The Aero-Hydrodynamic Characteristics of Yachts Sailing Upwind in Waves

A Step Towards the Development of a Dynamic VPP

Giovanni Bordogna

July 5, 2013

Faculty of Mechanical, Maritime and Materials Engineering · Delft University of Technology

The Aero-Hydrodynamic Characteristics of Yachts Sailing Upwind in Waves

A Step Towards the Development of a Dynamic VPP

Master of Science Thesis

For obtaining the degree of Master of Science in Marine Technology at
Delft University of Technology

Giovanni Bordogna

July 5, 2013

Faculty of Mechanical, Maritime and Materials Engineering · Delft University of Technology

Delft University Of Technology
Section Of
Ship Hydromechanics and Structures

The undersigned hereby certify that they have read and recommend to the Faculty of Mechanical, Maritime and Materials Engineering for acceptance a thesis entitled

The Aero-Hydrodynamic Characteristics of Yachts Sailing Upwind in Waves

by

Giovanni Bordogna

in partial fulfillment of the requirements for the degree of

Master of Science.

Dated: July 5, 2013

Head of the section: _____
Prof.Dr.Ir. R.H.M. Huijsmans

Supervisor: _____
Dr.Ir. J.A. Keuning

Co-supervisor: _____
Prof. F.V. Fossati

Reader: _____
Prof.Ir. J.J. Hopman

Summary

A common practice during the design of a sailing yacht is to assume an ideal environment. The wind is constant in intensity and direction and the sea is calm. In this situation, an equilibrium between the aerodynamic and hydrodynamic forces and moments can be found. The equations of equilibrium are thus solved to find the best setup (combination of sails, sail trim, etc.) in order to achieve the maximum boat speed.

This procedure is the core of a 'traditional' Velocity Prediction Program (VPP) , which was first introduced in 1976. Since then many improvements have been made and nowadays VPPs are capable of dealing with the most diverse designs. However, in nearly forty years of life, the nature of these programs has not changed and, still, important dynamic effects caused by the real environment, are not taken into account.

Investigating the performance of a yacht taking into account these effects, is far from easy. Indeed, the equations of equilibrium should be replaced by the more complicated equations of motion which need to be solved in the time domain. However, in recent years, the dynamic characteristics of a yacht sailing in waves and shifting winds (real environment) have become a more popular topic in the sailing yacht community.

In the wake of the increasing interest towards this subject, the present work aims to investigate some important dynamic aspects. The effect of the surge motion and of the heeling angle on the motions of heave and pitch, and on the mean added resistance, are studied by means of towing-tank tests. These are performed on two models of series 4 of the Delft Systematic Yacht Hull Series. Then, time-domain simulations are performed to study the effect of a pitch-induced oscillating aerodynamic force on the seakeeping of yachts sailing upwind in waves. The aerodynamic force is calculated using a quasi-steady as well as an unsteady method, whereas the hydrodynamic part of the problem is tackled using a strip-theory program which is capable of considering asymmetric hull shapes (e.g. hulls with a heeling angle). The results show that surge has a small influence on the motions and on the mean added resistance alike. The heeling angle on the other hand, prove to have a large effect on the seakeeping of the models. This effect can be qualitatively predicted by the strip-theory program, although the trend is not always correct. Finally, in same cases, the aerodynamic force significantly affects the pitch and heave motions and this results in a considerable reduction of the added resistance in waves.

Acknowledgements

I would like to express my gratitude to Dr. Lex Keuning for supervising me during the course of this thesis. I always enjoyed our discussions and his patience in dealing with my questions is sincerely appreciated. Equally I want to thank Prof. Fabio Fossati for his collaboration and for the time he took to come to Delft and engage with the research. This work would not have been possible without their expertise and support.

I would also like to thank Prof. Rene Huijsmans and Prof. Hans Hopman for revising my thesis draft. I am very grateful for their feedback and help.

The assistance of Guido Vish during the month I spent at the towing tank carrying out the experiments is very much appreciated. Likewise I thank the staff of the Ship Hydromechanics Laboratory for helping with the models.

The help and support from Ellen and my friends during this period is deeply appreciated.

Lastly, I want to thank my family for their love and unconditional support.

Delft, The Netherlands
July 5, 2013

Giovanni Bordogna

Contents

Nomenclature

Latin Symbols

A_x	Cross-sectional area
A_{tr}	Transom cross-sectional area
$A_{i,j}$	Infinite-frequency added mass
$a_{i,j}$	Added mass relative to the entire ship
B	Breadth waterline
$b_{i,j}$	Damping relative to the entire ship
C	Hydrostatic restoring matrix
C_{sails}	Sailplan chord length
Cx	Sail aerodynamic driving force coefficient
D	6-by-6 global complex added mass matrix
$d_{i,j}$	Sectional damping
E	Radiated energy for one period of oscillation of the ship
Fn	Froude number
F_{aero}	Sail aerodynamic force
$F_{aero,3}$	Heave aerodynamic force
$F_{aero,5}$	Pitch aerodynamic moment
$F_{wave,3}$	Wave-induced heave force
$F_{wave,5}$	Wave-induced pitch moment
F_x	Longitudinal force measured on the model parallell to the X-axis of the tank
$\vec{\hat{F}}_e$	6-component global force vector
$\vec{\hat{f}}_x$	3-component sectional force vector

G	3-by-3 sectional complex added mass matrix
g	Acceleration due to gravity
h	Water depth
I	Mass moment of inertia of the ship
$K_{i,j}$	Retardation function
k	Wave number
k_{yy}	Pitch radius of gyration
LCB	Longitudinal center of buoyancy
LWL	Length waterline
L_{pp}	Length between perpendiculars
M	Mass matrix
m	Mass of the ship
$n_{i,j}$	Sectional added mass
p	Pressure
R_{aw}	Mean added resistance in waves
SA	Sail area
T	Draft
T_e	Wave encounter period
t	Time
$\vec{u}$	6-component global vector of motions
$\vec{u_x}$	3-component sectional vector of motions
V_{AW}	Apparent wind speed
V_R	Reduced velocity
V_{ris}	Dynamic apparent wind speed
V_{TW}	True wind speed
Vs	Ship forward speed
V_{zb}	Mean relative vertical velocity
x_3	Heave amplitude
$\dot{x_3}$	Heave velocity
$\ddot{x_3}$	Heave acceleration
X, Y, Z	PDSTRIP output and calculation reference system
X_{in},Y_{in},Z_{in}	PDSTRIP input reference system
x_G, y_G, z_G	Coordinates of the ship center of gravity
x_{tr}, y_{tr}, z_{tr}	Coordinates of the center of gravity of the transom area
y_S, z_S	Coordinates of the sectional area center
$y_W(x)$	Sectional mean transverse coordinate of the waterline
Z_{COE}	Sail center of effort height

Greek Symbols

β_{AW}	Apparent wind angle
β_{din}	Dynamic apparent wind angle
β_{eff}	Effective dynamic apparent wind angle
β_{TW}	True wind angle
ζ	Wave elevation
ζ_a	Wave amplitude
θ	Pitch amplitude
$\dot{\theta}$	Pitch velocity
$\ddot{\theta}$	Pitch acceleration
λ	Wave length
λ_μ	Wave length in oblique waves
μ	Wave direction (180° for bow waves)
ρ	Density of water
ρ_{air}	Density of air
ϕ	Wave velocity potential
ω	Wave angular frequency
ω_e	Wave frequency of encounter

Abbreviations

CFD	Computational Fluid Dynamics
COG	Center Of Gravity
DOF	Degree Of Freedom
DVPP	Dynamic Velocity Prediction Program
EOM	Equations Of Motion
IACC	International America's Cup Class
IMS	International Measurement System
MARIN	Maritime Research Institute Netherlands
MIT	Massachusetts Institute of Technology
RANSE	Reynolds Averaged Navier-Stokes Equations
RAO	Response Amplitude Operator
VPP	Velocity Prediction Program

Chapter 1

Introduction

Sailing yachts are complex beings whose functioning is one of the most complicated in the maritime field. The difficulty of studying and predicting the behavior of sailing yachts resides in the fact that they operate at the interface of two fluids, water and air, and they have to comply equally with the natural laws of both. In fact, the sails are as important as the hull or the appendages. These three components cannot be imagined separately and the degree of their interaction directly depends on the wind and the waves. Furthermore, man is deeply involved in this loop because, apart from being responsible for the steering, he is also accountable for adjusting the sails which ultimately modifies the entire process again.
The will to predict what is happening in such a chaotic and unforeseeable situation seems hopeless. As a result, assumptions and simplifications need to be made.

What generally occurs during the design of a sailing yacht is to assume that, what in reality is chaotic and unpredictable, is actually steady and known: the wind is constant in intensity and direction, the water is calm and sailors always make the optimal decision. Also, the fact that yachts tack and gybe is generally neglected. One may argue that this might seem an oversimplification, however, in the past as much as nowadays, this could be deemed as the standard procedure in yacht design.
Based on these assumptions, a tool which could predict the performance of a sailing yacht was introduced already in 1976 by MIT researcher J.E.Kerwin [28] and named Velocity Prediction Program (VPP). The main scope of this tool was to establish a handicapping system to allow different yachts to compete at one same regatta. Since that moment, VPPs have spread enormously and nowadays are an essential tool in the yacht design and yacht handicapping communities alike.

In nearly forty years of life, VPPs have improved considerably. Now, the most diverse designs can be considered and they are able to deal with every sort of device such as canting keels or bulb winglets as well as with data provided by CFD simulations or towing-tank tests. However, the assumptions on which they are based remain unchanged.

Let us for now refrain from questioning the assumption that sailors are optimal decision makers but focus, instead, on the following questions:

- How different yachts react to a gust or shift of wind?
- How their performance are influenced by the waves of the ocean?
- How different yachts maneuver?

Although none of these questions can be answered by using VPPs, these programs are regularly employed to design yachts and make them compete equally together.
In the past, a number of studies have been published with the aim of tackling these questions. While some focused on the maneuverability of yachts, others investigated their seakeeping abilities and the related dynamic effects[1].

In the following sections the main works published on these topics are briefly summarized, paying particular attention to the assumptions made.

1.1 Literature review on maneuverability

In 1990, Larsson [37] reported about a sailing simulator at the SSPA Maritime Consulting in Sweden which was capable of simulating the maneuvering of a yacht by solving the equations of motion in the time domain for four degrees of freedom (DOF): surge, sway, roll and yaw. In the program there was also the possibility of considering a wind spectrum (wind varying in intensity and direction).

In 1993, Masuyama et al.[39] were the first to compare the results of a time-domain simulation with results obtained by means of full-scale tests. Again, only the surge, sway, roll and yaw equations of motion (EOM) were considered. The hydrodynamic forces and moments and all the hydrodynamic derivatives for the maneuvering model, were calculated with rather complicated towing-tank tests. The added mass and added mass moment of inertia were obtained by using strip-theory programs. The aerodynamic coefficients were obtained by means of steady wind-tunnel tests. In the results the authors plotted the trajectory, the heeling angle, the drift angle and the speed of the yacht before, during and after a tack, comparing the results of the simulation with full-scale results. The rudder angle which was recorded on board the actual yacht was used as input for the maneuvering simulation.
The same method was used by Masuyama and Fukasawa [38] in 2008. However, this time the aerodynamic forces were calculated by means of full-scale measurements, which improved the prediction of the attitude of the yacht during the actual tacking phase (i.e. when the jib begins to flog).

In 1995, Bilger [7] proposed a simplified method to predict the optimal tacking procedure. The tacking procedure was divided into two parts; the turning part and the accelerating part. The model was based on simple algebraic equations and no equations of motion were actually solved.

In 2003, Masuyama et al. [40] solved the same four equations of motion as described in [39], in order to predict the maneuverability of a traditional Japanese sailing trader.

[1] Studies related to the surf-riding of yachts sailing in following seas have not been reported due to the peculiarity of this problem

Due to the peculiarity of such a ship, the hydrodynamic coefficients and forces had to be obtained by means of towing-tank tests while the aerodynamic coefficients were obtained by performing wind-tunnel experiments.

In 2004, De Ridder, Vermeulen and Keuning [45] developed a time-domain tool which was capable of solving the EOM for surge, sway, roll and yaw, using the results of the Delft Systematic Yacht Hull Series (DSYHS) only. In this paper, the authors used the coordinate system as proposed by Hanamoto et al. [22]. The aerodynamic forces were calculated using the Hazen/IMS coefficients and by considering that the apparent wind speed and apparent wind angle were affected by the forward velocity of the yacht as well as by the sway-roll-yaw induced velocities.
The data relative to the DSYHS used in this work were based on results published in earlier papers ([31] and [30]) in which particular attention was given to the resistance of the hull and the appendages, the side force production of the appendages and the yaw moment of the hull (Munk moment).

In 2007, Keuning et al. [29] proposed an optimization model for the tacking procedure of an IACC yacht. The model was based on the same four equations of motion as described in [45], however, being an America's Cup yacht not compatible with the DSYHS range, the hydrodynamic part was improved using data obtained by means of dedicated towing-tank tests. Also the aerodynamic part was improved; the aerodynamic coefficients were calculated using CFD programs and wind-tunnel experiments. The results of the simulations were presented as distance lost during a tack against different combinations of rudder and trim-tab angles. They were also compared with data obtained during full-scale trials.

Although not strictly related to maneuvering, it is worthwhile mentioning the work of Verwerft and Keuning [52]. In their 2008 publication, the authors studied the effect of varying wind in intensity and direction on three different yachts (the main varying factor was the displacement). Once again, as presented in [45], all the calculations were based solely on the results of the DSYHS. However, this time the yaw moment was calculated using the side forces generated by each individual appendage and by separately considering the Munk moment generated by the bare hull (see also [31]) . The main advantage of this formulation was that the actual area of the appendages was taken into account, rather than the effective draft of the keel as suggested by the Extended Keel Method. Also, the effects on the lift production of the appendages caused by the heeling angle, the presence of the hull and the asymmetry of the heeled hull, were taken into account. So was the downwash of the keel on the rudder.

Finally, another time-domain simulator for the tacking procedure of a yacht was presented in 2007 by Ledri and Battistin [3]. The equations of motion were solved for surge, sway, roll and yaw. The hydrodynamic forces and moments were calculated with the same approach used by Verwerft and Keuning [52], with the exception that the lift generated by the canoe body and the appendages was calculated according to formulas reported by van Oossanen [51]. The added mass and damping coefficients were obtained using the results of the DSYHS or the Clarke's method as presented by Lewis [36], while the Hazen/IMS aerodynamic coefficients, as presented by Claughton [9], were used to calculate the quasi-steady aerodynamic forces and moments. An optimization routine based on a genetic algorithm was also employed to find the optimal tacking procedure and the results were presented in terms of Distance Made Good (gain in distance).

1.2 Literature review on wave-induced dynamic effects

For the sake of clarity, this section has been divided in two parts: whilst the first one deals with the seakeeping-related problems of yachts sailing in waves, the second is dedicated to the wave-induced dynamic effects on sails. Due to the scarcity of publications on the topic, a section dedicated to the dynamic effects caused by the sail aerodynamic force on the motions, has not been included.

1.2.1 Seakeeping of sailing yachts

In 1967, Spens, Desaix and Brown [48] were among the first to investigate the dynamic-related problems of a yacht sailing in waves. Towing-tank tests were performed at the Davidson Laboratory to study the influence of the waves on the performance of a yacht sailing upwind. Tests with and without appendages were performed in head as well as oblique waves. One important conclusion was that, for the latter case, the waves only affected the leeway of the yacht by a negligible amount. Also, the added resistance in oblique waves could be estimated from tests in head waves, having the same effective wave length and the same frequency of encounter.

One year later, Gerritsma reported in [19] the case of a 'half-ton' yacht sailing upwind. The experiments were compared with results obtained with a strip-theory program for the heave and pitch motions. The effect of the heeling angle and forward velocity were not included in the calculation, while the effect of the lift-producing appendages was. The results showed poor agreement when the wave length was larger than 1.5 LWL as the responses were shifted to longer waves when compared with the experiments. The author pointed out that this was probably due to the fact that the forward velocity had not been taken into account. The towing-tank tests were performed in regular as well as irregular waves for three different wave amplitudes. For a wave height up to $2 \cdot \zeta_a/Lwl = \frac{1}{14}$, the motions of heave and pitch appeared to scale linearly with the wave height, both when the model was heeled and upright.

Again, in 1972 Gerritsma and Moeyes [21] tested three models with the aim of investigating the effect of the pitch radius of gyration on a yacht sailing upwind in waves. The results showed that the radius of gyration played an important role in the determination of the pitch motion and the added resistance alike.

One of the first and only attempts to couple the aero and hydrodynamic effects of a yacht sailing in waves was done by Skinner in 1982 [47]. The main scope of his research was to show that the aerodynamic damping of the sails could considerably reduce the motions due to the waves, in particular for pitch and roll. A quasi-steady approach was used to calculate the aerodynamic force, while the damping of the sails was calculated with the lifting line theory. The yacht motions were calculated with a strip-theory program. The author concluded that by considering the aerodynamic damping, the pitch motion was reduced by approximately 14%, while roll appeared to be highly over-damped. Another conclusion was that these results could be over predicted by the use of a quasi-steady approach as unsteady effects could diminish the significance of the aerodynamic pitch damping.

In 1987, Klaka and Penrose [32] carried out towing-tank experiments on a 12-Meter sailing yacht, both upright and with 15° of heel without drift. The results showed that the mean added resistance, if the model was heeled, was about half of that measured for the upright condition.

Three years later, Kapsenberg [27] reported a new technique employed at MARIN to test yachts sailing upwind in waves. The experiments were performed letting the model free to move in all the six DOF. The model was towed from the hypothetical sail center of effort height using a constant tension winch mounted on the carriage. Appendages were mounted on the model and an autopilot system was used to keep the model on course. The tests were performed with the correct combination of forward speed, heel and drift angle so that the hydrodynamic forces and moments were in equilibrium. Kapsenberg also compared the results of the experiments with calculations carried out with a strip-theory program, in which the yacht was assumed to be upright, with no appendages. The conclusion was that the heave and pitch motions, and the added resistance in waves, were largely over predicted by the calculations, especially at the resonance peak.

In 1995 Levadou [35] carried out a series of towing-tank tests to study the seakeeping abilities of the models of series 4 of the DSYHS. The models were tested upright and with a heeling angle of 20°, free to heave and pitch, and restrained in the other directions. The experiments were performed at zero drift and trim angle. The results showed that the heeling angle had a significant influence on the motions and the mean added resistance alike. Levadou reported however that, during the heeled tests, the models had a considerable undesired sway and yaw motions caused by the force generated by the asymmetric hull, and this may have had an influence on the results.

Day et al. [11] in 2002 were among the first to carry out a time-domain simulation considering all six degrees of freedom. The authors proposed a new tool called Performance Prediction Program (PPP), which was the result of coupling a quasi-steady model to calculate the hydrodynamic and the aerodynamic forces with a non-linear ship-motion program. In this model the hydrodynamic forces were calculated by using the results of the DSYHS and the aerodynamic coefficients were based on the Hazen/IMS method. As the ship-motion program operated in the frequency domain, spectral techniques and convolution had to be used in order to express the results in the time domain. The results compared the pitch motion calculated with the PPP against the data obtained during full-scale trials. The PPP overestimated the pitch motion and the authors argued that the possible cause was the fact that the damping sources (damping of the sails but mostly damping due to slamming) had not been taken into account.

In the same year, Ottosson et al. [42] also proposed a time-domain simulator called Dynamic VPP (DVPP) which was capable of solving the equations of motion for the six DOF. The hydrodynamic and aerodynamic forces were calculated by using standard theory as described in van Oossanen [51] and Larsson and Eliasson [34]. The motions were calculated by means of a strip-theory program. The main scope of the simulations was to study the influence of the pitch radius of gyration on the added resistance in waves. For this purpose, the mean added resistance was calculated with the Gerritsma and Beukelman formulation [20].

In 2005, Jacquin et al. [25] and Harris [23] used CFD techniques for the prediction of unsteady hydrodynamic and aerodynamic forces. Jacquin tackled the hydrodynamic

problem by using a RANSE solver, while a panel method was used for the aerodynamic part. The problem was solved for six degrees of freedom. While the effect of the sails on the motions was considered, the change of the aerodynamic forces due to the motions of the yacht was neglected.

Harris also took into account the six equations of motion. This time, however, potential flow solvers were used to calculate the forces both for the hydrodynamic and the aerodynamic part. The added mass, damping and wave forces were calculated using a strip-theory program. The results were then transformed into the time domain by using the Cummins Equations [10]. The sails were divided into sixteen strips. The lift and the (inviscid) drag were calculated by considering on each strip the apparent wind speed, the apparent wind angle and the motion-induced velocities. The sail-related viscous phenomena were calculated with a simple empirical formulation.

Richardt et al. [44] proposed in 2005 a time-domain simulator for sailing yachts (called FS-equilibrium) capable of solving the equations of motion up to six degrees of freedom. The main idea behind this program was that the information necessary to solve the problem should be provided by the user in form of modules. However, a range of modules was already available and these are substantially based on the results of the DSYHS and the Hazen/IMS model.

In 2012, Bordogna [8] developed a time-domain VPP which was able to consider the motions of a yacht in six DOF although only the equations for surge, sway, roll and yaw were directly solved. These four EOM were solved using the same formulation as proposed by Verwerft and Keuning [52] and also the hydrodynamic forces were calculated in the same way. The pitch and heave motions were not directly solved, but instead an external strip-theory program was used. The waves were assumed to be regular and that they affected the pitch and heave motions only. The wave-induced forces and moments relative to all the other motions, were neglected. The main novelty of the program was that the aerodynamic forces were calculated with a two-dimensional Unsteady Thin Airfoil Theory as introduced by Gerhardt [16]. The results were also compared with data obtained with full-scale tests but they showed poor agreement.

More recently, Fossati [12] proposed a simple model which considered a yacht as a single mass point which followed the profile of long waves. According to this assumption, the time and length scales of the yacht were much shorter than those of the waves. Two equations of motion were solved numerically in the time domain, namely one tangential to the wave surface and one normal to it. The hydrodynamic resistance of the yacht was assumed to be composed by the wave making resistance (which was thought to be dependent mainly on the displaced volume) and the viscous resistance. The added resistance in waves was not considered due to the assumptions made. The aerodynamic forces were calculated using a rheological model tuned on the basis of unsteady wind-tunnel tests. The results were reported for regular and irregular waves. In the second case, the frequency of oscillation needed to choose the correct value of the stiffness and damping coefficients of the rheological model, was assumed to be the modal encounter frequency of the wave spectrum under consideration.

1.2.2 Wave-induced dynamic effects on sails

In the last few years, there has been a number of authors who investigated the unsteady effects on sail aerodynamics caused by the pitching of a yacht sailing upwind in waves.

As reported in [14], [13] and [15], Fossati studied, by means of unsteady wind-tunnel tests, the influence on the sail aerodynamics of the so-called reduced frequency and the pitch angle (i.e. the degree of oscillation of the sails). The results of his research clearly identify the presence of a hysteresis loop caused by the unsteady effects. Different values of the aerodynamic coefficients were in fact obtained depending on whether the pitch angle was increased or decreased. Furthermore, for large pitch angles, it was shown that viscous effects (i.e. separation) played an important role. The author also proposed a rheological model which was able to predict the unsteady aerodynamic driving force coefficient using as input the pitch angle and the dynamic apparent wind angle.

In [17], [18] and [16], Gerhardt showed that a quasi-steady approach should be avoided in the situation of a yacht pitching while sailing upwind in waves. The author therefore derived a new Unsteady Thin Airfoil Theory for two interacting sail 'slices' in a two-dimensional potential flow (all the viscous effects were neglected). In particular, he applied this theory to a IACC yacht sailing in a moderate sea state and he concluded that the aerodynamic forces were better predicted with this new technique rather than by using a quasi-steady method.

Finally, Augier [2] used Fluid-Structure Interaction techniques to investigate the effects of harmonic pitch-induced motions on flexible and rigid sails. The results presented were in agreement with those of Fossati; the dynamic behavior of a sail plan subject to pitch motions strongly deviated from the quasi-steady theory due to the presence of a hysteresis loop.

1.3 Considerations and aim of the research

The previous sections have reported several studies that aimed to address the three primary questions presented at the beginning of this chapter. As it can be seen, maneuverability has arguably been the topic studied most rigorously, with different techniques being employed and compared. In contrast, the effects of a realistic environment (i.e. the presence of waves and a varying wind) have been investigated in a more sporadic way and often the assumptions made seem to oversimplify the problem or have even been proven wrong by later studies (i.e. using a quasi-steady aerodynamic theory and neglecting the unsteady effects due to pitch).

In the early stage of this thesis, the problem of a yacht sailing in waves was considered in its entire complexity. In fact discussed was the possibility of conducting time-domain simulations considering the six degrees of freedom and using the unsteady aerodynamic theory as presented by Fossati. The results would have then been compared with experiments similar to those carried out by Kapsenberg [27]. However, due to the extreme difficulty of considering the seakeeping of a yacht in the six degrees of freedom, taking also into account the aero-hydrodynamic unsteady effects, it was instead decided to adopt a step-by-step approach. It is believed that a first step towards a better understanding of the

effects of the aero-hydrodynamic coupling in a dynamic environment can be achieved by simplify the seakeeping problem, considering three degrees of freedom only: surge, heave and pitch. Doing so, maneuverability is no longer part of the problem and the appendages can be neglected. On the other hand, the unsteady effects caused by the pitch on the sails, and the way, in turn, the unsteady aerodynamic force influences the motions, is taken into account. Therefore, a collaboration with Professor Fossati of Politecnico di Milano, who recently published research regarding a similar problem [12], was established.

On the basis of these considerations, of the three primary questions presented earlier in this chapter, the focus of this thesis is on the second question: How are the performance of yachts influenced by the waves of the ocean? From this basic question stem more particular issues that the research presented in this work aims to investigate:

1. How does surge influence the motions of heave and pitch, and the added resistance of yachts sailing upwind in waves?
2. How does a certain heeling angle influence the performance of yachts sailing in waves and can this effect be predicted by a strip-theory program?
3. Does the trim angle have an influence on the seakeeping of yachts?
4. What is the relationship between the surge force amplitude and the amplitude of the wave causing that force?
5. Does the pitch-induced oscillating aerodynamic force affect the performance of yachts sailing upwind in waves? And are the unsteady aerodynamic effects of importance?

In order to answer these questions, several techniques were employed during the present research. First, towing-tank tests were carried out on two models of series 4 of the DSYHS to study the influence of the surge motion on the motions of heave and pitch, and on the mean added resistance. Similar experiments were then performed to study the effect of the heeling angle. During these experiments, attention was given to avoid undesired sway and yaw motions caused by the asymmetric hull. For each test, the surge force was measured and then analyzed. This in fact becomes of interest when the dynamic behavior of a ship is intended to be studied.

The effect of the trim angle on the seakeeping of the models was also investigated. This was done by comparing the results of the current experiments with the output of similar tests carried out in 1995 [35] on the same models of the DSYHS.

Furthermore, the strip-theory program PDSTRIP [6] was used to verify whether the influence of the heeling angle on the motions of heave and pitch, and on the mean added resistance, could be properly predicted. In fact, this program has the peculiarity of being able to consider asymmetric hull shapes, which makes it suitable for this type of investigation. Finally, time-domain simulations were performed to study the effect of a varying aerodynamic force on the seakeeping of yachts sailing upwind in waves. For this purpose, the frequency-dependent coefficients computed with PDSTRIP were transformed in the time domain by means of the so-called Cummins Equations [10]. The time-dependent aerodynamic force was computed using a quasi-steady, as well as an unsteady method and, in the latter case, the rheological model proposed by Fossati was used.

In conclusion, the research carried out in this thesis should be seen as a first step towards the development of a so-called Dynamic Velocity Prediction Program. This tool should be able to take into account the main interactions between the three components of a yacht (the hull, the sails and the appendages) considering a realistic environment and the related unsteady effects.

1.4 Thesis outline

Before discussing the results of the experiments and the calculations, the theory used in this thesis is presented. In Chapter 2, the characteristics of PDSTRIP, which are of particular importance for the present work, are treated. Then, it is explained how the hydromechanical coefficients computed with PDSTRIP can be transformed into the time domain by means of Cummins Equations. These equations present various numerical issues, and the way these have been treated is discussed. Furthermore, the concept of instationary sail aerodynamics is presented. Here the difference between the quasi-steady and the unsteady method to calculate the aerodynamic force is stressed. Lastly, the equations of motion for heave and pitch are given.
In Chapter 3 the details of the models tested and the setup used during the towing-tank experiments are reported. The results of the experiments and the calculations are then presented and discussed. This is done in Chapter 4. Some conclusions and final remarks are given in Chapter 5.

Chapter 2

Background Theory

This chapter deals with the different techniques adopted during the present research to predict the behavior of yachts sailing upwind in waves. First, the characteristics important for this thesis of the strip-theory program PDSTRIP are revised. The frequency-dependent added mass and damping calculated with this program are then transformed into the time domain by using the Cummins Equations. Here the focus is on some numerical issues related to these equations and the way they have been treated in the present work. The principles of unsteady sail aerodynamics are then presented, stressing the difference between two different methods (i.e. a quasi-steady and an unsteady method) to calculate the aerodynamic force. At last, the equations of motions are solved in the time domain.

2.1 PDSTRIP

PDSTRIP is an open-source computer program to calculate the seakeeping of ships and other floating bodies according to the Ordinary Strip Theory of Korvin-Kroukowsky and Jacobs [33]. The program was originally written in FORTRAN 77 by Söding (the program was called STRIP, see [6]) and then was translated into FORTRAN 90/95 by Bertram [5] and made publicly available in 2006. Apart from the features aimed to study the seakeeping of commercial vessels, which are present in many similar programs, PDSTRIP also includes routines particularly tailored to study the seakeeping of sailing yachts. These features are:

- Possibility of considering asymmetrical cross sections (e.g. heeled ships)
- Possibility of including fins such as keels and rudders (and the forces generated by them)
- Possibility of considering the effect of a harmonically oscillating (linear) aerodynamic force on the motions

Among these characteristics, only the first is of interest for the present research. In fact, the appendages have not been taken into account, and the rheological model of Fossati has been used to calculate the unsteady (non-linear) aerodynamic force.
For these reasons, it has been included in a MATLAB program only those routines of PDSTRIP which are necessary to calculate the RAOs of a generic bare hull (i.e. symmetric as well as asymmetric). This resulted in an easy-to-use program and, most importantly, made it possible to quickly implement those functions necessary to perform the time-domain simulations.

It should also be mentioned that, although not implemented in the original PDSTRIP, it has been included in the MATLAB version the possibility to calculate the mean added resistance in waves according to the Gerritsma and Beukelman formulation [20]. The description of this method, together with the entire derivation of the equations of motion in the frequency domain, may be found in Appendix A.

2.1.1 Coordinate system

PDSTRIP adopts two different coordinate systems; one to input the data for the calculations and one to perform the calculations. In the input coordinate system, the origin is assumed to be at the interception of the water line with the midship plane. The X_{in}-axis points forward, the Y_{in}-axis points to port and the Z_{in}-axis points upward. In contrast, the coordinate system used to perform the calculations has the 3 axis X,Y and Z which respectively point forward, starboard and downward. This coordinate system moves forward with the average ship velocity but it does not follow the periodical oscillations of the ship. Its origin is located at the interception of the baseline with the midship plane. The translations are positive according to the directions of the axis while the rotations are positive according to the right-hand rule. The results of the calculations refer to the XYZ coordinate system (see Figure 2.1).

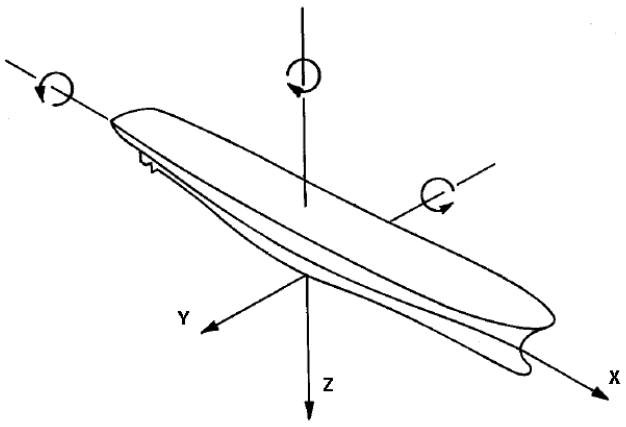

Figure 2.1: PDSTRIP coordinate system used during the calculations

2.1.2 Calculation of the added mass and damping

In PDSTRIP the section contour of the floating body is defined by the actual offset points of the hull, allowing it to consider symmetrical as well as asymmetrical hull shapes. No mapping techniques are used. The boundary conditions are satisfied according to the patch method (see [46] and [4]). This method considers the integral of the boundary conditions over each segment, instead of at the collocation point in the middle of each segment as the panel method does.

Once the boundary conditions are satisfied, and the velocity potential ϕ is calculated, the pressure on the body contour can be calculated according to Bernoulli's equation:

$$p = -\rho \frac{\partial \phi}{\partial t} \tag{2.1}$$

Integrating the pressure over each cross-section contour, the complex values of the sectional sway and heave force, and roll moment, are obtained. These forces and moment can also be considered in the following form:

$$\hat{f} = -n \cdot \left(-\omega^2 \hat{u}\right) - d\left(i\omega\hat{u}\right) \tag{2.2}$$

in which, $\hat{f}$ is the generic complex force (or moment) caused by one of the 3 motions, n is the added mass and d is the damping. The terms $\left(-\omega^2\hat{u}\right)$ and$(i\omega\hat{u})$ are the complex amplitudes of the sinusoidal acceleration and sinusoidal velocity, respectively. The complex added mass $\hat{n}$, the real added mass n and the damping d are related according to the following formulation:

$$\hat{n} = n - \frac{id}{\omega} \tag{2.3}$$

Eq. (2.3) holds for each of the 3 forces and the 3 motions, resulting in the sectional complex added mass matrix G:

$$G = \begin{bmatrix} \hat{n}_{2,2} & \hat{n}_{2,3} & \hat{n}_{2,4} \\ \hat{n}_{3,2} & \hat{n}_{3,3} & \hat{n}_{3,4} \\ \hat{n}_{4,2} & \hat{n}_{4,3} & \hat{n}_{4,4} \end{bmatrix} \tag{2.4}$$

The 3-by-3 matrix G is then integrated over the ship length. The 6-by-6 complex added mass matrix D is then obtained. In this procedure, the surge added mass and damping are not computed. As it occurs in any strip-theory program, these need to be calculated in some other ways. In PDSTRIP, it is assumed that the surge damping is zero and the surge added mass can be approximated according to the following empirical formula:

$$n_{1,1} = \frac{m}{\pi \cdot \sqrt{\rho L_{pp}^3/m} - 14} \tag{2.5}$$

The 6-by-6 ΔD matrix, which contains the effects of the surge added mass $n_{1,1}$ on all the other terms, is then summed to the matrix D, resulting in the global 6-by-6 radiation matrix. This comprises of the real added mass ($a_{i,j}$) and damping ($b_{i,j}$) terms relative to the entire ship.

2.2 Cummins Equations

The main idea behind the Cummins Equations, (named after W.E. Cummins, see [10]) is to apply the theory of impulse to the problem of ship motions in waves. The interested reader may find the complete derivation of the Cummins Equations in Appendix B.

In the situation of a ship with forward speed, the Cummins Equations read:

$$\sum_{j=1}^{6}\{(M_{i,j}+A_{i,j})\cdot\ddot{x}_j(t)+b_{i,j}(\omega_\infty)\cdot\dot{x}_j(t)+ \int_0^\infty K_{i,j}(\tau)\cdot\dot{x}_j(t-\tau)\cdot d\tau+C_{i,j}\cdot x_j(t)\}=X_i(t) \quad (2.6)$$

in which, $M_{i,j}$ is the mass term, $C_{i,j}$ is the restoring term and $X_i(t)$ is the external time-dependent exciting force. The term $b_{i,j}(\omega_\infty)$ indicates the speed-dependent infinite-frequency damping coefficient.

A convenient aspect of the Cummins Equations is that, although they need to be solved in the time domain, a frequency-domain method can be used to calculate the added mass and damping. Indeed, according to [41] the terms $A_{i,j}$ and $K_{i,j}$ can be defined as:

$$K_{i,j}(\tau)=\frac{2}{\pi}\cdot\int_0^\infty b_{i,j}(\omega)\cdot\cos(\omega\tau)\cdot d\omega \quad (2.7)$$

$$A_{i,j}=a_{i,j}(\omega_\infty)+\frac{1}{\omega_\infty}\cdot\int_0^\infty K_{i,j}(\tau)\cdot\sin(\omega\tau)\cdot d\tau \quad (2.8)$$

in which the damping $b_{i,j}(\omega)$ should be calculated considering the non-zero forward speed.

As Eq. (2.8) is valid for any frequency, it also holds for $\omega=\infty$, which provides:

$$A_{i,j}=a_{i,j}(\omega_\infty) \quad (2.9)$$

In contrast, the infinite-frequency added mass term $a_{i,j}(\omega_\infty)$ should be calculated for zero forward speed.

An interesting feature of the Cummins Equations is that they allow simultaneously to take into account linear, as well as non-linear, effects of the seakeeping of a ship. Indeed, the left-hand side of Eq.(A.1) is linear as it is simply the specular representation in the time domain of its frequency-domain counterpart. This means that all the terms which appear in the left-hand side of the equation are calculated relative to the average, steady position of the ship. On the other hand, the time-dependent exciting force $X_i(t)$, which appears in the right-hand side of the equation, can be any sort of linear as well as non-linear force and moment.

The 'memory' effects of the system are contained in the retardation function $K_{i,j}(\tau)$ which, for this reason, acts like damping in the time domain. A typical trend of the retardation function is shown in Figure 2.2.

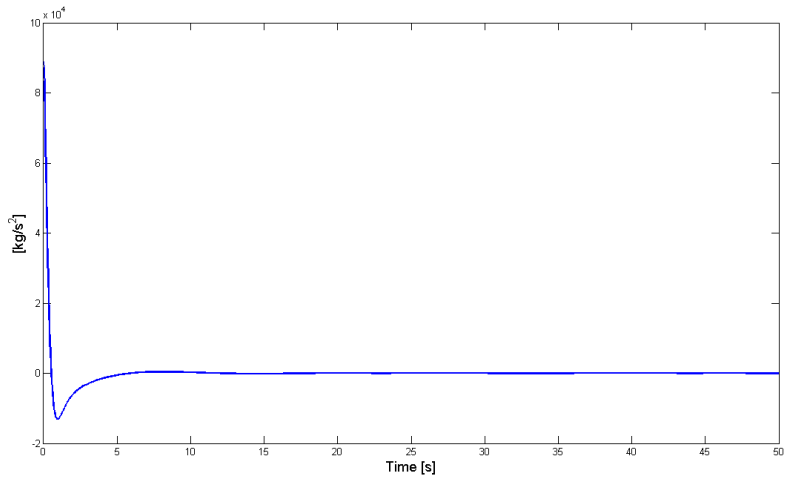

Figure 2.2: Example of retardation function $K_{3,3}$

The Cummins Equations present several numerical issues which need to be treated with care. Among these, the most troublesome are arguably related to the computation of $K_{i,j}(\tau)$. The first problem is that the integral which appears in Eq. (2.7) needs to be taken over an infinite frequency range. Strip-theory programs fail in calculating the damping coefficient $b_{i,j}(\omega)$ at very high frequencies. This means that the numerical integration can only be properly carried out till a certain frequency value Ω, so that the retardation function becomes:

$$K_{i,j}(\tau) = \frac{2}{\pi} \cdot \int_0^{\Omega} b_{i,j}(\omega) \cdot \cos(\omega\tau) \cdot d\omega \tag{2.10}$$

and this, in turn, introduces a truncation error defined as:

$$\Delta K_{i,j}(\tau) = \frac{2}{\pi} \cdot \int_{\Omega}^{\infty} b_{i,j}(\omega) \cdot \cos(\omega\tau) \cdot d\omega \tag{2.11}$$

Studies carried out in the past (see [26]) proved that, in case Ω is sufficiently large, the error due to $\Delta K_{i,j}(\tau)$ is generally small.

The second and more troublesome problem is that the damping $b_{i,j}(\omega)$ needs to be calculated very accurately over the entire frequency range. Errors are otherwise introduced, which would result in a miscalculated retardation function. This, in turn, would largely influence the prediction of the response, especially at the resonance peak.

In the situation of a ship with zero forward speed, it is known that the damping $b_{i,j}(\omega)$ tends to zero at a rate of approximately ω^{-2}, as the frequency ω approaches an infinite value (see Figure 2.3). Use can be made of this property to approximate the high-frequency tail of the damping curves which, in turn, facilitates the computation the retardation function. The responses computed using the Cummins Equations for Fn=0 appear to have a good degree of accuracy when compared to the results obtained with the frequency-domain calculations. An example relative to a wave length $\lambda = 1.5 \cdot LWL$ is shown in Figure 2.4.

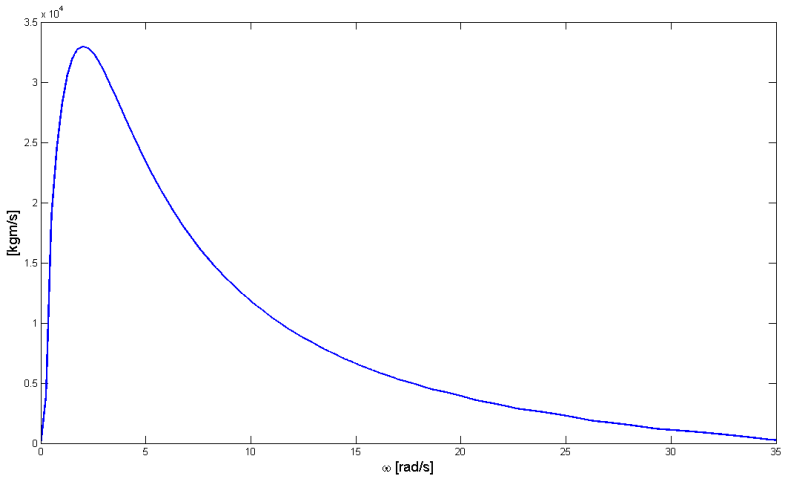

Figure 2.3: Damping curve relative to $b_{5,3}(\omega)$. Fn=0

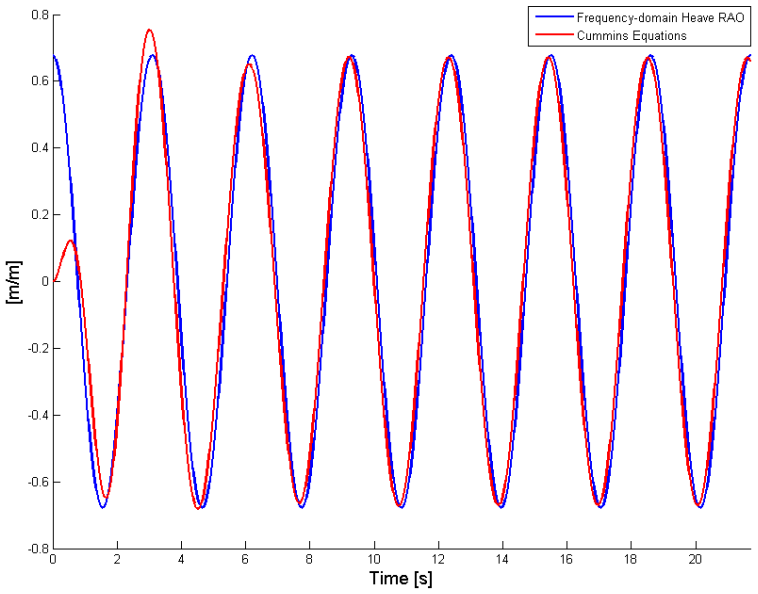

Figure 2.4: Comparison of the heave response calculated using the Cummins Equations and the heave response computed in the frequency domain. Fn=0, $\lambda = 1.5 \cdot LWL$

On the other hand, if the ship is moving with a certain forward speed, only the damping terms on the main diagonal of the matrix D (e.g.$b_{3,3}(\omega)$, $b_{5,5}(\omega)$ etc.) still have this property. Indeed, due to the effects caused by the forward velocity, the off-diagonal damping terms (e.g. $b_{3,5}(\omega)$, $b_{5,3}(\omega)$ etc.) do not tend to zero as the frequency tends to infinity (see Figure 2.5).

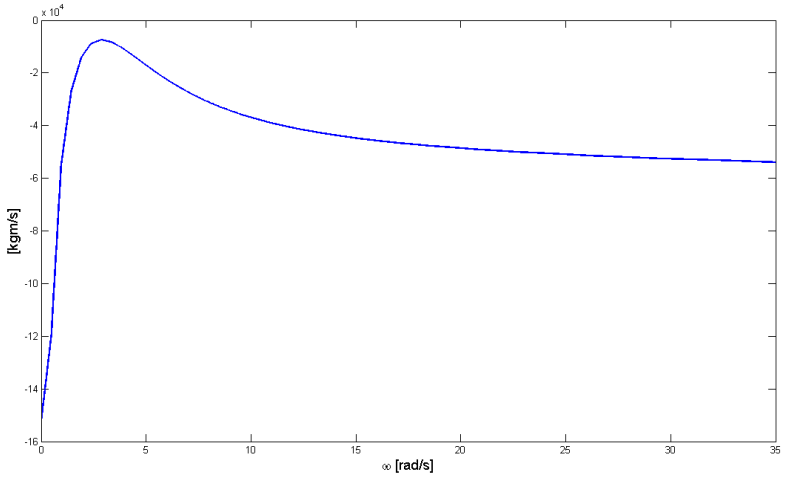

Figure 2.5: Damping curve relative to $b_{5,3}(\omega)$. Fn=0.35

In this situation, the accuracy of the computation of $K_{i,j}(\tau)$ depends on the ability of the frequency-domain program to properly calculate the damping at high frequencies. PDSTRIP uses an interpolation function which smoothes the damping curve at high frequencies removing the kinks caused by numerical errors. However, this is done at the cost of loosing some accuracy. The retardation function is therefore not properly calculated, resulting in a wrongly predicted response (see Figure 2.6).

A lot of effort has been put in trying to solve this problem, in particular using different shapes of the high frequency tail of the off-diagonal damping curves. However, no significant improvements have been achieved. For the time-domain simulations therefore, the retardation functions have been modified to achieve results analogous to those obtained with the frequency-domain calculations (see 'Cummins with correction' in Figure 2.6). This has been done by multiplying the retardation functions by coefficients empirically found (e.g. $0.9 \cdot K_{i,j}(\tau)$). Although this may appear as a brutal approach, it allowed to properly perform the time-domain simulations, which ultimately was the scope of using the Cummins Equations.

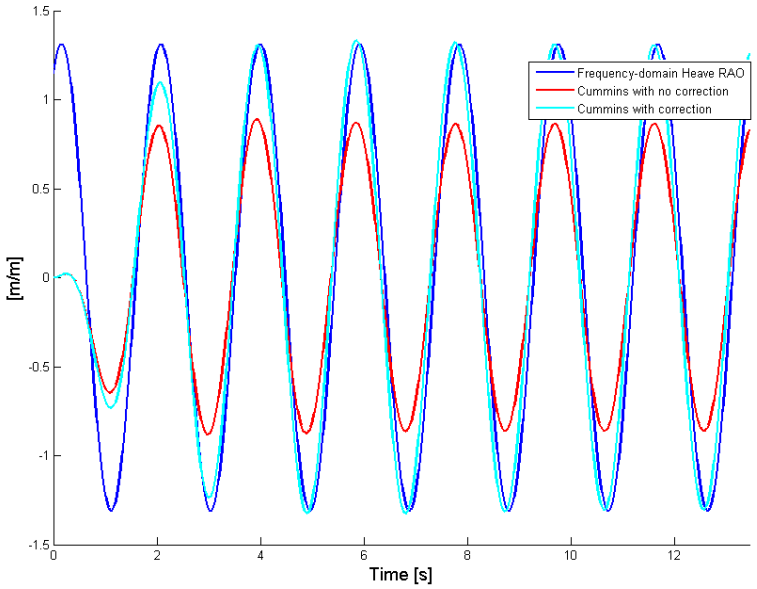

Figure 2.6: Comparison of the heave response calculated using the Cummins Equations and the heave response computed in the frequency domain. Fn=0.35, $\lambda = 1.5 \cdot LWL$

Furthermore, attention should also be paid to the infinite-time integral of the retardation function necessary to calculate the added mass term $A_{i,j}$ (see Eq. (2.8)). After a certain time $\Gamma_{i,j}$, however, the oscillations present in the retardation function become of a negligible magnitude. Thus, according to [26], the infinite-frequency added mass can be numerically computed as:

$$A_{i,j} = a_{i,j}(\Omega) + \frac{1}{\Omega} \cdot \int_0^{\Gamma_{i,j}} K_{i,j}(\tau) \cdot \sin(\Omega\tau) \cdot d\tau \tag{2.12}$$

It should also be mentioned that nowadays the convolution integral present in the Cummins Equations (see Eq. (A.1)) is often approximated using a state-space model in order to save computation time (see for instance [43]). However, being this behind the scope for this thesis, the Cummins Equations have been solved by actually computing the convolution integral.

2.3 Sail aerodynamics

In this section the dynamic effects on the sails caused by the pitch motion of a yacht sailing in waves are discussed. Particular attention is given to the main differences between two methods available to tackle this problem; a quasi-steady method and an unsteady method. Finally, the aerodynamic force and moment used in the equations of motion are presented.

2.3.1 Dynamic wind triangle and effective angle theory

In the dynamic situation of a yacht sailing in waves, the wind triangle is influenced by the yacht's motions. In the present work, though, the wind triangle is assumed to be affected by the pitch motion only. This is because only the equations of heave and pitch are considered during the simulations (see 2.4) and heave can be deemed to have a negligible effect. A dynamic wind triangle in which the apparent wind speed, V_{AW}, and apparent wind angle, β_{AW}, are also function of the time-varying pitch-induced velocity, is then obtained. This results in a new apparent wind speed, V_{ris}, and a new apparent wind angle, β_{din}, which are calculated relative to the (steady) center of effort height of the sails Z_{COE}.

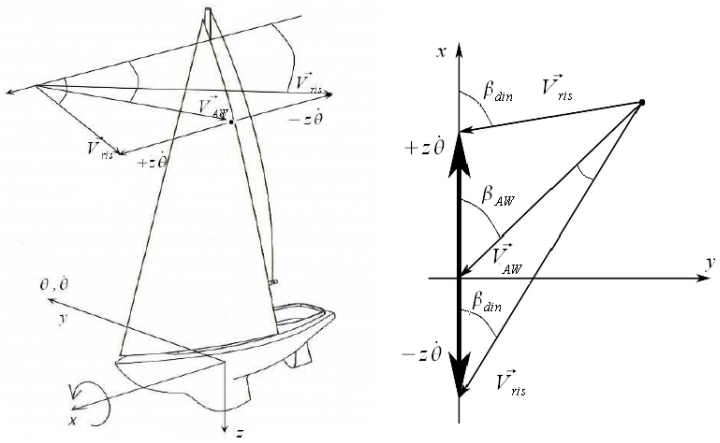

Figure 2.7: Pitch-induced dynamic wind triangle. (Fossati [12])

According to [2], the time-varying resultant apparent wind speed can then be written as:

$$V_{ris}(t) = \sqrt{(V_{TW} \cdot \sin\beta_{TW})^2 + \left(V_{TW} \cdot \cos\beta_{TW} + Vs + Z_{COE} \cdot \dot{\theta}(t)\right)^2} \tag{2.13}$$

and time-varying resultant apparent wind angle as:

$$\beta_{din}(t) = \sin^{-1}\left(\frac{V_{TW} \cdot \sin\beta_{TW}}{V_{ris}(t)}\right) \tag{2.14}$$

Another effect caused by the pitch motion which needs to be taken into account is that the onset flow is no longer perpendicular to the leading edge of the sails.

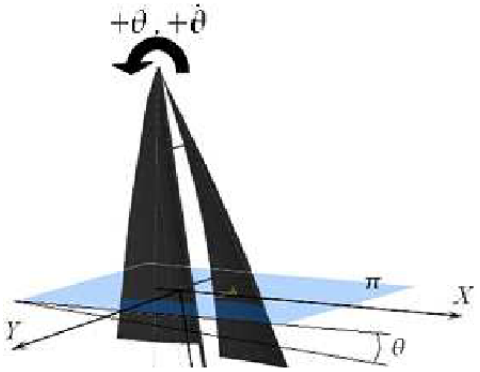

Figure 2.8: Effective angle theory. (Fossati [12])

Using the same concept as presented in the effective angle theory [24], an effective apparent wind angle can be calculated on the π-plane perpendicular to the leading edge of the sails. This is done according to the following formulation:

$$\beta_{eff}(t) = \tan^{-1}\left(\frac{\tan\beta_{din}(t)}{\cos\theta(t)}\right) \tag{2.15}$$

It should be noted that the pitch-induced dynamic effects presented here above are independent from the method adopted to calculate the aerodynamic force. In fact, the only difference between a quasi-steady and an unsteady method is the way the driving force coefficient Cx is calculated.

2.3.2 Quasi-steady and unsteady driving force coefficient

In a quasi-steady approach the driving force coefficient Cx is assumed to be only function of the instantaneous apparent wind angle β_{din}. Indeed, Cx is calculated in a static manner for different apparent wind angles, completely neglecting any dynamic effect. Given a certain value of β_{din}, the corresponding value of Cx is found regardless of whether the pitch angle is increased or decreased.

The unsteady method employed in the present work, on the other hand, it is able to consider all the main dynamic and viscous effects related to the problem of a yacht pitching in waves. This consists in the rheological model proposed by Fossati [12] and it is based on dedicated dynamic wind-tunnel tests. In the past few years in fact, a large number of experiments have been performed at the Politecnico di Milano wind-tunnel. The aim was to investigate the most influencing pitch-induced dynamic effects on the sails of a yacht beating upwind; the reduced velocity V_R and the pitch angle θ[1].

[1] The effect of using rigid instead of soft sails has also been investigated however this is not treated in the present work.

The reduced velocity V_R (or its inverse, the reduced frequency f_R) is a fundamental parameter of unsteady aerodynamics. It indicates the degree of unsteadiness of the system and it is defined as:

$$V_R = \frac{VT}{C} \quad \text{or} \quad f_R = \frac{C}{VT} \tag{2.16}$$

in which, V is the flow velocity, T the period of oscillation and C the chord length of the airfoil. In relation to the unsteady aerodynamics of sails, the reduced velocity can also be expressed as:

$$V_R = \frac{V_{AW} \cdot T_e}{C_{sails}} \tag{2.17}$$

in which the airfoil chord length C_{sails} can be assumed to be the sum of the main sail chord length, C_{main}, and the jib chord length C_{jib}, measured at the center of effort height of the sails Z_{COE}.

Reported in Figure 2.9 are the results of experiments performed in a static, as well as dynamic manner. The most striking difference between the two is the appearance of hysteresis loops which are dependent on the reduced velocity (indicated as $\dot{V}$ in the figure). It should also be noted, that lower the value of the reduced velocity, larger the hysteresis loop area.

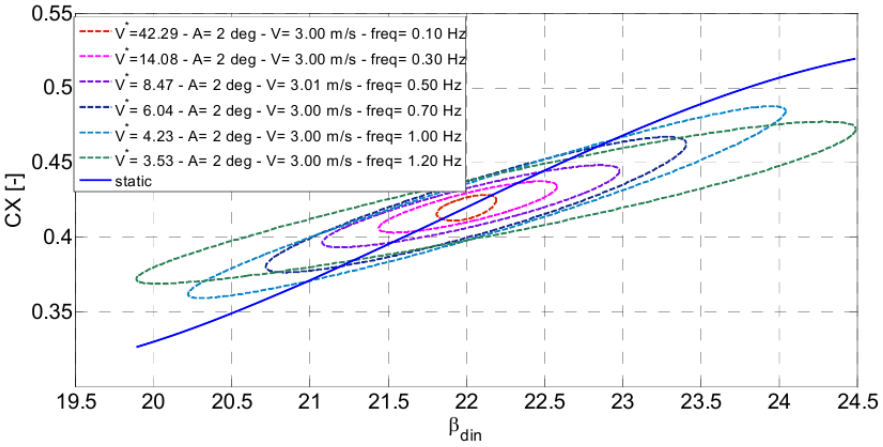

Figure 2.9: Effect of the reduced velocity on the driving force coefficient. (Fossati [15])

The other fundamental parameter is the pitching angle of the yacht. Indeed, as it can be seen in Figure 2.10, by keeping the reduced velocity constant and increasing the pitching angle (defined as A in the figure), the shape of the hysteresis loop deforms into an irregular, non-elliptical shape. This indicates that separation occurs, as in fact it has been observed during the wind-tunnel tests.

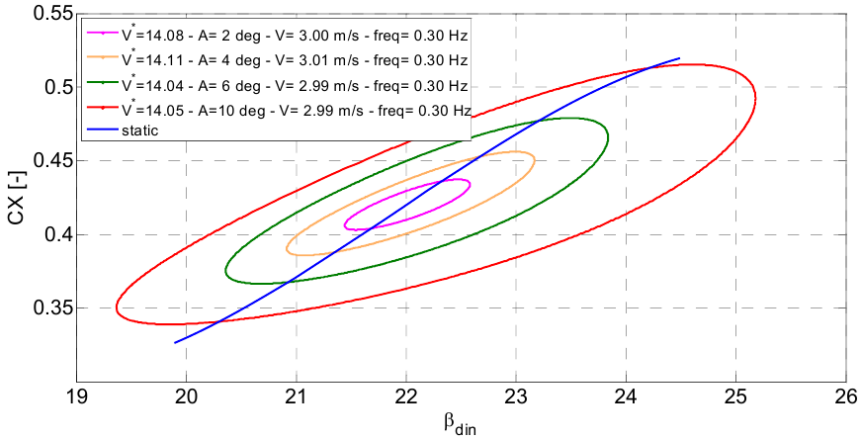

Figure 2.10: Effect of the pitching angle on the driving force coefficient. (Fossati [15])

In the second part of the research carried out at Politecnico di Milano, a rheological model based on the large amount of data acquired during the wind-tunnel tests was developed. The scope of this tool was to predict the unsteady effects caused by the pitch motion on the driving force coefficient Cx.

Rheological models are mechanical systems which comprise several different basic components such as springs, dampers, bump stops, etc.. These are interconnected in order to properly describe the behavior of non-linear and non-conservative systems. The rheological model presented by Fossati [12] consists in a linear spring, k, connected with one extremity to a linear damper, r. The input of such a model are the instantaneous apparent wind angle β_{din}, and its time derivative $\dot{\beta}_{din}$, (see Figure 2.11).

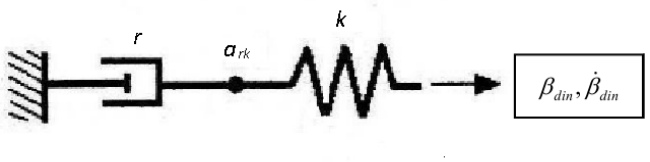

Figure 2.11: Representation of the rheological model. (Fossati [12])

The dynamic behavior of this rheological model can be described with the following equations:

$$\begin{cases} C_x = k\,(\beta - \alpha_{rk}) \\ r\dot{\alpha}_{rk} = k\,(\beta - \alpha_{rk}) \end{cases} \tag{2.18}$$

In this formulation, the driving force coefficient Cx is assumed to be the force transmitted to the ground (see Figure 2.11). This depends on the instantaneous apparent wind angle β_{din}, its time derivative $\dot{\beta}_{din}$ and the displacement of the spring-damper connecting point α_{rk}, which can be calculated according to the following time-incremental relationship:

$$\alpha_{rk}(t+\Delta t) = \alpha_{rk}(t) + \frac{\Delta t}{r} \cdot k \cdot (\beta_{din}(t) - \alpha_{rk}(t)) \tag{2.19}$$

In Eq. (2.19), the parameters r and k, are the damping and stiffness parameters which need to be tuned on the basis of the results of the wind-tunnel experiments.

The parameters r-damping and k-stiffness used in the present rheological model refer to 3 different steady apparent wind angles, namely 22°, 27° and 32°, and to values of the reduced velocity included in the range $3.5 < V_R < 14$ (see Figure 2.12).

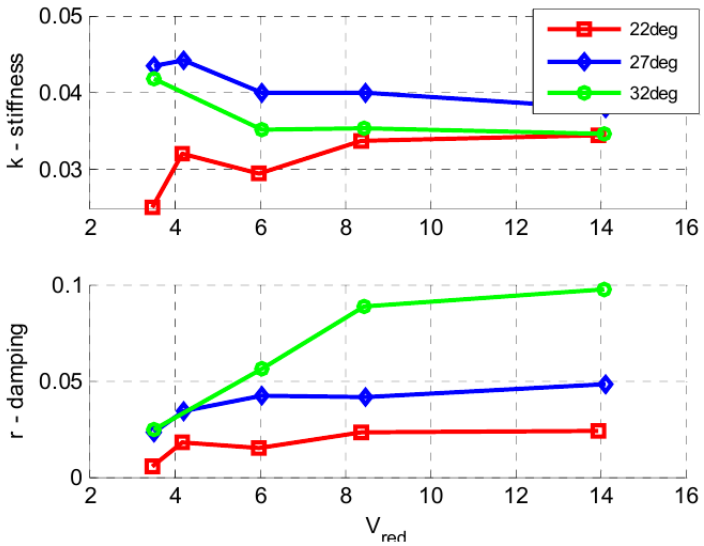

Figure 2.12: Values of the damping and stiffness parameters. (Fossati [12])

2.3.3 Sail aerodynamic force and moment

Once the instantaneous apparent wind speed V_{ris} and the instantaneous driving force coefficient Cx have been calculated, the time-dependent aerodynamic force can be computed according to:

$$F_{aero}(t) = \frac{1}{2} \cdot \rho_{air} \cdot SA \cdot Cx(\beta_{din}) \cdot V_{ris}^2 \tag{2.20}$$

in which SA is the sail area.

The aerodynamic force $F_{aero}(t)$ can then be used to calculate the aerodynamic pitch moment:

$$F_{aero,5}(t) = -F_{aero}(t) \cdot Z_{COE} \tag{2.21}$$

and the heave component of the aerodynamic force:

$$F_{aero,3}(t) = -F_{aero}(t) \cdot \sin(\theta) \tag{2.22}$$

The minus sign in Eq. (2.21) and Eq. (2.22) is due to the reference system adopted (see 2.1.1).

2.4 Solving the equations of motion in the time domain

In the previous sections, all the elements necessary to solve the equations of motion in the time domain have been presented. Time-domain simulations can now be performed to study the influence of the aerodynamic force on the motions of heave and pitch of a yacht sailing upwind in waves. For the time being, the waves are assumed to be regular and to have an angle $\mu = 180°$ with the centerline of the yacht. The appendages are neglected and only the translations along the X and Z-axis (surge and heave) and the rotation about the Y-axis (pitch) are considered. This results in a two-dimensional problem as depicted in Figure 2.13.

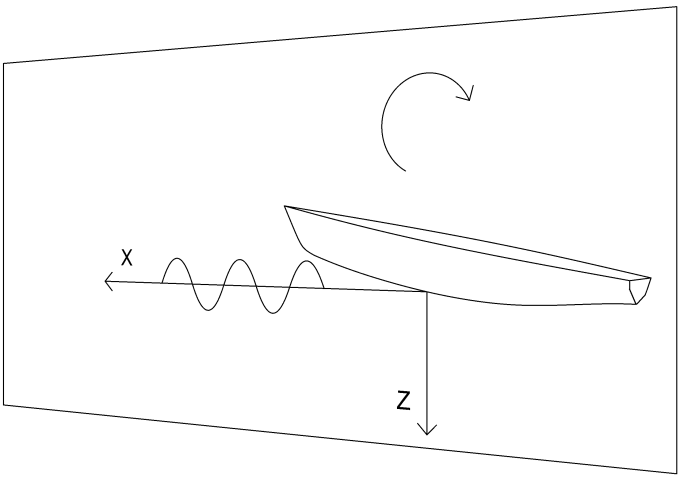

Figure 2.13: Surge, heave and pitch 2-dimensional problem

In principle, for the problem here described, the 3 coupled equations of motion of surge, heave and pitch, should be considered. At the moment, however, a formulation for the surge force is not available. The surge force is the total force experienced by the ship along the X-axis. In the case of a ship sailing in waves, it comprises the calm water resistance plus the additional, oscillating resistance due to the waves.

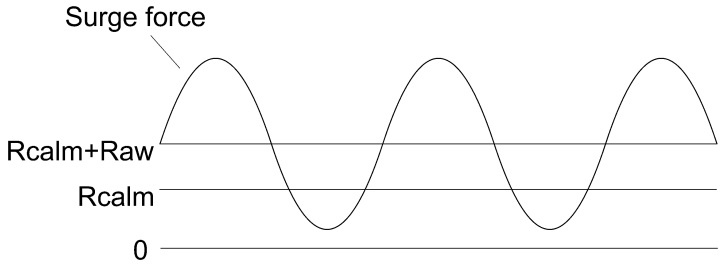

Figure 2.14: Surge force, calm water and mean added resistance Raw

Furthermore, surge is not treated as the other motions by strip theory programs (i.e. PDSTRIP assumes a constant, frequency-independent surge added mass and a zero surge damping), thus the Cummins Equations could not be used in this situation. For these reasons, only the equations of heave and pitch have been solved assuming a constant forward speed.

Recalling the equations of motions presented in Eq. A.1, the heave and pitch accelerations can be computed according to:

$$\ddot{x}_3(t) = [F_{wave,3}(t) + F_{areo,3}(t) - b_{3,3}(\omega_\infty)\cdot\dot{x}_3(t) - b_{3,5}(\omega_\infty)\cdot\dot{\theta}(t) - \int_0^\infty K_{3,3}(t)\cdot\dot{x}_3(t-\tau)\cdot d\tau - \int_0^\infty K_{3,5}(t)\cdot\dot{\theta}(t-\tau)\cdot d\tau + C_{3,3}\cdot x_3(t) + C_{3,5}\cdot\theta(t) - (M_{3,5}+A_{3,5})\cdot\ddot{\theta}(t)]/(M_{3,3}+A_{3,3}) \quad (2.23)$$

$$\ddot{\theta}(t) = [F_{wave,5}(t) + F_{areo,5}(t) - b_{5,5}(\omega_\infty)\cdot\dot{\theta}(t) - b_{5,3}(\omega_\infty)\cdot\dot{x}_3(t) - \int_0^\infty K_{5,5}(t)\cdot\dot{\theta}(t-\tau)\cdot d\tau - \int_0^\infty K_{5,3}(t)\cdot\dot{x}_3(t-\tau)\cdot d\tau + C_{5,5}\cdot\theta(t) + C_{5,3}\cdot x_3(t) - (M_{5,3}+A_{5,3})\cdot\ddot{x}_3(t)]/(M_{5,5}+A_{5,5}) \quad (2.24)$$

in which, $F_{wave,3}$ and $F_{wave,5}$ are the wave-induced heave force and pitch moment defined as:

$$F_{wave,3} = |F_{FK,3}|\cdot\cos(\omega_e t + \epsilon_{FK,3}) + |F_{diff,3}|\cdot\cos(\omega_e t + \epsilon_{diff,3}) \quad (2.25)$$

$$F_{wave,5} = |F_{FK,5}|\cdot\cos(\omega_e t + \epsilon_{FK,5}) + |F_{diff,5}|\cdot\cos(\omega_e t + \epsilon_{diff,5}) \quad (2.26)$$

$F_{FK,3}$, $F_{FK,5}$, $F_{diff,3}$ and $F_{diff,5}$ are respectively the linear Froude-Krilov and diffraction heave force and pitch moment calculated in the frequency domain.

Finally, Eq. (2.23) and Eq. (2.24) are solved numerically in the time-domain using the Newmark integration scheme to compute the heave and pitch velocities, $\dot{x}_3$ and $\dot{\theta}$, and displacements, x_3 and θ.

Chapter 3

Towing-Tank Experiments

For the present research, a large number of experiments were carried out in the towing tank Nr. 1 of the Delft Ship Hydromechanics Laboratory.
The tank has a length of 142 m, a width of 4.22 m and a maximum depth of 2.5 m. An image of the tank is given in Figure 3.1.

Figure 3.1: Towing tank Nr. 1 of the Delft Ship Hydromechanics Laboratory

The towing-tank has an electric-motor driven carriage which is able to reach a maximum speed of 8 m/s and a hydraulic wave maker which is capable of generating regular as well as irregular waves of different lengths and amplitudes.

3.1 Aim of the experiments

The towing-tank tests were carried out with the aim of investigating the following issues:

- Influence of surge on the motions of heave and pitch, and on the mean added resistance in waves
- Influence of the heeling angle on the motions of heave and pitch, and on the mean added resistance in waves
- Relationship between the surge force and the wave amplitude causing that force

Depending on the type of investigation, different setups were used. These are discussed in Section 3.3.

3.2 Models

The experiments were performed on two models of series 4 of the DSYHS, namely model # 43 and model # 45. The parent hull of series 4 is model # 44. This was designed in the early nineties by Jim Teeters of the design office Sparkman & Stephens and it resembles the typical lines of an IMS yacht.

Models # 43 and model # 45 are made of fiberglass and were constructed in 1995. The hydrostatic data and coefficients of the models are reported in Table 3.1 and in Table 3.2.

Model	LWL	BWL	Tc	Disp.	Aw	Ax	Sc
	[m]	[m]	[m]	[kg]	$[m^2]$	$[m^2]$	$[m^2]$
# 43	1.71	0.614	0.097	40.53	0.705	0.042	0.774
# 45	1.71	0.409	0.146	40.53	0.467	0.042	0.642

Table 3.1: Model # 43 and # 45 hydrostatic data

Model	$\frac{LCB_{fpp}}{LWL}$	Cp	$\frac{\nabla c^{1/3}}{AW}$	$\frac{BWL}{LWL}$	$\frac{LCB_{fpp}}{LCF_{fpp}}$	$\frac{\nabla c^{1/3}}{LWL}$	Cm	$\frac{BWL}{Tc}$
	[-]	[-]	[-]	[-]	[-]	[-]	[-]	[-]
# 43	0.533	0.553	0.167	0.359	0.943	0.20	0.712	6.29
# 45	0.533	0.554	0.252	0.24	0.947	0.20	0.711	2.79

Table 3.2: Model # 43 and # 45 hydrostatic coefficients

The main differences between the two models are due to the beam and draft variation. This can be seen, for instance, looking at the beam over length ratio $\frac{BWL}{LWL}$ as well as at the beam over draft ratio $\frac{BWL}{Tc}$. These two parameters have a strong influence on the heave and pitch damping, and this is one of the reason why these two models were chosen. The other reason is that, in the past (see [35]), similar experiments have been performed on the same models. The results of those experiments can then be compared with the findings of the tests carried out during this thesis.

Here below are shown the cross sections of the models.

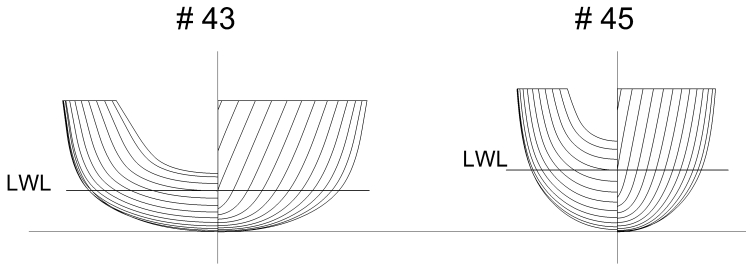

Figure 3.2: Cross sections of models # 43 and # 45

3.3 Setup and measurement techniques

Three different setups were employed during the experiments:

- Model upright, free to heave and pitch and restrained in all the other motions
- Model upright, free to surge, heave and pitch and restrained in all the other motions
- Model heeled by 20°, free to heave and pitch and restrained in all the other motions

Experiments in which the model was 20° heeled and free to surge, heave and pitch were not performed due to technical problems related to the large side force generated by the asymmetric shape of the heeled hull. For each setup the motions of heave and pitch, and the surge force (which was then used to calculate the mean added resistance) were measured. It should be noted that the models were tested without appendages and with no drift angle.

In each of the 3 setups, and for both of the models, the center of gravity (COG) was assumed to have the same x coordinate of the center of buoyancy ($x = LCB$), to be at the center line of the model ($y = 0$), and to have a z coordinate $z = 0.03$ [m], with respect to the water line. The COG was located 3 cm above the water line in order to resemble the experiments which were carried out in 1995. In those experiments in fact, due to some difficulties to fit the hinge at the water level, this was the adopted vertical position of the COG.
The hinge, together with the transducer to measure the surge force, was located at the

COG. The motions were measured using a system of 3 cameras mounted on the carriage and a square plate with 4 leds fixed on the aft of the models (see Figure 3.3).

In order to prevent the model from swaying and yawing, a vertical plate was mounted on the aft of the models. Such a construction was particularly important for the tests in which the model was heeled. In fact, during these tests, additional clamps were used to stiffen the installation (see Figure 3.3).

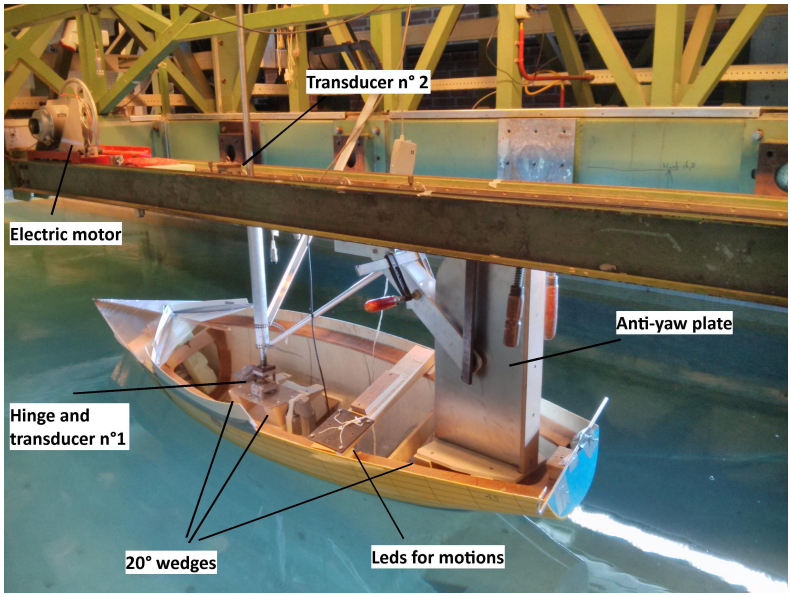

Figure 3.3: Arrangement used in the setups. Side view

As turbulence stimulator, three carborundum grain stripes with a width of 4 cm were placed at ordinate six, eight and ten.

In the free-to-surge tests, a constant-tension electric motor was used to deliver a constant towing-force to the model. The towing force, given as input to the motor, was the sum of the calm water resistance and the mean added resistance, measured during the corresponding experiment in which the model was restrained in surge. Whenever needed, the input towing force could also be manually adjusted during a test. This force was measured on a second transducer (called 'Transducer n° 2' in Figure 3.3) to verify to what extent the force delivered was actually constant. For this type of test, the clamps which were fitted in front and behind the trolleys to prevent the model from surging, were removed to allow the model to freely move along the rails (see Figure 3.4).

The correct displacement was achieved by adding weights in the models. The weights were located in the upright models paying attention to accomplish the desired location of the COG and the desired value of the longitudinal radius of gyration k_{yy}. In this regard, the target value of the radius of gyration, expressed as k_{yy}/LWL, was 0.25 for both models. This value was relative to the upright models without trimming moment. However, it

should be pointed out that such a value was realized for model # 45 only. In fact, due to its shape and its own weight distribution, it was impossible to accomplish the value of $k_{yy}/LWL = 0.25$ for model # 43. The nearest value which was possible to reach was $k_{yy} = 0.28$.

For the heeled tests, the weights were moved to the port side till a heeling angle of 20° had been reached. During this procedure the longitudinal position of the weights was kept constant. Their vertical position inevitably changed, however by a small amount. Furthermore, wedges with an angle of 20° were fitted under the hinge as well as under the 'anti-yaw' vertical plate (see Figure 3.3). Doing so, the heave and pitch motions of the models were measured relative to the tank reference system as it occurred during the upright tests. This means that the radius of gyration k_{yy} calculated for the upright tests was also effective for the heeled tests.

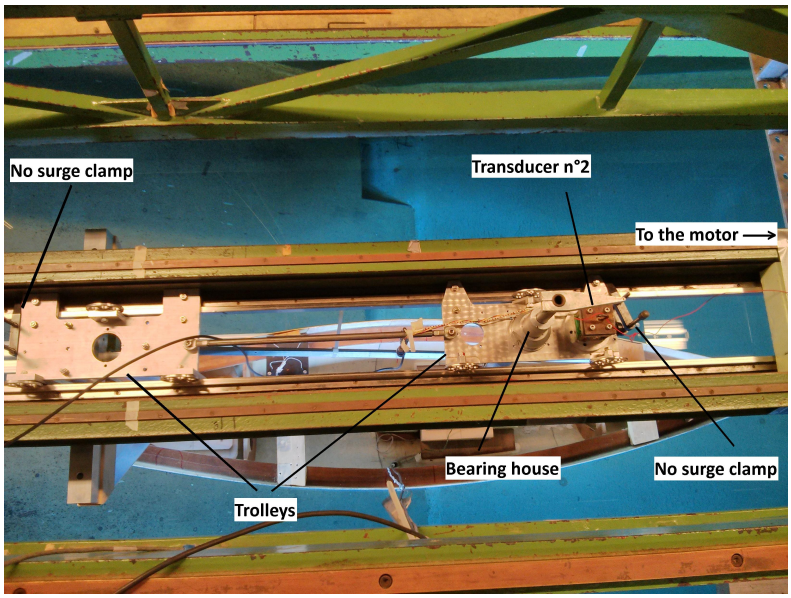

Figure 3.4: Arrangement used in the setups. Top view

The models were tested for two speeds, namely Fn=0.325 and Fn=0.4. For each speed a bow-down trimming moment was given to the models for both the calm water tests and the tests in waves (upright and heeled). The trimming moment was calculated assuming a steady condition in which the calm water resistance of the model was equal to the aerodynamic propulsive force. The weights placed in the model were then be moved according to the following formulation:

$$\Delta x_{weight} = \frac{R_{calm} \cdot Z_{CEO}}{W} \tag{3.1}$$

R_{calm} is the calm water resistance of the model expressed in kilograms, Z_{CEO} is the hypothetical sail center of effort height of the model and W is the weight which needs to

be moved. It is obvious that, by moving a weight, also the position of the COG and the value of k_{yy} changes. However, such a change was inevitable and nevertheless small.

In Table 3.3 are reported the trim angles used for each model, depending on the forward speed.

	Fn=0.325	Fn=0.4
	[deg]	[deg]
Model # 43	0.12	0.55
Model # 45	0.23	1.02

Table 3.3: Trim angles used during the tests

The wave frequency given as input for the wave maker was calculated using the dispersion relation and taking into account the actual depth of the towing tank. A twin-wire wave probe was mounted on the carriage in correspondence to the longitudinal position of the COG of the model. This probe was used only to measure the phase shift of the responses, as the measurements of the wave amplitude were disturbed by the presence of the model and the forward speed. For a more accurate assessment, the amplitudes of the waves were measured for each frequency and each nominal wave amplitude, having the carriage still in the middle of the tank. This was done once after all the experiments were completed.

Two nominal wave amplitudes were tested, namely of $\zeta_a = 25$ [mm] and $\zeta_a = 35$ [mm]. However, depending on the wave frequency, the wave maker delivers waves with slightly different amplitudes. In Table 3.4 the amplitudes of the waves measured by the wave probe are reported. These have been used to calculate the results presented in Chapter 4.

	$\lambda = 2$ [m]	$\lambda = 2.25$ [m]	$\lambda = 2.5$ [m]	$\lambda = 3$ [m]	$\lambda = 3.5$ [m]
	[mm]	[mm]	[mm]	[mm]	[mm]
$\zeta_a = 25$ [mm]	23.5	22.9	23.2	24.0	22.3
$\zeta_a = 35$ [mm]	34.1	33.6	33.8	34.0	31.3

Table 3.4: Amplitudes of the waves measured by the wave probe

3.4 Matrix of experiments

The tests were performed on model # 43 and model # 45 of the DSYHS. Two conditions were considered, namely upright and with a heeling angle $\phi = 20°$. The tests upright were repeated also allowing the model to surge. The Froude numbers tested were Fn=0.325 and Fn=0.4, and two wave amplitudes were used (i.e. $\zeta_a = 25$ [mm] and $\zeta_a = 35$ [mm]).

For all of these conditions, 5 wave lengths were considered: $\lambda = 2$ [m], $\lambda = 2.25$ [m], $\lambda = 2.5$ [m], $\lambda = 3$ [m] and $\lambda = 3.5$ [m]. All these conditions combine in the following matrix of experiments:

	Model	Speed	Wave amplitude	Wave length	
$\phi = 0°$, No surge	2	x 2	x 2	x 5	= 40
$\phi = 0°$, Free to surge	2	x 2	x 2	x 5	= 40
$\phi = 20°$, No Surge	2	x 2	x 2	x 5	= 40
-	-	-	-	N° experiments	= 120

Table 3.5: Matrix of experiments

It should be noted that the number of tests actually performed was much larger (more than 200). The runs which are not reported in Table 3.5 comprise of calm water tests, tests repeated to verify the reliability of certain results and also runs which were disregarded for various reasons. It should also be mentioned that, due to lack of time, only 3 wave lengths (i.e. $\lambda = 2$ [m], $\lambda = 2.5$ [m], and $\lambda = 3.5$ [m]) were tested for the runs made with model # 45 having a heeling angle $\phi = 20°$ and using a wave amplitude $\zeta_a = 35$ [mm].

Chapter 4

Results

In this chapter the results of the research are presented. First, the findings of the towing-tank tests are discussed. These are also compared with similar tests performed on the same models in 1995 (see [35]) to study the influence of the trim angle on the seakeeping of the models. The results of the computations are then provided. The aim is to investigate whether PDSTRIP is capable of predicting the effects caused by the heeling angle on the motions and on the mean added resistance, which were found during the experiments. Lastly, the results of the time-domain simulations are reported to show the influence of the aerodynamic force on the motions of heave and pitch, and the mean added resistance in waves.

4.1 Results of the towing-tank experiments

In Section 4.1.1 and Section 4.1.2 are reported the results relative to the influence of the surge motion and of the heeling angle on the seakeeping of the models. In Section 4.1.3 the surge force is analyzed. It should be noted that values of the heave and pitch amplitudes, used throughout this section, were obtained by filtering the signals with a sine-fit function, having a frequency equal to the frequency of encounter.

4.1.1 Effects of surge on the motions and added resistance

From the findings of the experiments it appears that surge has a small influence on the motions of heave and pitch. Regarding the heave response, the difference measured when the models were restrained in surge, or free to surge, appears to be negligibly small. Generally, the pitch response seems to be reduced by the surge motion. The maximum reduction, of about 5%, was measured for model # 43, relative to Fn=0.4 (see Figure 4.2). As it appears from the reliability study reported in Appendix C, the measurements of the motions have a good degree of precision. The measurement error is, in fact, generally

below 1%. It should be noted that, due to lack of time, the reliability study was performed on model # 43 only. However, the results are assumed to be valid also for model # 45.

All of these considerations hold true for model # 43 and model # 45, relative to the results obtained for both the low speed and high speed tests.

Some results obtained for the wave amplitude $\zeta_a = 25$ [mm] are shown in Figure 4.1 to Figure 4.4. The reader may find the complete results of this investigation in Appendix D.1.

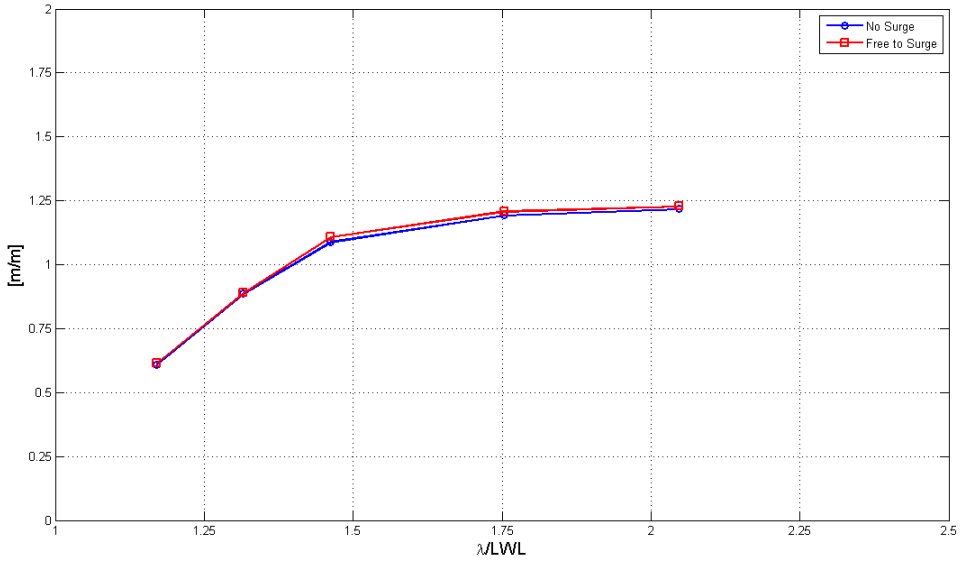

Figure 4.1: Model # 43· Surge vs NO Surge - Heave: Fn=0.325, $\zeta_a = 25$ mm

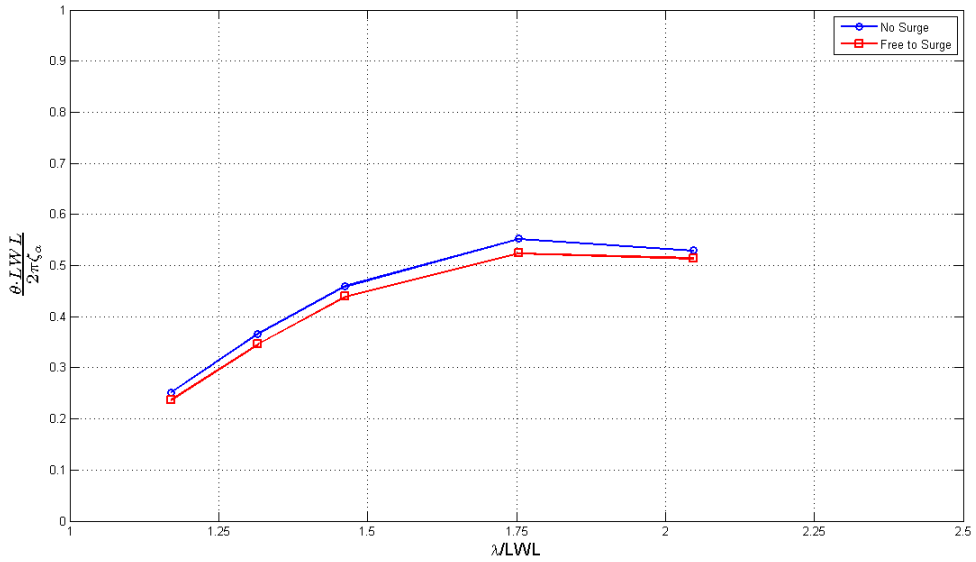

Figure 4.2: Model # 43· Surge vs NO Surge - Pitch: Fn=0.4, $\zeta_a = 25$ mm

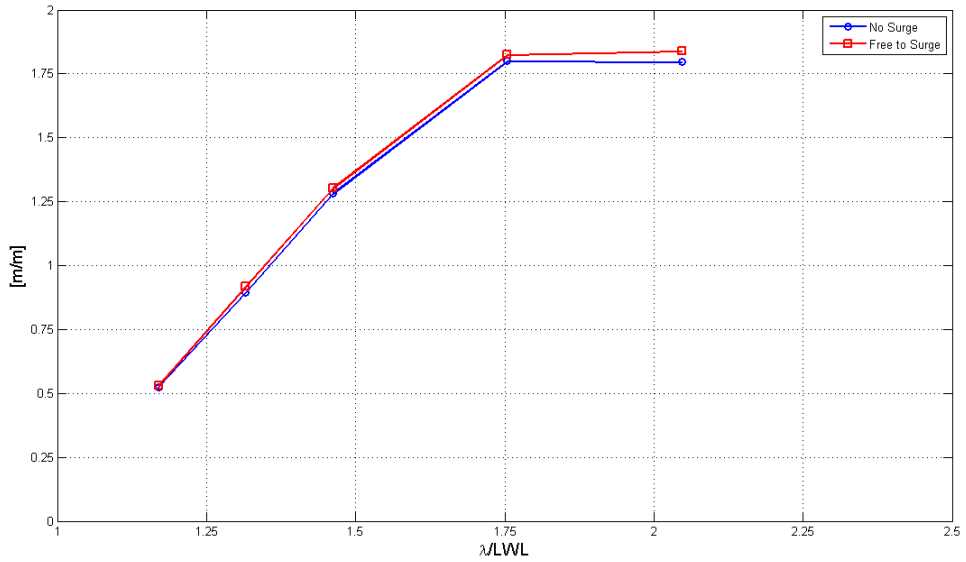

Figure 4.3: Model # 45· Surge vs NO Surge - Heave: Fn=0.4, $\zeta_a = 25$ mm

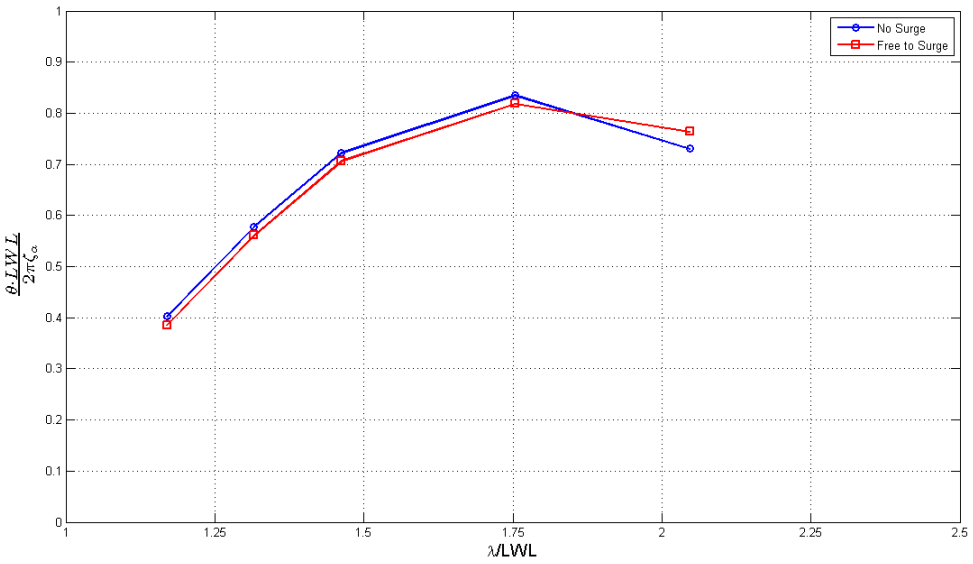

Figure 4.4: Model # 45· Surge vs NO Surge - Pitch: Fn=0.325, $\zeta_a = 25$ mm

The tests were also repeated with a larger wave amplitude, $\zeta_a = 35$ [mm], to investigate whether a larger surge motion would have a more noticeable effect. The results found,

however, are analogous to those obtained for $\zeta_a = 25$ [mm]. See, for example, Figure 4.5 and Figure 4.6.

From a theoretical point of view, these results can be explained by the fact that the motions of surge and heave are uncoupled, while those of surge and pitch are coupled but only to a minor extent.

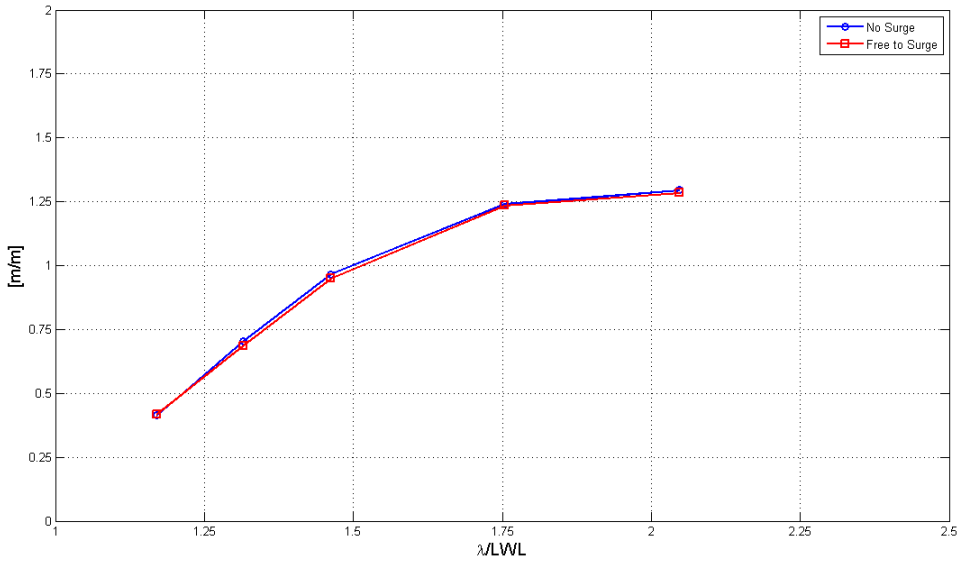

Figure 4.5: Model # 43· Surge vs NO Surge - Heave: Fn=0.4, $\zeta_a = 35$ mm

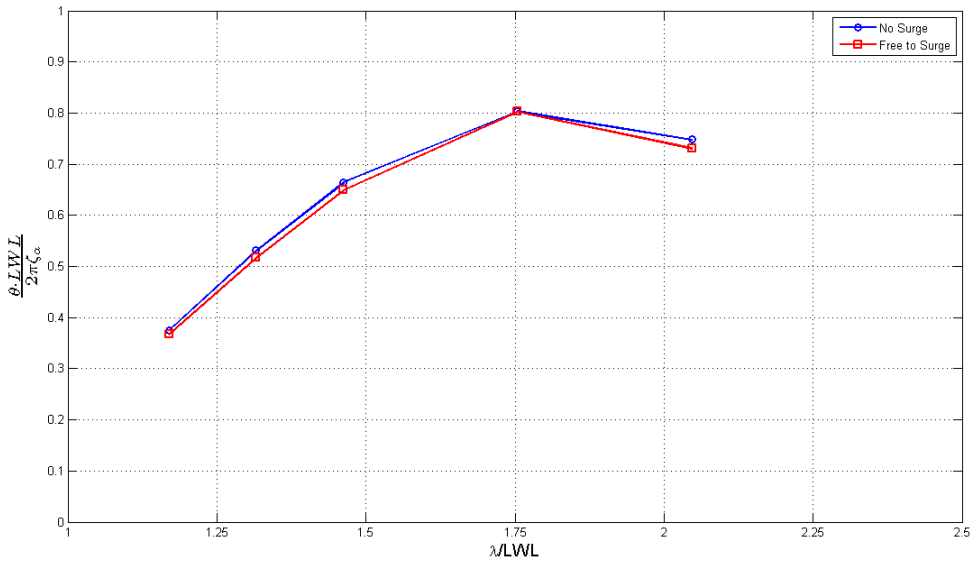

Figure 4.6: Model # 45· Surge vs NO Surge - Pitch: Fn=0.325, $\zeta_a = 35$ mm

In contrast, the results relative to the influence of surge on the mean added resistance, appear to be more heterogeneous.

Let us first consider the results relative to Fn=0.325, for model # 43 and model # 45 alike (see Figure 4.7 and Figure 4.9). Analogously to the motions of heave and pitch, also for the mean added resistance, it seems that the effect of surge is small (if not negligible). This is confirmed by the results obtained for the same speed but using the larger wave amplitude (see Figure 4.8 and Figure 4.10).

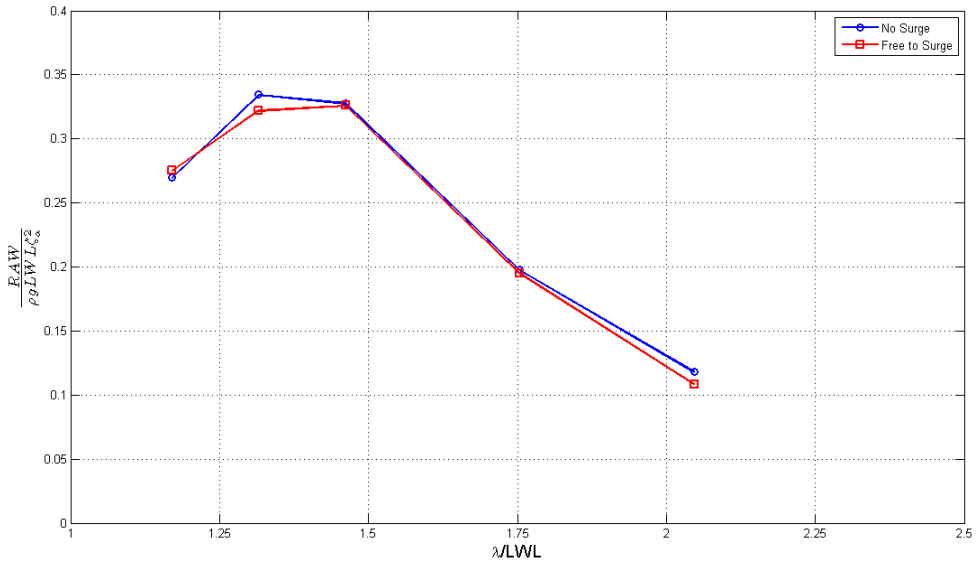

Figure 4.7: Model # 43· Surge vs NO Surge - Added resistance: Fn=0.325, $\zeta_a = 25$ mm

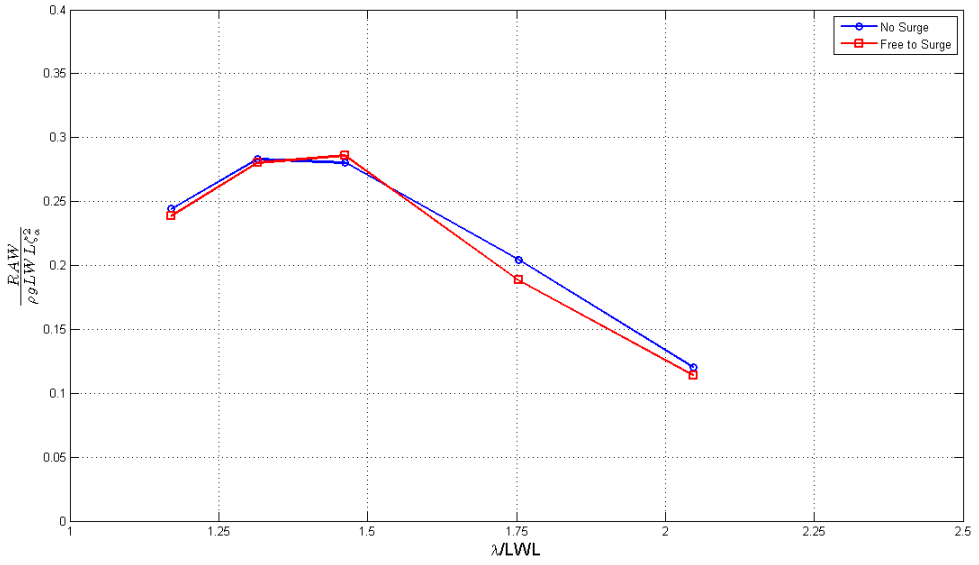

Figure 4.8: Model # 43· Surge vs NO Surge - Added resistance: Fn=0.325, $\zeta_a = 35$ mm

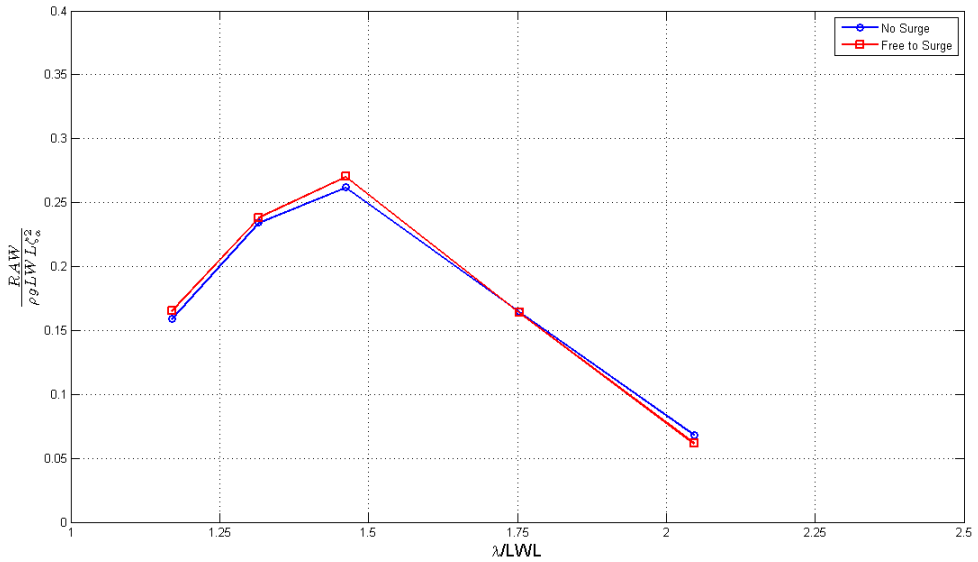

Figure 4.9: Model # 45· Surge vs NO Surge - Added resistance: Fn=0.325, $\zeta_a = 25$ mm

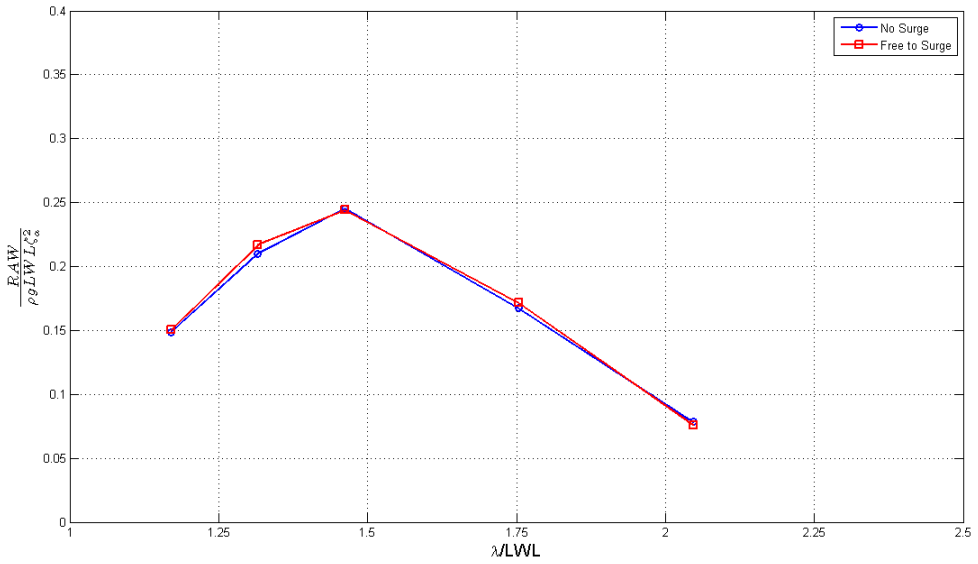

Figure 4.10: Model # 45· Surge vs NO Surge - Added resistance: Fn=0.325, $\zeta_a = 35$ mm

However, when the speed is increased to Fn=0.4 (see Figure 4.11 and Figure 4.13), the difference is generally large. To verify whether a significant trend can be identified, these results should be compared with those obtained for $\zeta_a = 35$ [mm], and reported in Figure

4.12 and Figure 4.14 respectively. As it can be seen, it is not possible to identify a clear trend.

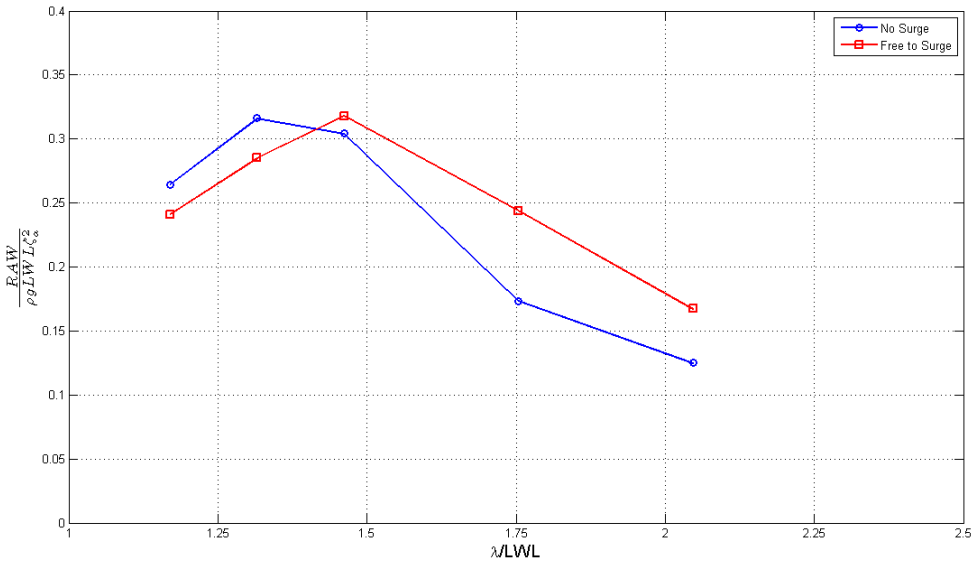

Figure 4.11: Model # 43· Surge vs NO Surge - Added resistance: Fn=0.4, $\zeta_a = 25$ mm

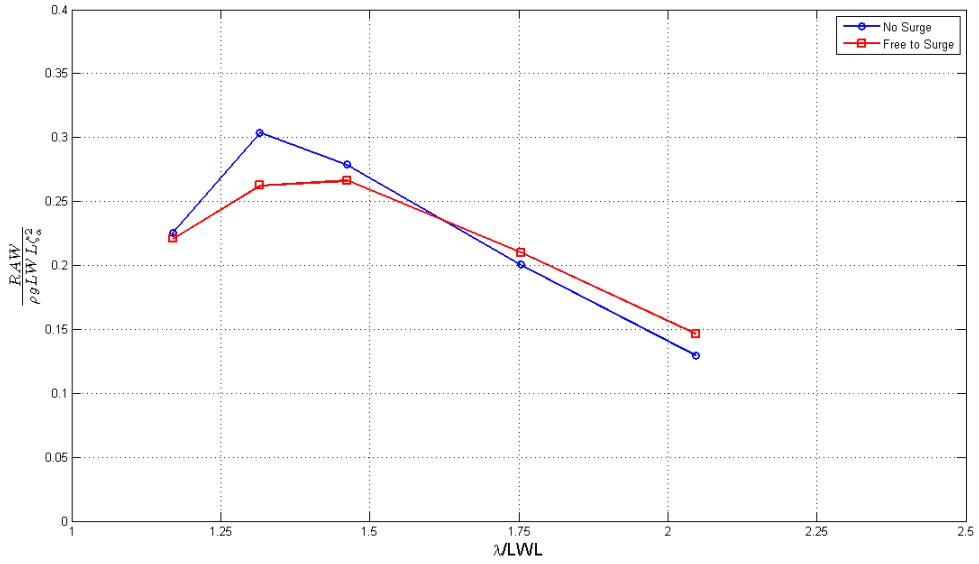

Figure 4.12: Model # 43· Surge vs NO Surge - Added resistance: Fn=0.4, $\zeta_a = 35$ mm

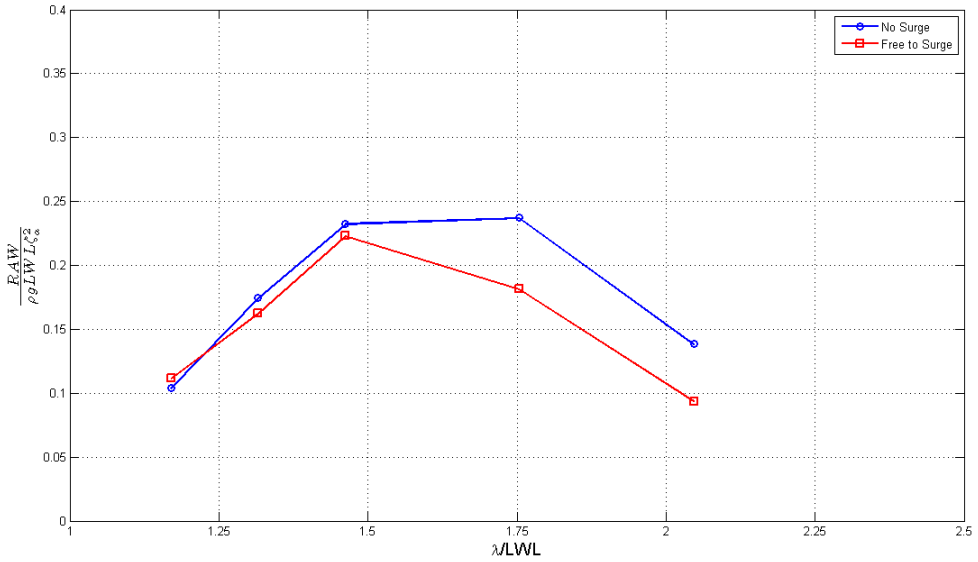

Figure 4.13: Model # 45· Surge vs NO Surge - Added resistance: Fn=0.4, $\zeta_a = 25$ mm

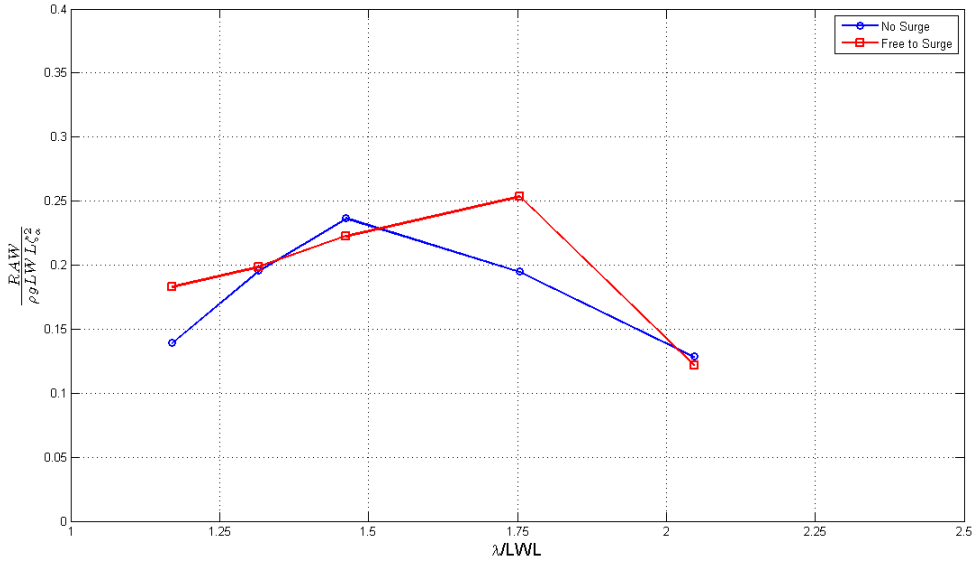

Figure 4.14: Model # 45· Surge vs NO Surge - Added resistance: Fn=0.4, $\zeta_a = 35$ mm

These results were unexpected and appear to be unjustifiable with a theoretical explanation. The reason for such a large difference can be found looking at the repeatability of the measurements (see Appendix C). In fact, the measurement error, relative to the mean added resistance for Fn=0.325, is in the range of 0.5% to 5%. On the other hand, when the forward speed is increased to Fn=0.4, the measurement error is typically 6%, with

a peak up to 20%. The reliability of these measurements should be therefore deemed as poor. As a reference, it should be mentioned that the mean added resistance is on average 60% of the calm water resistance (i.e. $0.15 \cdot R_{calm} < R_{AW} < 1.1 \cdot R_{calm}$).

Although it is not clear why the accuracy of the measurements decreases so drastically when the speed is increased, it is believed that this is due to the large vibrations in the setup caused by the speed Fn=0.4. This problem, indeed, was also detected for the same speed during the tests in which the model was heeled.

4.1.2 Effects of the heeling angle on the motions and added resistance

The results of the towing-tank tests show that, in general, the heeling angle has a considerable influence on the motions of heave and pitch and the mean added resistance alike. It appears, however, that it has a different effect depending on the model considered.

In reference to model # 43, it can be seen that the heeling angle reduces the heave motion by about 5-7%. This is the case when the forward speed is Fn=0.325, for both the small and the large wave amplitudes (see Figure 4.15 and Figure 4.16). Looking at Figure 4.17, it can be noted that for Fn=0.4, the reduction is even more consistent, as, for some wave lengths, it becomes as large as 19%. Analogously to the considerations made in Section 4.1.1, the results of the motions appear to have a good degree of reliability, being the average measurement error about 1.5% (see Appendix C).

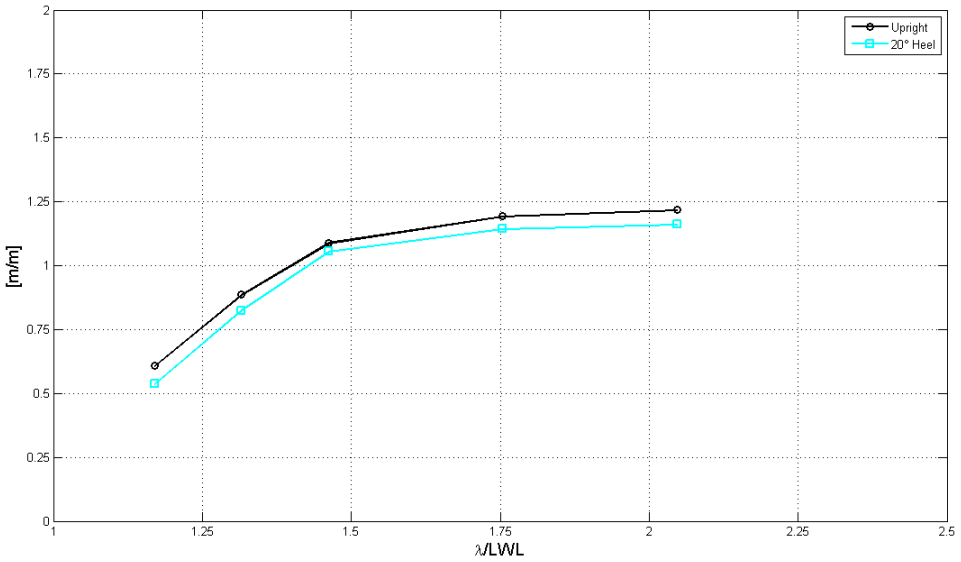

Figure 4.15: Model # 43· Upright vs 20° Heel - Heave: Fn=0.325, $\zeta_a = 25$ mm

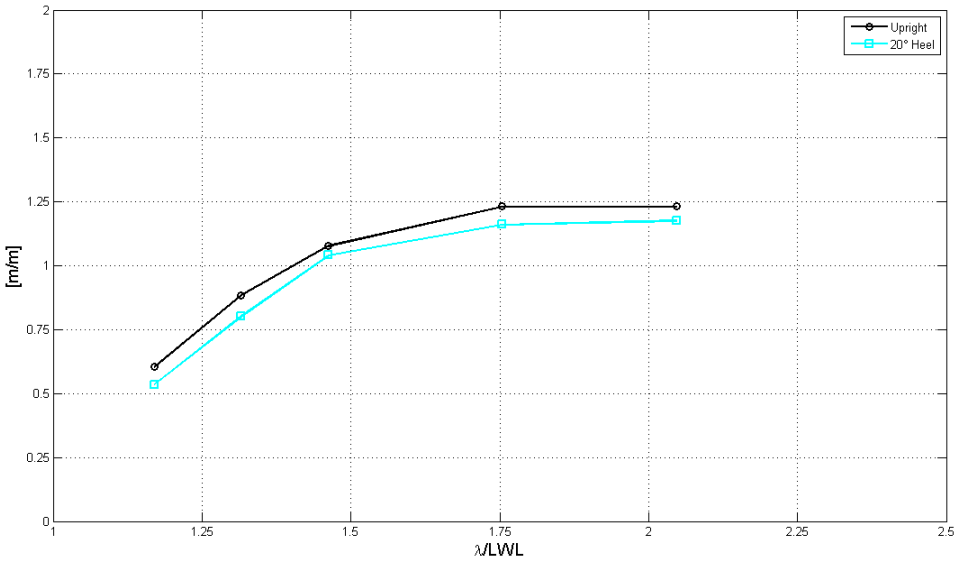

Figure 4.16: Model # 43· Upright vs 20° Heel - Heave: Fn=0.325, $\zeta_a = 35$ mm

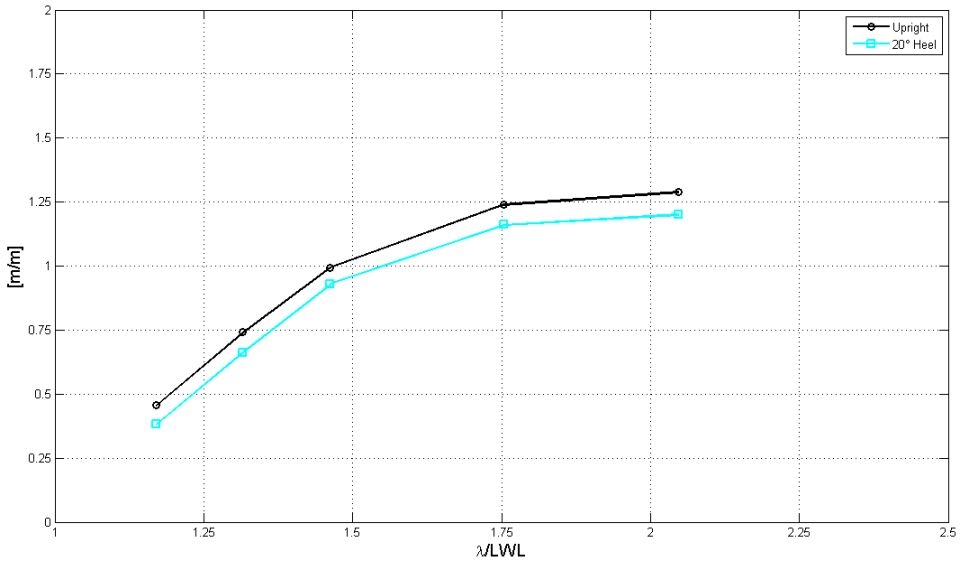

Figure 4.17: Model # 43· Upright vs 20° Heel - Heave: Fn=0.4, $\zeta_a = 25$ mm

On the other hand, it seems that the influence of the heeling angle on the pitch motion has an opposite trend. For Fn=0.325, indeed, pitch is increased by 5-6% (see Figure 4.18). For the higher speed, the increase is slightly lower, typically around 2%, which is nearly as large as the average measurement precision (i.e. 1.5%). This is reported in Figure 4.19.

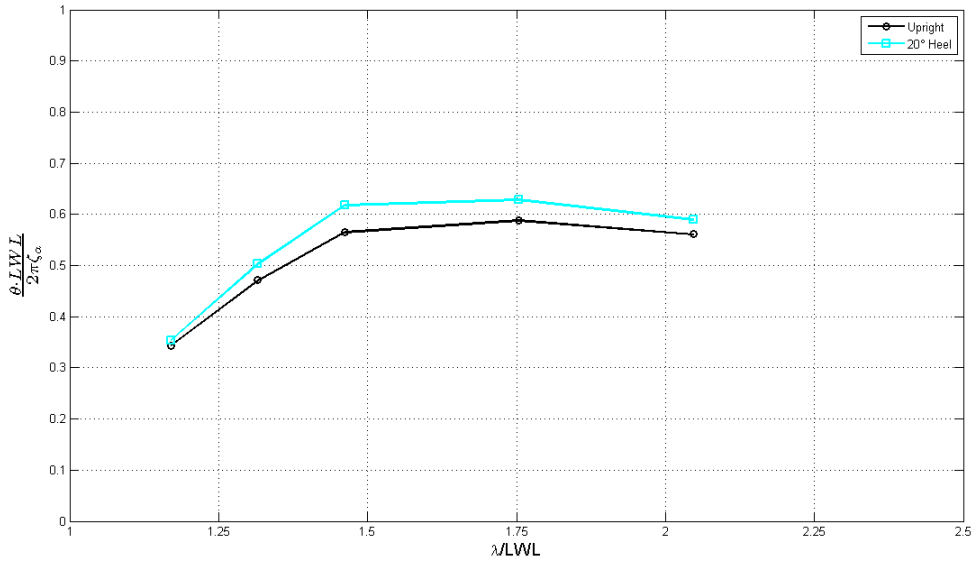

Figure 4.18: Model # 43· Upright vs 20° Heel - Pitch: Fn=0.325, $\zeta_a = 25$ mm

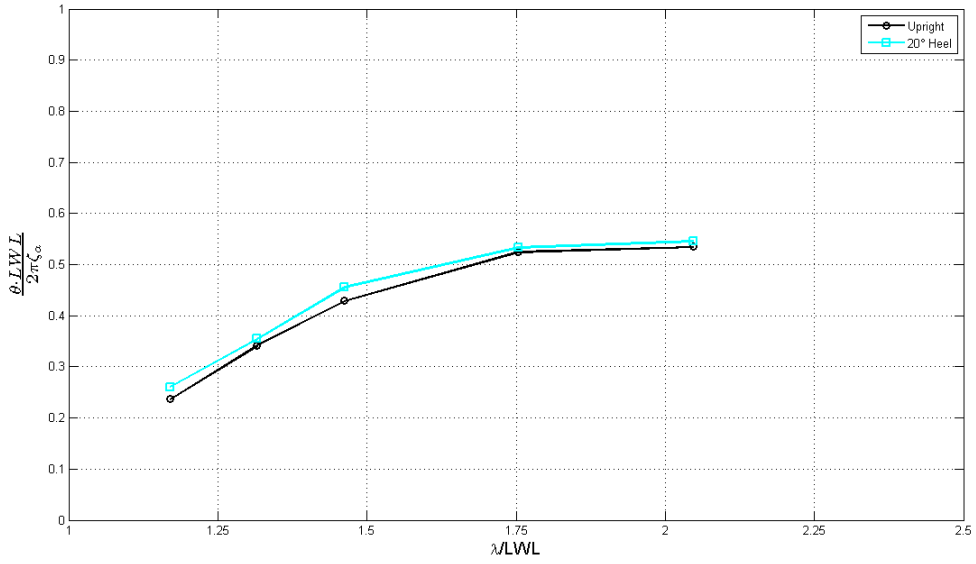

Figure 4.19: Model # 43· Upright vs 20° Heel - Pitch: Fn=0.4, $\zeta_a = 35$ mm

In order to explain these differences, some suggestions may be found by looking at the waterplane areas of the upright and heeled model. Looking at Figure 4.20, it can be seen that when the model is heeled there is a noticeable reduction in the waterplane area at the aft of the model. This may explain the increase of the pitch motion. In contrast, heave is reduced by the heeling angle although the waterplane area of the heeled model

is slightly smaller when compared to the upright model. This is counter intuitive and arguably caused by the prominent flare of the model, which ingresses the water as the model heaves and pitches.

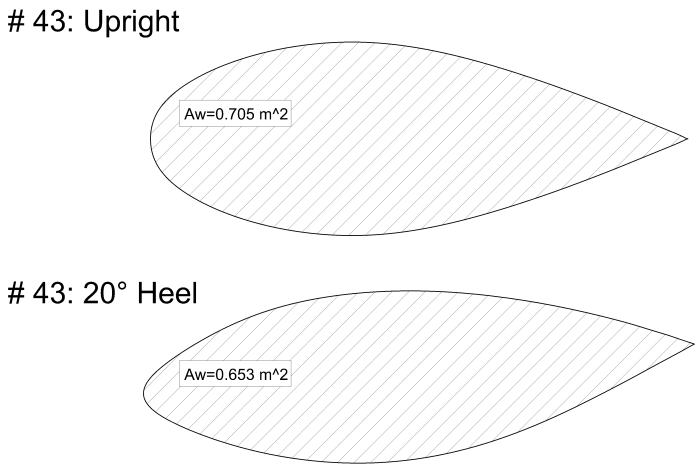

Figure 4.20: Model # 43 · Comparison of the upright and heeled waterplane areas

As a result of this dual effect of the heeling angle on the motions of heave and pitch, the mean added resistance appears to be substantially unchanged. This can be seen in Figure 4.21, relative to Fn=0.325 and to the wave amplitude $\zeta_a = 25$ [mm].

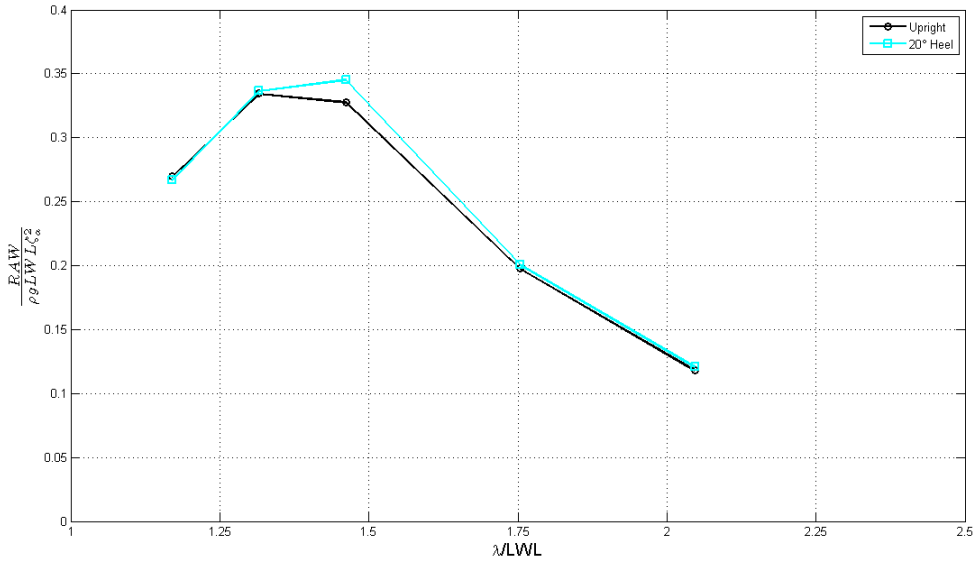

Figure 4.21: Model # 43· Upright vs 20° Heel - Added resistance: Fn=0.325, $\zeta_a = 25$ mm

The results relative to the mean added resistance obtained for Fn=0.325, appear to have a satisfactory degree of repeatability (the largest discrepancy was found at the resonance and it is as large as 8%). In contrast, those regarding the forward speed Fn=0.4 should be considered as unreliable, having in fact an average error of about 15% (refer to Appendix C for more details). For this reason they have not been reported in this section. The complete results of the investigation on the effects of the heeling angle may be found in Appendix D.2.

Let us now focus on model #45.

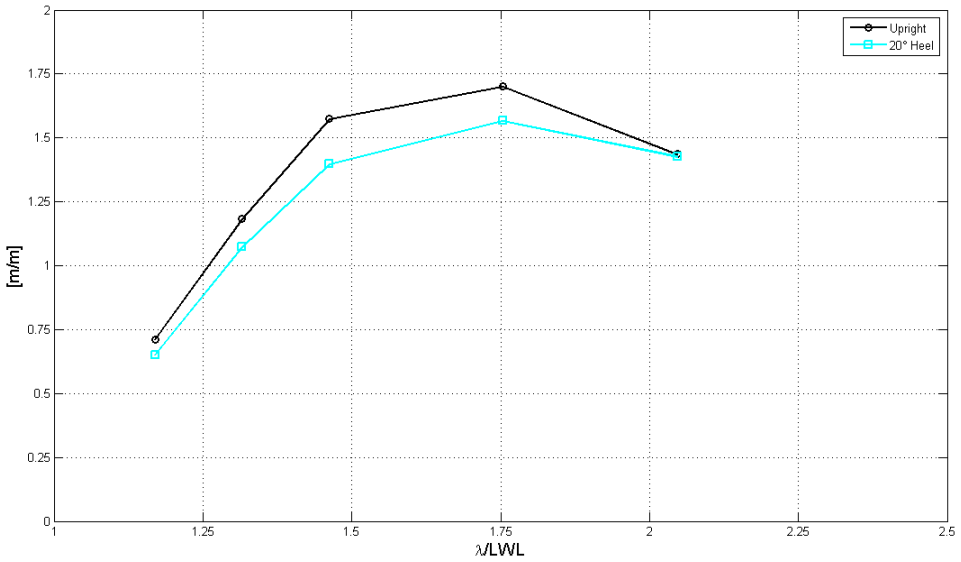

Figure 4.22: Model # 45· Upright vs 20° Heel - Heave: Fn=0.325, $\zeta_a = 25$ mm

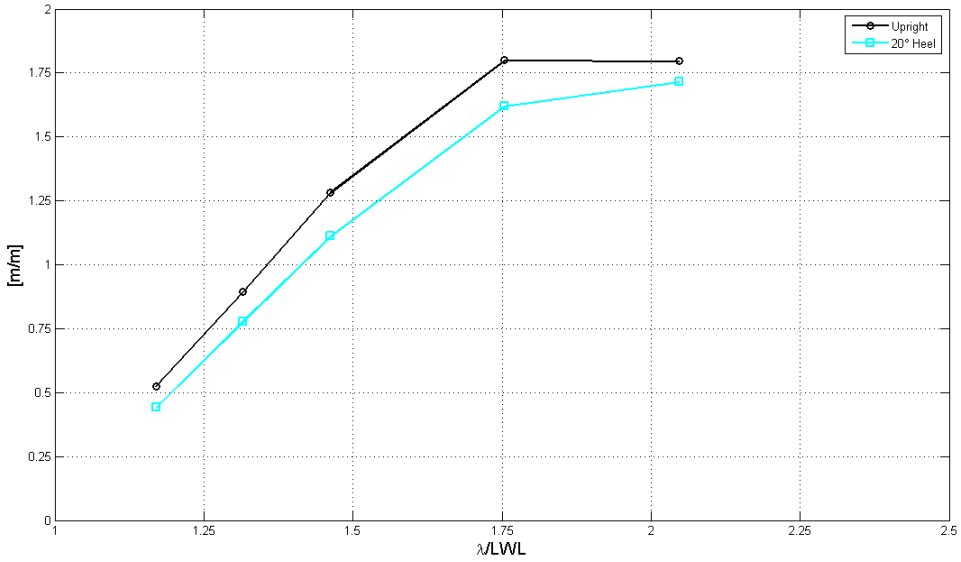

Figure 4.23: Model # 45· Upright vs 20° Heel - Heave: Fn=0.4, $\zeta_a = 25$ mm

As it can be seen in Figure 4.22 and Figure 4.23, the heeling angle has the effect of reducing the heave motion. In fact, heave is typically reduced by about 10% when the speed is equal to Fn=0.325. The reduction becomes even more consistent for Fn=0.4.

Looking at Figure 4.24 and Figure 4.25, it can be noted that also the pitch motion is considerably reduced by the heeling angle. This appears to be so for both of the speeds at which the model was tested during the experiments.

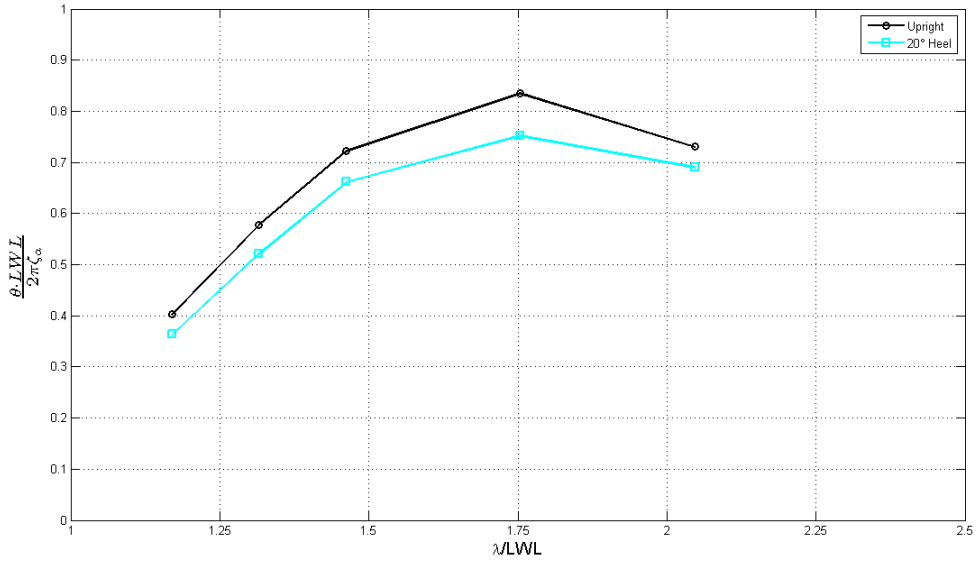

Figure 4.24: Model # 45· Upright vs 20° Heel - Pitch: Fn=0.325, $\zeta_a = 25$ mm

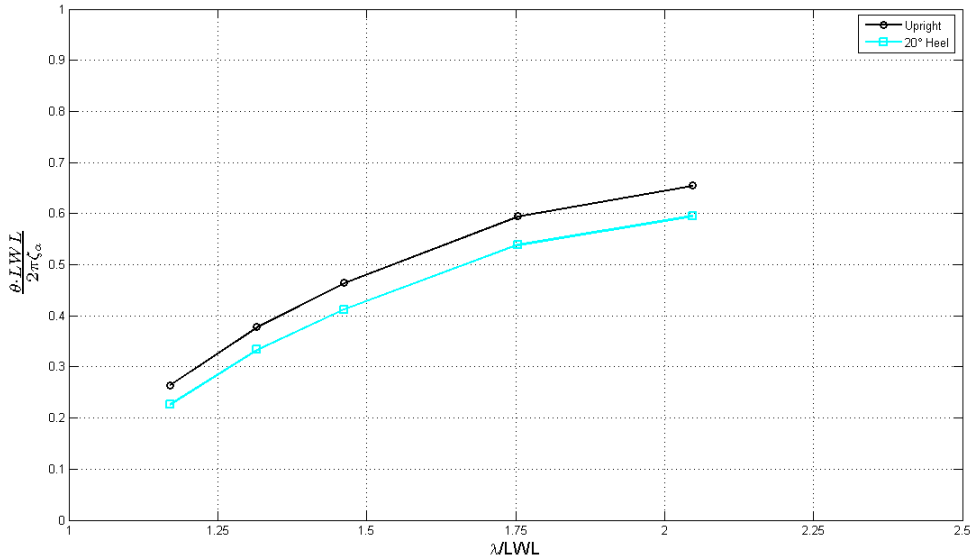

Figure 4.25: Model # 45· Upright vs 20° Heel - Pitch: Fn=0.4, $\zeta_a = 25$ mm

As it can be seen in Figure 4.26, the waterplane area of the model increases of about 5% when under heel. This indicates that the damping of the heeled model is larger than that of the same model in the upright condition. This may explain the reducing effect of the heeling angle on the heave and pitch motions.

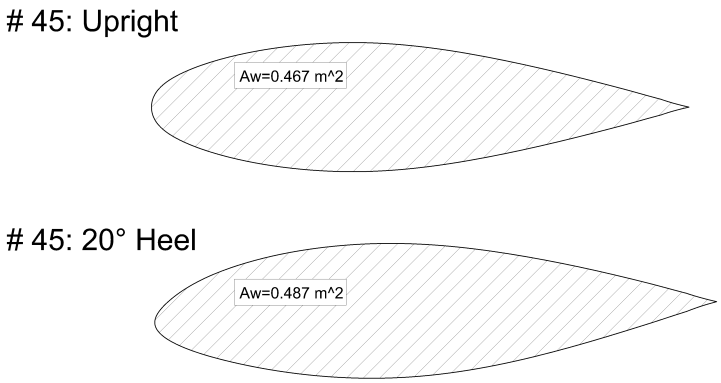

Figure 4.26: Model # 45 · Comparison of the upright and heeled waterplane areas

The effects caused by the increase in damping can also be noted on the mean added resistance. Looking at Figure 4.27, it can be seen that the mean added resistance for the heeled model is indeed generally larger than that measured for the same model upright. It can be argued that the increase in added resistance is due to the larger damping. In fact, although the motions of the heeled model are reduced by the larger heave and pitch damping, this is done at the cost of a larger dissipation of energy.

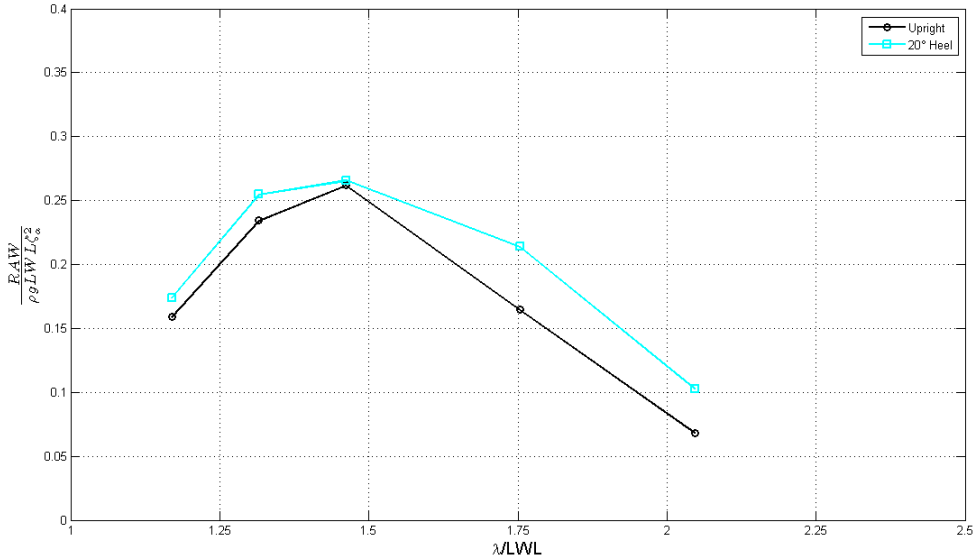

Figure 4.27: Model # 45· Upright vs 20° Heel - Added resistance: Fn=0.325, $\zeta_a = 25$ mm

4.1.3 Analysis of the surge force

When a model is tested in waves, it is a common procedure to discard the time signal of the surge force, instead only its mean is kept in order to calculate the mean added resistance. Information regarding the shape of the signal and its amplitude are lost as generally they are not of interest. However, when the behavior of a ship is going to be studied in the time domain, one would preferably have the time signal of the surge force rather than its mean. For this reason, for each test, the time signal of the force F_x was kept and analyzed.

The force F_x can be defined as the total force acting on the model, parallel to the longitudinal X-axis of the tank. After being measured by the transducer, F_x generally looks like a signal which has a frequency equal to the frequency of encounter of the model, which is disturbed by higher frequency signals caused by any sort of vibration. In this section, the term surge force refers to the filtered F_x signal. Similarly to the motions, it is assumed that the amplitude of the surge force is equal to the amplitude of the sinusoid (of frequency equal to the frequency of encounter) fitted to the signal. An example is reported in Figure 4.28.

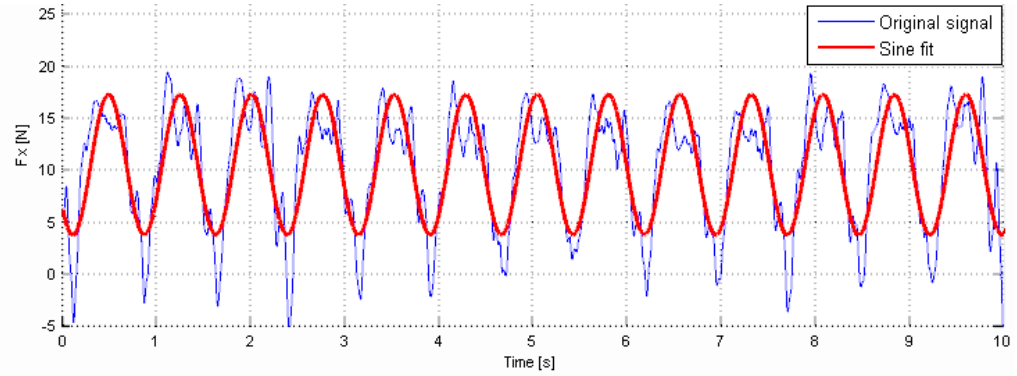

Figure 4.28: Example of sine fit to the F_x original signal

In the present research, the analysis of the surge force mainly focuses on its amplitude. In particular, the relationship between the amplitude of the surge force and the amplitude of the wave causing this force was investigated. The surge force, in fact, is a resistive force and for this reason its behavior may differ from that of the other hydrodynamic forces (heave force, sway force, etc.).

First studied was whether the amplitude of the surge force had a quadratic relation with the wave amplitude, as its mean does. An example of this investigation is shown in Figure 4.29, in which is depicted the surge force divided by the square of the wave amplitudes $\zeta_a = 25$ [mm] and $\zeta_a = 35$ [mm].

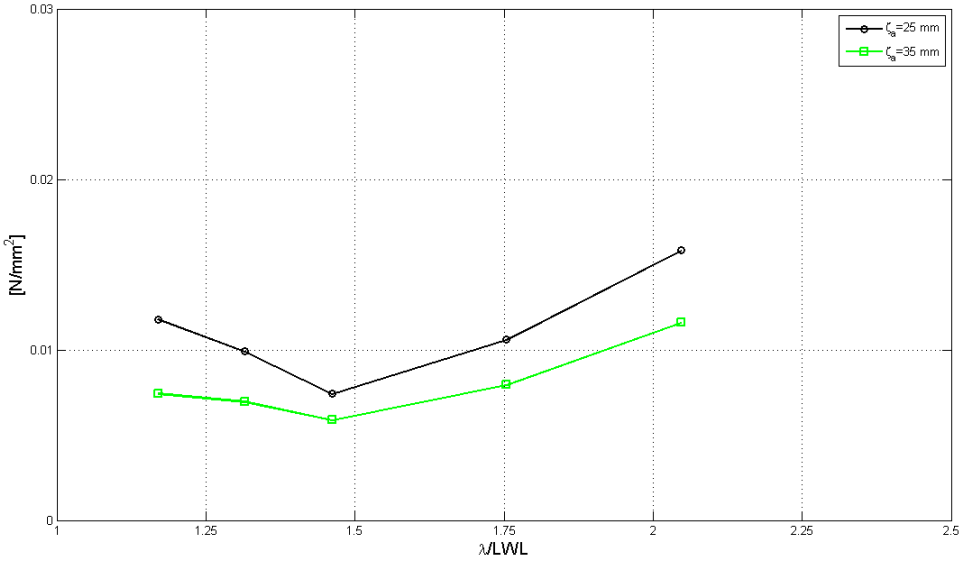

Figure 4.29: Model # 43· $\frac{|\text{Surge Force}|}{\zeta_a^2}$ - Fn=0.325, Upright

Then, the surge force was divided by the wave amplitudes only, to verify whether it could have a linear relation. This was done for both Fn=0.325 and Fn=0.4. (see Figure 4.30 and Figure 4.31).

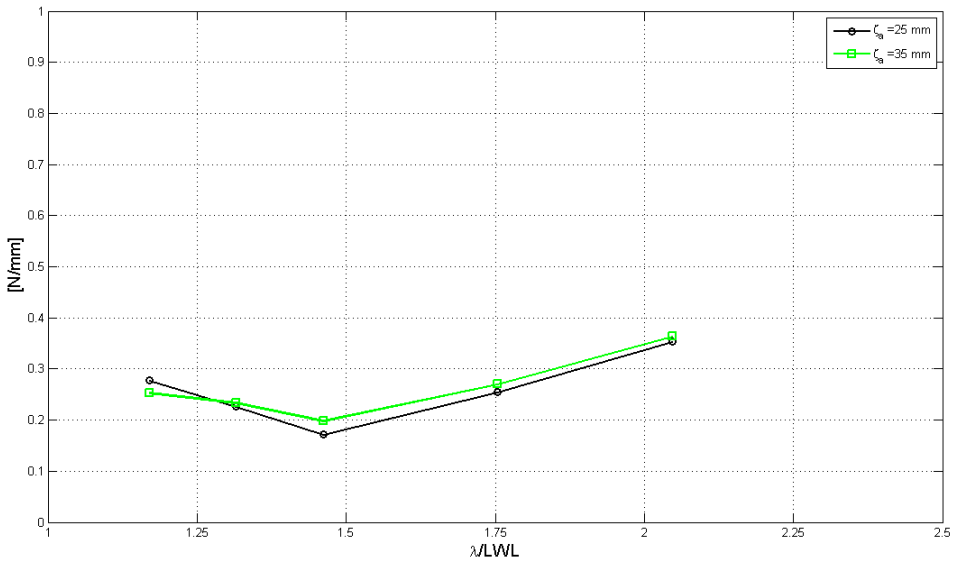

Figure 4.30: Model # 43· $\frac{|\text{Surge Force}|}{\zeta_a}$ - Fn=0.325, Upright

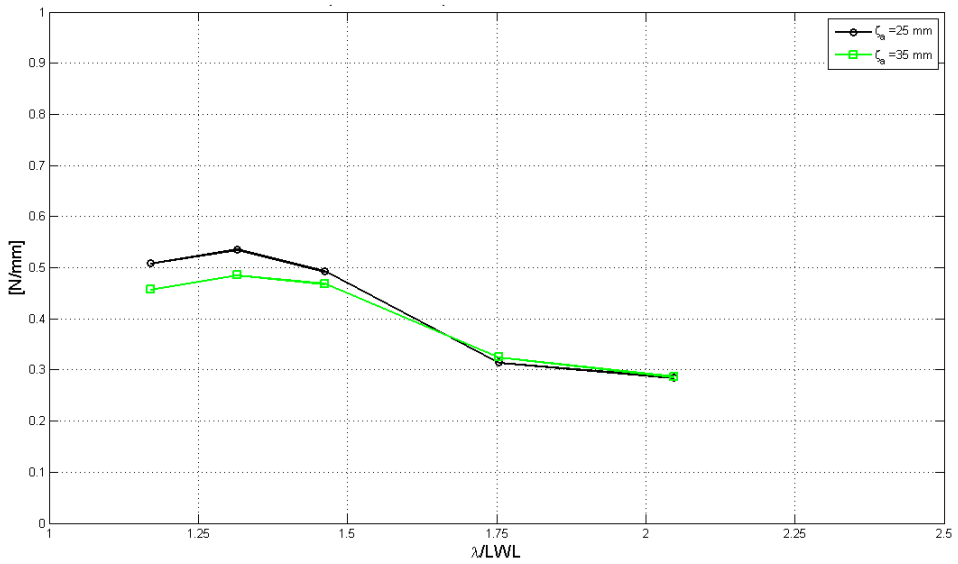

Figure 4.31: Model # 43· $\frac{|\text{Surge Force}|}{\zeta_a}$ - Fn=0.4, Upright

As it can be noted, it appears that the amplitude of the surge force scales linearly with the wave amplitude rather than quadratically. The results relative to model # 45 seem to confirm this trend (see Figure 4.32 and Figure 4.33).

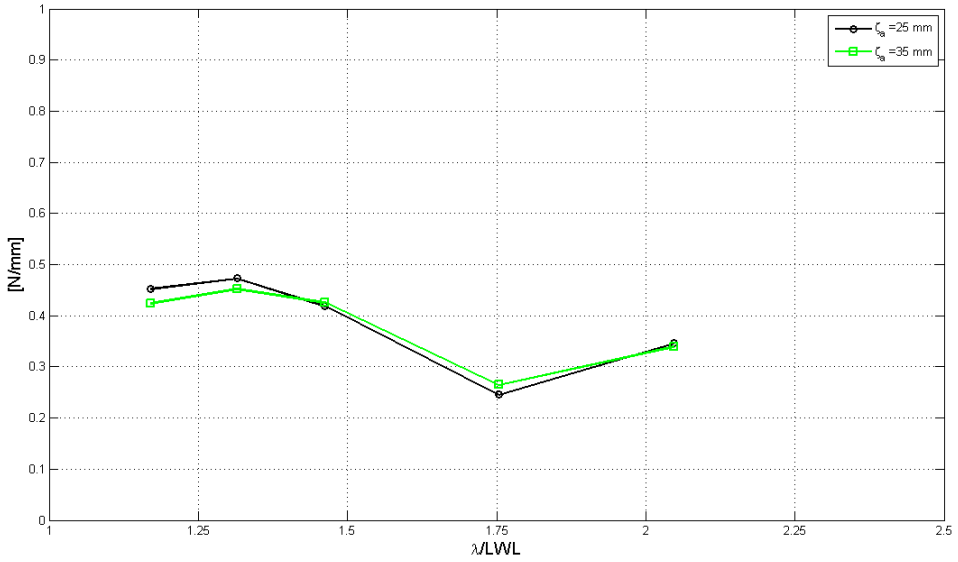

Figure 4.32: Model # 45· $\frac{|\text{Surge Force}|}{\zeta_a}$ - Fn=0.325, Upright

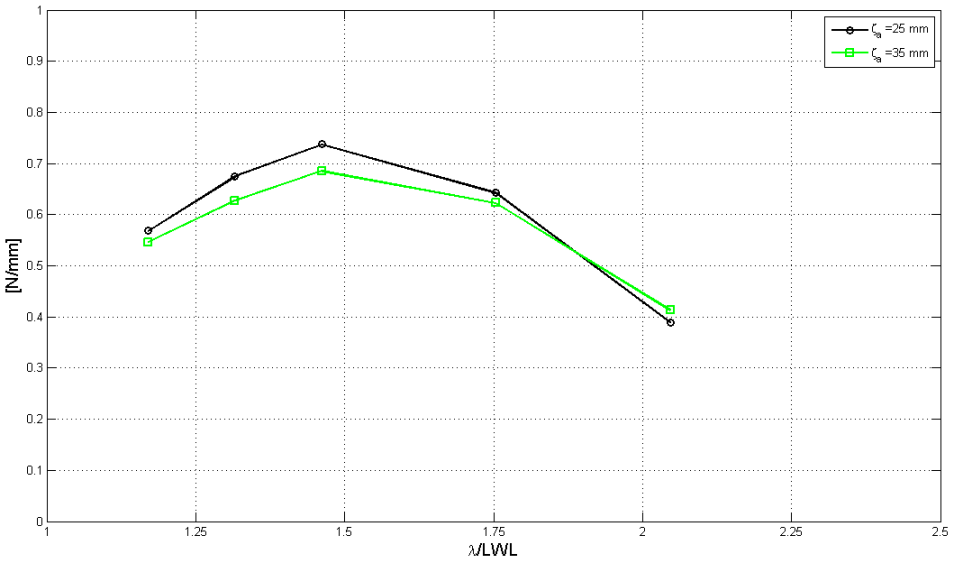

Figure 4.33: Model # 45· $\frac{|\text{Surge Force}|}{\zeta_a}$ - Fn=0.4, Upright

Similar results were also obtained for the heeled tests. An example is shown in Figure 4.34. The complete results relative to the analysis of the linearity of the surge force may be found in Appendix D.3.

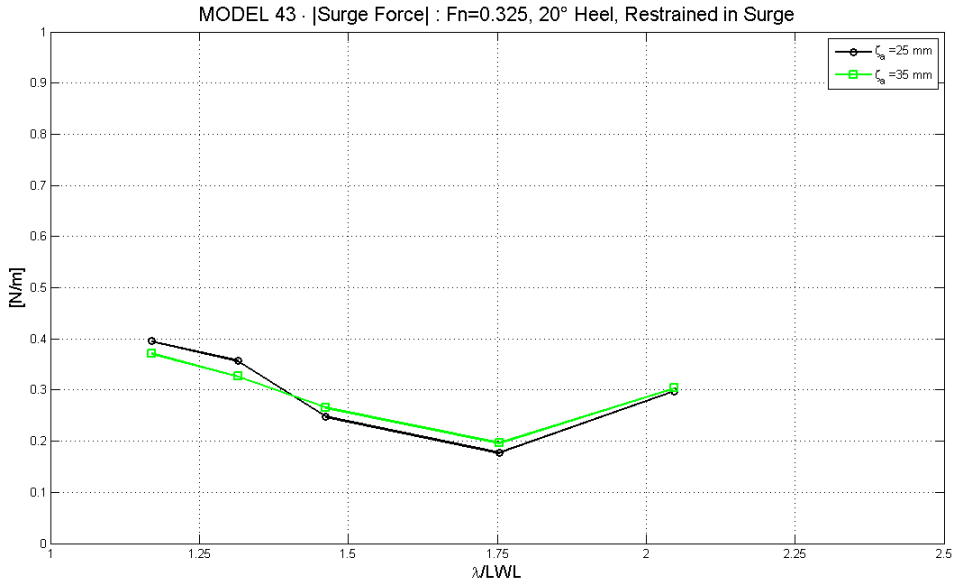

Figure 4.34: Model # 43· $\frac{|\text{Surge Force}|}{\zeta_a}$ - Fn=0.325, 20° Heel

To further investigate the linearity of the surge force, a harmonic analysis of the surge force signals was performed. It is in fact known that, signals which have a non-negligible quadratic component, present a conspicuous amount of energy at a frequency twice as large as the main frequency of the signal. From this investigation, it appears that the surge force do not have such a component. Indeed, it is found that, in general, the majority of the energy is located in correspondence of the frequency of encounter. Some smaller quantities of energy, caused by the vibrations of the setup, are located at higher frequencies. A typical example is given in Figure 4.35.

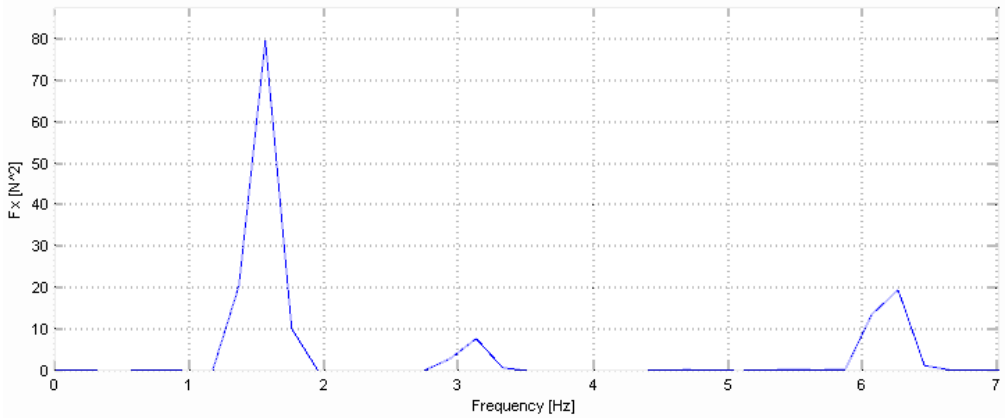

Figure 4.35: Typical result of the harmonic analysis relative to a 'moderate' testing condition. This refers to model # 43: Fn=0.325, $\zeta_a = 25$ [mm], $\lambda = 2$ [m]. Upright

In some extreme cases (model heeled, high speed and short waves), a larger amount of energy is found at the high-frequencies. However, this does not seem to concentrate around $\omega = 2 \cdot \omega_e$, which indicates that this is caused by the larger vibrations rather than a possible quadratic component of the signal (see Figure 4.36).

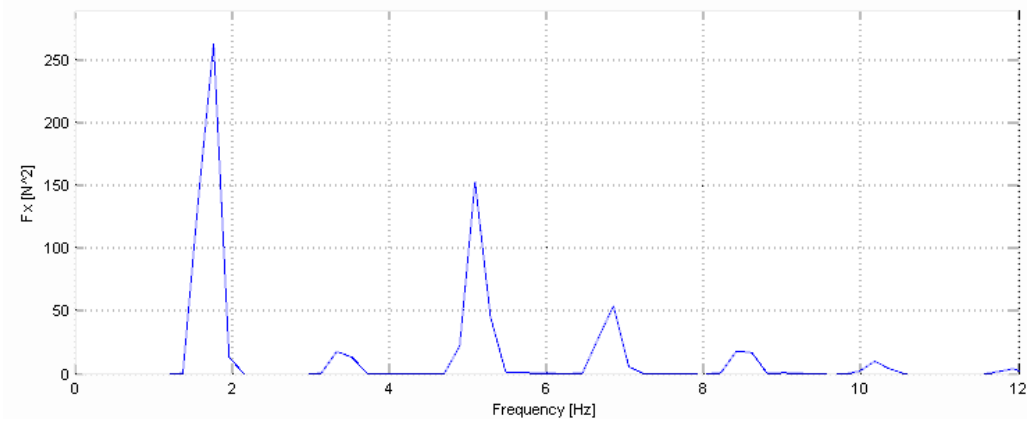

Figure 4.36: Typical result of the harmonic analysis relative to a 'severe' testing condition. This refers to model # 43: Fn=0.4, $\zeta_a = 25$ [mm], $\lambda = 2$ [m]. 20° Heeled

Another aspect of the surge force which was noted during this investigation is that, under certain circumstances, it may become negative. A negative force is a propulsive force. The nature of this phenomenon is still unclear, but it is believed that is due to a favorable pressure distribution along the hull. Also in such a situation, it appears that the amplitude of the surge force scales linearly with the wave amplitude. This can be seen, for instance, looking at Figure 4.37 and Figure 4.38.

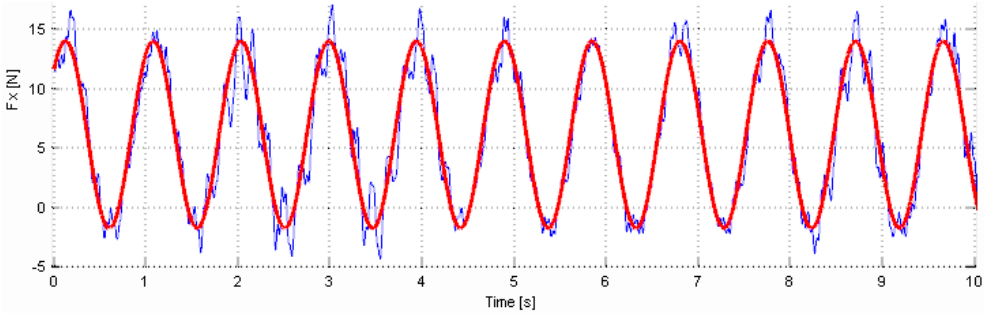

Figure 4.37: Model # 43·Surge force: Fn=0.325, $\lambda = 3.5$[m], $\zeta_a = 25$ [mm]. Upright

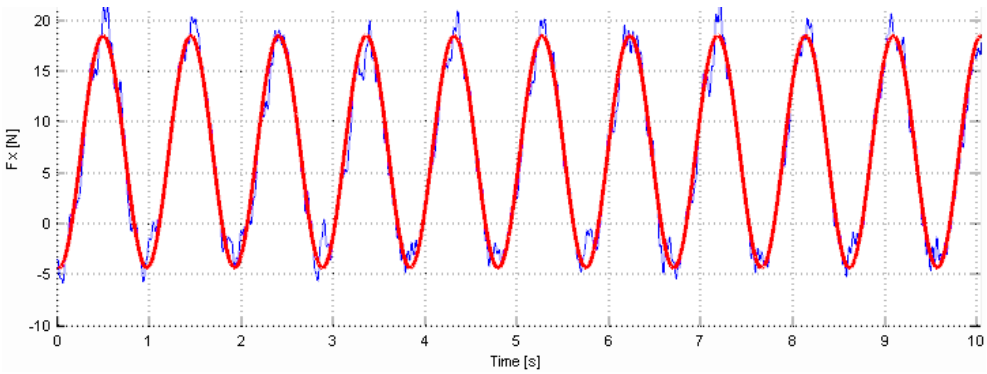

Figure 4.38: Model # 43·Surge force: Fn=0.325, $\lambda = 3.5$[m], $\zeta_a = 35$ [mm]. Upright

The data reported here above refer to the tests in which the models were restrained in surge. However, the tests in which the models were free to surge provided similar results, with respect to the linearity of the surge force. The only difference between the two is that, in the second case, the surge force is considerably smaller. This can be explained by considering that in one case, the inertia of the model is included in the result, whereas it is not in the other case. These results are reported in Appendix D.3.

4.2 Comparison with previous experiments: study of the trim angle

In 1995 during his MSc Thesis, Marc Levadou [35] carried out experiments similar to those performed for the present research. The setup used during his experiments and for the current tests were intentionally kept the same, as it has been described in Chapter 3. However, two important differences should be mentioned. The first is that in 1995 the models were tested without trim angle. The second is that the radius of gyration of model # 43 was $k_{yy} = 0.28$ during the tests carried out in this work, while it was $k_{yy} = 0.25$ for the experiments performed by Levadou. This difference is due to the large 'anti-yaw' vertical plate (see Figure 3.3), which was not used in the previous experiments. Due to the lack of a similar system, it is reported by Levadou that the tests in which the models were heeled suffered by large undesired sway and yaw motions.

On the basis of these considerations, and with the aim of this investigation being the influence of the trim angle on the seakeeping of the models, only the experiments relative to model # 45, in a upright condition, are here discussed. The complete results relative to this study can be found in Appendix D.4.

Figure 4.39, Figure 4.40 and Figure 4.41, show the comparison of the results relative to Froude number Fn=0.325[1], for the model upright.

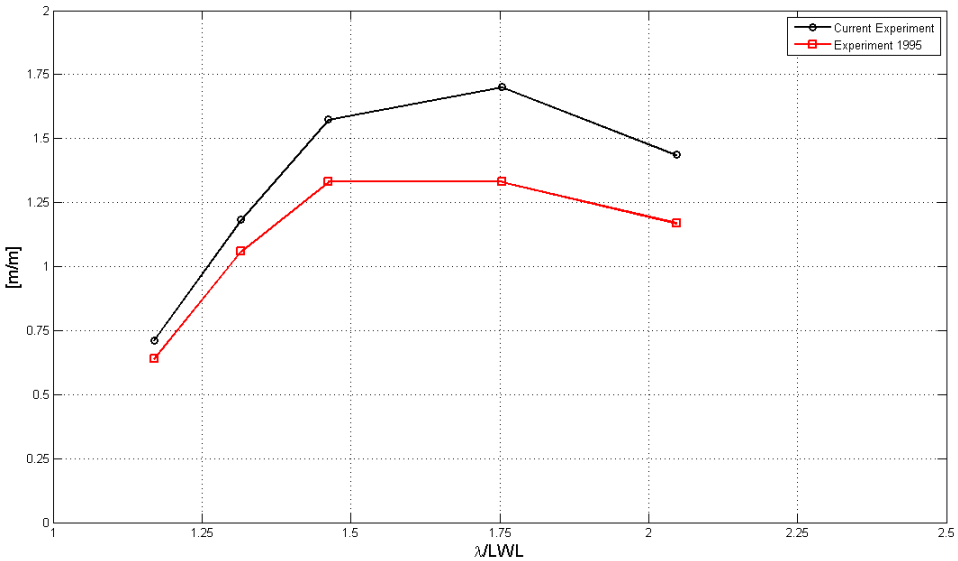

Figure 4.39: Model # 45·Comparison with experiments 1995 - Heave: Fn=0.325

[1]Fn=0.325 was the highest speed used during the experiments of 1995. No tests were carried out for Fn=0.4.

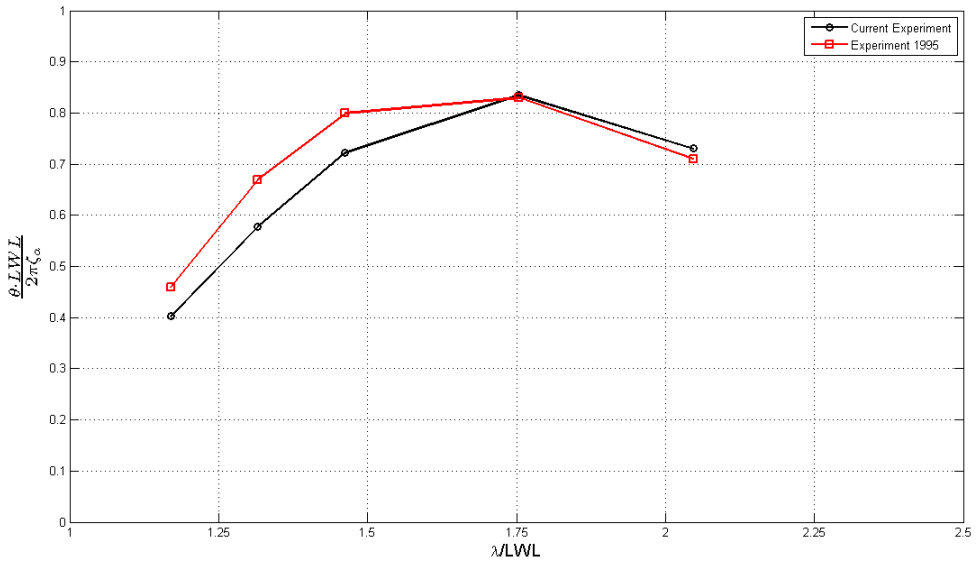

Figure 4.40: Model # 45·Comparison with experiments 1995 - Pitch: Fn=0.325

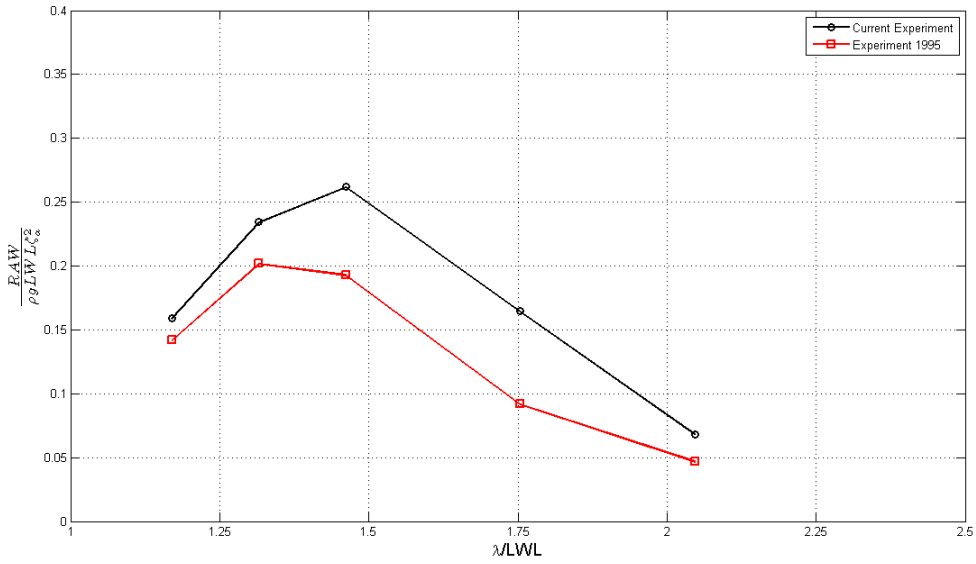

Figure 4.41: Model # 45·Comparison with experiments 1995 - Added resistance: Fn=0.325

As it can be seen the difference is very large, and it is particularly so for the heave response at the resonance peak. The difference relative to pitch, however, seems to have an opposite trend; it is large for the short waves and it decreases as the waves become longer. These differences also lead to a large discrepancy in the mean added resistance, as that measured during the experiments of 1995 is considerably lower.

The differences between the results of the current experiments and those relative to the experiments carried out in 1995 appear to be surprisingly large. And it is particularly so considering that the trim angle correspondent to Fn=0.325 is only 0.23°.

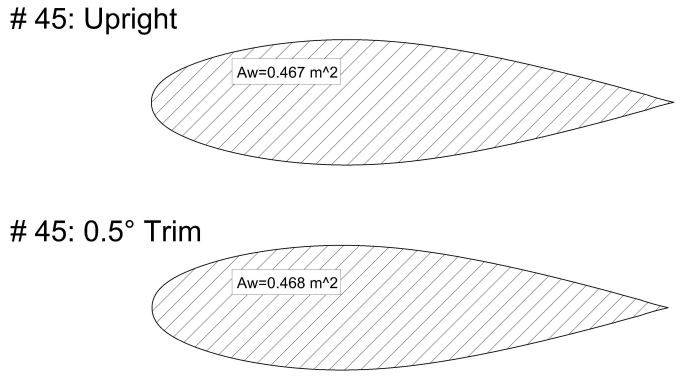

Figure 4.42: Model # 45 · Comparison of the upright and trimmed waterplane areas

Although sailing yachts have conspicuous overhangs and flare, looking at Figure 4.42, it can be seen that the waterplane area of the trimmed model remains substantially unchanged. Another possible cause of these unexpected results, is that in 1995 the motions were measured using a different technique. In fact a potentiometer was used instead of the system of cameras and leds which is used nowadays. It should also be noted that no information regarding the reliability of the experiments performed in 1995 is known.

4.3 Study of the effects of the heeling angle using PDSTRIP

The strip-theory program PDSTRIP has the capability of considering asymmetric hulls. Now the aim is to investigate whether the program is able to correctly predict the effects caused by the heeling angle on the motions, and on the mean added resistance, found during the experiments in the towing tank. As, for the time being, this is the main intent rather than investigating the absolute accuracy of the program, the results reported in this section show the comparison of the calculations performed for the upright and heeled models.

For the calculations, the values of the radii of gyration and the location of the COG of the models, were set equal to those adopted during the tests. Also the correct trim angles were used (see Table 3.3). The computations were carried out considering head waves. Furthermore, the condition of restraint in surge, in which the models were tested, was resembled by eliminating the surge effect (which is however small) on the motions of heave and pitch. It was assumed that this was possible to be achieved by setting the surge-pitch coupling terms to zero in the added mass and restoring matrices. During the heeled tests, the models were also restrained to sway, roll and yaw, although they tended to do so due to the forces caused by the asymmetry of the hull. These motions are, in

general, coupled with the motions of heave and pitch, and thus they have an influence on them. Similarly to the surge, it was assumed that the motions of sway, roll and yaw, could have been decoupled from those of heave and pitch by setting the coupling terms of the complex added mass and restoring matrices to zero[2]. In Figure 4.43 and Figure 4.44 an example of heave and pitch RAOs, which were obtained with and without decoupling, is reported.

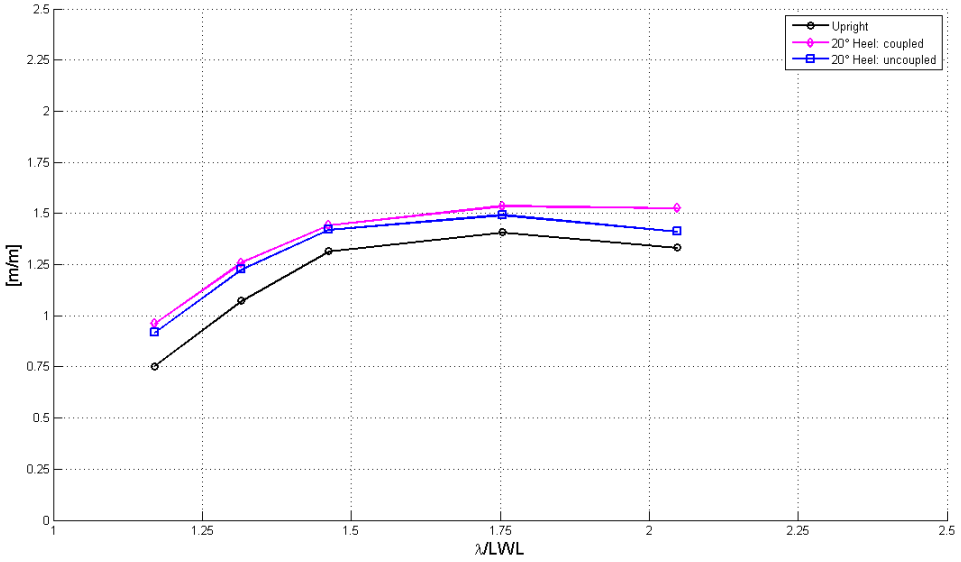

Figure 4.43: Effect of the decoupling on the heave motion - Model # 43-Fn=0.325

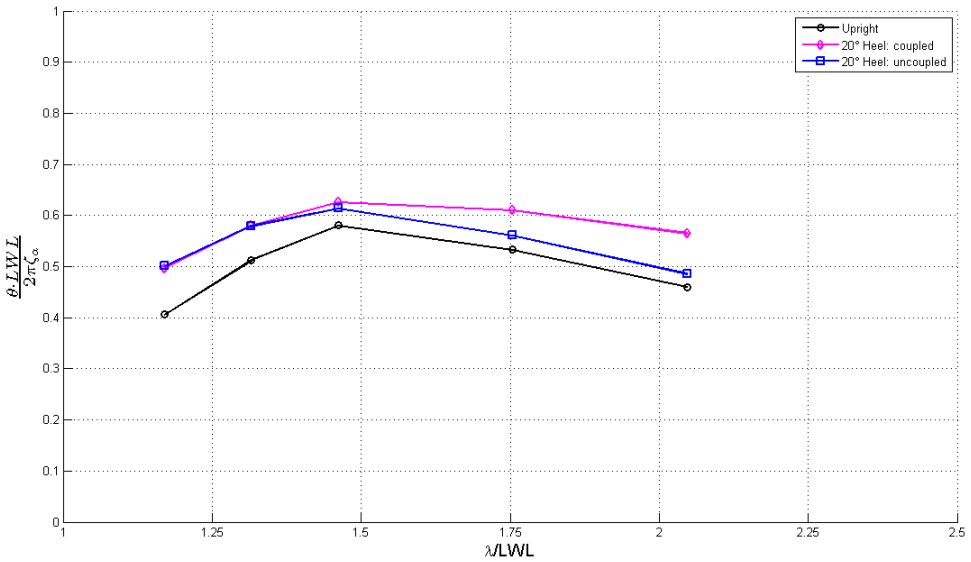

Figure 4.44: Effect of the decoupling on the pitch motion - Model # 43-Fn=0.325

[2]Setting to zero also the coupling terms of the mass matrix would generate a singular matrix

The results reported in this section were obtained using the above mentioned decoupling system.

In Figure 4.45 and Figure 4.46 the results relative to model # 43 at a forward speed equal to Fn=0.325 are shown.

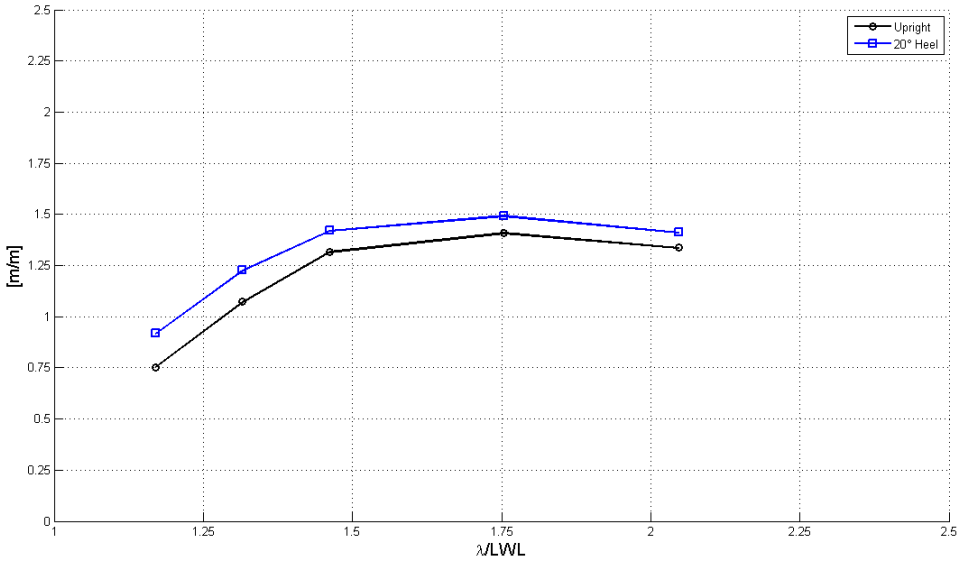

Figure 4.45: Model # 43·Upright vs 20° Heel - Heave: Fn=0.325. PDSTRIP

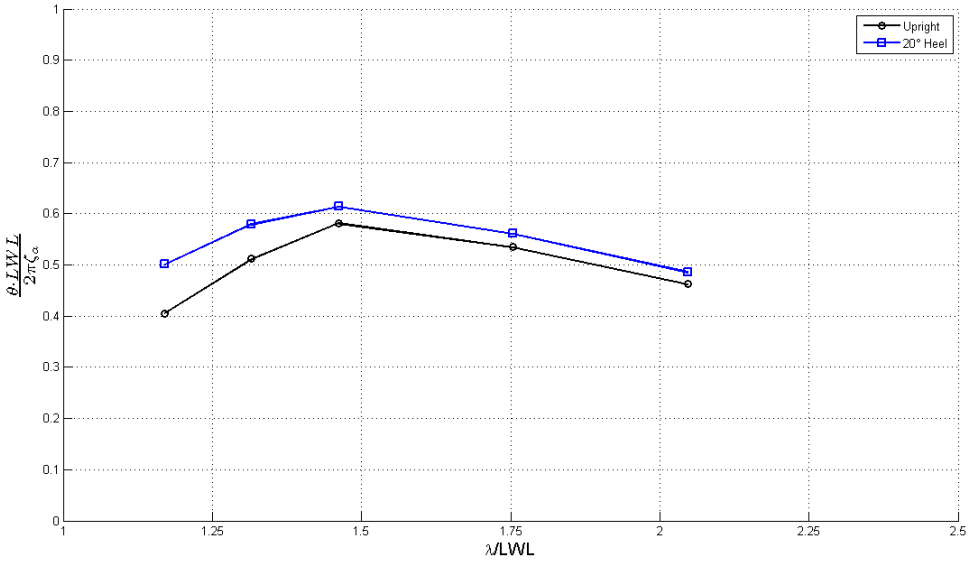

Figure 4.46: Model # 43·Upright vs 20° Heel - Pitch: Fn=0.325. PDSTRIP

The first thing that can be noted is that PDSTRIP predicts a considerable influence of heeling angle on the motions. In particular, the effects of the heeling angle on the pitch motion seems to be substantially in agreement with the trend found during the experiment. Pitch is in fact larger, when the model is heeled, compared to the upright case. On the other hand, the effect of the heeling angle on heave is wrongly predicted. While the measurements show that heave is slightly reduced when the model is heeled, PDSTRIP predicts an opposite trend. As it has already been mentioned in Section 4.1.2, this result is arguably due to the prominent flare of the model, which ingresses the water as the model heaves and pitches. However, this effect cannot be taken into account by strip-theory programs, which may explain the difference.

The mean added resistance was computed using the Gerritsma and Beukelman formulation (see Appendix A.2 for the details regarding this method), which is well know for providing reliable results, especially in the situation of ships sailing in bow-quarteting and head waves. In Figure 4.47 the mean added resistance calculated for the upright and heeled model is shown.

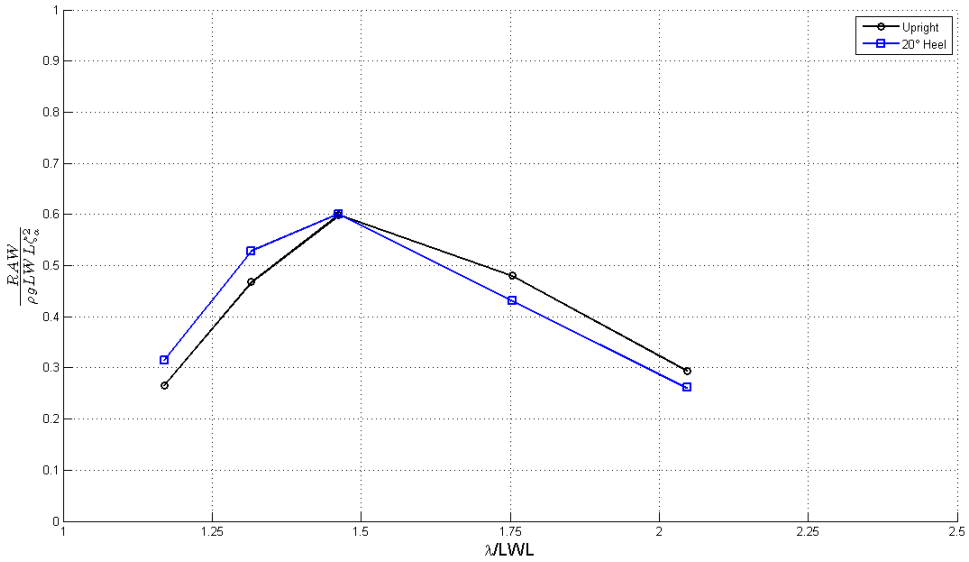

Figure 4.47: Model # 43-Upright vs 20° Heel - Added resistance: Fn=0.325. PDSTRIP

As it can be seen, the heeling angle has the effect of increasing the mean added resistance at the short waves, and decreasing it, at the long waves. At the resonance, the result remain substantially unchanged. Considering that the degree of repeatability of these tests have a measurement error which, at the resonance, becomes as large as 8%, the trend predicted by PDSTRIP doesn't deviate too much from the result of the experiments. However, a certain difference should be expected due to the wrong prediction of the heave motion.

In Figure 4.48 and Figure 4.49 the results of the heave and pitch responses for the forward speed Fn=0.4 are reported.

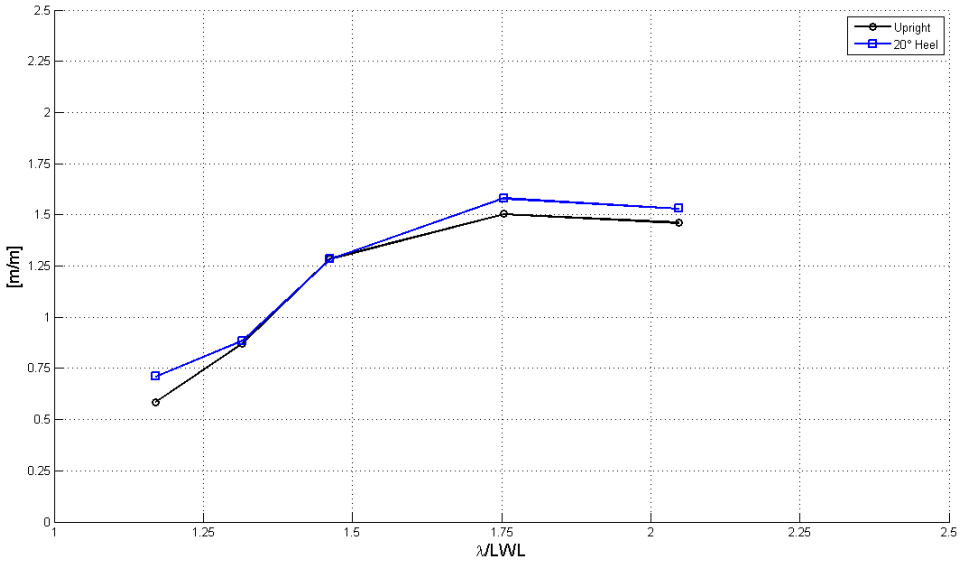

Figure 4.48: Model # 43·Upright vs 20° Heel - Heave: Fn=0.4. PDSTRIP

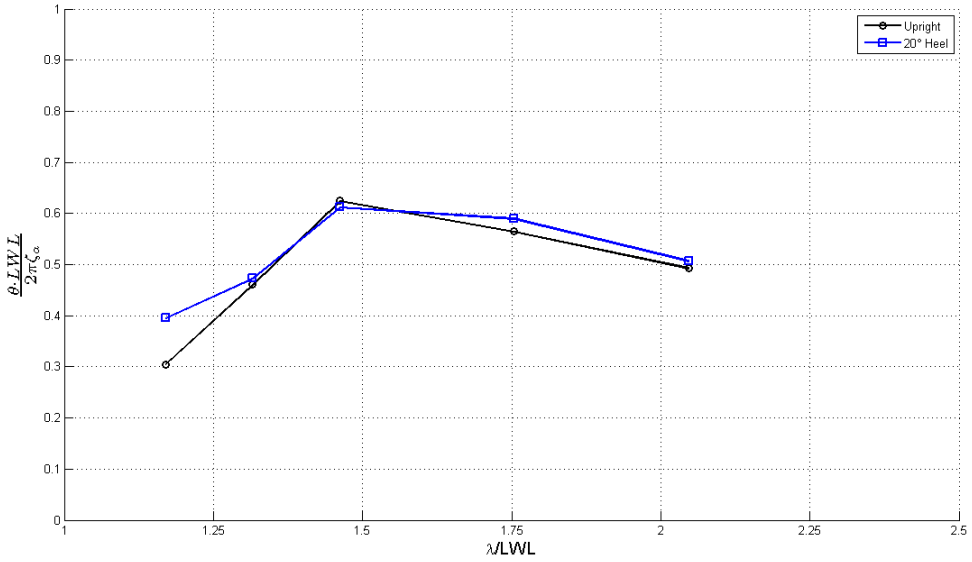

Figure 4.49: Model # 43·Upright vs 20° Heel - Pitch: Fn=0.4. PDSTRIP

It can be seen that, in general, the heave response is still increased by the heeling angle, although by a smaller amount when compared to the speed Fn=0.325. This trend is not in agreement with the results of the experiments, as it was that pitch is still considerably reduced by the heeling angle, also for this speed. Also the influence of the heeling angle on the pitch response is less relevant for Fn=0.4. This trend, in contrast, was detected

during the tests in the towing tank. As a result the mean added resistance appears to be increased by the heeling angle, at the short waves, whilst is slightly decreased, at the long waves (see Figure 4.50). Due to the poor degree of reliability of the results of the mean added resistance obtained at Fn=0.4 (see Appendix C), it is not possible to judge whether the trend predicted by PDSTRIP is correct or not.

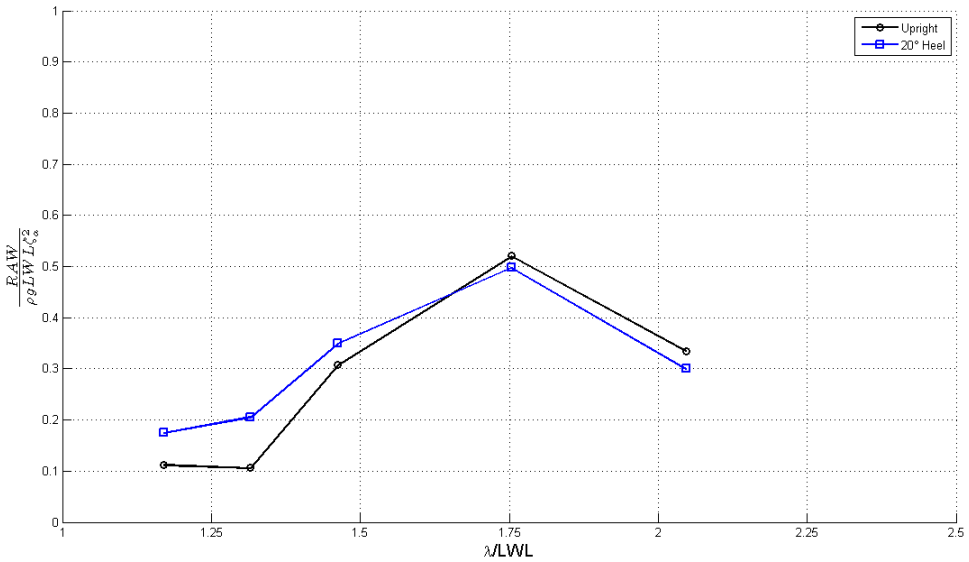

Figure 4.50: Model # 43 ·Upright vs 20° Heel - Added resistance: Fn=0.4. PDSTRIP

Let us now consider the results relative to model # 45. From the computations performed with PDSTRIP, it can be seen that the heeling angle has the effect of reducing the motions. This holds true for heave and pitch alike. The responses are in fact considerably reduced at the resonance and for the long waves. For the short waves the effect of the heeling angle on the motions appears to be small, if not negligible (see Figure 4.51 and Figure 4.52). These results are qualitatively in agreement with the findings of the experiments obtained for the same model and the same speed.

On the other hand, the results relative to the mean added resistance appear to deviate from the results of the towing-tank tests. In fact PDSTRIP predicts a considerable reduction of the added resistance caused by the heeling angle, while an opposite trend was detected during the experiments. This can be seen in Figure 4.53. It should be noted that such a difference appears to be larger than the precision of the measurements, thus it cannot be claimed to be caused by measurement inaccuracies (see Appendix C).

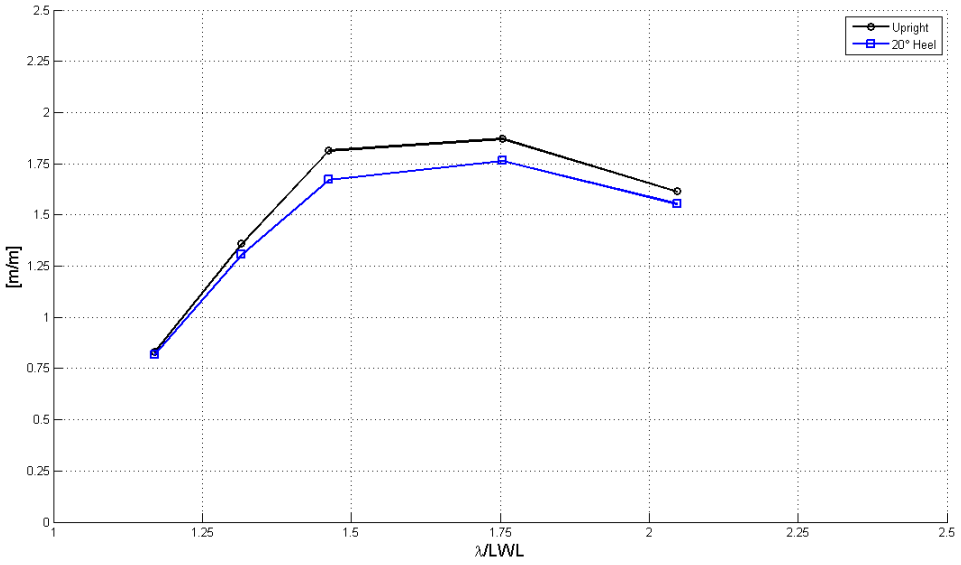

Figure 4.51: Model # 45·Upright vs 20° Heel - Heave: Fn=0.325. PDSTRIP

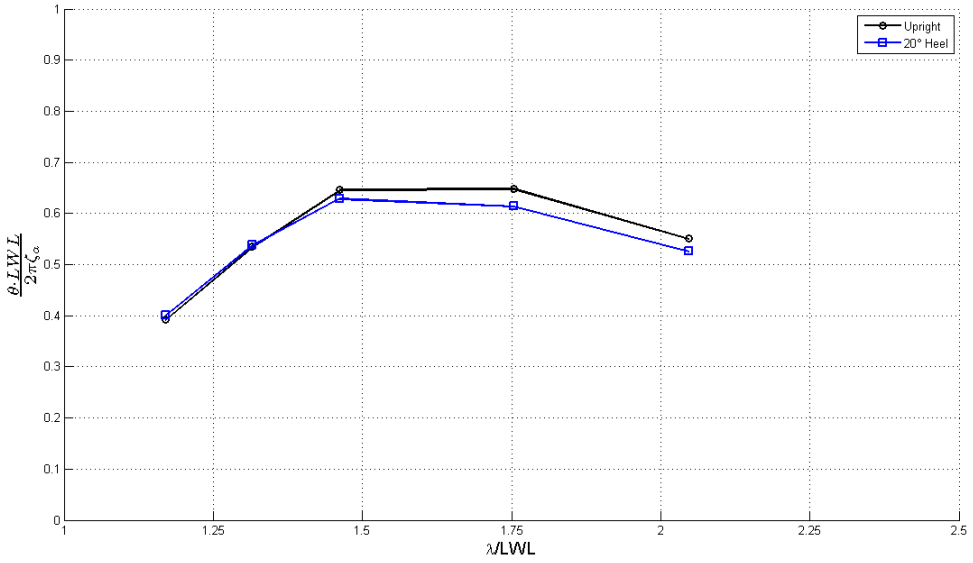

Figure 4.52: Model # 45·Upright vs 20° Heel - Pitch: Fn=0.325. PDSTRIP

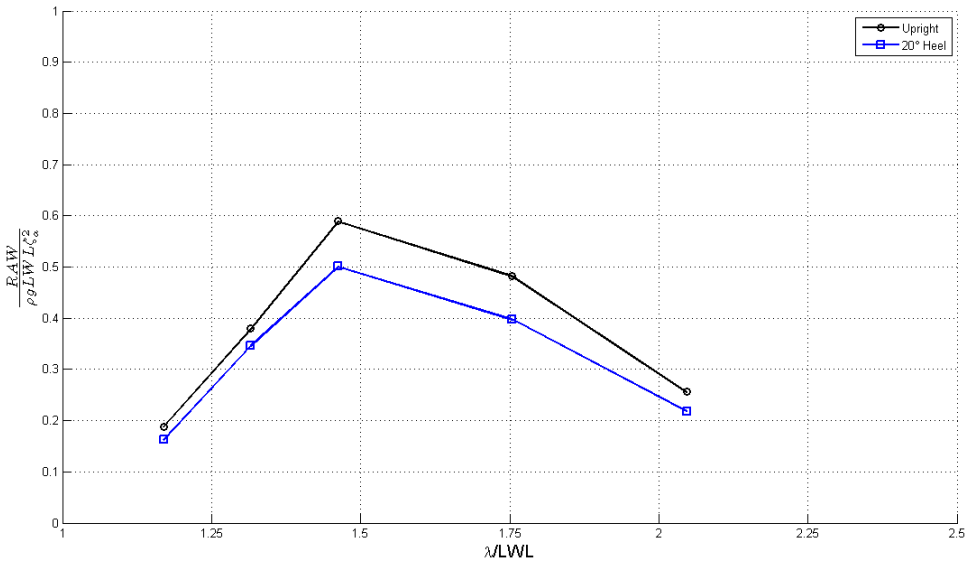

Figure 4.53: Model # 45·Upright vs 20° Heel - Added resistance: Fn=0.325. PDSTRIP

For the forward speed Fn=0.4, the results provided by PDSTRIP, relative to the motions of heave and pitch, are still qualitatively in agreement with the findings of the experiments. However, a few discrepancies should be noted by looking at Figure 4.54 and Figure 4.55.

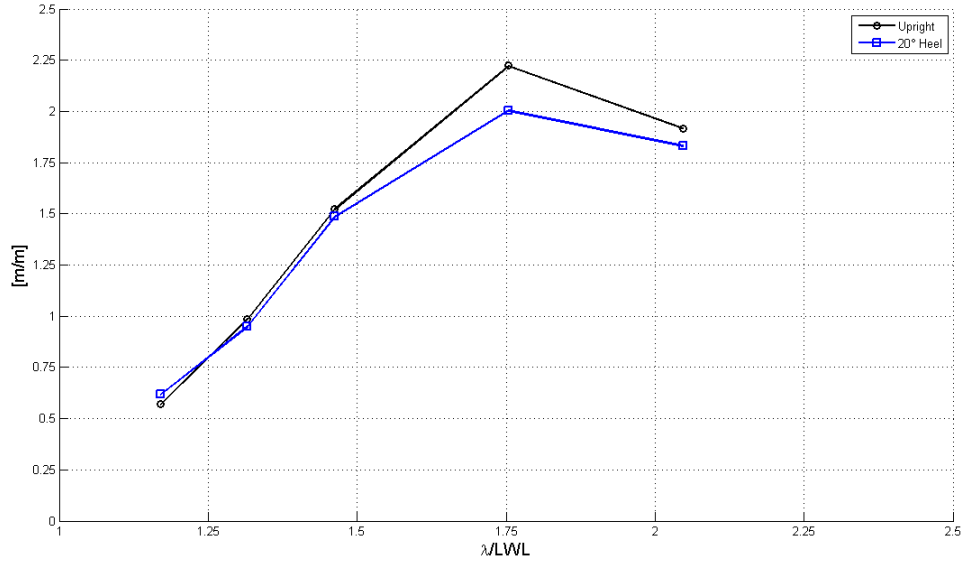

Figure 4.54: Model # 45·Upright vs 20° Heel - Heave: Fn=0.4. PDSTRIP

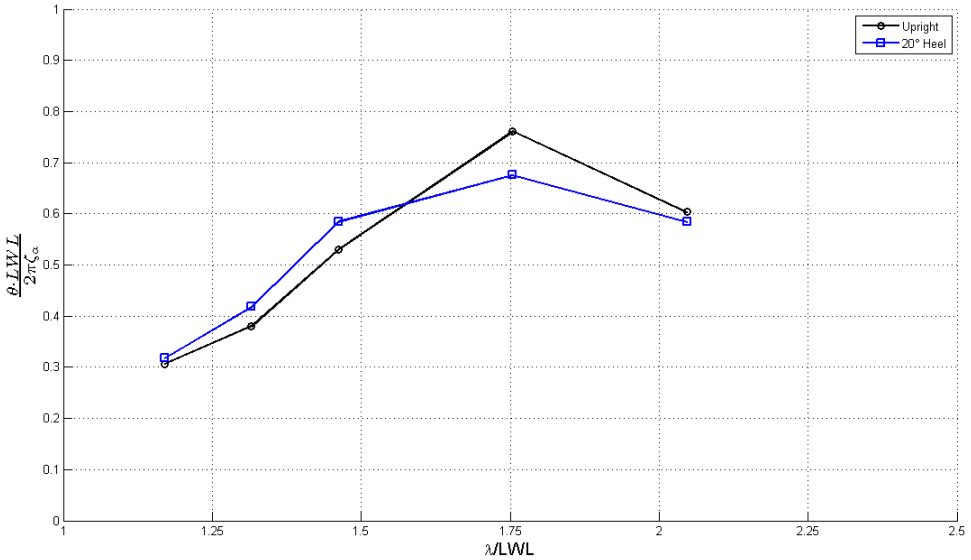

Figure 4.55: Model # 45·Upright vs 20° Heel - Pitch: Fn=0.4. PDSTRIP

The pitch response predicted by the program appears to be increased by the heeling angle, for a relative wave length $\lambda/LWL < 1.5$. Such a trend was not detected during the tests, as the pitch motion was reduced by the heeling angle for the entire range of wave lengths considered. Also the heave response appears to deviate from the results of the measurements in case of short waves. PDSTRIP indeed underestimates the decreasing effect that the heeling angle has on the heave response, which was found during the experiments.

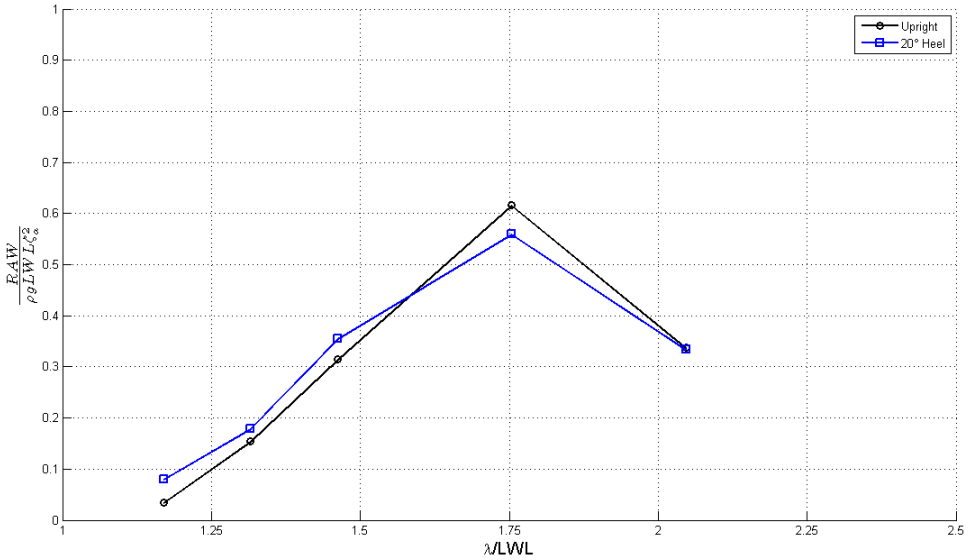

Figure 4.56: Model # 45·Upright vs 20° Heel - Added resistance: Fn=0.4. PDSTRIP

Lastly, the results relative to the mean added resistance are given in Figure 4.56. As it can be seen, the heeling angle seems to slightly decrease the added resistance at the resonance peak, whilst it has an opposite effect at the short waves. For this model, similarly to model # 43, it is not possible to judge whether this trend is in agreement with the findings of the experiments. In fact, the results of the mean added resistance obtained at Fn=0.4, are contaminated by a measurement error which is on average as large as 15%, making these results unreliable (see Appendix C).

4.4 Results of the time domain simulations

Time-domain simulations were carried out to study the influence of the aerodynamic force on the motions of heave and pitch and how, in turn, this would affect the mean added resistance in waves. For this reason, a sail plan which could be suitable for a yacht similar to the models under consideration was designed. The main characteristics are shown in Figure 4.57.

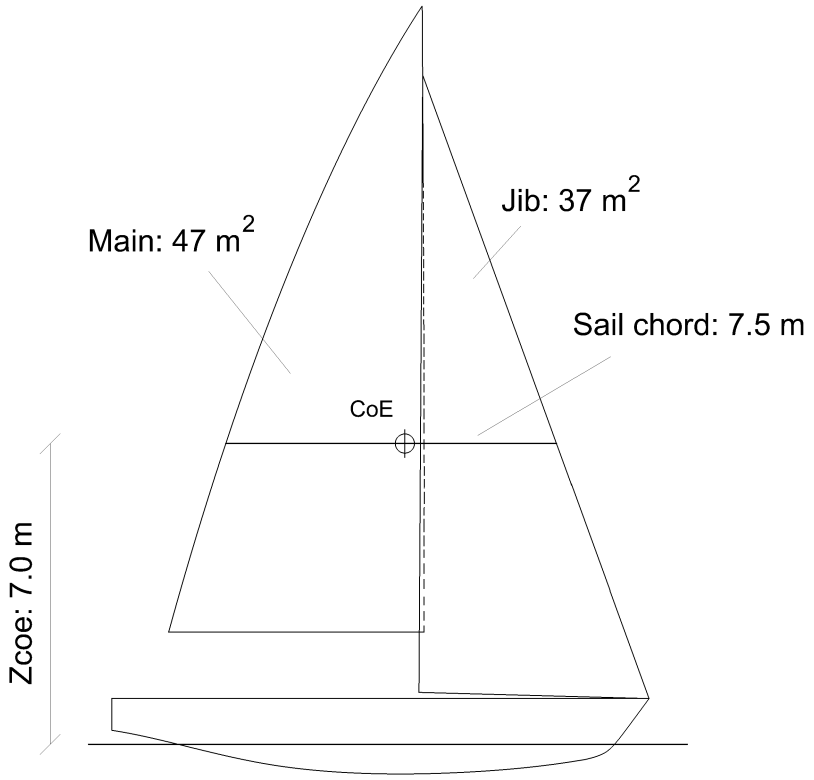

Figure 4.57: Sail plan used for the time-domain simulations. It should be pointed out that the models are now considered in their full-scale version having LWL=10 [m].

A typical upwind sailing condition was hypothesized and used throughout the calculations. The true wind speed was assumed to be $V_{TW} = 16$ [kt] and the true wind angle to be $\beta_{TW} = 40°$. This resulted in a apparent wind angle $\beta_{AW} = 27°$ and an apparent wind speed $V_{AW} = 22$ [kt], having the yacht a forward speed equal to Fn=0.35. This condition was tested for 2 wave amplitudes ($\zeta_a = 0.25$ [m] and $\zeta_a = 0.6$ [m]), 3 wave lengths ($\lambda = 20$ [m], $\lambda = 35$ [m] and $\lambda = 50$ [m]) and 2 heeling angles ($\phi = 0°$ and $\phi = 20°$). For each combination, the simulations were performed without considering the aerodynamic force and taking into account the aerodynamic force calculated using the quasi-steady and the unsteady method.
As it has been explained in 2.4, the time-domain simulations were performed in a two-dimensional environment in which the regular waves are assumed to have an angle $\mu = 180°$ with the centerline of the yacht. Only the motions of heave and pitch were considered and the forward speed was assumed to be constant. According to the considerations made so far, the reduced velocity (which is used to compute the unsteady aerodynamic force) is only dependent on the wave length λ. The values of the reduced velocities, correspondent to the 3 wave lengths chosen, are VR=3.35, VR=4.87 and VR=6.14. It should be mentioned that the value VR=3.35 is actually just outside the range of reduced velocities tested by Fossati ($3.5 < VR < 14$). In this case the aerodynamic stiffness and damping coefficients were assumed to be equal to those correspondent to the reduced velocity VR=3.5. It should also be noted that, due to the limitations imposed by the reduced velocity range, it was impossible to consider shorter waves.

In Figure 4.58 a typical result of a time-domain simulation relative to the pitch motion is shown. Analogous results were obtained also for heave. However, for convenience in this section the results of the time-domain simulations are presented as function of the wave length expressed as λ/LWL, rather than function of time.

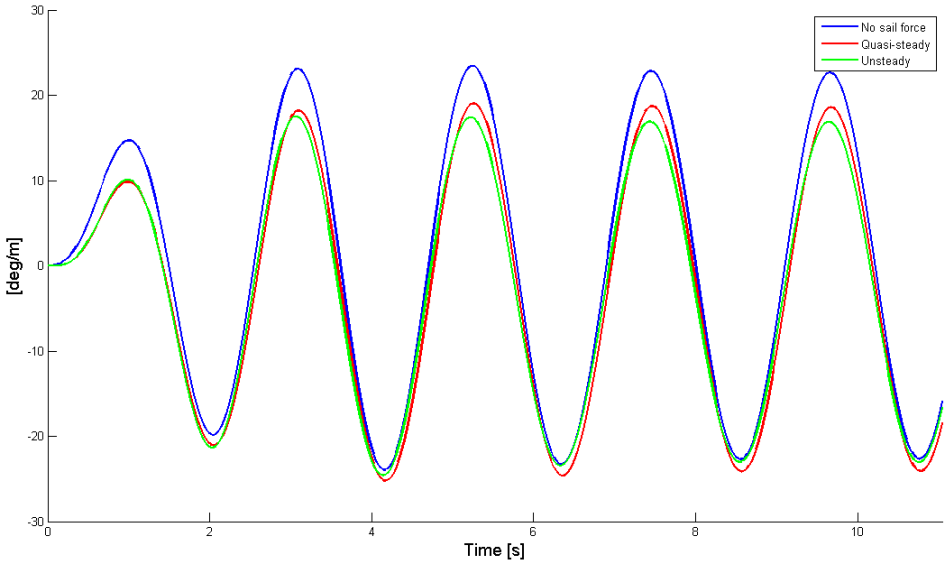

Figure 4.58: Typical result of a time-domain simulation relative to pitch

The aerodynamic force has a double effect on the heave and pitch motions of a yacht. In fact, it influences the amplitude as well as the mean of the responses. In other words, it imposes a certain trim and sinkage to the yacht. This can be seen in Figure 4.59. It also appears that the results are substantially independent from the method employed to calculate the aerodynamic force. Nevertheless, the results reported in this section focus on the influence of the aerodynamic force on the amplitude of the heave and pitch motions, rather than its effect on the sinkage and trim.

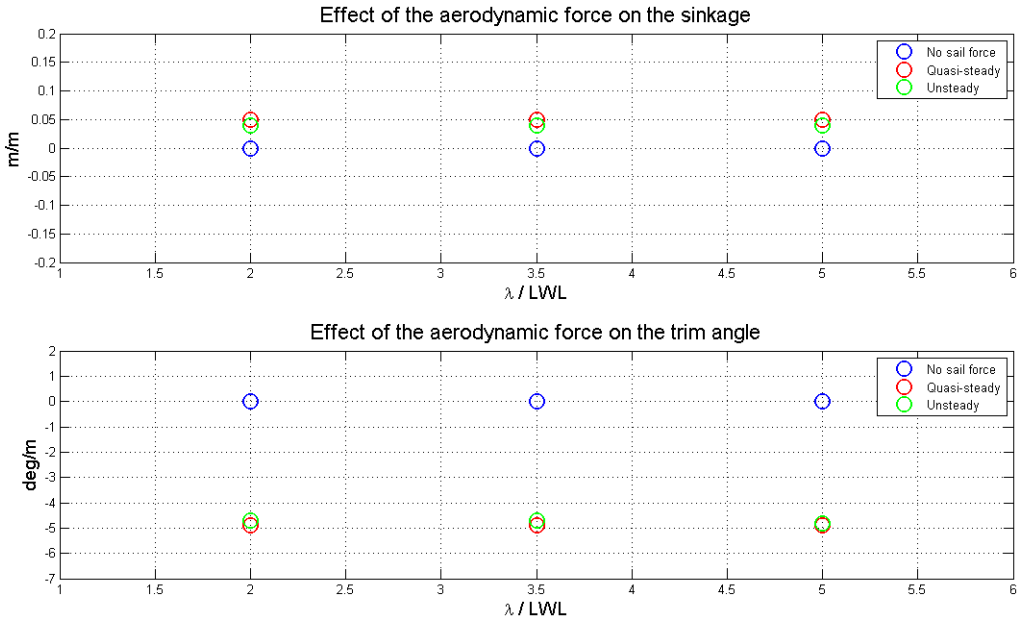

Figure 4.59: Typical example of sinkage and trim angle caused by the aerodynamic force. It should be noted that a negative trim angle corresponds to bow down

Let us now consider model # 43. Presented in Figure 4.60 and Figure 4.61 are the results relative to heave and pitch, obtained considering the model to be upright and the wave amplitude to be $\zeta_a = 0.25$ [m]. As it can be seen, the amplitude of the responses of heave and pitch appear to be influenced by the aerodynamic force. It is particularly so for the short wave ($\lambda/LWL = 2$), being near the resonance area. For the medium and long wave, on the other hand, the effect of the aerodynamic force is less noticeable. It is also interesting to note that the results obtained using the two different theories to calculate the aerodynamic force, produce considerably different results. For $\lambda/LWL = 2$, the heave response is increased by 2% when the quasi-steady method is used, whilst a reduction of the same amount is obtained by using the unsteady method (see Figure 4.60). On the other hand, the reduction of the pitch response (of about 6%) seems to be predicted similarly by both methods. This is no longer true when the wave amplitude is increased to $\zeta_a = 0.6$ [m]. For this case, in fact, using the unsteady method results in a reduction of the pitch response of about 6%, whereas a reduction of only 3% is obtained by using the quasi-steady approach (see Figure 4.62).

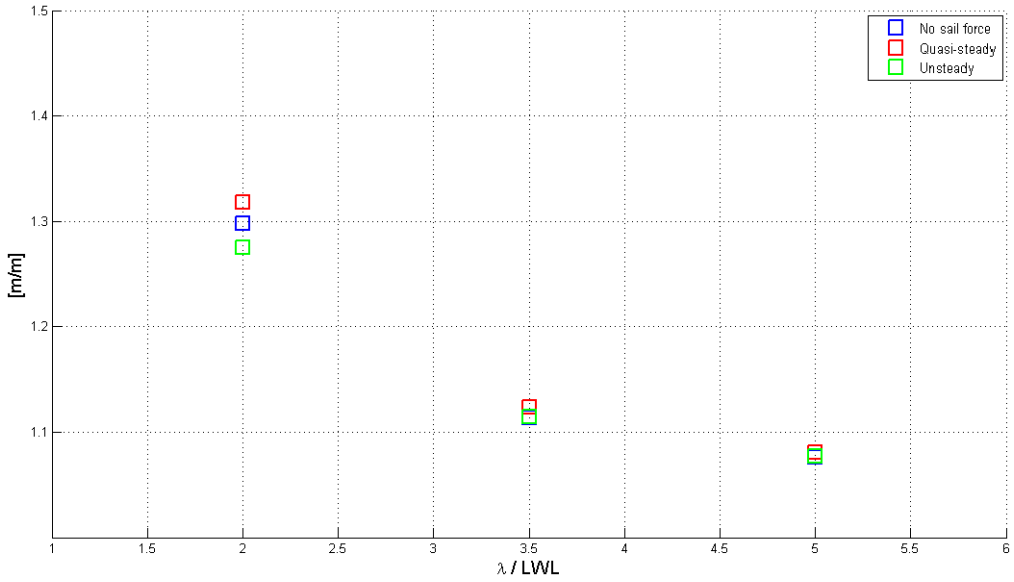

Figure 4.60: Model # 43· Heave: Fn=0.35, $\zeta_a = 0.25$ m, Upright

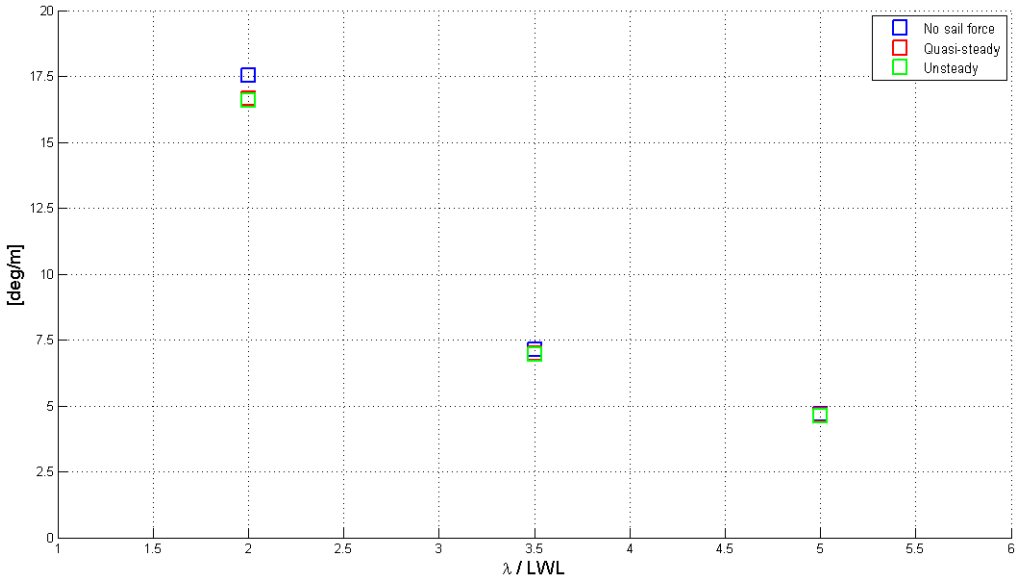

Figure 4.61: Model # 43· Pitch: Fn=0.35, $\zeta_a = 0.25$ m, Upright

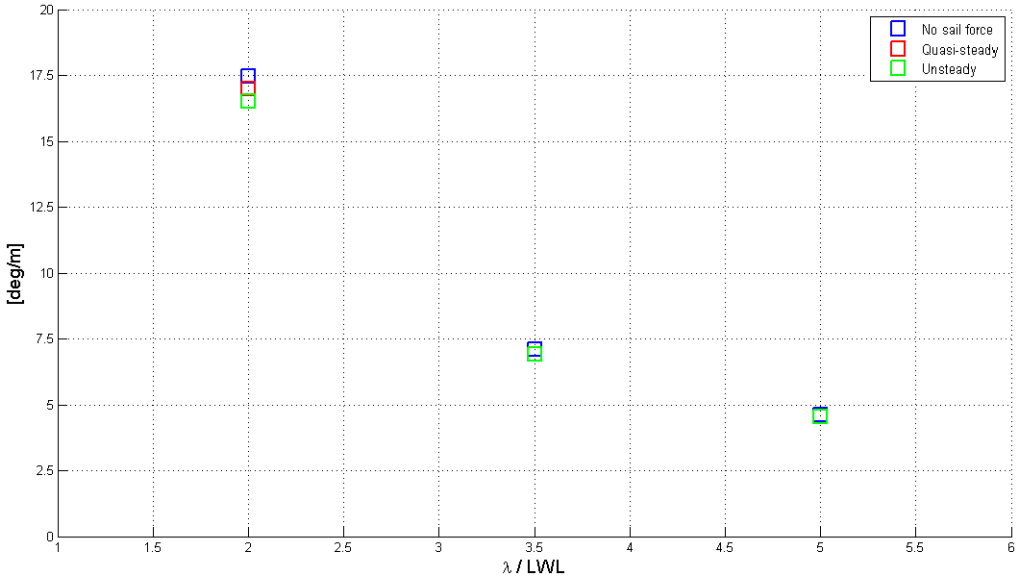

Figure 4.62: Model # 43· Pitch: Fn=0.35, $\zeta_a = 0.6$ m, Upright

Similar results were also obtained for the simulations in which the model was heeled by 20°. This can be seen, for example, in Figure 4.63, in which the pitch response obtained for $\zeta_a = 0.6$ [m] is depicted. Once again, pitch appears to be reduced by the aerodynamic force and the unsteady method results in a reduction nearly twice as large the reduction obtained by using the quasi-steady method (5.5% and 3%). The other results relative to the heeled model are given in Appendix D.6.

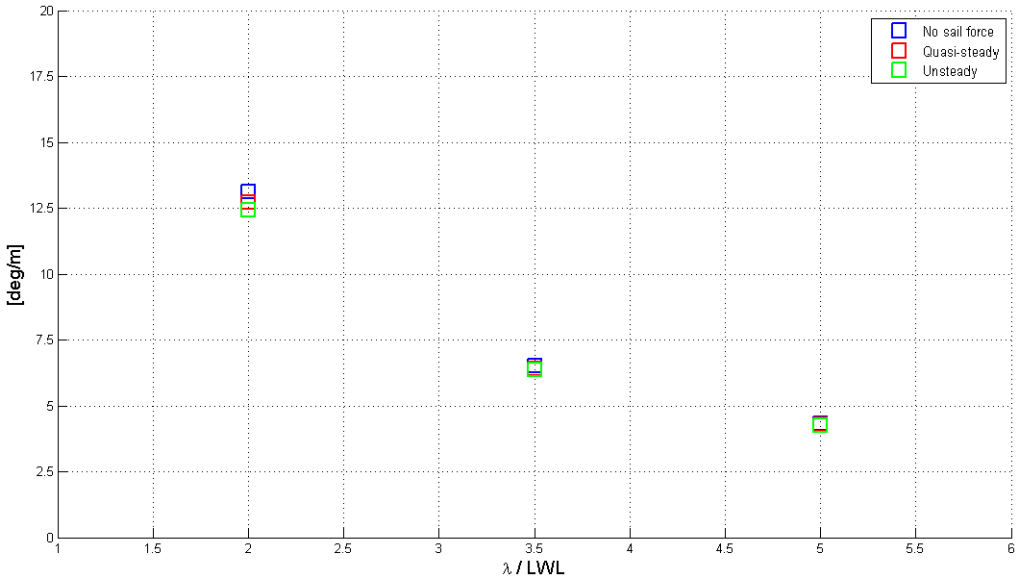

Figure 4.63: Model # 43· Pitch: Fn=0.35, $\zeta_a = 0.6$ m, 20° Heel

Similarly to the results obtained for model # 43, it seems that model # 45 the aerodynamic force has the largest influence on the responses for the case $\lambda/LWL = 2$. In particular, looking at Figure 4.64, it appears that, for this situation, the heave response is reduced by the aerodynamic force of nearly 6%. This result refers to the situation in which the unsteady method was used. If, in contrast, the quasi-steady method was adopted, the reduction appears to be negligibly small.

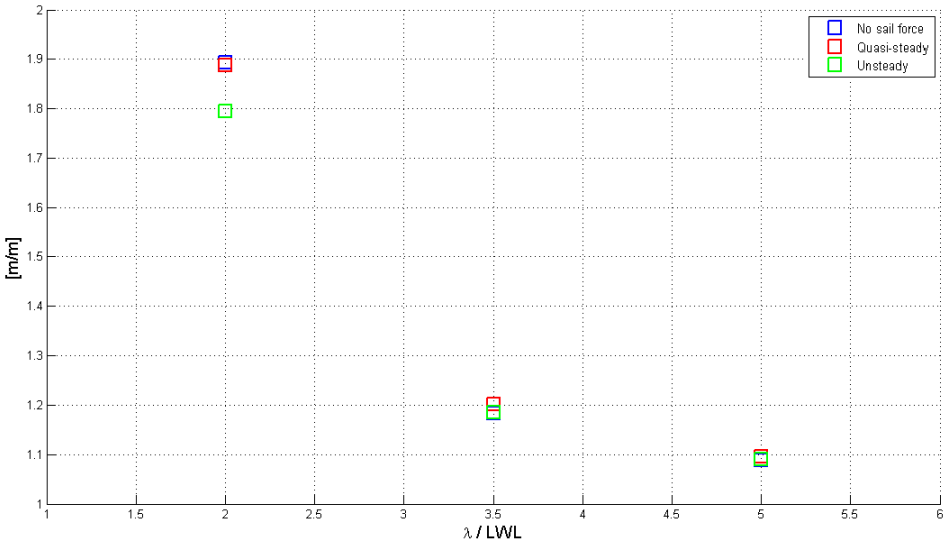

Figure 4.64: Model # 45·Heave: Fn=0.35, $\zeta_a = 0.25$ m, Upright

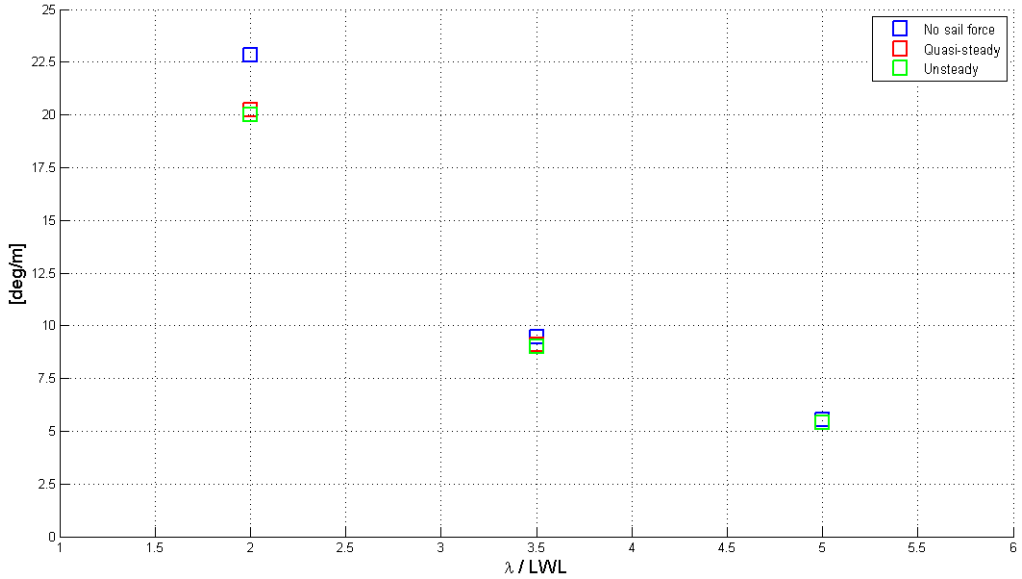

Figure 4.65: Model # 45· Pitch: Fn=0.35, $\zeta_a = 0.25$ m, Upright

On the other hand, the two methods seem to have a similar reducing effect on the pitch response (see Figure 4.65). In this case, indeed, both methods give a reduction of about 14%. This occurs for the wave amplitude $\zeta_a = 0.25$ [m]. For the larger wave amplitude ($\zeta_a = 0.6$ [m]) however, the two methods provide different results. While the unsteady method provides a reduction of the pitch motion of nearly 14%, the reduction obtained by using the quasi-steady method is only 6%. This can be seen in Figure 4.66.

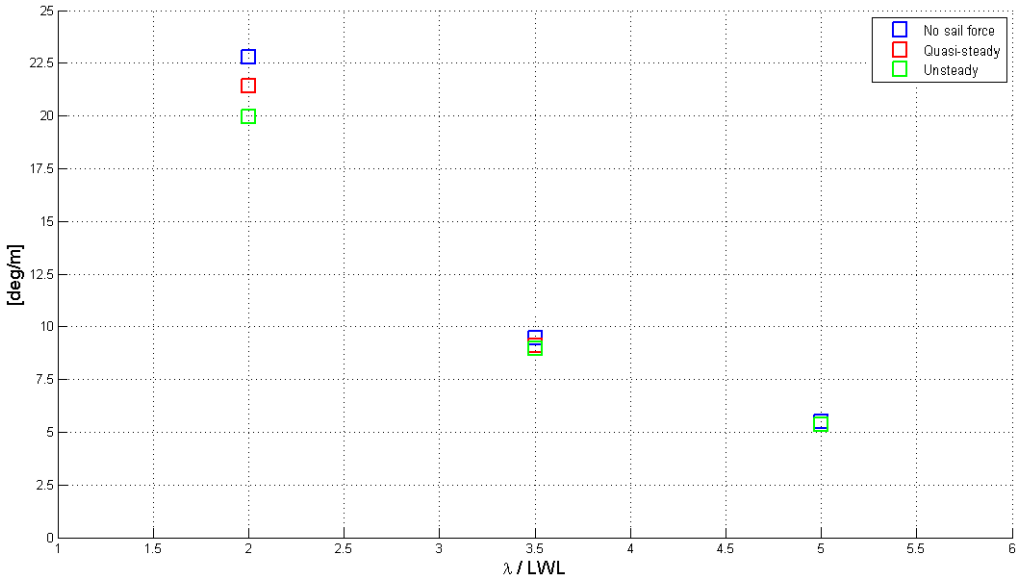

Figure 4.66: Model # 45· Pitch: Fn=0.35, $\zeta_a = 0.6$ m, Upright

Although different yachts were considered and a different approach was employed, the findings of this investigation are qualitatively in agreement with those presented by Skinner [47] in 1982. In his research, Skinner noted that, for some conditions, the aerodynamic force reduced the pitch motion by up to 14%. However, differently from what Skinner hypothesized, the results presented in this section prove that the aerodynamic force has a larger reducing effect on the motion when the unsteady effects are taken into account (unsteady method), rather than when they are neglected (quasi-steady method).

In Figure 4.67 the quasi-steady and the unsteady aerodynamic force are compared. Three main differences may be noted: amplitude, phase and shape of the signals. The differences in amplitude and phase were expected and they were caused by the nature of the method employed to calculate the aerodynamic force (considering or not the unsteady effects). The difference in shape, i.e. the fact that the quasi-steady force presents a peculiar double peak, was not expected but it may be explained by looking at Figure 4.68. As it can be seen, the driving force coefficient Cx, calculated in a static manner, has a more or less linear relation with the apparent wind angle β_{din}, up to $\beta_{din} \approx 24°$. After this threshold,

the relationship is no longer linear. It should be also recalled that the mean apparent wind angle used for the simulations was $\beta_{din} = 27°$. Thus, when the wave amplitude is large enough (i.e. $\zeta_a = 0.6$ m), due to the large motion of pitch, Cx spans an area which also comprises the hump of the curve, resulting in that peculiar double-peak shape shown in Figure 4.67.

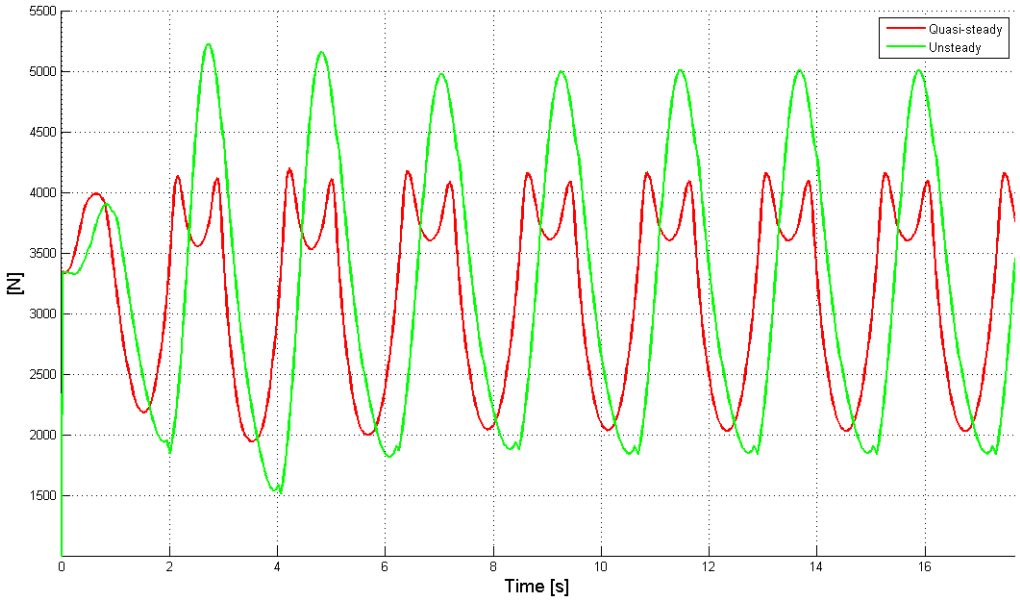

Figure 4.67: Comparison of the aerodynamic force calculated with the quasi-steady and the unsteady method. Model # 45 · Fn=0.35,$\zeta_a = 0.6$ m. Upright

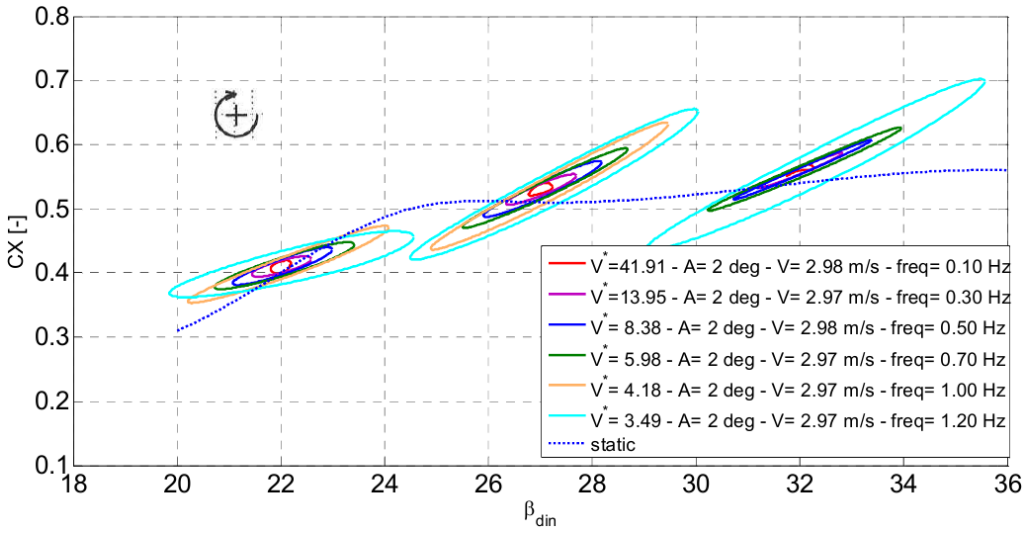

Figure 4.68: Static vs Dynamic driving force coefficients. (Fossati [12])

If, on the other hand, a wave amplitude $\zeta_a = 0.25$ [m] is considered, the shape of the aerodynamic force, calculated with the quasi-steady method, becomes more similar to a sinusoid. This can be seen in Figure 4.69.

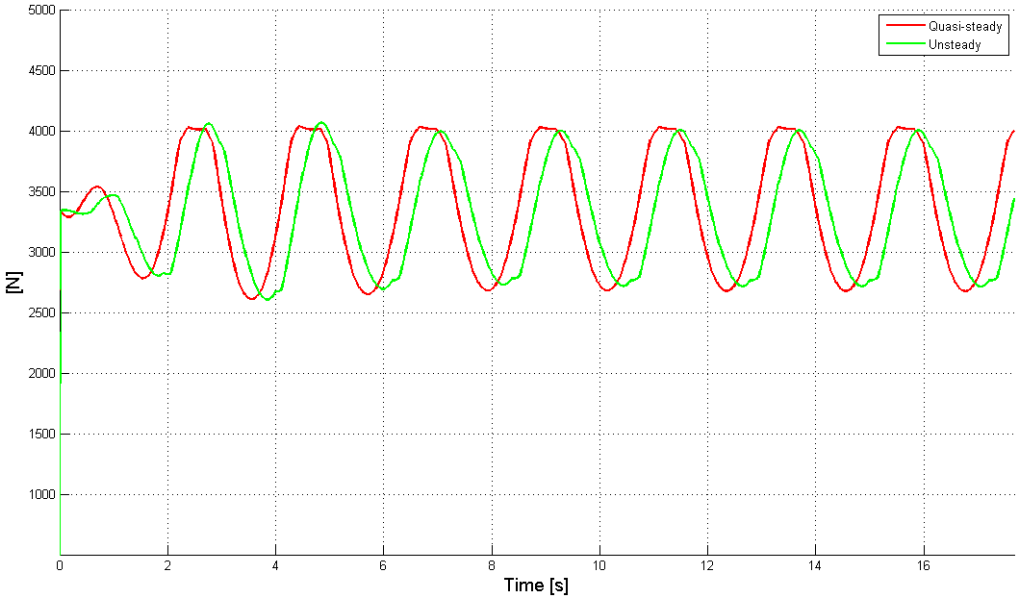

Figure 4.69: Comparison of the aerodynamic force calculated with the quasi-steady and the unsteady method. Model # 45 · Fn=0.35,$\zeta_a = 0.25$ m. Upright

After having studied the effect of the aerodynamic force on the motions, it is now interesting to investigate how, in turn, this influences the mean added resistance in waves. For this purpose the Gerritsma and Beukelman formulation was used and the motions of heave and pitch were reduced according to the findings discussed above. An example is given in Figure 4.70, in which the mean added resistance relative to model # 45 is shown. The results refer to the upright condition, considering a wave amplitude $\zeta_a = 0.25$ [m]. It can be seen that, for $\lambda/LWL = 2$, there is a considerable reduction caused by the aerodynamic sailing force. The mean added resistance is indeed reduced by 7.5%, if the quasi-steady method is used, and by nearly 19% if instead the unsteady method is adopted. It should also be noted that such a large discrepancy is mainly caused by the difference in phase of the aerodynamic force, when calculated with one method or the other. For $\zeta_a = 0.25$ [m], the two methods provide, in fact, a similar amplitude of the aerodynamic force (see Figure 4.69).

When the wave amplitude is $\zeta_a = 0.6$ [m], the results obtained using the quasi-steady or the unsteady method deviate even more considerably. The mean added resistance is reduced by only 2.5% if the quasi-steady method is used, and by 20% for the unsteady method. This large difference is due to the peculiar double-peak shape of the quasi-steady aerodynamic force, shown in Figure 4.67. Lastly, it should be noted that, for the longer waves ($\lambda/LWL = 3.5$ and $\lambda/LWL = 5$), the influence of the aerodynamic force

on the mean added resistance is considerably smaller. This holds true for both the wave amplitudes considered in this investigation.

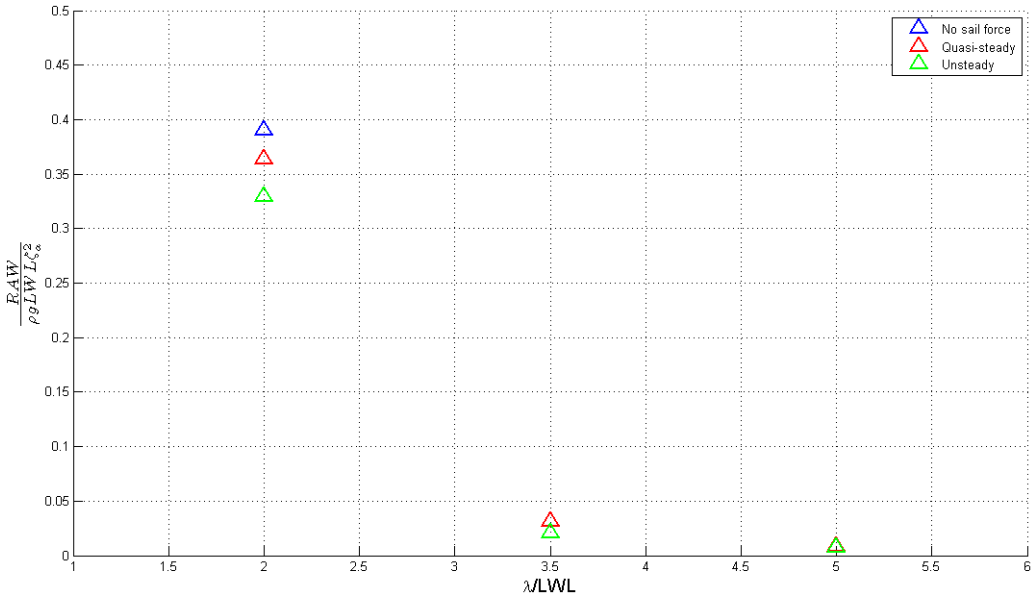

Figure 4.70: Effect of the aerodynamic sailing force on the mean added resistance. Model # 45· Fn=0.35, $\zeta_a = 0.25$ m. Upright

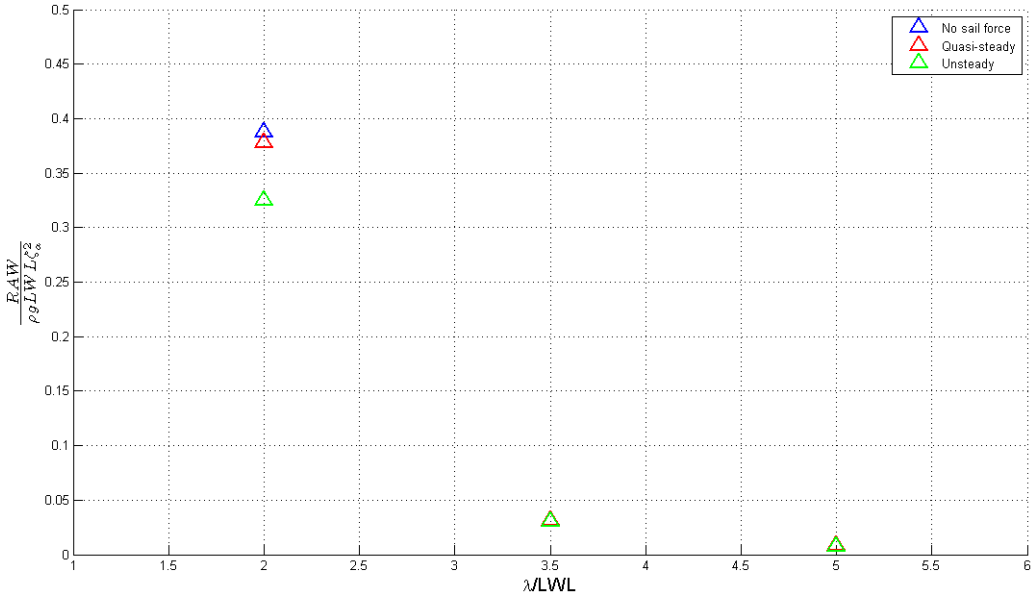

Figure 4.71: Effect of the aerodynamic sailing force on the mean added resistance. Model # 45 · Fn=0.35, $\zeta_a = 0.6$ m. Upright

Chapter 5

Conclusions

5.1 Conclusions

During the course of this thesis, various techniques were employed to investigate the five issues presented in Section1.3 that stemmed from the basic question: how are the performance of yachts influenced by the waves of the ocean? Some conclusions can now be drawn based on those particular five research questions.

From the findings of the experiments, it appears that surge generally reduces the pitch motion, but by a small amount (below 5%), and its influence on heave is negligible. As a result the mean added resistance in waves seems to be substantially unchanged. In contrast, the heeling angle proves to have a large influence on the heave and pitch motions, and on the mean added resistance. In turn, the way these are affected depends on the shape of the upright hull. This result is qualitatively in agreement with the findings of other authors who performed similar tests in the past ([32], [27] and [35]). The strip-theory program PDSTRIP, which has the ability of being able to consider asymmetric hulls, was used to investigate whether it could properly predict the effects caused by the heeling angle on the motions found during the experiments. It appears that the program does, in fact, predict a large influence of the heeling angle on the motions, but the trend is not always correct. However, the discrepancies seem to be caused by effects which strip-theory programs, by their nature, cannot take into account (i.e. effects caused the emerged part of the hull).

The effects of the trim angle on the motions and added resistance were investigated by comparing the results of the current experiments with those performed in 1995 on the same models of the DSYHS [35]. The trim angle appears to have a surprisingly large influence on the seakeeping of the models, arguably caused, at least in part, by the different testing techniques employed. Due to lack of time, it was not possible to further investigate the effects of the trim angle by using the strip-theory program PDSTRIP.

From the tests it also resulted that the surge force amplitude, although being a resistive force, has a linear dependency with the wave amplitude, rather than quadratically as its

mean does. It also appears that, in some conditions, the surge force may turn negative, becoming a propulsive force.

Finally, the time-domain simulations show that the aerodynamic force has a considerable influence on the seakeeping of yachts sailing upwind in waves. The motions of heave, and mainly pitch, are considerably reduced by the aerodynamic force, resulting in a reduction of the mean added resistance which, in some cases, may be as large as 20%. The reducing effect of the aerodynamic force on the motions depends on the motions themselves; it is large near the resonance and becomes small for the long waves at which the responses are less significant. The way the aerodynamic force is calculated appears to be of paramount importance. If the unsteady effects are taken into account (unsteady method), the aerodynamic force appears to have a more significant reducing effect on the motions than when these effects are neglected (quasi-steady method). In fact, in the case of a large wave amplitude (i.e. $\zeta_a = 0.6$ [m]), the reduction in the motions obtained by using the quasi-steady method, results to be about 50% lower than that provided by the unsteady method. This, in turn, results in a reduction of the mean added resistance that is underestimated by approximately a factor of 10 (i.e. reduction of 2.5% using the quasi-steady method and 20% using the unsteady method).

5.2 Final remarks

The results reported in this work prove that the seakeeping of sailing yachts is largely influenced by the effects caused by the sails and that in general, different yachts are affected in a different manner. The first consideration, which appears evident, is that the seakeeping abilities of sailing yachts cannot be properly studied without taking these effects into account.

The second consideration is that sails appear to have a double beneficial influence on a vessel. Apart, of course, from their capability of transforming the wind power into a propulsive force, they also work as damper for the motions, which may results in a lower dissipation of energy of the oscillating vessel in waves.

The third and final consideration is that the performance of yachts sailing in waves might be significantly improved by a proper study of the dynamic effects caused by the coupling between the aero and hydrodynamic forces and moments. Although a lot more work still needs to be done, in the author's opinion, the use of a tool (i.e. Dynamic Velocity Prediction Program) which is able to consider such a condition would allow designers to better judge the performance of their designs as well as give them the opportunity of studying innovative concepts.

Bibliography

[1] Alexandersson, M.: 2009, 'A Study of Methods to Predict Added Resistance in Waves'. MSc Thesis, KTH Centre for Naval Architecture, Stockholm.

[2] Augier, B., F. Hauville, P. Bot, and M. Durand: 2012, 'Numerical Investigation on the Unsteady Fluid Structure Interation of a Yacht Sail Plan'. *Proc. 4th High Performance Yacht Design Conference.* Auckland, RINA.

[3] Battistin, D. and L. Ledri: 2007, 'A Tool for Time Dependent Performance Prediction and Optimization of Sailing Yachts'. *Proc. 18th Chesapeake Sailing Yacht Symposium.*

[4] Bertram, V., *Practical Ship Hydrodynamics.* Butterworth and Heinemann, Oxford. 2000.

[5] Bertram, V. and K. Graf: 2006, 'Program PDSTRIP: Public Domain Strip Method'. http://sourceforge.net/projects/pdstrip/.

[6] Bertram, V., H. Söding, and K. Graf: 2006, 'PDSTRIP - A Strip Method for Ship And Yacht Seakeeping'. *9th Numerical Towing Tank Symposium.* Le Croisic, France.

[7] Bilger, R.: 1995, 'A simplified Theory for the Tacking of a Sailboat'. *12th Australasian Fluid Mechanics Conference.* Sydney.

[8] Bordogna, G.: 2012, 'Development of a Generic Dynamic VPP Based on an Unsteady Thin Airfoil Theory for Two Interacting Sails in Two-Dimensional Potential Flow'. Internship Report, Yacht Research Unit, The University of Auckland, Auckland.

[9] Claughton, A.: 1999, 'Developments in the IMS VPP Formulations'. *Proc. 14th Chesapeake Sailing Yacht Symposium.* Annapolis, SNAME.

[10] Cummins, W.: 1962, 'The Impulse Response Function and Ship Motions'. *Symposium on Ship Theory.* Institut für Shiffbau der Universität Hamburg.

[11] Day, S., L. Letizia, and A. Stuart: 2002, 'VPP VS PPP: Challenges in the Time-Domain Prediction of Sailing Yacht Performance'. *Proc. 1st High Performance Yacht Design Conference.* Auckland, RINA.

[12] Fossati, F. and S. Muggiasca: 2012, 'Motions of a Sailing Yacht in Large Waves: an Opening Simple Instationary Modelling Approach'. *Proc. 22nd HISWA symposium.* Amsterdam, RINA.

[13] Fossati, F. and S.Muggiasca: 2010, 'Numerical Modelling of Sail Aerodynamic Behaviour in Dynamic Conditions'. *Proc. 2nd International Conference on Innovation in High Performance Sailing Yachts.* Lorient, RINA.

[14] Fossati, F. and S.Muggiasca: 2011, 'Experimental Investigation of Sail Aerodynamic Behavior in Dynamic Conditions'. *Journal of Sailboat Technology, Article 2011-02.* SNAME.

[15] Fossati, F. and S.Muggiasca: 2012, 'An Experimental Investigation of Unsteady Sail Aerodynamics Including Sail Flexibility'. *Proc. 4th High Performance Yacht Desgin Conference.* Auckland, RINA.

[16] Gerhardt, F.: 2010, 'Unsteady Aerodynamics of Upwind-Sailing and Tacking'. Ph.D. thesis, Department of Mechanical Engineering. The University of Auckland. Auckland.

[17] Gerhardt, F., R. Flay, and P. Richards: 2008, 'Unsteady Aerodynamic Phenomena Associated With Sailing Upwind in Waves'. *Proc. 3rd High Performance Yacht Design Conference.* Auckland, RINA.

[18] Gerhardt, F., R. Flay, and P. Richards: 2011, 'Unsteady Aerodynamics of Two Interacting Yacht-Sails in Two-Dimensional Potential Flow'. *Journal of Fluid Mechanics.* 668: 551-581.

[19] Gerritsma, J.: 1968, 'Course Keeping Qualities and Motions in Waves of a Sailing Yacht'. Technical Report, Delft University of Technology.

[20] Gerritsma, J. and W. Beukelman: 1972, 'Analysis of the Resistance Increase in Waves of a Fast Cargo Ship'. *International Shipbuilding Progress.* 19:285-293.

[21] Gerritsma, J. and G. Moeyes: 1972, 'The Seakeeping Performance and Steering Properties of Sailing Yachts'. Technical Report, Delft University of Technology.

[22] Hanamoto, M.: 1988, 'Study on Ship Motions and Capsizing in Following Seas'. *Journal of the Society of Naval Architects of Japan.* No 147.

[23] Harris, D.: 2005, 'Time Domain Simulation of Yacht Sailing Upwind in Waves'. *Proc. 17th Chesapeake Sailing Yacht Symposium.* Annapolis, SNAME.

[24] Jackson, P.: 2001, 'An Improved Upwind Sail Model for VPP's'. *Proc. 15th Chesapeake Sailing Yacht Symposium.* Annapolis, SNAME.

[25] Jacquin, E., Y. Roux, P. Guillerm, and B. Alessandrini: 2005, 'Toward Numerical VPP with the Full Coupling of Hydrodynamic and Aerodynamic Solvers for ACC Yacht'. *Proc. 17th Chesapeake Sailing Yacht Symposium.* Annapolis, SNAME.

[26] Journée, J.: 1993, 'Hydromechanical Coefficients for Calculating Time Domain Motions of Cutter Suction Dredges by Cummins Equations'. *Report N° 968.* Delft Ship Hydromechanics Laboratory. Delft University of Technology.

[27] Kapsenberg, G.: 1990, 'A New Technique for Testing a Sailing Yacht in Waves'. *Proc. 10th Chesapeake Sailing Yacht Symposium.* SNAME.

[28] Kerwin, J.: 1976, 'A Velocity Prediction Program for Ocean Racing Yachts'. Report 78-11, Department of Ocean Engineering, Massachusetts Institute of Technology.

[29] Keuning, J., M. Katgert, and A. Mohnhaupt: 2007, 'The Use of a Manouvering Model for the Optimization of the Tacking Procedure of an IACC Sailing Yacht'. *Proc. The Modern Yacht.* Southampton, RINA.

[30] Keuning, J. and U. Sonnenberg: 1998, 'Approximation of the Hydrodynamic Forces on a Sailing Yacht based on the 'Delft Systematic Yacht Hull Series". *Proc. 15th HISWA symposium.* Amsterdam, RINA.

[31] Keuning, J. and K. Vermeulen: 2003, 'The Yaw Balance of Sailing Yachts Upright and Heeled'. *Proc. 16th Chesapeake Sailing Yacht Symposium.* Annapolis, SNAME.

[32] Klaka, K. and J. Penrose: 1987, 'Performance Prediction of Sailing Yachts in Waves'. *Conference on Yachting Technology.* University of Western Australia.

[33] Korvin-Kroukowsky, B. and W. Jacobs: 1957, 'Pitching and Heaving Motions of a Ship in Regular Waves'. SNAME Transactions.

[34] Larsson, L. and R. Eliasson, *Principles of Yacht Design.* Adlar Coles, London. 2000.

[35] Levadou, M.: 1995, 'Added Resistance in Waves of Sailing Yachts'. *Report N° 1032-S MSc Thesis.* Delft Shiphydromechanics Laboratory. Delft University of Technology.

[36] Lewis, E., *Principles of Naval Architecture.* SNAME, 1988.

[37] L.Larsson: 1990, 'Scientific Methods in Yacht Design'. *Ann. Rev. Fluid Mechanics.* Transactions 22: 349-385.

[38] Masuyama, Y. and T. Fukasawa: 2008, 'Tacking Simulation of Sailing Yachts with New Model of Aerodynamic Force Variation'. *Proc. 3rd High Performance Yacht Design Conference.* Auckland, RINA.

[39] Masuyama, Y., I. Nakamura, H. Tatano, and K.Takagi: 1993, 'Dynamic Performance of Sailing Cruiser by Full-Scale Sea Tests'. *Proc. 11th Chesapeake Sailing Yacht Symposium.* Annapolis, SNAME.

[40] Masuyama, Y., K. Nomoto, and A. Sakurai: 2003, 'Numerical Simulation of Maneuvring of 'Naniwa-maru', a Full-scale Reconstruction of Sailing Trader of Japonese Heritage'. *Proc. 16th Chesapeake Sailing Yacht Symposium.* Annapolis, SNAME.

[41] Ogilvie, H.: 1964, 'Recent Progress Towards the Understanding and Prediction of Ship Motions'. *5th Symposium on Naval Hydrodynamics.* Bergen, Norway.

[42] Ottosson, P., M. Brown, and L. Larsson: 2002, 'The Effect of Pitch Radius of Gyration on Sailing Yacht Performance'. *Proc. 1st High Performance Yacht Design Conference.* Auckland, RINA.

[43] Pérez, T. and T.I.Fossen: 2008, 'Time-vs. Frequency-domain Identification of Parametric Radiation Force Models for Marine Structures at Zero Speed'. *Modeling, Identification and Control, Vol. 29, No. 1, pp. 1-19.*

[44] Richardt, T., S. Harries, and K. Hochkirch: 2005, 'Maneuvering Simulations for Ships and Sailing Yachts using FS-Equilibrium as an Open Modular Workbench'. Hamburg.

[45] Ridder, E. D., K.J.Vermeulen, and J. Keuning: 2004, 'A Mathematical Model for the Tacking Manoeuvre of a Sailing Yacht'. *Proc. 18th HISWA symposium.* Amsterdam, RINA.

[46] Söding, H.: 1993, 'A Method for Accurate Force Calculation in Potential Flow'. *Ship Technology Research 40, pp. 176-186.*

[47] Skinner, G.: 1982, 'Sailing Vessel Dynamics: Investigations into Aero-Hydrodynamic Coupling'. MSc Thesis, Department of Oceanl Engineering, Massachussets Institute of Technology, Boston.

[48] Spens, P., P. Spens, and P.W.Brown: 1967, 'Some Further Experimental Studies of the Sailing Yacht'. SNAME.

[49] Tasai, F.: 1969, 'Improvements in the Theory of Ship Motions in Longitudinal waves'. *12th ITTC.*

[50] Ursell, F.: 1949, 'On the Heaving Motion of a Circular Cylinder on the Surface of a Fluid'. Quartely Journal of Mechanics and Applied Mathematics, Vol. II.

[51] van Oossanen, P.: 1993, 'Predicting the Speed of Sailing Yachts'. SNAME, Transactions: 101(12): 337-397.

[52] Verwerft, B. and J. Keuning: 2008, 'The Modification and Application of a Time Dependent Performance Prediction Model on the Dynamic Behaviour of a Sailing Yacht'. *Proc. 20th HISWA symposium.* Amsterdam, RINA.

Appendix A

Strip Theory and Mean Added Resistance in Waves

A.1 Strip-theory method

One of the most popular tools to study the seakeeping of ships and other floating bodies is undoubtedly the strip theory. This method, although relatively simple and inexpensive, proved to be capable of predicting the motions of the most diverse type of vessels with a satisfactory degree of accuracy.

The basic idea behind the strip theory is to divide the ship under consideration into a certain number of cross sections (typically 20 to 30). For each of them, two-dimensional added mass and damping coefficients as well as the wave loads are calculated in the frequency domain. These are then integrated over the ship length in order to obtain the three-dimensional values relative to the entire vessel. Finally, the mass and the restoring terms are computed so that the equations of motions can be solved in the frequency domain for the six degrees of freedom.

The first step towards the development of the strip theory was taken in 1949 with the publication of Ursell [50]. This used a potential-flow method to calculate the two-dimensional hydromechanical coefficients of a heaving cylinder with zero forward speed. This method has then been improved by adopting an already existing mapping technique (2-parameter Lewis conformal mapping) in order to be able to consider proper hull forms. In 1957, Korvin-Kroukowsky and Jacobs [33] made another substantial improvement by considering the effect of forward speed caused by the three-dimensional potential mass. This is often referred to as 'Ordinary Strip Theory' in opposition to the 'Modified Strip Theory', introduced in 1969 by Tasai [49], which also considered the effect of forward speed due to the potential damping.

Hereafter the equations of motion in the frequency domain as reported in PDSTRIP [5] are derived.

Velocity potential and boundary conditions

In order to calculate the two-dimensional hydromechanical coefficients of each cross section, strip-theory programs make use of linear potential theory. The fundamental assumption of this theory is that the fluid is inviscid and incompressible and the flow is irrotational (i.e. potential flow). Moreover, this theory also implies that the wave steepness is infinitely small so that the motions can be assumed to scale linearly with the wave amplitude. Once these assumptions are fulfilled, the two-dimensional wave velocity potential can be written as:

$$\phi(y,z,t) = Re\left[\hat{\phi}(y,z)\, e^{i\omega t}\right] \tag{A.1}$$

In Eq. (A.1), ω is the circular frequency of oscillation. Therefore, in the case of a ship with forward speed, this coincides with the frequency of encounter, which is defined as:

$$\omega_e = \omega - k \cdot Vs \cdot cos\mu \tag{A.2}$$

Being two-dimensional, the flow is assumed to be excited only by sinusoidal translations of the body along the Y and Z axis (sway and heave), and sinusoidal rotations about the X-axis (roll).

In order to be properly solved, the velocity potential needs to satisfy a number of boundary conditions.

Laplace equation: The Laplace equation is directly derived from the continuity equation and is needed to enforce the condition of incompressibility to the flow. The equation reads:

$$\nabla^2\phi = \frac{\partial\phi}{\partial y^2} + \frac{\partial\phi}{\partial z^2} = 0 \tag{A.3}$$

Seabed boundary condition: This boundary condition is needed to prevent the flow from leaking through the seabed. Thus the vertical velocity of the water particles is imposed to be zero at z=h, being h the water depth:

$$\frac{\partial\phi}{\partial z} = 0 \tag{A.4}$$

Dynamic boundary condition at the free surface: The dynamic boundary condition is necessary to impose that, at free surface of the fluid $z = \zeta$, the pressure p is equal to the atmospheric pressure. This is done by considering the linearised Bernoulli equation:

$$p = -\rho \cdot \frac{\partial\phi}{\partial t} - \rho \cdot g \cdot z \tag{A.5}$$

At the free surface the pressure is constant, thus, because of the linearisation, the vertical velocity of a water particle becomes:

$$\frac{dz}{dt} = \frac{\partial \phi}{\partial t} \approx \frac{\partial \zeta}{\partial t} \tag{A.6}$$

Combining these two requirements, the following boundary condition is obtained:

$$\frac{\partial^2 \phi}{\partial t^2} + g \cdot \frac{\partial \phi}{\partial z} = 0 \quad \text{for z=0} \tag{A.7}$$

Kinematic boundary condition on the body surface: This boundary condition is to prevent the fluid from leaking into the oscillating body. The velocity of the a water particle at a certain point on the submerged hull needs therefore to be equal to the velocity of that point. This can be written as:

$$\nabla \phi \cdot \vec{n} = \vec{v} \cdot \vec{n} \quad \text{Along the hull contour} \tag{A.8}$$

In which $\vec{v}$ is the motion velocity of the floating body at that contour point and $\vec{n}$ is the inward unit normal on the contour.

Radiation condition: The radiation boundary condition states that the value of the potential tends to zero as the distance R of a water particle from the oscillating body increases. In mathematical terms this is:

$$\lim_{R \to \infty} \phi = 0 \tag{A.9}$$

Finally, using Eq.(A.1), the boundary conditions for the complex amplitude of the potential become:

$$\text{Laplace:} \quad \frac{\partial \hat{\phi}}{\partial y^2} + \frac{\partial \hat{\phi}}{\partial z^2} = 0 \quad \text{For z>0 and outisde the body} \tag{A.10}$$

$$\text{Seabed:} \quad \frac{\partial \hat{\phi}}{\partial z} = 0 \quad \text{at z=h} \tag{A.11}$$

$$\text{Free surface:} \quad \frac{\omega^2}{g} \cdot \hat{\phi} + \frac{\partial \hat{\phi}}{\partial z} = 0 \quad \text{at z=0} \tag{A.12}$$

$$\text{Hull:} \quad \nabla \hat{\phi} \cdot \vec{n} = \vec{v} \cdot \vec{n} \quad \text{Along the hull contour} \tag{A.13}$$

$$\text{Radiation:} \quad \frac{\partial \hat{\phi}}{\partial y} = \pm \mathrm{i} k \hat{\phi} \tag{A.14}$$

Solution method for the radiation problem

The solution method employed by PDSTRIP is called patch method and it approximates the potential $\hat{\phi}$ as a superposition of point sources defined as:

$$\hat{\phi}(y,z) = \sum_{i=1}^{n} q_i \frac{1}{2} \ln\left[(y-y_i)^2 + (z-z_i)^2\right] \tag{A.15}$$

The term q_i indicates the strength of the n sources located at (y_i,z_i). This satisfies the Laplace equation everywhere but at the location of the sources. For this reason, the sources are located within the hull contour and just above the free surface at $z = 0$.

One source is generated near the midpoint of each segment between two points. This is true for the offset points of the submerged hull, as well as for the free-surface points. The total number of free-surface grid points is 110 (55 for each side) and, in order to be able to consider asymmetrical hulls, both sides need to be discretized.

The patch method satisfies the integral of boundary conditions over each segment. For the kinematic boundary condition on the body surface this is simply done by using the following expression:

$$\int_A^B \nabla\hat{\phi} \cdot \vec{n} \cdot ds \tag{A.16}$$

Eq. (A.16) states that a flux induced by a source located at S, through a segment between points A and B, is equal to the source strength multiplied by the angle ASB and divided by 2π. This same method is also used for the second term in the boundary condition at the free surface ($\frac{\partial\hat{\phi}}{\partial z}$). On the other hand, the first term of this boundary condition is approximated according to:

$$\int_A^B \hat{\phi} \cdot ds \approx \frac{1}{2} \cdot \{\phi(A + 0.316 \cdot [B-A]) + \phi(A + 0.684 \cdot [B-A])\} \cdot |B-A| \tag{A.17}$$

The constants 0.316 and 0.684 are determined such that the integral is correctly approximated near the midpoint of the segment AB.
The seabed boundary condition is satisfied exactly by mirroring at points $(y_i, 2h - z_i)$ all the sources below the bottom, being a source located at (y_i, z_i). In order to improve the accuracy of the vertical motions, additional sources are placed at y=0 and at a distance above the free surface equal to half of the distance of the furthest free-surface grid point.

The radiation boundary condition is satisfied by considering the integral over a segment between point A, near the body, and a point B, far away from it. The same type of approximation shown in Eq. (A.17) is used, resulting in:

$$\phi_B - \phi_A = \pm\frac{ik}{2} \{\phi(A + 0.316 \cdot [B-A]) + \phi(A + 0.684 \cdot [B-A])\} \cdot (y_B - y_A) \tag{A.18}$$

from which follows:

$$i\left(\phi_B-\phi_A\right)-\frac{k}{2}\cdot|y_B-y_A|\cdot\left\{\phi\left(A+0.316\cdot[B-A]\right)+\phi\left(A+0.684\cdot[B-A]\right)\right\}=0 \quad \text{(A.19)}$$

The manner in which the radiation boundary condition is satisfied is of paramount importance for the accuracy of the method. For this purpose, it is improved as explained hereafter.
Waves with decreasing amplitude in the direction of the wave propagation are generated using a complex number of the form:

$$k=k_r+ik_i \quad \text{(A.20)}$$

in which k_i is a negative wave number. This generates a damping region at some distance from the body which is advantageous in the outer range of the free surface. The imaginary part of the wave number k of Eq. (A.20) introduces into Eq. (A.19) the term:

$$ik_i\cdot|y_B-y_A|\cdot\phi_{average} \quad \text{(A.21)}$$

Now, taking the derivative of the radiation boundary condition with respect to y, i.e.:

$$\frac{\partial\phi}{\partial y^2}=-k^2\cdot\phi \quad \text{(A.22)}$$

the term described in Eq. (A.21) transforms into:

$$i\frac{k_i}{k^2}\cdot|y_B-y_A|\cdot\frac{\partial\phi_{average}}{\partial y^2} \quad \text{(A.23)}$$

This can be interpreted as a Taylor expansion of the first term of Eq. (A.19) with reference to potentials ϕ shifted by δy from the original points A and B:

$$i\left[\phi\left(y_B+\delta_y\right)-\phi\left(y_A+\delta_y\right)\right]\approx i\left[\phi\left(y_B\right)-\phi\left(y_A\right)\right]+i\delta_y\left(y_B-y_A\right)\cdot\frac{\partial\phi_{average}}{\partial y^2} \quad \text{(A.24)}$$

On the other hand, the Taylor expansion of the second term of Eq. (A.19) corresponds to (A.23) if the following condition holds:

$$\pm\frac{k_i}{k^2}\approx\pm\frac{k_i}{k_r^2}=\delta_y \quad \text{(A.25)}$$

The potentials ϕ_A and ϕ_B are in fact determined not at y_A and y_B but instead at $y_A\pm k_i/k_r^2$ and $y_B\pm k_i/k_r^2$, respectively.

To gain further accuracy, for each frequency the calculations are performed twice considering 2 different values of the distance y_D at which the damping region on the free surface

begins. The 2 values of y_D differ 1/4 of the radiated wave length from each other and the results found in both the calculations are averaged.
The 55 free-surface panels considered for each side of the body are divided into 2 areas of 25 and 28 panels. In the first area only the free-surface boundary condition is satisfied, while in the second one the radiation boundary condition.

The linear equation system which is obtained by considering the boundary conditions is then solved in order to find the complex values of the sources' strenght. The velocity potential is then obtained from equation Eq.(A.15).
Now, the pressure on the body contour can be calculated by considering Bernoulli's equation:

$$p = -\rho \frac{\partial \phi}{\partial t} \tag{A.26}$$

The pressure amplitude is then integrated over each cross-section contour so that the complex values of the sway and heave force, and roll moment are obtained.

Let us now consider only one of the force terms, $\hat{f}$, caused by one of the 3 motion amplitudes $\hat{u}$ and rewrite it as:

$$\hat{f} = -\hat{n} \cdot \left(-\omega^2 \hat{u}\right) \tag{A.27}$$

The term $\hat{n}$ can be interpret as the complex added mass as the term $-\omega^2\hat{u}$ is the complex amplitude of the sinusoidal acceleration. However, the complex force $\hat{f}$ may also be considered as the sum of an added mass and a damping term:

$$\hat{f} = -n \cdot \left(-\omega^2 \hat{u}\right) - d\left(i\omega\hat{u}\right) \tag{A.28}$$

in which $i\omega\hat{u}$ is the complex amplitude of the sinusoidal velocity. Both Eq.(A.27) and Eq.(A.28) hold only if the following condition is met:

$$\hat{n} = n - \frac{id}{\omega} \tag{A.29}$$

This explains the relation between the complex added mass, real added mass and damping. The relation reported in Eq. (A.29) holds for each of the 3 forces and the 3 motions which generate the 3-by-3 matrix G containing the added mass and damping terms.
This is done for each cross section of the body.

Sectional wave-excitation forces

The wave-excitation forces comprise the Froude-Krilov forces and the diffraction forces. The former is obtained by considering the dynamic pressure in a wave on a non-moving cross section, neglecting the influence of the section on the pressure. The latter is due to the pressure change caused by the presence of the non-moving section.

Considering the complex amplitude of the wave pressure as:

$$\hat{p} = \rho \cdot \frac{-\omega^2 e^{iky\sin\mu}}{2k\sinh kh} \cdot \left(e^{k(z-H)} + e^{-k(z-h)}\right) \tag{A.30}$$

the Froude-Krilov force can be computed as the integral of the wave pressure over each segment of each section of the body:

$$\int_{\vec{x}_{i-1}}^{\vec{x}_i} \hat{p} ds = -\rho g \frac{e^{iky_{i-1}\sin\mu}}{2k\cosh kh} \cdot \left(e^{kz_1}e^{-kh}\frac{e^{k(\Delta z + i\Delta y\sin\mu)}-1}{k\left(\Delta z + i\Delta y\sin\mu\right)} + e^{-kz_1}e^{kh}\frac{e^{k(-\Delta z + i\Delta y\sin\mu)}-1}{k\left(-\Delta z + i\Delta y\sin\mu\right)}\right) \cdot |\vec{x}_i - \vec{x}_{i-1}| \tag{A.31}$$

in which $\Delta y = y_i - y_{i-1}$ and $\Delta z = z_i - z_{i-1}$, being $\vec{x}_i = (y_i, z_i)$ and $\vec{x}_{i-1} = (y_{i-1}, z_{i-1})$ two adjacent points on the body contour. The total Froude-Krilov force of each cross section is the sum of the integrals over each segment.

The diffraction forces and moment are computed similarly to the added mass forces and moment. However, now the inhomogeneous terms in the body boundary condition are treated as the fluxes which would occur between a panel endpoints $\vec{x}_i$ and $\vec{x}_{i-1}$ in case there was no change of the wave-induced flow caused by the presence of the body. In the diffraction calculation, these fluxes need to cancel out with the source-generated flow. Mathematically the fluxes can be written as:

$$\begin{aligned}\int_{\vec{x}_{i-1}}^{\vec{x}_i} \left(\hat{\phi}_y, \hat{\phi}_z\right) d\vec{x} = \frac{-i\omega e^{iky_{i-1}\sin\mu}}{2k\sinh kh} \cdot [e^{kz_1}e^{-kh}\frac{e^{k(\Delta z + i\Delta y\sin\mu)}-1}{k\left(\Delta z + i\Delta y\sin\mu\right)} \cdot (\Delta y - i\Delta z\sin\mu) \\ + e^{-kz_1}e^{kh}\frac{e^{k(-\Delta z + i\Delta y\sin\mu)}-1}{k\left(-\Delta z + i\Delta y\sin\mu\right)} \cdot (\Delta y + i\Delta z\sin\mu)] \cdot |\vec{x}_i - \vec{x}_{i-1}|\end{aligned} \tag{A.32}$$

Integration over the ship length

Once the two-dimensional hydromechanical coefficients have been obtained they need to be integrated over the ship length also taking into account the effect of the forward speed of the ship as described by the Ordinary Strip Theory.
First, let us consider the 3-component force vector $\vec{\hat{f}}_x$ which is proportional to the 3-component motion vector $\vec{\hat{u}}_x = \{\hat{u}_2, \hat{u}_3, \hat{u}_4\}$. This can also be rewritten as:

$$\vec{\hat{f}}_x = G\omega_e^2 \vec{\hat{u}}_x = \begin{bmatrix} \hat{n}_{2,2} & \hat{n}_{2,3} & \hat{n}_{2,4} \\ \hat{n}_{3,2} & \hat{n}_{3,3} & \hat{n}_{3,4} \\ \hat{n}_{4,2} & \hat{n}_{4,3} & \hat{n}_{4,4} \end{bmatrix} \cdot \omega_e^2 \vec{\hat{u}}_x \tag{A.33}$$

The elements of the complex added mass matrix G can be interpreted as real-value added mass and damping. For each element, the first index refers to the force component while the second index refers to the motion component causing the force. It should also be noted that the motions and moments refer to the origin of the cross section at $y = 0$ and $z = 0$.

Eq.(A.33) can be rewritten as:

$$\vec{\hat{f}}_x = \left(-i\omega_e + Vs \cdot \frac{d}{dx}\right) \cdot G \cdot \left(\omega_e^2 \vec{\hat{u}}_x\right) \tag{A.34}$$

and this can be interpreted as the substantial derivative of the momentum, also taking into account the forward speed of the ship Vs.

The 6-by-6 complex added mass matrix D relative to the entire ship is then obtained according to:

$$\mathrm{D} = \int_L V \cdot \left(-i\omega_e + Vs \cdot \frac{d}{dx}\right) \cdot G \cdot W \, dx \tag{A.35}$$

in which V is the transformation matrix between the 3-component cross-section force $\vec{\hat{f}}_x$ and the global force:

$$V = \begin{bmatrix} 0 & 0 & 0 \\ 1 & 0 & 0 \\ 0 & 1 & 0 \\ 0 & 0 & 1 \\ 0 & -x & 0 \\ x & 0 & 0 \end{bmatrix} \tag{A.36}$$

Also, W is the transformation matrix between the 3-component cross-section velocity $\vec{\hat{u}}_x$ and the 6-component motions of the ship:

$$W = \begin{bmatrix} 0 & i\omega_e & 0 & 0 & 0 & i\omega_e x \\ 0 & 0 & i\omega_e & 0 & -i\omega_e x + Vs & 0 \\ 0 & 0 & 0 & i\omega_e & 0 & 0 \end{bmatrix} \tag{A.37}$$

As it occurs in any strip-theory program, the surge added mass and damping cannot be computed with the procedure described above, thus they need to be calculated or estimated in other ways. In PDSTRIP it is assumed that the surge damping is zero whereas the surge added mass can be approximated with the following empirical formula:

$$n_{11} = \frac{m}{\pi \cdot \sqrt{\rho L_{pp}^3 / m} - 14} \tag{A.38}$$

The additional 6-by-6 matrix ΔD, which includes the influence of the surge added mass on all the other terms, is computed as:

$$\Delta \mathrm{D} = \omega_e^2 n_{11} \vec{U} \vec{U}^T \tag{A.39}$$

in which U is the transformation vector:

$$U = \begin{Bmatrix} 1 \\ 0 \\ 0 \\ 0 \\ z_S \\ -y_S \end{Bmatrix} \tag{A.40}$$

and (y_S,z_S) indicates the center of the cross sections. The total 6-by-6 radiation matrix is finally obtained by summing D and ΔD.

In a similar manner the global force vector is calculated.

First, let $\hat{\vec{f}}_{e,x}$ be the complex amplitude 3-component force vector which acts on each cross section of the body. This vector is proportional to the complex amplitude $\hat{\zeta}_x$ of the wave at $x = y = 0$. This force vector consists of the Froude-Krilov component (index 0) and the diffraction component (index 7), so that:

$$\hat{\vec{f}}_{e,x} = \left(\hat{\vec{f}}_{e,x0} + \hat{\vec{f}}_{e,x7}\right) \cdot \hat{\zeta}_x \tag{A.41}$$

For a ship with forward speed, similarly to Eq. (A.34), $\hat{\vec{f}}_{e,x7}$ should be replaced by:

$$\hat{\vec{f}}_{e,x7} - \frac{Vs}{i\omega} \cdot \frac{d\hat{\vec{f}}_{e,x7}}{dx} \tag{A.42}$$

Moreover, the complex amplitude of the wave elevation ζ of a regular Airy wave can be written as:

$$\hat{\zeta}_x = \hat{\zeta}_0 e^{-ikx\cos\mu} \tag{A.43}$$

The first part of the global force vector thus becomes:

$$\hat{\vec{f}}_{e,1} = \int_L V \cdot \left(\hat{\vec{f}}_{e,x0} + \hat{\vec{f}}_{e,x7} + \frac{Vs}{i\omega} \cdot \frac{d\hat{\vec{f}}_{e,x7}}{dx} \right) \cdot e^{-1kx\cos\mu}\, dx \cdot \hat{\zeta}_0 \tag{A.44}$$

In order to better calculate the motions of surge, yaw and pitch, the longitudinal wave force should also be considered. However, only the Froude-Krilov component of this force may be taken into account as the diffraction part is negligibly small. This component can be written as:

$$\int_L \hat{p} \frac{dA_x}{dx} dx + \hat{p}_{tr} A_{tr} \tag{A.45}$$

in which, $\hat{p}$ is the complex value of the pressure at the center of the cross section and A_x is the area of the cross section. The term relative to the transom (A_{tr}) is zero if there is no transom stern or in case the transom stern is wetted at zero or low speed.

Now, the second part of the global force vector can be written as:

$$\hat{\vec{f}}_{e,2} \left(\int_L \begin{Bmatrix} 1 \\ 0 \\ 0 \\ 0 \\ z_S \\ -y_S \end{Bmatrix} \cdot \alpha \frac{dA_x}{dx} e^{-ikx\cos\mu} dx + \begin{Bmatrix} 1 \\ 0 \\ 0 \\ 0 \\ z_S \\ -y_S \end{Bmatrix} \cdot \alpha A_{tr} e^{-ikx_{tr}\cos\mu} \right) \cdot \hat{\zeta}_0 \tag{A.46}$$

in which the term α is defined as:

$$\alpha = -\rho g e^{-k(z_x+T)} e^{iky_x \sin\mu} \tag{A.47}$$

Finally, the global force vector is obtained by summing the two components:

$$\hat{\vec{F}}_e = \hat{\vec{f}}_{e,1} + \hat{\vec{f}}_{e,2}$$

Mass matrix and hydrostatics matrix

The last elements necessary to solve the equations of motion are the mass matrix M, and the matrix C containing the hydrostatic restoring terms. These are defined as follows:

$$M = \begin{bmatrix} m & 0 & 0 & 0 & mz_G & -my_G \\ 0 & m & 0 & -mz_G & 0 & mx_G \\ 0 & 0 & m & my_G & -mx_G & 0 \\ 0 & -mz_G & my_G & I_{xx} & -I_{xy} & -I_{xz} \\ mz_G & 0 & -mx_G & -I_{xy} & I_{yy} & -I_{yz} \\ -my_G & mx_G & 0 & -I_{xz} & -I_{yz} & I_{zz} \end{bmatrix} \tag{A.48}$$

$$C = \begin{bmatrix} 0 & 0 & \rho g A_{tr} & \rho g y_{tr} A_{tr} & -\rho g x_{tr} A_{tr} + gm \; -\rho g \int A_x dx & 0 \\ 0 & 0 & 0 & \rho g \int A_x dx - gm & 0 & 0 \\ 0 & 0 & \rho g \int B dx & \rho g \int y_W B dx & -\rho g \int x B dx & 0 \\ 0 & 0 & \rho g \int y_W B dx & \rho g \int y_W^2 B dx + gm z_G \; -\rho g \int A_x z_S dx & -\rho g \int x y_W B dx & 0 \\ 0 & 0 & \rho g z_{tr} A_{tr} \; -\rho g \int x B dx & \rho g y_{tr} z_{tr} A_{tr} \; -\rho g \int x y_W B dx & -\rho g \int A_x z_S dx \; +gm z_G + \rho g \int x^2 B dx & 0 \\ 0 & 0 & -\rho g y_{tr} A_{tr} & \rho g \int x A_x dx - gm x_G \; -\rho g y_{tr}^2 A_{tr}^2 & -gm y_G \; +\rho g \int y_S A_x dx & 0 \end{bmatrix} \tag{A.49}$$

Solving the equations of motion in the frequency domain

The equations of motion can now be written as:

$$\left(-\omega_e^2 M - D + C\right) \cdot \hat{\vec{u}} = \hat{\vec{F}}_e \tag{A.50}$$

Once the system is solved for $\hat{\vec{u}}$, the RAO of each motion can be calculated. In particular, the real amplitude of the motions is obtained by taking the absolute value of $\hat{\vec{u}}$, whereas the phase shift between the response and the exciting wave can be calculated as the ratio between the imaginary and the real part of $\hat{\vec{u}}$.

A.2 Mean added resistance in waves

The Gerritsma and Beukelman [20] formulation for the mean added resistance, introduced in 1972, it is based on the concept of energy dissipation. The main hypothesis is that energy is carried away from a ship by the radiated waves generated by its oscillations and this is experienced by the ship as an additional resistance.

According to [20], the mean added resistance is calculated by considering regular waves so that the radiated energy for one period of oscillation can be written as:

$$E = \int_0^{T_e} \int_0^{LWL} d' \cdot V_{zb}^2 \cdot dx \cdot dt \tag{A.51}$$

The term d' indicates the sectional damping coefficients of each strip, corrected for the effects due to forward speed. Mathematically this becomes:

$$d' = d_{3,3} - Vs \cdot \frac{dn_{3,3}}{dx} \tag{A.52}$$

in which $d_{3,3}$ is the sectional heave damping and $n_{3,3}$ is the sectional heave added mass.

The term V_{zb} in Eq.(A.51) refers to the mean relative vertical velocity between the ship and the wave and, according to [1], can be defined as:

$$V_{zb} = -Vs \cdot \theta - \dot{x}_3 + x \cdot \dot{\theta} + i \cdot \omega \cdot \zeta_a \cdot e^{kz} \cdot e^{i(\omega_e t - kx \cdot \cos\mu)} \tag{A.53}$$

Being V_{zb} a harmonic function, it can also be written in the form:

$$V_{zb} = |V_{zb}| \cdot \cos\left(\omega_e t + \epsilon_{zb}\right) \tag{A.54}$$

so that the time integral in Eq.(A.51) can be computed as:

$$E = \int_0^{T_e} \int_0^{LWL} d' \cdot V_{zb}^2 \cdot dx \cdot dt = \frac{T_e}{2} \cdot \int_0^{LWL} d' \cdot |V_{zb}^2| \cdot dx_b = \frac{\pi}{\omega_e} \cdot \int_0^{LWL} d' \cdot |V_{zb}^2| \cdot dx \tag{A.55}$$

The radiated energy during one period of oscillation can also be defined in terms of added resistance according to the following formulation:

$$E = R_{aw} \cdot \lambda_\mu = R_{aw} \cdot \left(\frac{\lambda}{-\cos\mu}\right) = R_{aw} \cdot \left(\frac{2\pi}{-k \cdot \cos\mu}\right) \tag{A.56}$$

From this follows the mean added resistance in waves R_{aw}:

$$R_{aw} = \left(\frac{-k \cdot \cos\mu}{2 \cdot \omega_e}\right) \cdot \int_0^{LWL} d' \cdot |V_{zb}^2| \cdot dx \tag{A.57}$$

Appendix B

Derivation of the Cummins Equations

The derivation of the Cummins Equations presented hereafter follows from [26].

Applying the impulse theory to the study of the seakeeping of ships, a certain floating body can be assumed to be a linear system. The velocities due to its translations and rotations are considered to be the input, and the reaction forces and moments of the water surrounding the body, the output. At the time $t = 0$, the body is assumed to be at rest. However, after having applied a velocity V for a short time Δt, an impulsive displacement Δx is obtained, so that:

$$\Delta x = V \cdot \Delta t \tag{B.1}$$

Being the system linear, potential theory can be used to compute the velocity of the surrounding water particles due to the displacement of the body. A velocity potential, proportional to the velocity V, can then be defined as:

$$\phi = V \cdot \Psi \quad \text{for } t_0 < t < t_0 + \Delta t \tag{B.2}$$

in which Ψ is the normalized velocity potential. As a result of the impulsive displacement Δx, the water particles will continue to move so that the velocity potential can be assumed to be proportional to Δx:

$$\phi = \chi \cdot \Delta x \quad \text{for t}{>}t_0 + \Delta t$$

Again, χ is the normalized velocity potential.

As it can be seen, according to the impulse theory, the system has a 'memory'. In fact a certain impulsive displacement Δx influences the motions of the surrounding water during the time in which it occurs, as well as the motions at any other point further in time. The

total displacement of a body can then be considered as the succession of all the impulsive displacements which occurred in time. Mathematically, this can be written as:

$$\phi(t) = \sum_{j=1}^{6} \left\{ V_{j,n} \cdot \Psi_j + \sum_{k=1}^{n} \left[\chi_j \left(t_{n-k}, t_{n-k} + \Delta t \right) \cdot V_{j,n} \cdot \Delta t \right] \right\} \tag{B.3}$$

in which the index n denotes the number of time steps and the index 6 refers to the 6 degrees of freedom. Moreover, letting Δt go to zero, Eq.(B.3) becomes:

$$\phi(t) = \sum_{j=1}^{6} \left\{ \dot{x}_j(t) \cdot \Psi_j + \int_{-\infty}^{t} \chi_j(t-\tau) \cdot \dot{x}_j(\tau) \cdot d\tau \right\} \tag{B.4}$$

in which $\dot{x}_j$ is the j^{th} velocity component at time t. After having calculated the pressure p using Bernoulli's equation, and having integrated it over the submerged hull of the floating body S, the hydrodynamic reaction forces and moments become:

$$F_i = \sum_{i=1}^{6} \left\{ A_{i,j} \cdot \ddot{x}_j(t) + \int_{-\infty}^{t} K_{i,j}(t-\tau) \cdot \dot{x}_j(\tau) \cdot d\tau \right\} \quad \text{for } i = 1, 2....6 \tag{B.5}$$

The term $A_{i,j}$ is defined as:

$$A_{i,j} = \rho \iint_S \Psi_j \cdot n_i \cdot dS \tag{B.6}$$

and the term $K_{i,j}$ as:

$$K_{i,j} = \rho \iint_S \frac{\partial \chi_j(t-\tau)}{\partial t} \cdot n_i \cdot dS \tag{B.7}$$

Taking into account the mass terms $M_{i,j}$, the hydrostatic restoring terms $C_{i,j}$ (described in (A.1)) and the external loads, the following equations of motion are obtained:

$$\sum_{j=1}^{6} \left\{ (M_{i,j} + A_{i,j}) \cdot \ddot{x}_j(t) + \int_{-\infty}^{t} K_{i,j}(t-\tau) \cdot \dot{x}_j(\tau) \cdot d\tau + C_{i,j} \cdot x_j \right\} = X_i(t) \tag{B.8}$$

Finally, replacing τ with $t - \tau$ and changing the integration boundaries, Eq.(B.8) can be rewritten as:

$$\sum_{j=1}^{6} \left\{ (M_{i,j} + A_{i,j}) \cdot \ddot{x}_j(t) + \int_{0}^{\infty} K_{i,j}(\tau) \cdot \dot{x}_j(t-\tau) \cdot d\tau + C_{i,j} \cdot x_j(t) \right\} = X_i(t) \tag{B.9}$$

These equations of motion are generally referred to as the Cummins Equations.

Appendix C

Reliability of the Experiments

After having completed the towing-tank experiments, a number of tests were repeated in order to investigate their reliability. Due to the short time available, the repeated tests were performed using model # 43 only, and just for a certain number of conditions. The results reported hereafter were obtained using either a wave amplitude $\zeta_a = 25$ [mm] or $\zeta_a = 35$ [mm], depending on the wave length used. This is indicated in the legend of each graph.

As it can be seen looking at Figure C.1 to Figure C.15, independently of the condition considered, the motions of heave and pitch appear to have a good degree of reliability. This also holds for the mean added resistance in waves, measured for a forward speed Fn=0.325 (see Figure C.3 and Figure C.12). However, for Fn=0.4, the results relative to the mean added resistance appear to have a poor degree of repeatability and thus should be deemed as unreliable. This is shown in Figure C.6, Figure C.9 and Figure C.15. Although reliability tests were not performed for model # 45, it is assumed that similar results would be obtained.

It is not well understood why the measurements of the mean added resistance relative to Fn=0.4 have such a large scatter, however, it is arguably due to the large vibrations in the setup caused by the high forward speed.

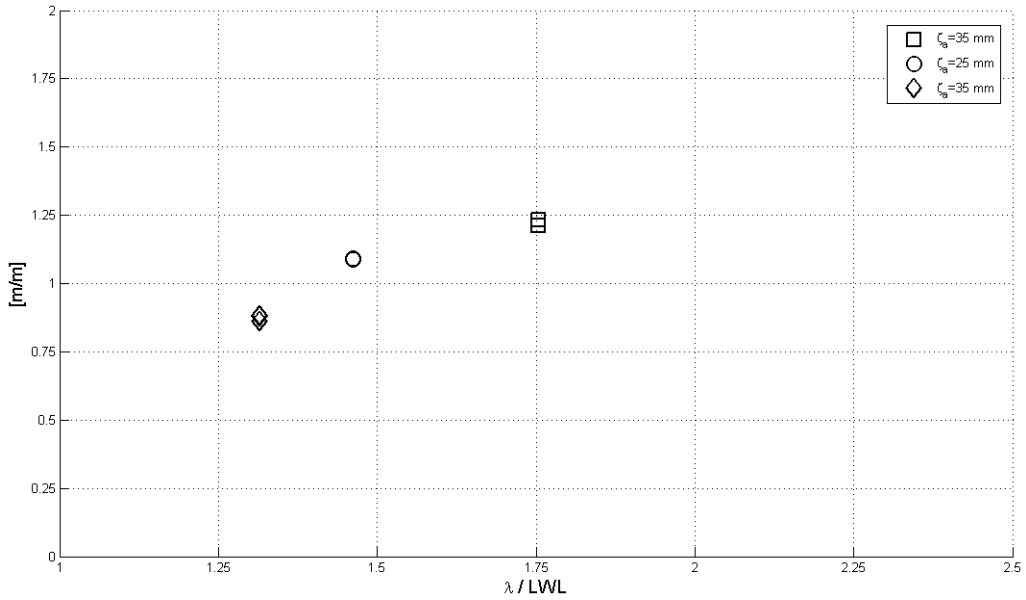

Figure C.1: Accuracy study - Heave: Upright, Fn=0.325, No surge

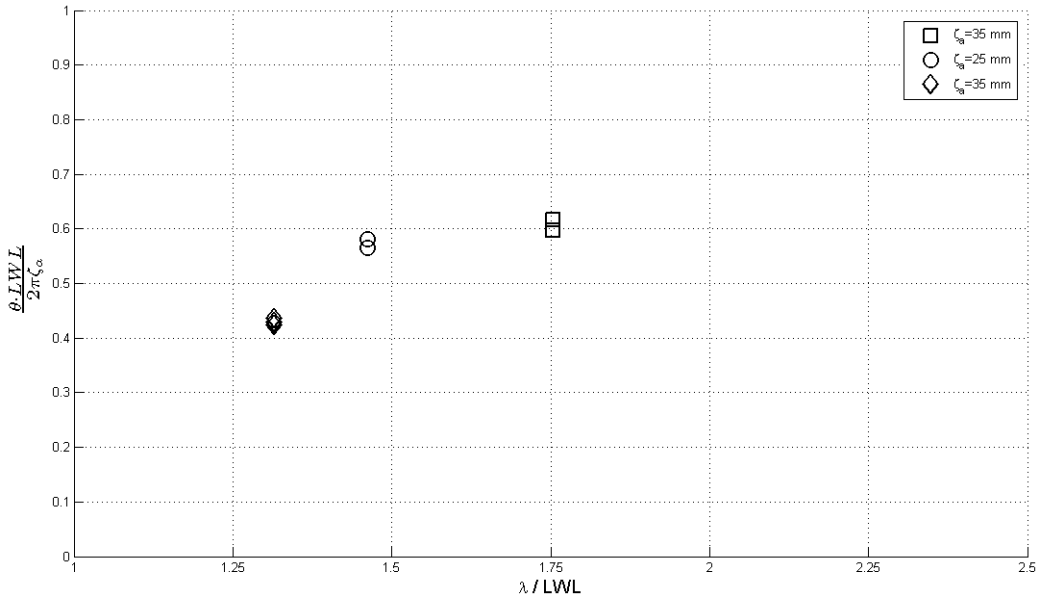

Figure C.2: Accuracy study - Pitch: Upright, Fn=0.325, No surge

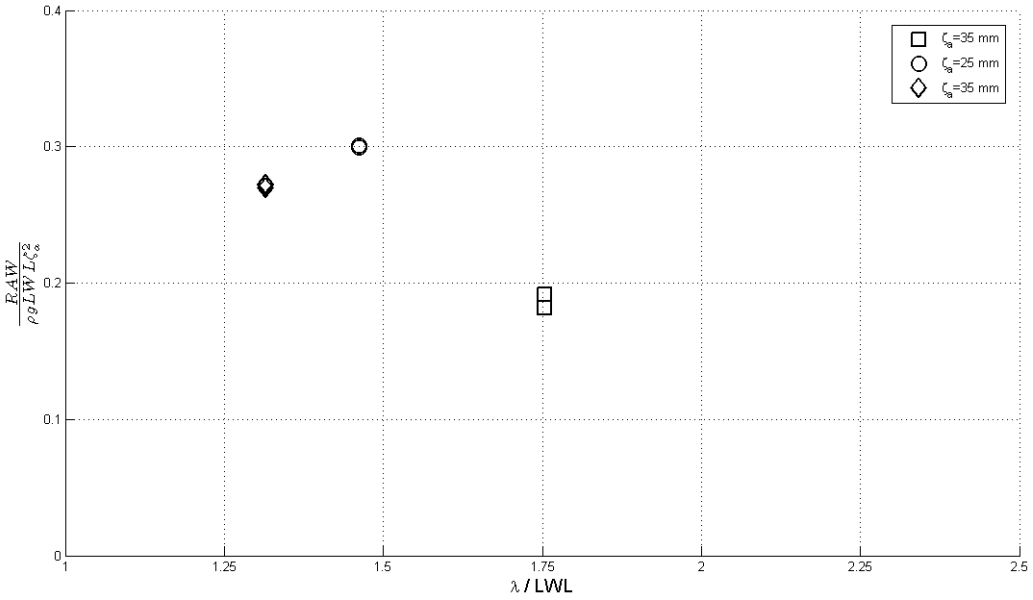

Figure C.3: Accuracy study - Added resistance: Upright, Fn=0.325, No surge

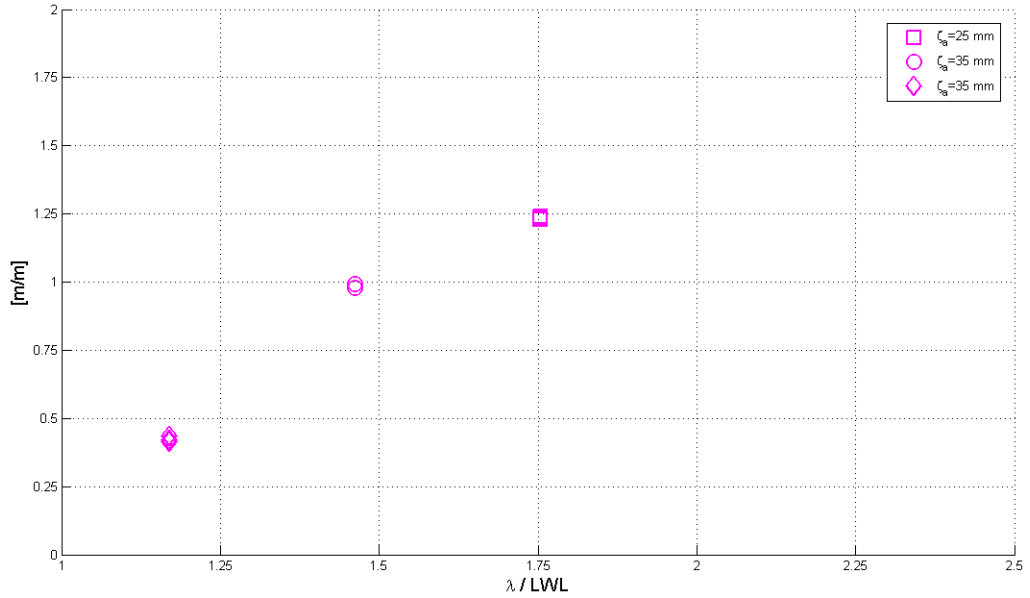

Figure C.4: Accuracy study - Heave: Upright, Fn=0.4, No surge

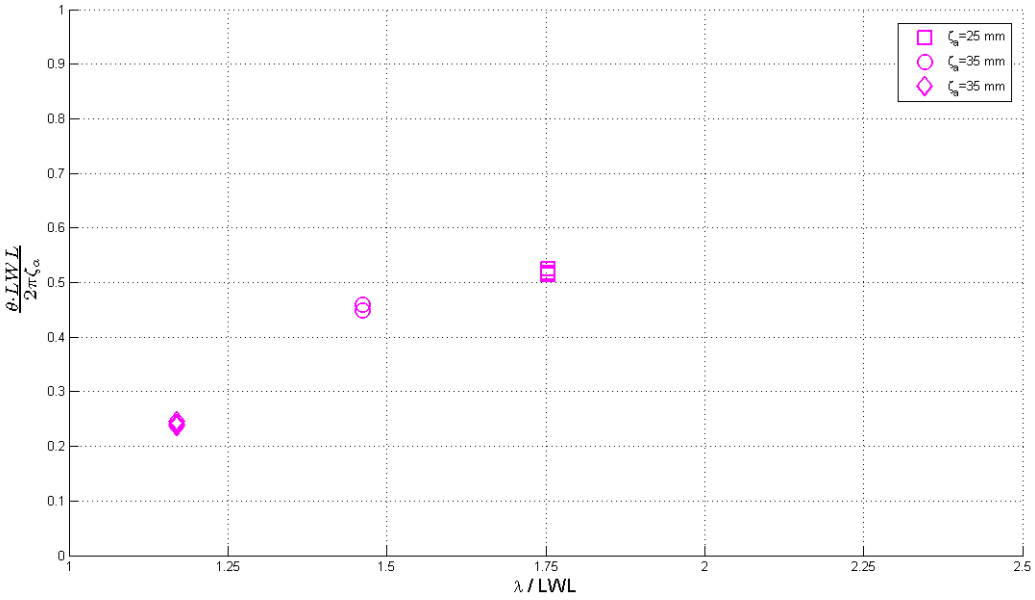

Figure C.5: Accuracy study - Pitch: Upright, Fn=0.4, No surge

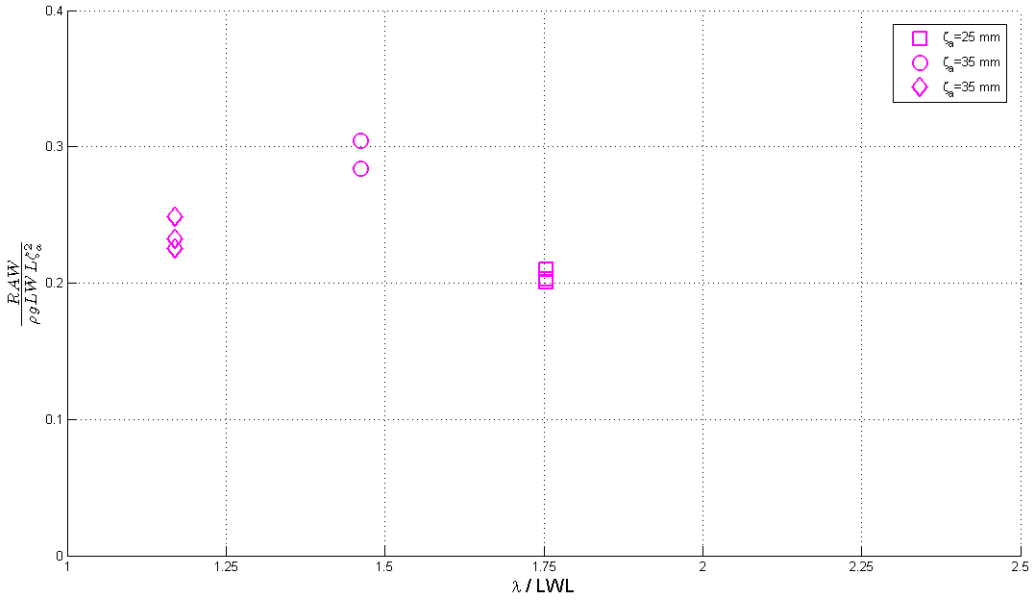

Figure C.6: Accuracy study - Added resistance: Upright, Fn=0.4, No surge

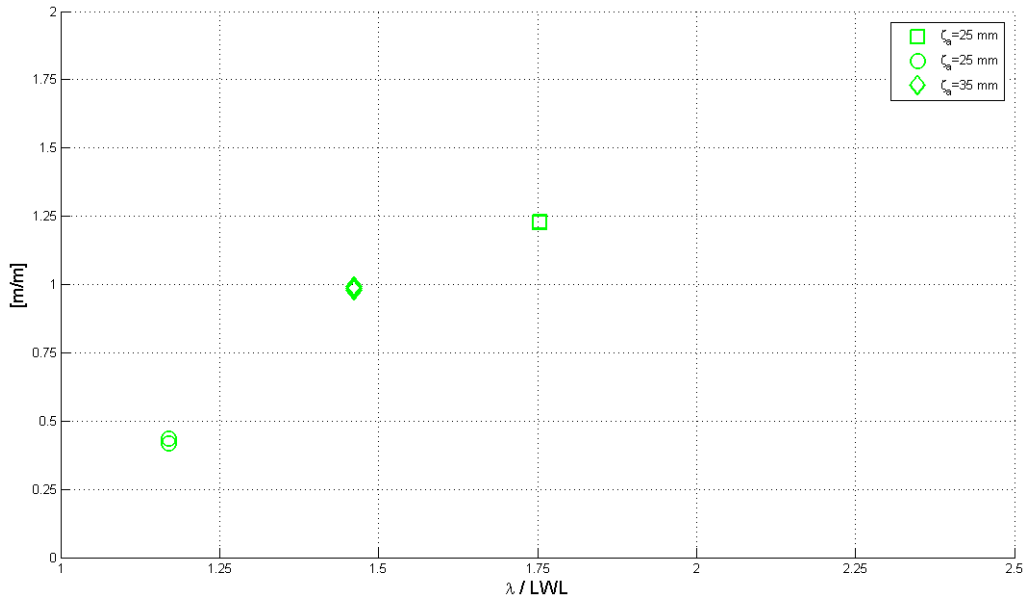

Figure C.7: Accuracy study - Heave: Upright, Fn=0.4, Free to surge

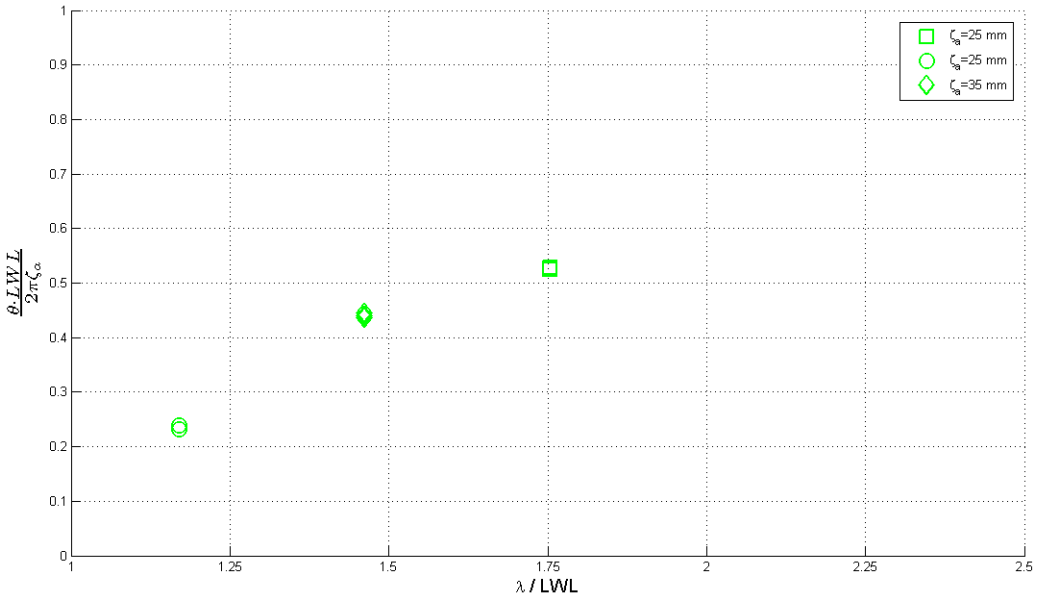

Figure C.8: Accuracy study - Pitch: Upright, Fn=0.4, Free to surge

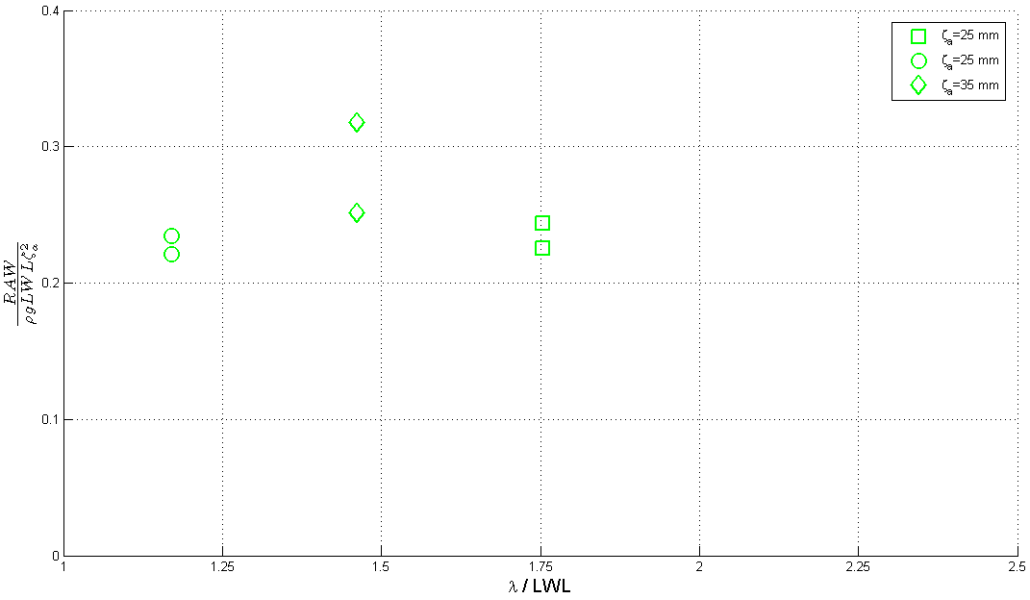

Figure C.9: Accuracy study - Added resistance: Upright, Fn=0.4, Free to surge

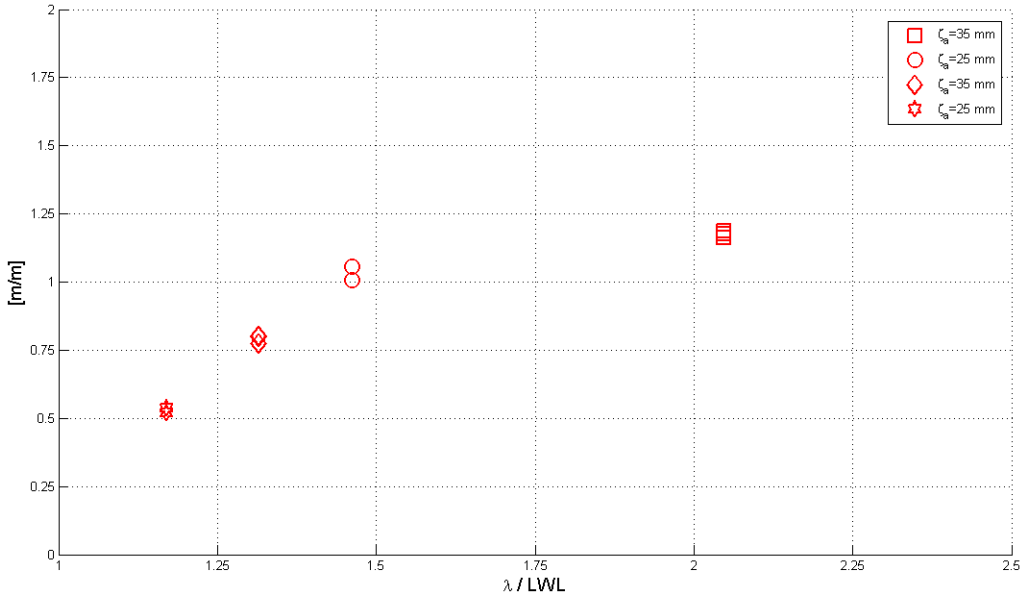

Figure C.10: Accuracy study - Heave: 20° Heel, Fn=0.325

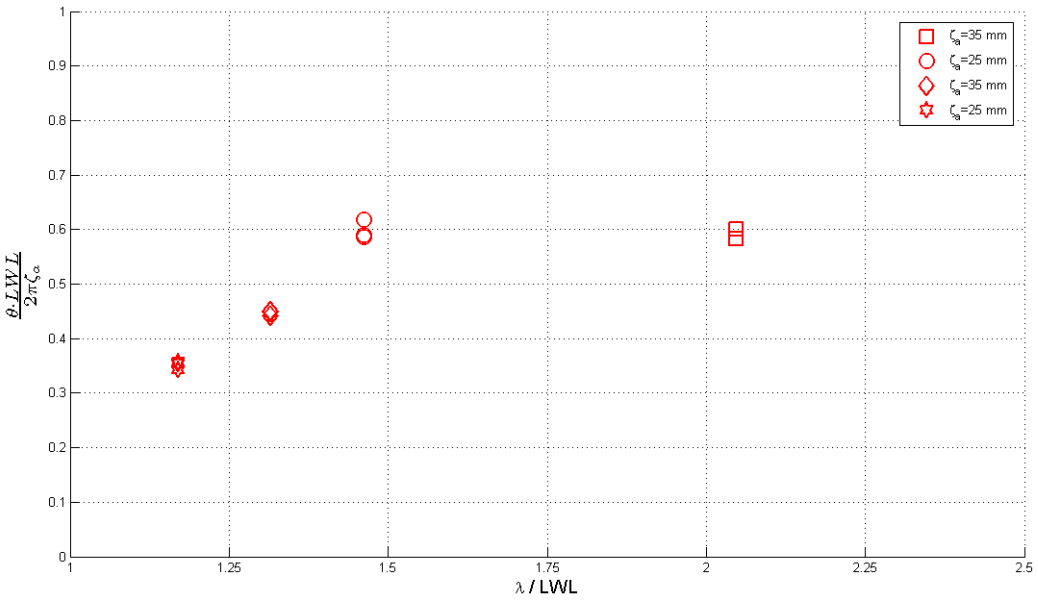

Figure C.11: Accuracy study - Pitch: 20° Heel, Fn=0.325

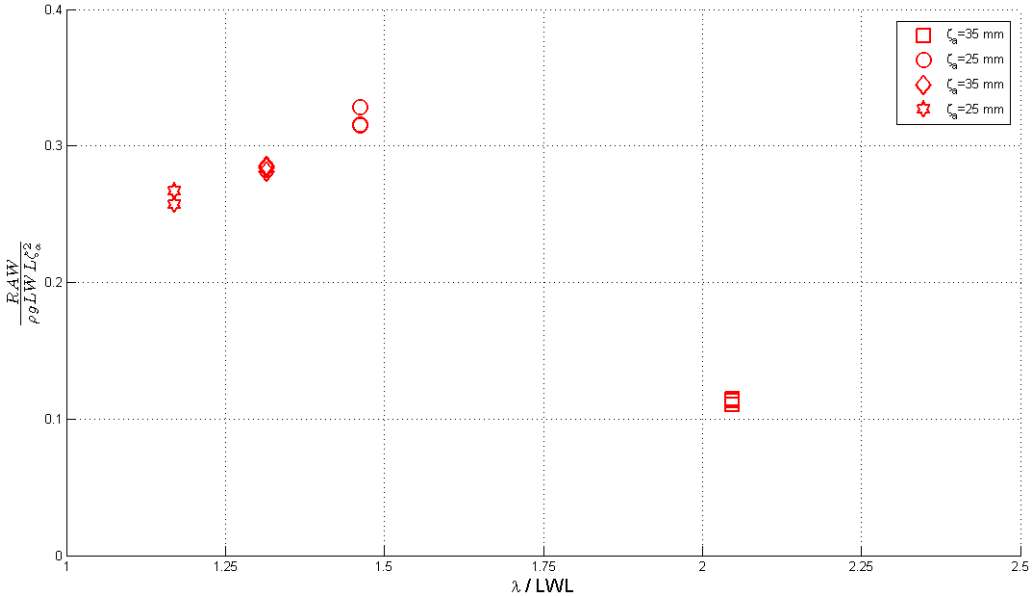

Figure C.12: Accuracy study - Added resistance: 20° Heel, Fn=0.325

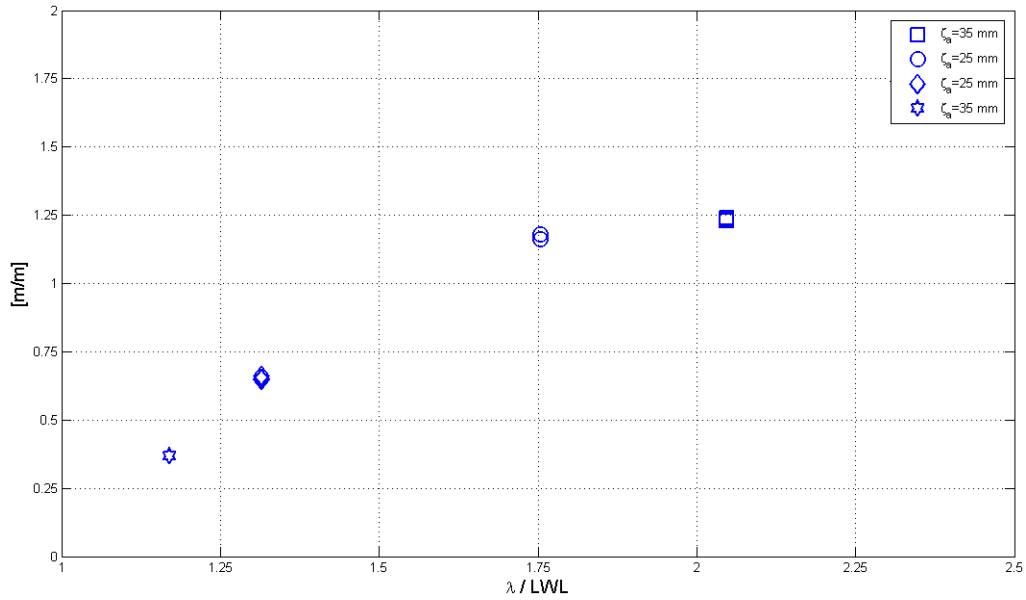

Figure C.13: Accuracy study - Heave: 20° Heel, Fn=0.4

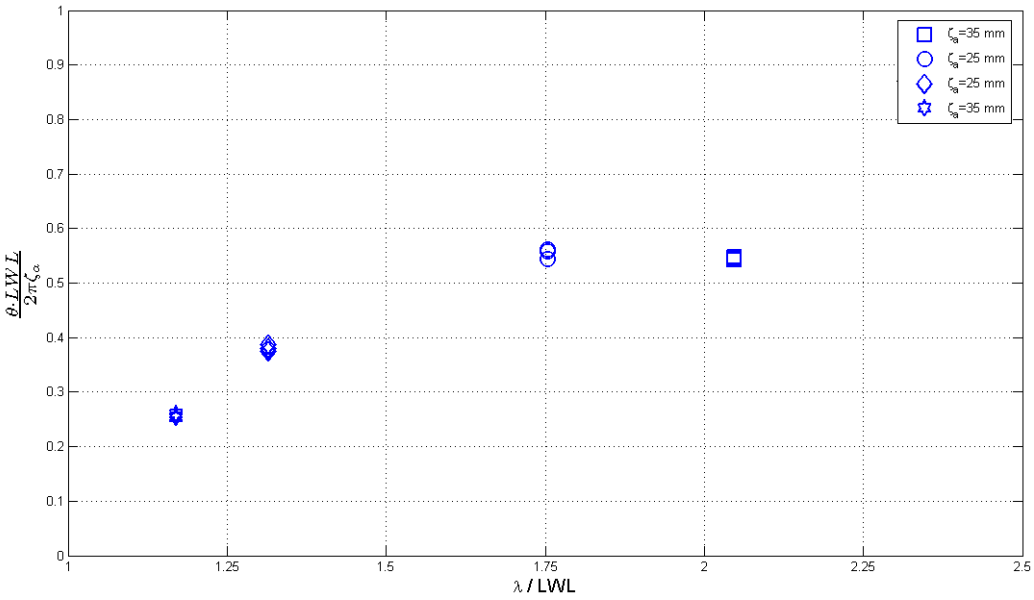

Figure C.14: Accuracy study - Pitch: 20° Heel, Fn=0.4

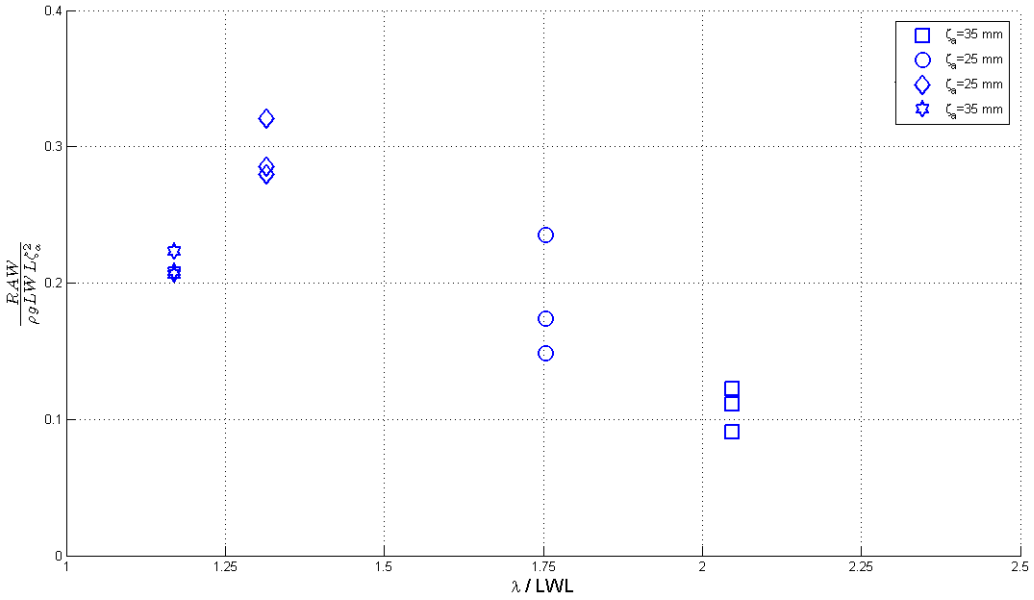

Figure C.15: Accuracy study - Added resistance: 20° Heel, Fn=0.4

Appendix D

Results of the Experiments and Calculations

D.1 Study of the effect of surge on the motions and added resistance

Model # 43

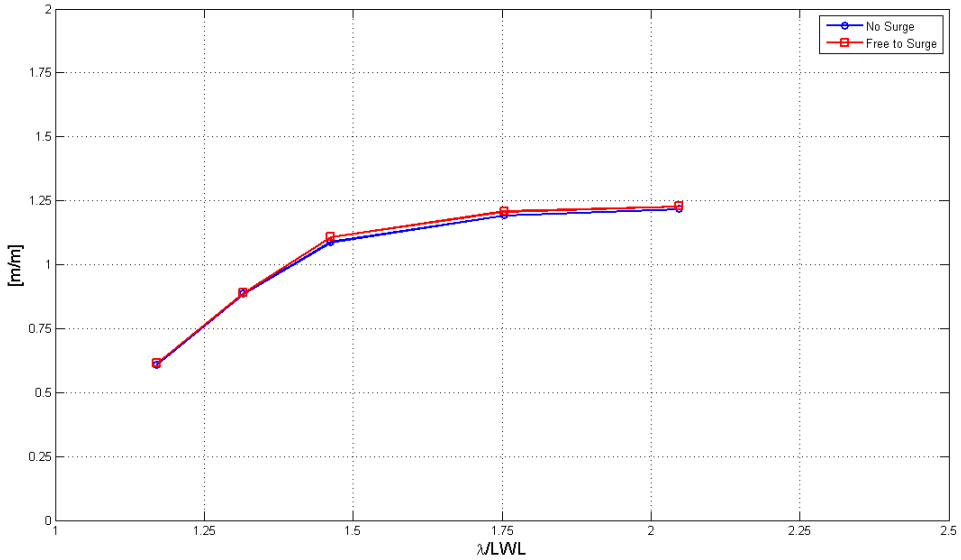

Figure D.1: Model # 43· Surge vs NO Surge - Heave: Fn=0.325, $\zeta_a = 25$ mm

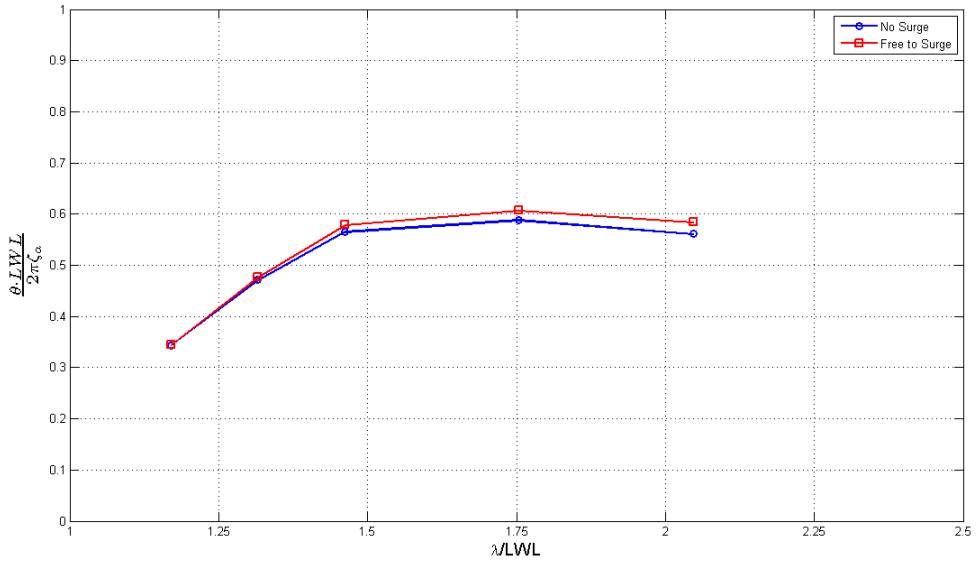

Figure D.2: Model # 43· Surge vs NO Surge - Pitch: Fn=0.325, $\zeta_a = 25$ mm

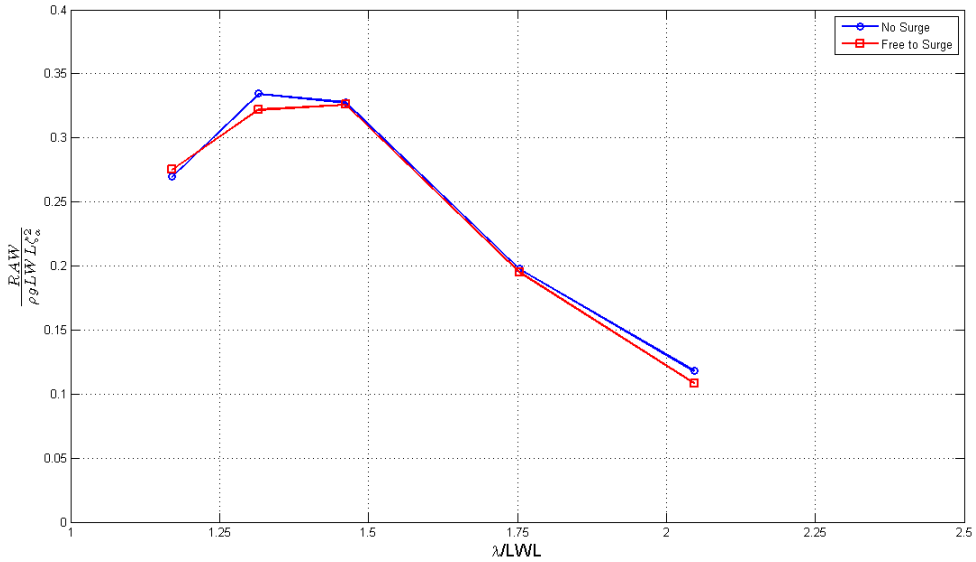

Figure D.3: Model # 43· Surge vs NO Surge - Added resistance: Fn=0.325, $\zeta_a = 25$ mm

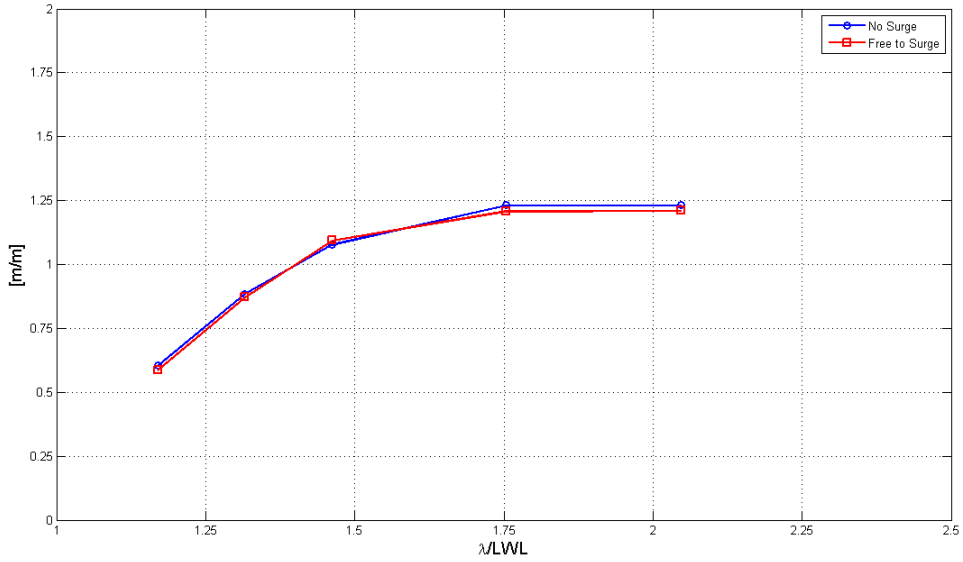

Figure D.4: Model # 43· Surge vs NO Surge - Heave: Fn=0.325, $\zeta_a = 35$ mm

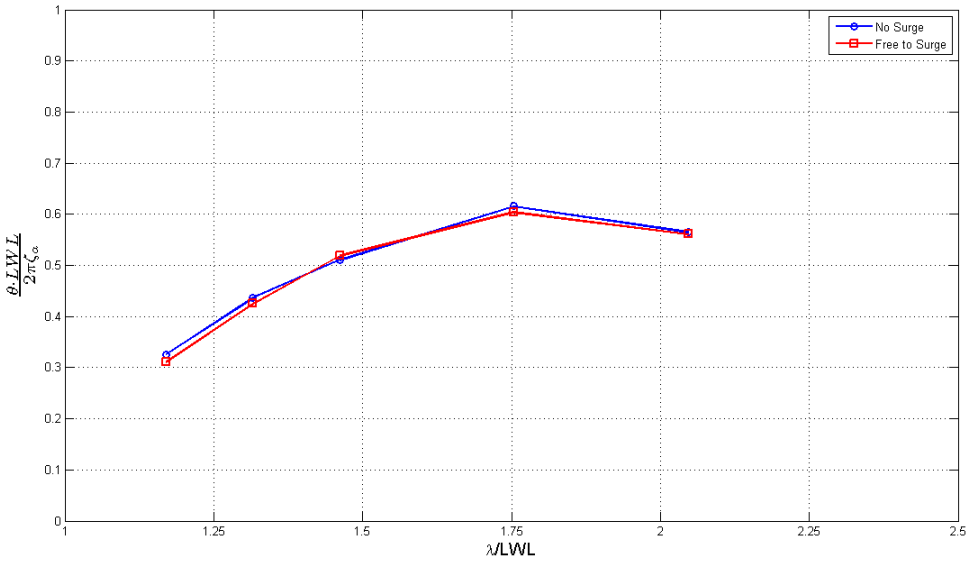

Figure D.5: Model # 43· Surge vs NO Surge - Pitch: Fn=0.325, $\zeta_a = 35$ mm

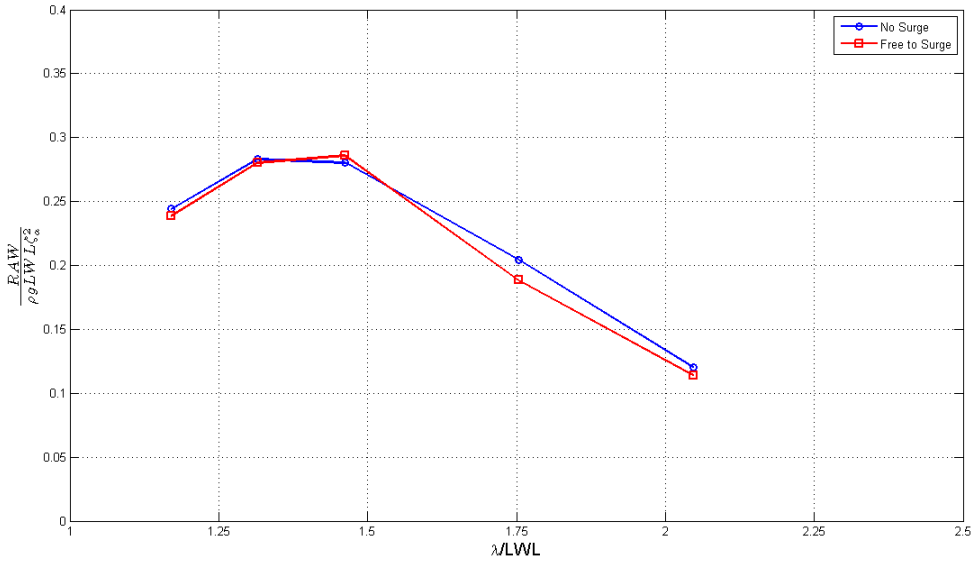

Figure D.6: Model # 43· Surge vs NO Surge - Added resistance: Fn=0.325, $\zeta_a = 35$ mm

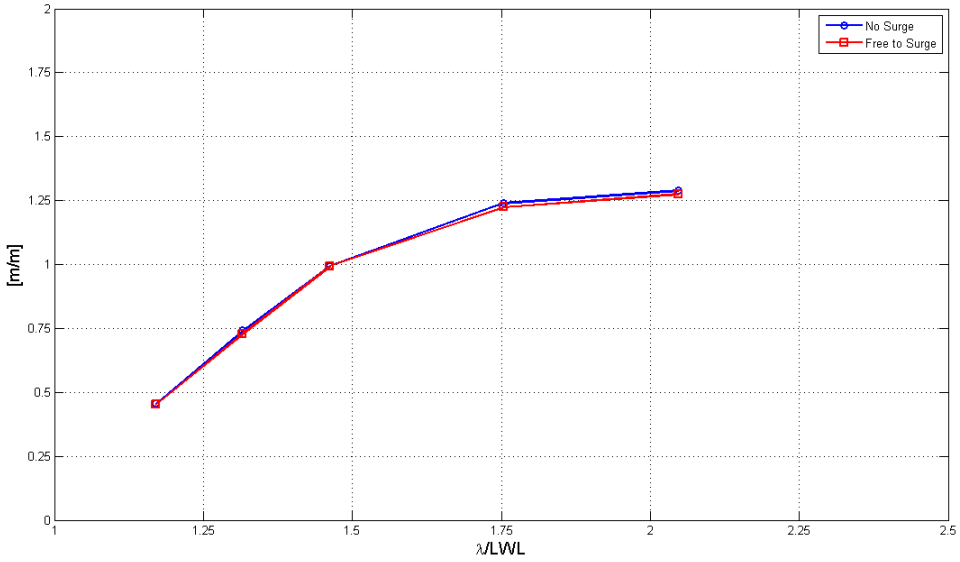

Figure D.7: Model # 43· Surge vs NO Surge - Heave: Fn=0.4, $\zeta_a = 25$ mm

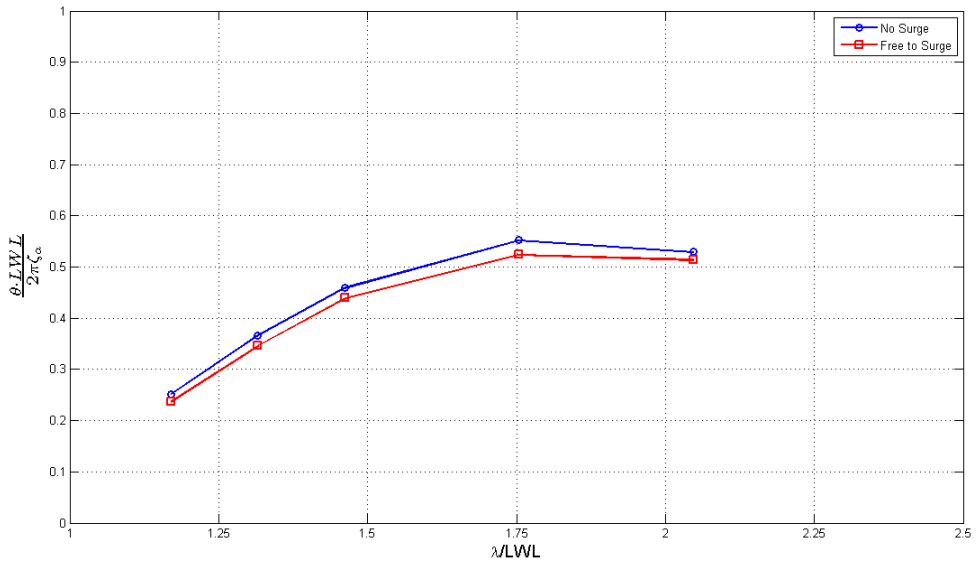

Figure D.8: Model # 43· Surge vs NO Surge - Pitch: Fn=0.4, $\zeta_a = 25$ mm

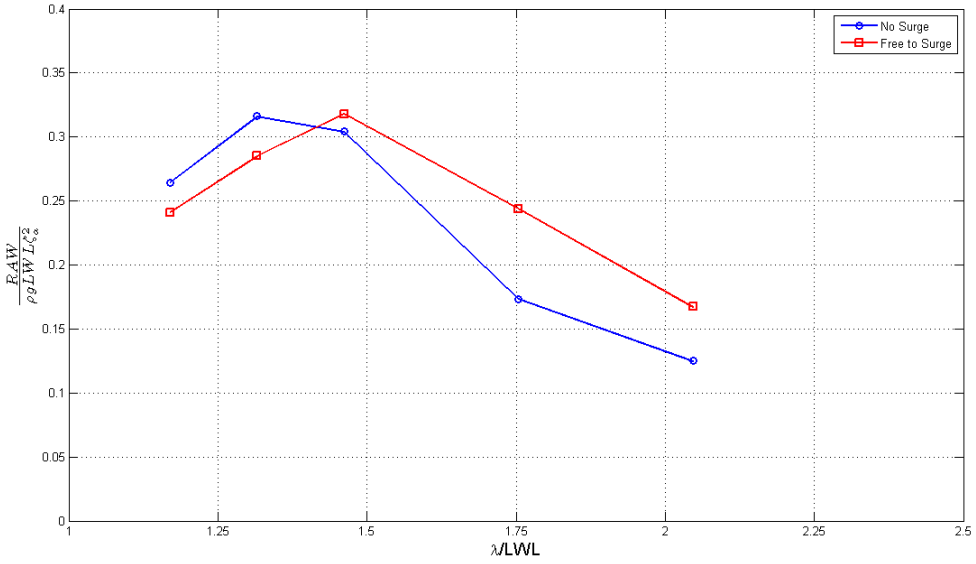

Figure D.9: Model # 43· Surge vs NO Surge - Added resistance: Fn=0.4, $\zeta_a = 25$ mm

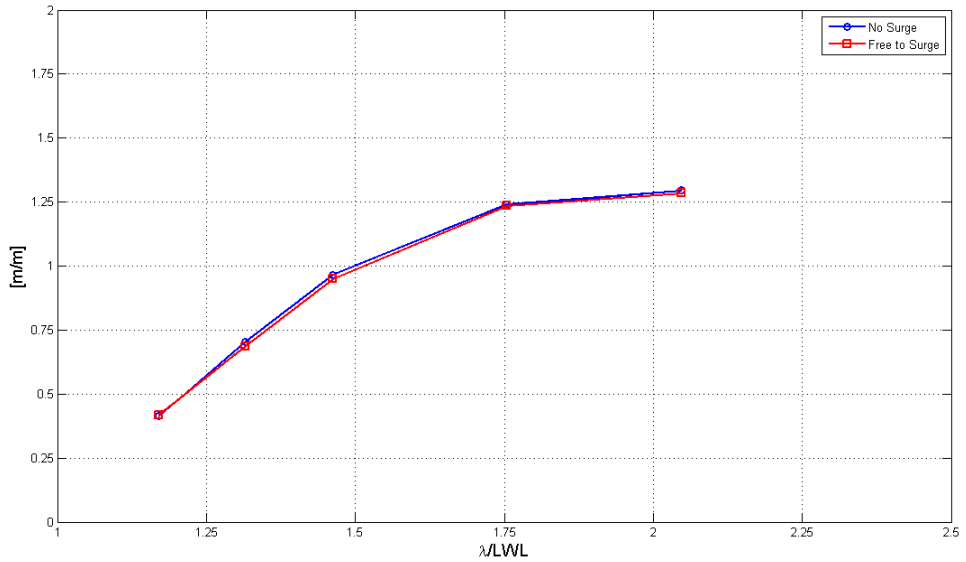

Figure D.10: Model # 43· Surge vs NO Surge - Heave: Fn=0.4, $\zeta_a = 35$ mm

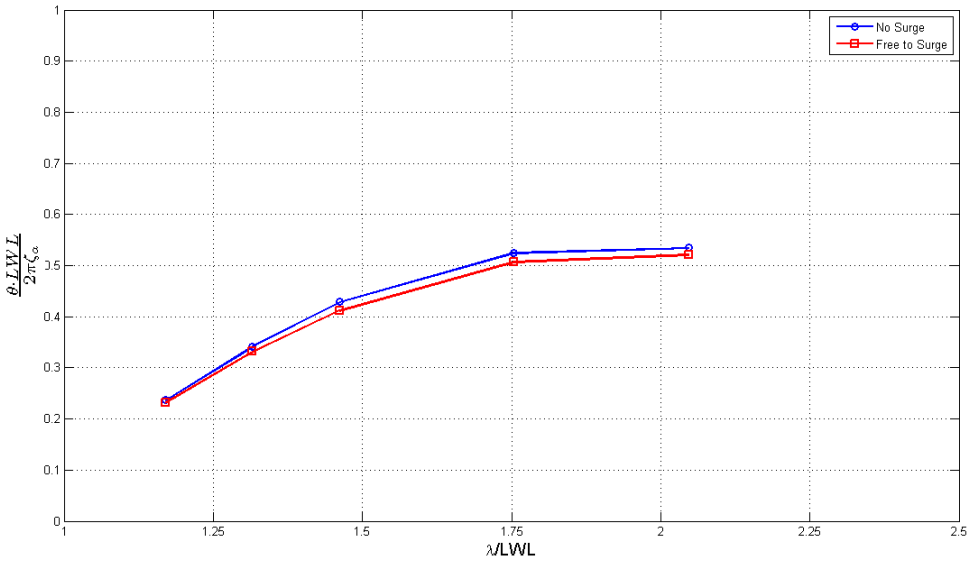

Figure D.11: Model # 43· Surge vs NO Surge - Pitch: Fn=0.4, $\zeta_a = 35$ mm

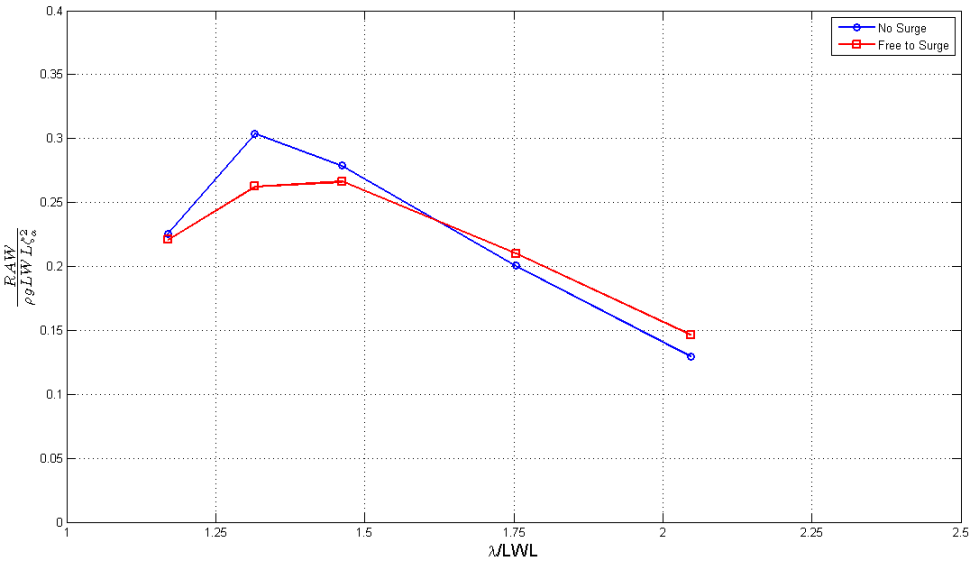

Figure D.12: Model # 43· Surge vs NO Surge - Added resistance: Fn=0.4, $\zeta_a = 35$ mm

Model # 45

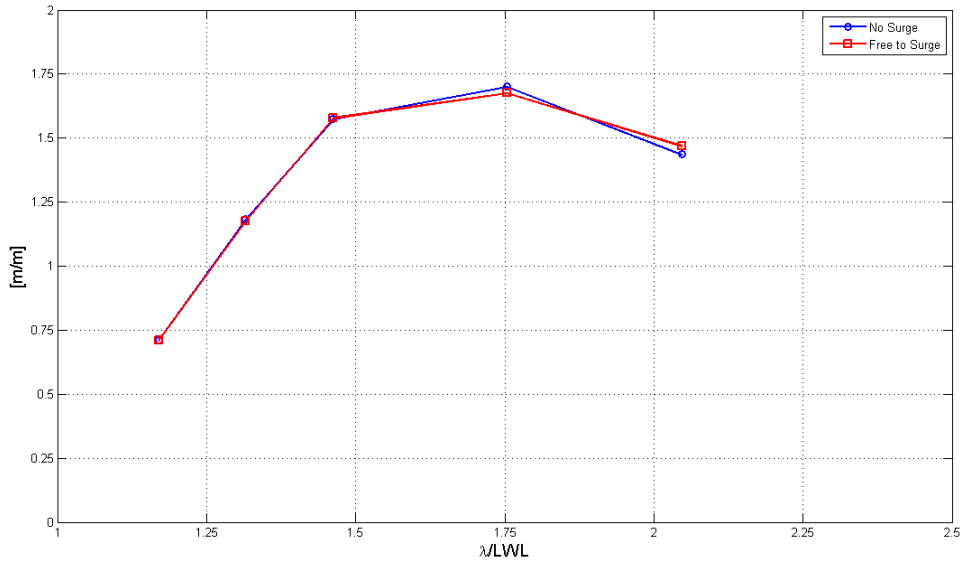

Figure D.13: Model # 45· Surge vs NO Surge - Heave: Fn=0.325, $\zeta_a = 25$ mm

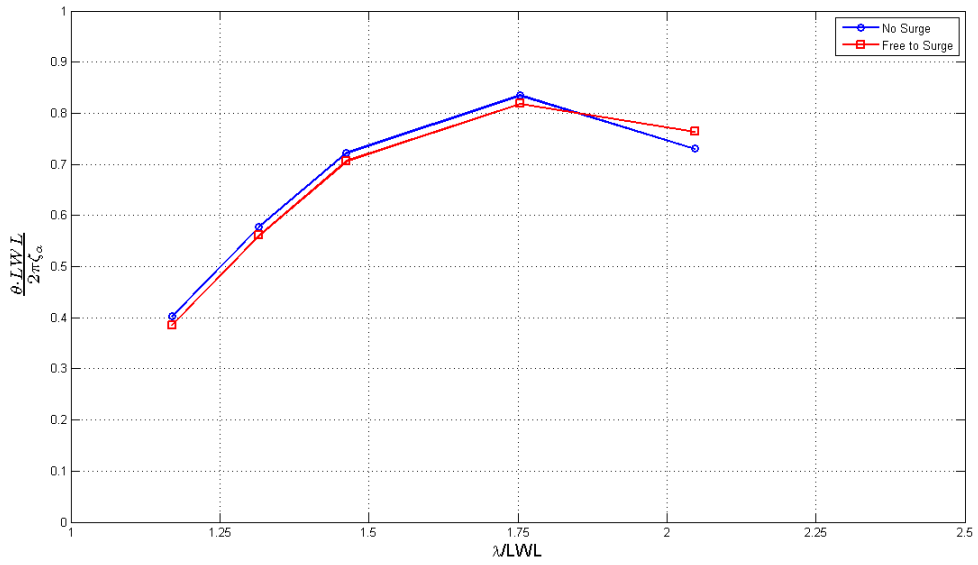

Figure D.14: Model # 45· Surge vs NO Surge - Pitch: Fn=0.325, $\zeta_a = 25$ mm

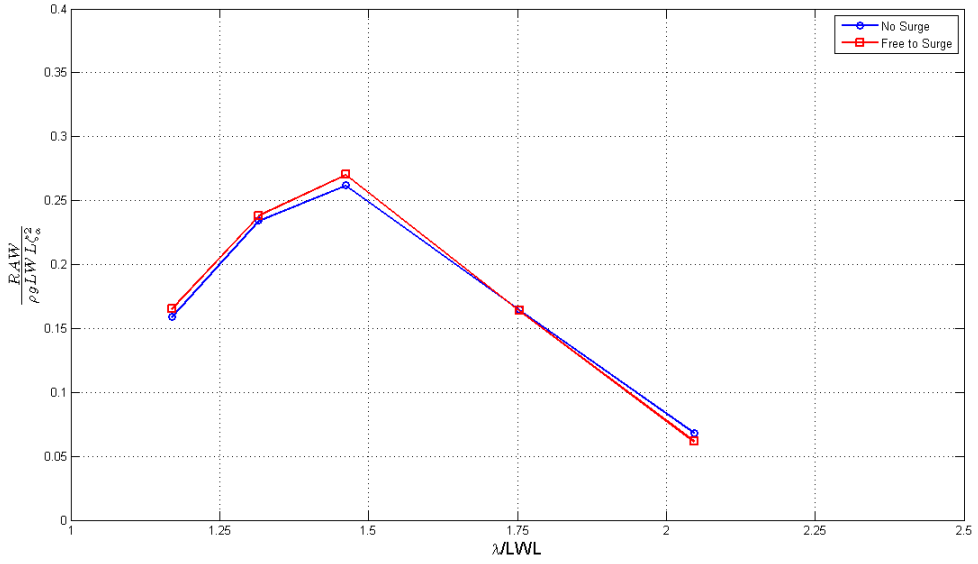

Figure D.15: Model # 45· Surge vs NO Surge - Added resistance: Fn=0.325, $\zeta_a = 25$ mm

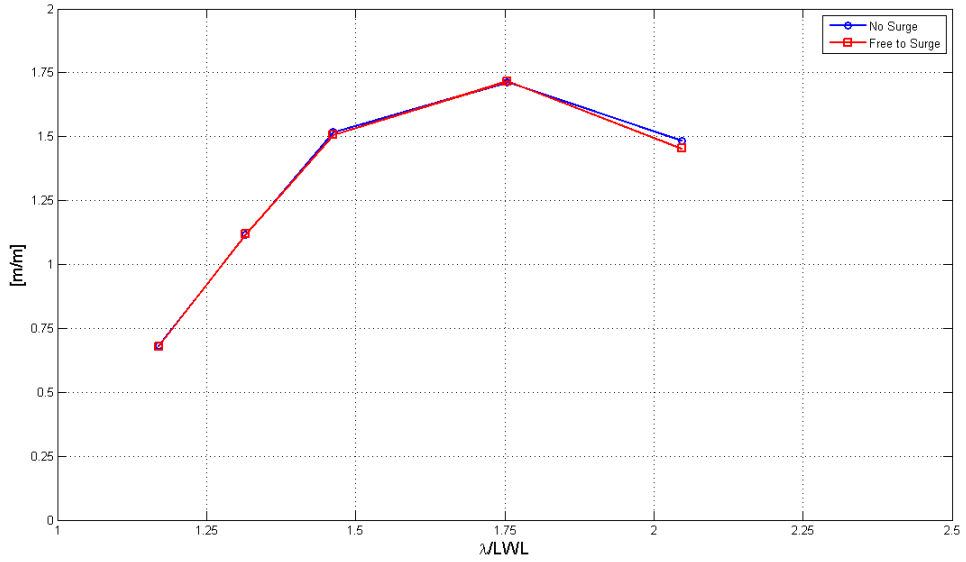

Figure D.16: Model # 45· Surge vs NO Surge - Heave: Fn=0.325, $\zeta_a = 35$ mm

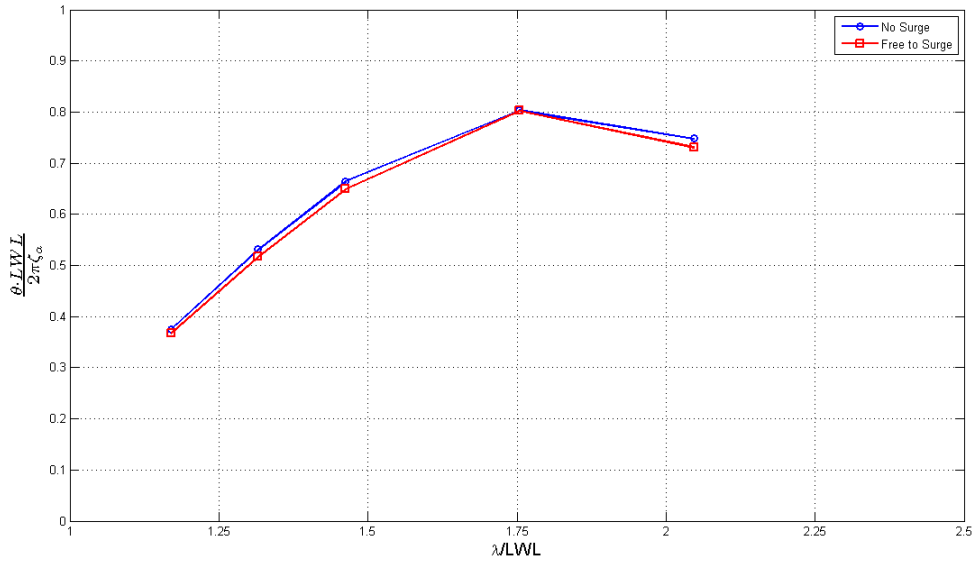

Figure D.17: Model # 45· Surge vs NO Surge - Pitch: Fn=0.325, $\zeta_a = 35$ mm

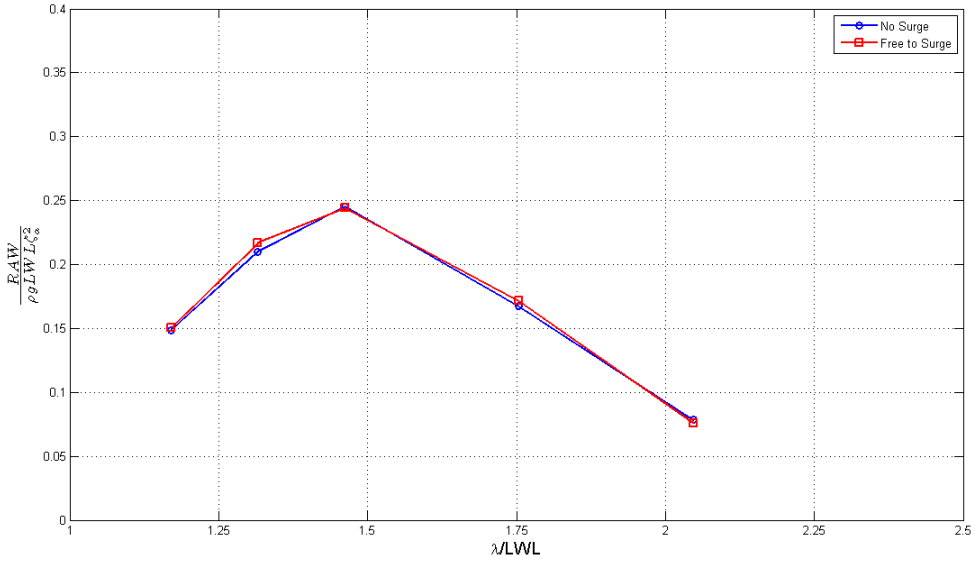

Figure D.18: Model # 45· Surge vs NO Surge - Added resistance: Fn=0.325, $\zeta_a = 35$ mm

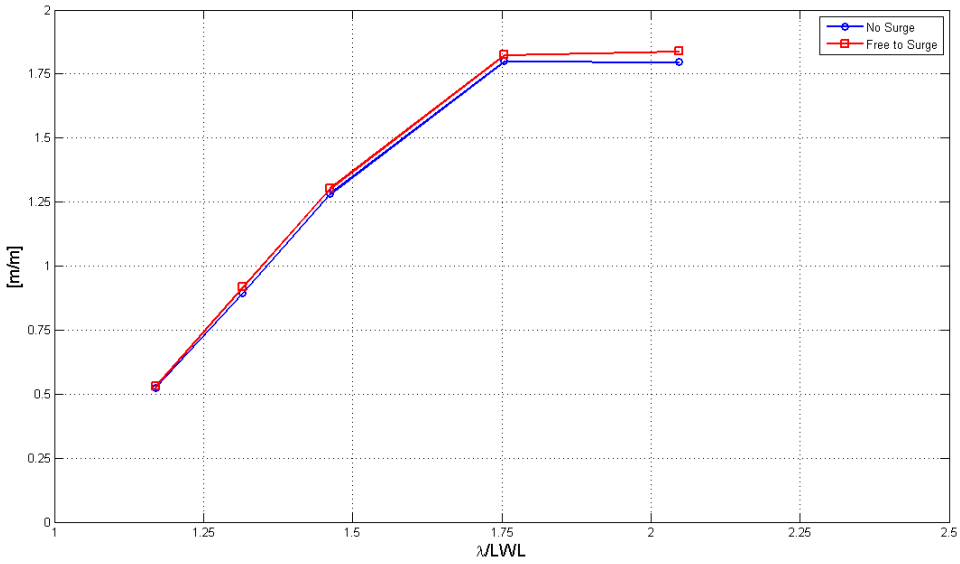

Figure D.19: Model # 45· Surge vs NO Surge - Heave: Fn=0.4, $\zeta_a = 25$ mm

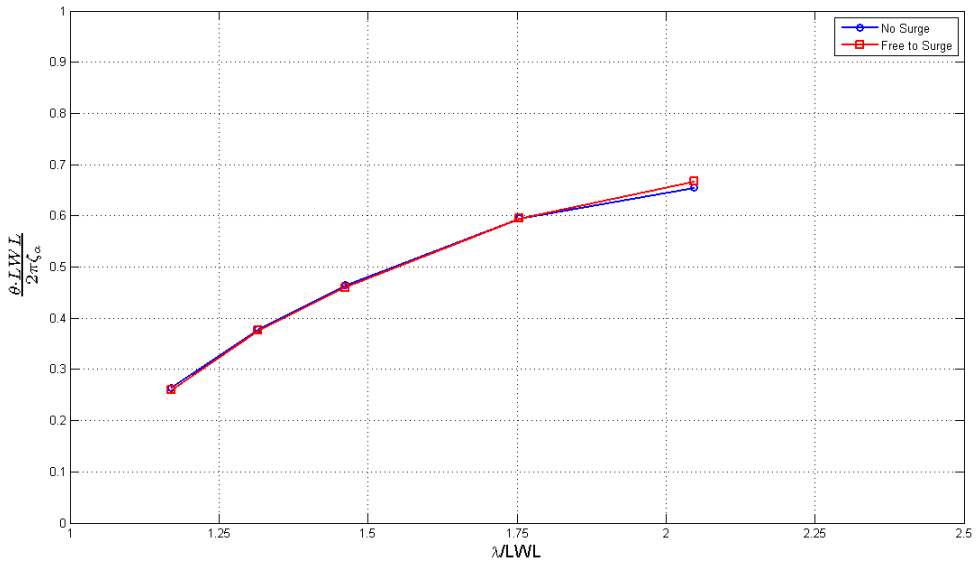

Figure D.20: Model # 45· Surge vs NO Surge - Pitch: Fn=0.4, $\zeta_a = 25$ mm

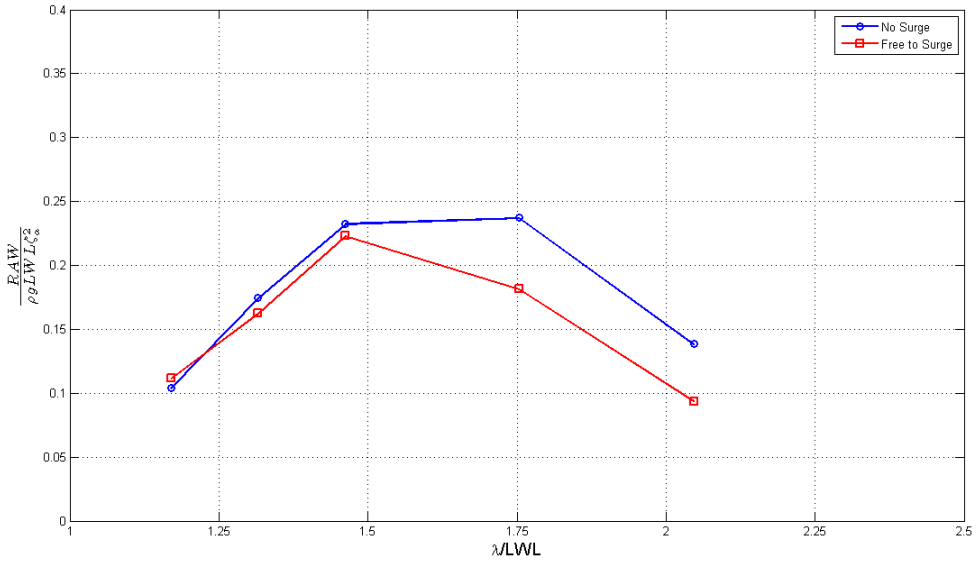

Figure D.21: Model # 45· Surge vs NO Surge - Added resistance: Fn=0.4, $\zeta_a = 25$ mm

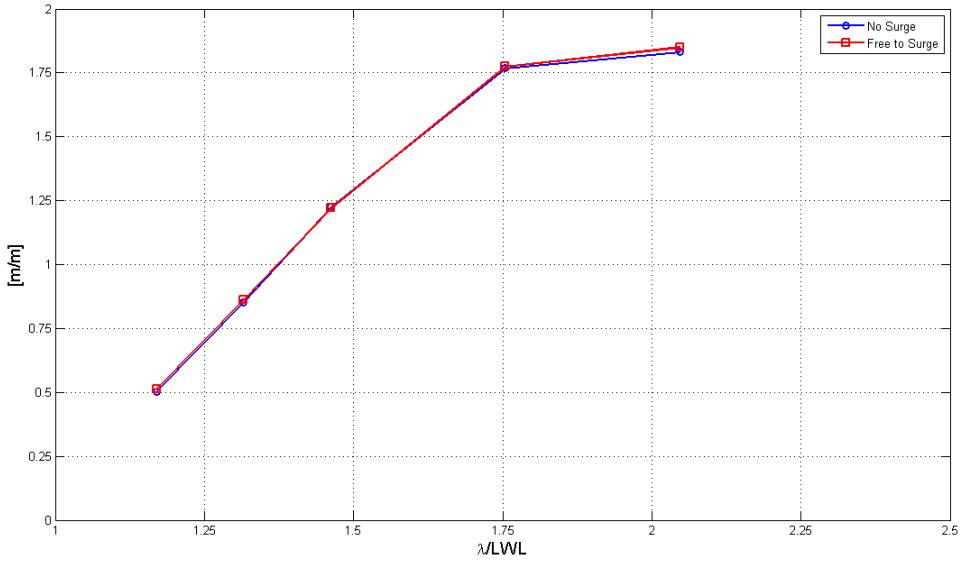

Figure D.22: Model # 45· Surge vs NO Surge - Heave: Fn=0.4, $\zeta_a = 35$ mm

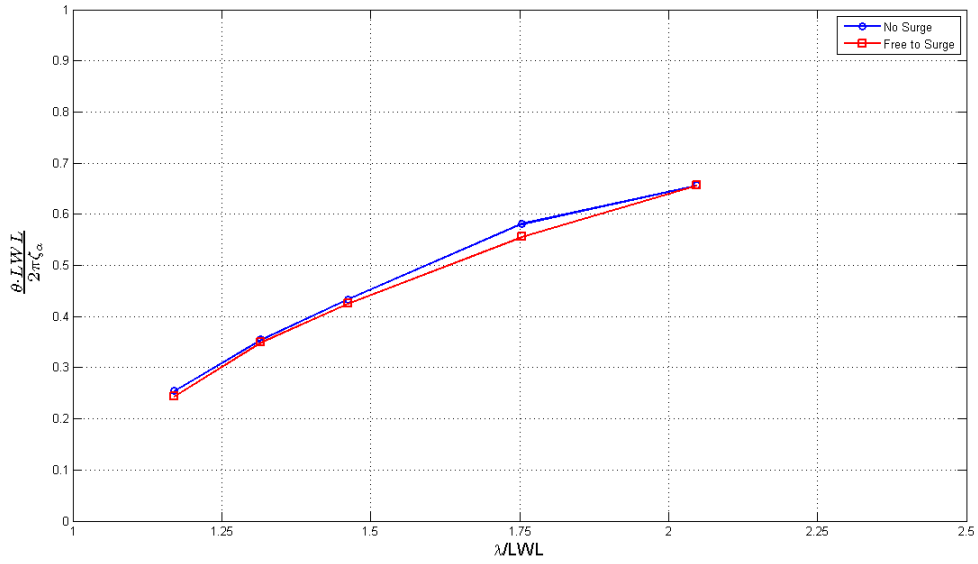

Figure D.23: Model # 45· Surge vs NO Surge - Pitch: Fn=0.4, $\zeta_a = 35$ mm

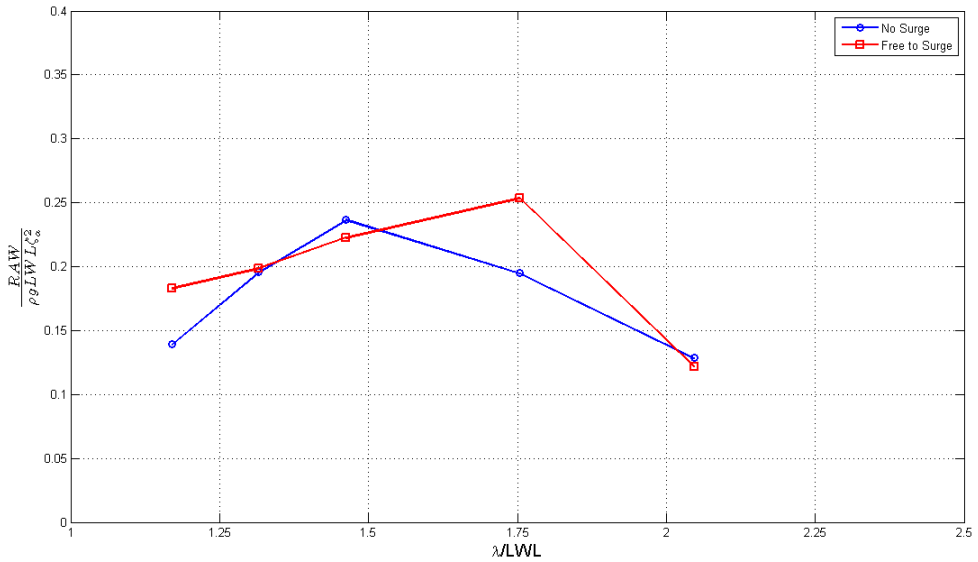

Figure D.24: Model # 45· Surge vs NO Surge - Added resistance: Fn=0.4, $\zeta_a = 35$ mm

D.2 Study of the effect of the heeling angle on the motions and added resistance

Model # 43

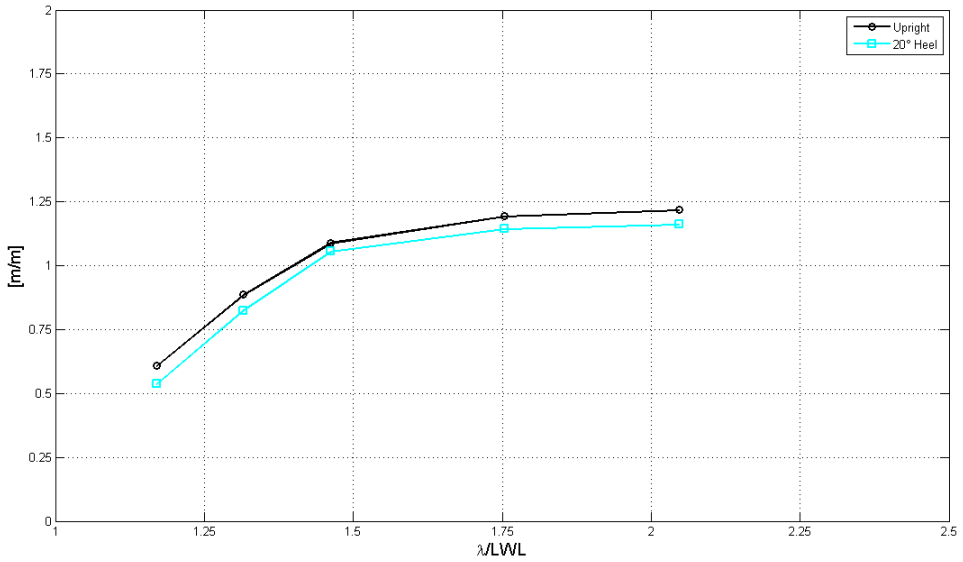

Figure D.25: Model # 43· Upright vs 20° Heel - Heave: Fn=0.325, $\zeta_a = 25$ mm

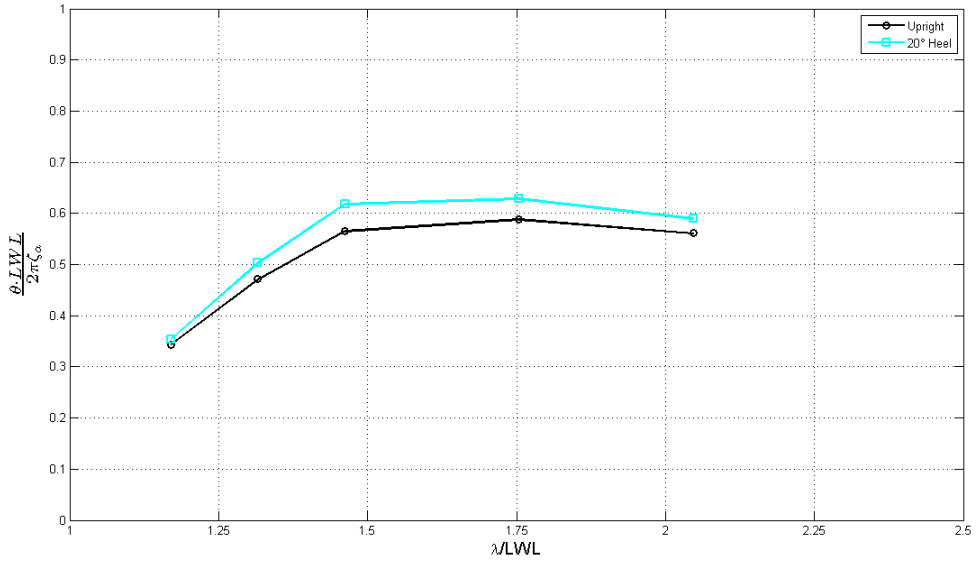

Figure D.26: Model # 43· Upright vs 20° Heel - Pitch: Fn=0.325, $\zeta_a = 25$ mm

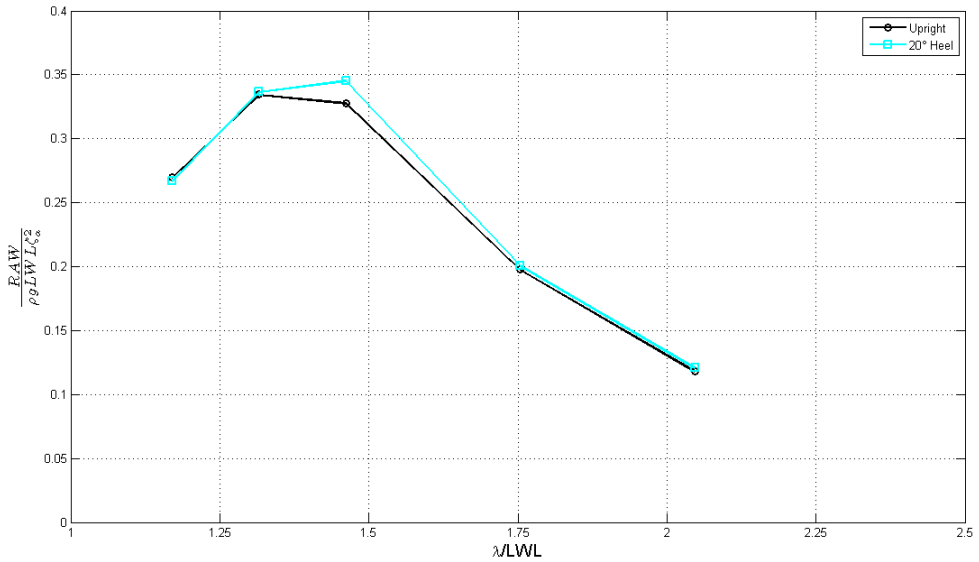

Figure D.27: Model # 43· Upright vs 20° Heel - Added resistance: Fn=0.325, $\zeta_a = 25$ mm

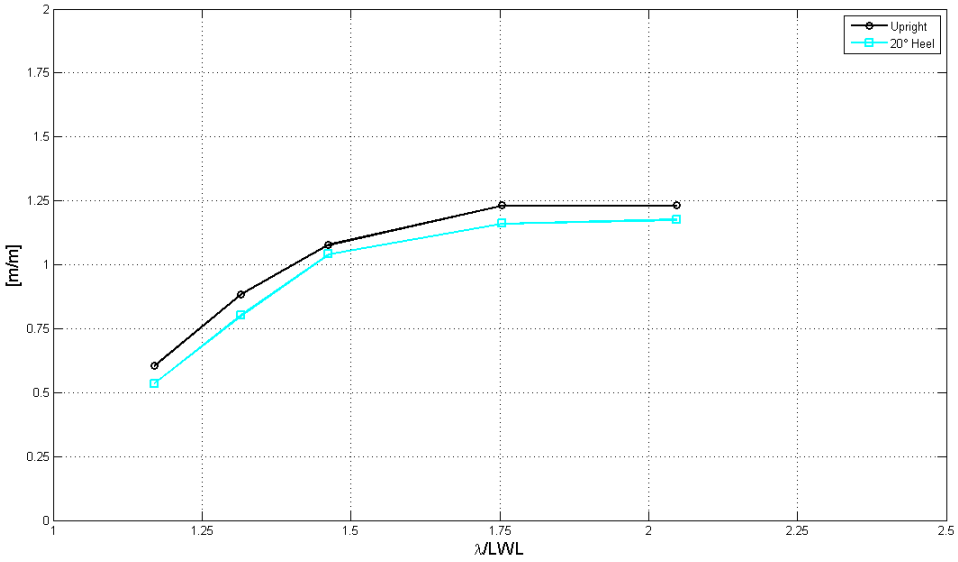

Figure D.28: Model # 43· Upright vs 20° Heel - Heave: Fn=0.325, $\zeta_a = 35$ mm

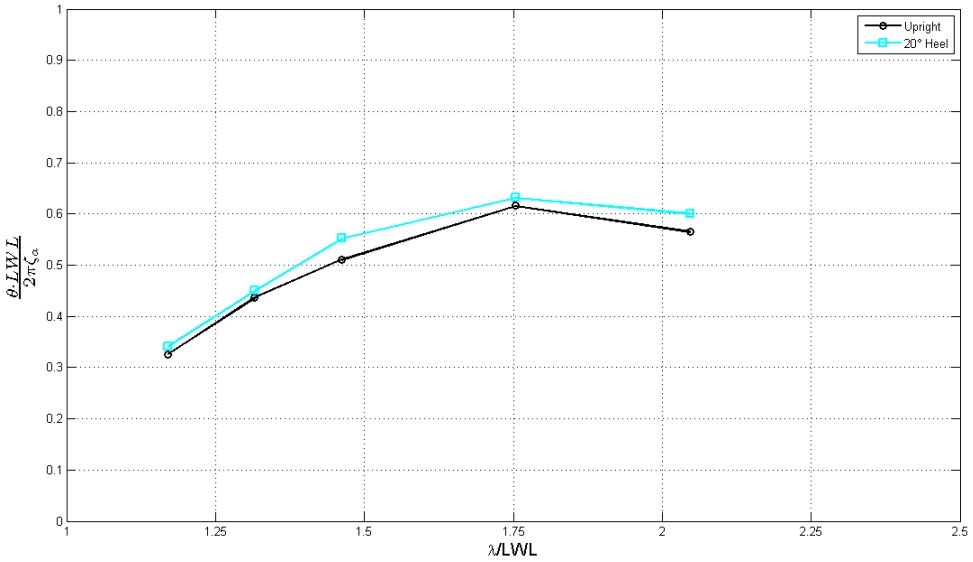

Figure D.29: Model # 43· Upright vs 20° Heel - Pitch: Fn=0.325, $\zeta_a = 35$ mm

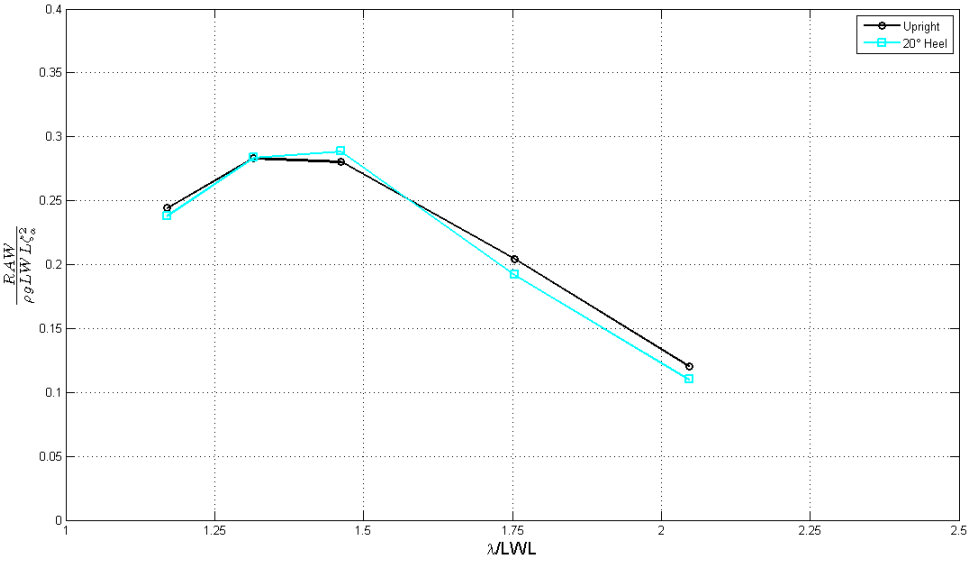

Figure D.30: Model # 43· Upright vs 20° Heel - Added resistance: Fn=0.325, $\zeta_a = 35$ mm

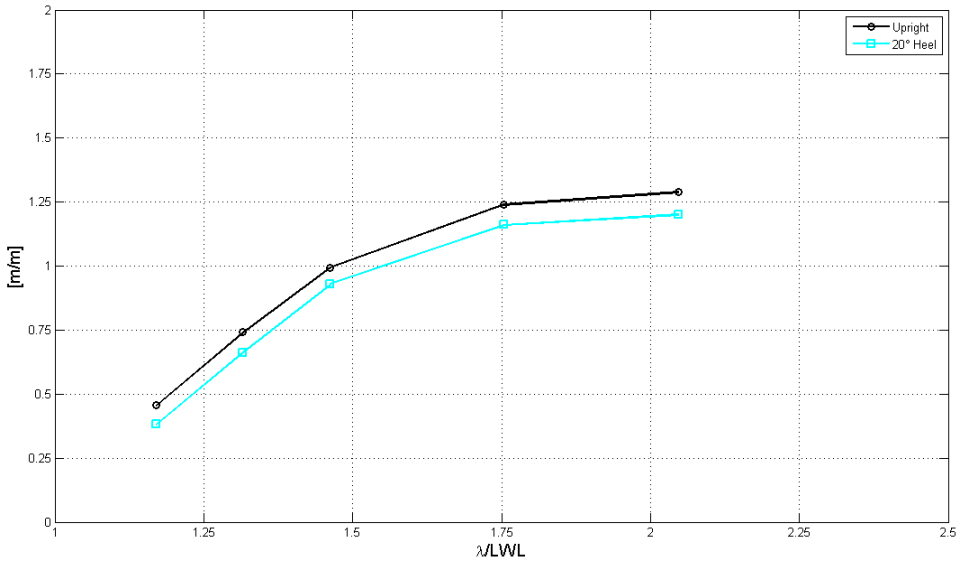

Figure D.31: Model # 43· Upright vs 20° Heel - Heave: Fn=0.4, $\zeta_a = 25$ mm

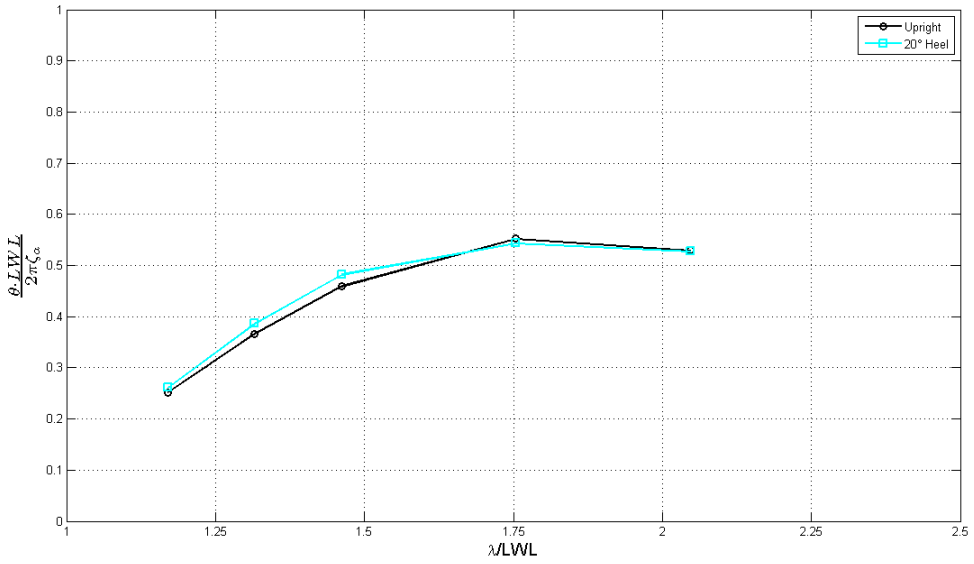

Figure D.32: Model # 43· Upright vs 20° Heel - Pitch: Fn=0.4, $\zeta_a = 25$ mm

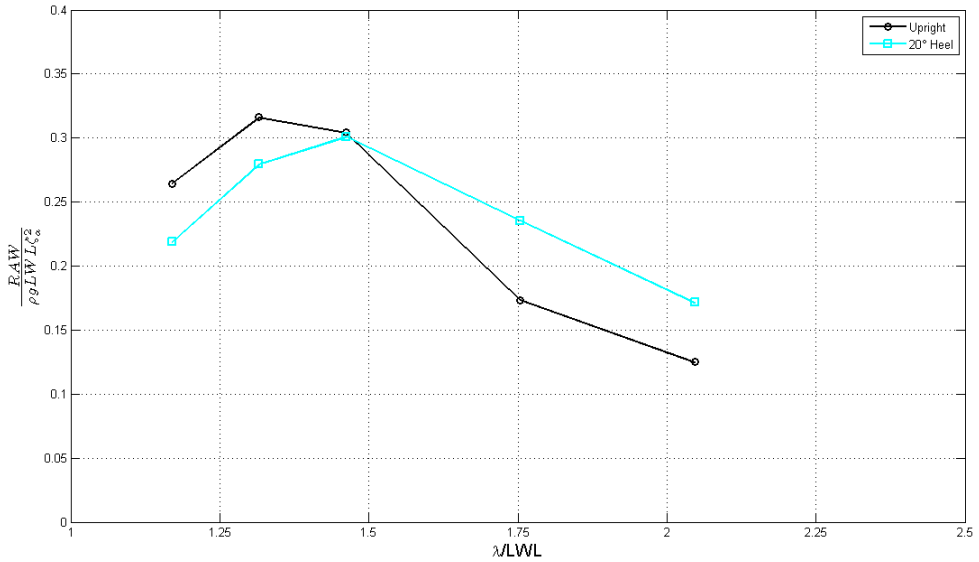

Figure D.33: Model # 43· Upright vs 20° Heel - Added resistance: Fn=0.4, $\zeta_a = 25$ mm

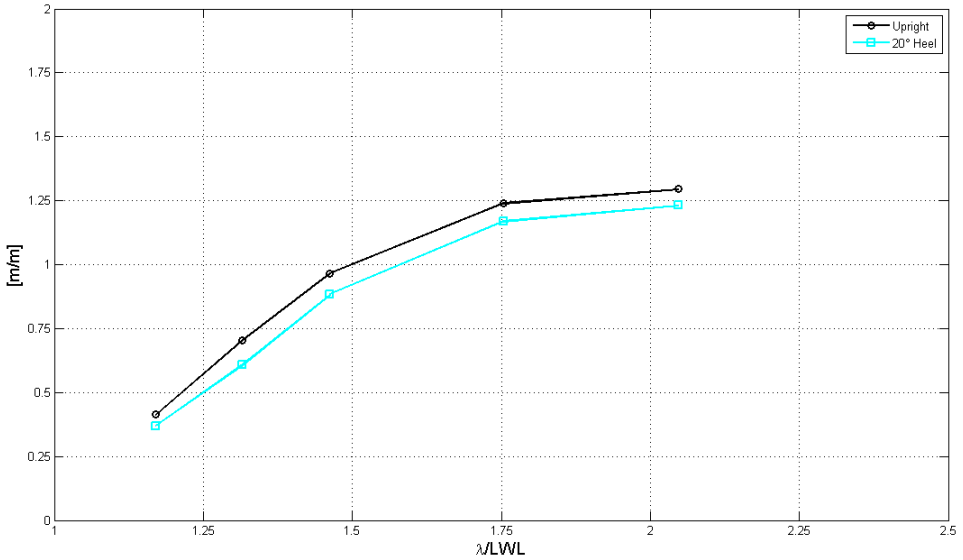

Figure D.34: Model # 43· Upright vs 20° Heel - Heave: Fn=0.4, $\zeta_a = 35$ mm

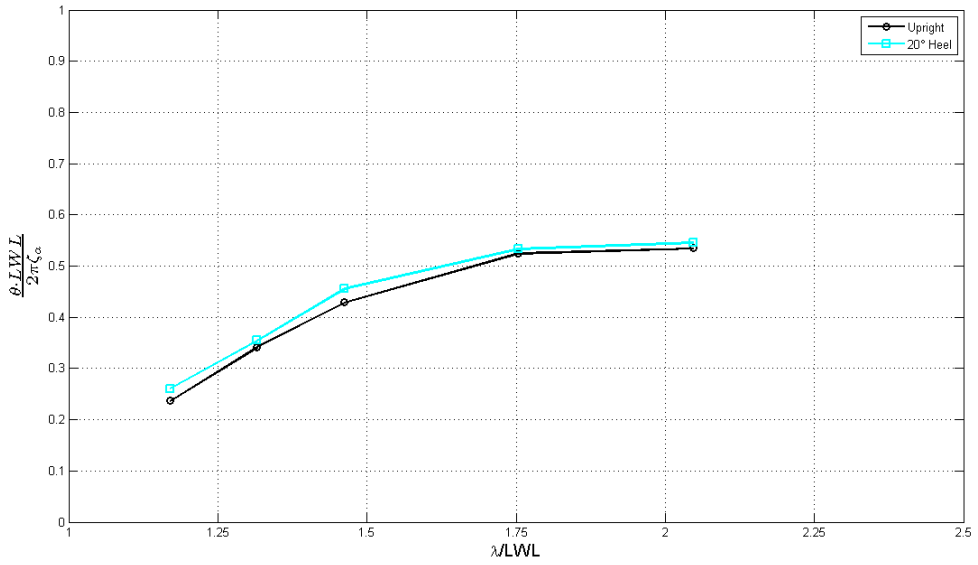

Figure D.35: Model # 43· Upright vs 20° Heel - Pitch: Fn=0.4, $\zeta_a = 35$ mm

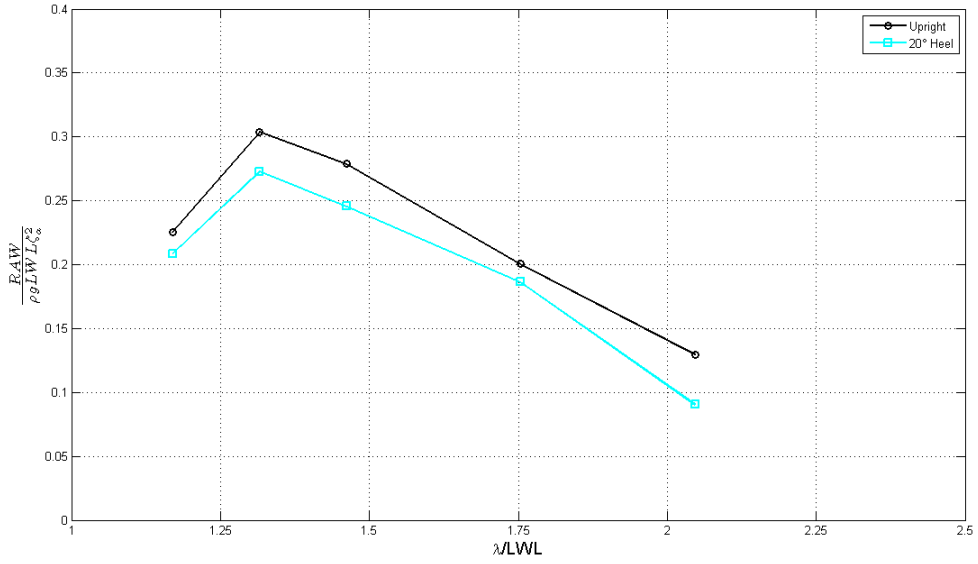

Figure D.36: Model # 43· Upright vs 20° Heel - Added resistance: Fn=0.4, $\zeta_a = 35$ mm

Model # 45[1]

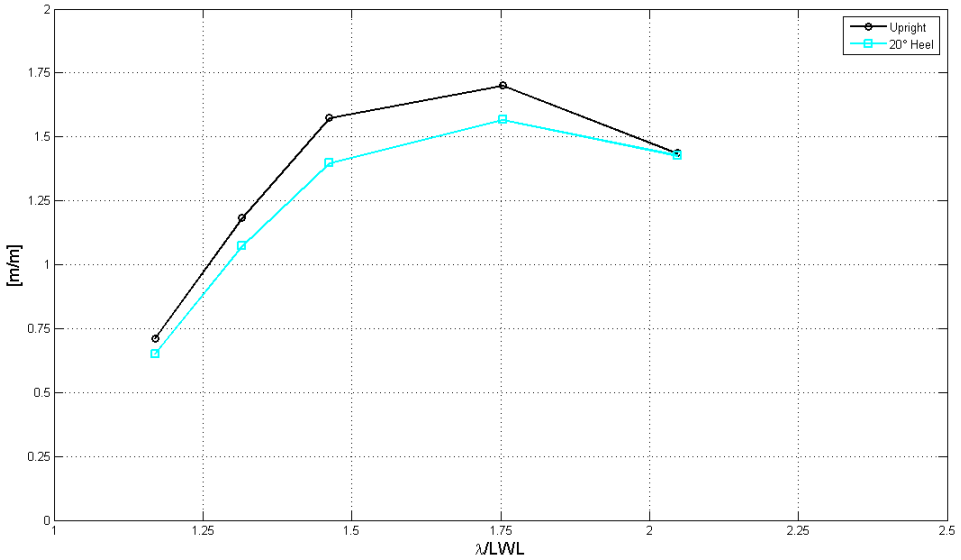

Figure D.37: Model # 45· Upright vs 20° Heel - Heave: Fn=0.325, $\zeta_a = 25$ mm

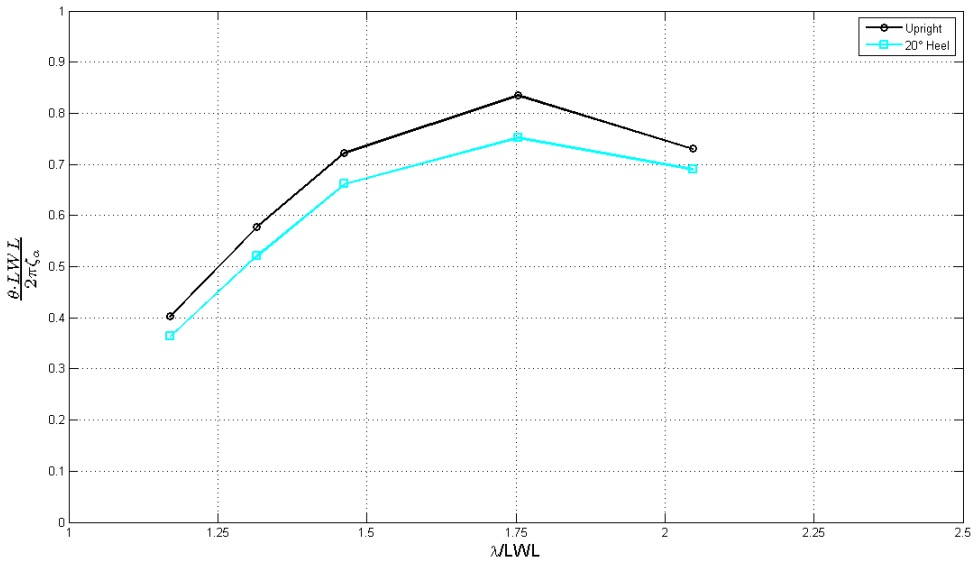

Figure D.38: Model # 45· Upright vs 20° Heel - Pitch: Fn=0.325, $\zeta_a = 25$ mm

[1]It should be recalled that only 3 waves lengths ($\lambda = 2$ [m], $\lambda = 2.5$ [m] and $\lambda = 3.5$ [m]) were tested for $\zeta_a = 35$ [mm]

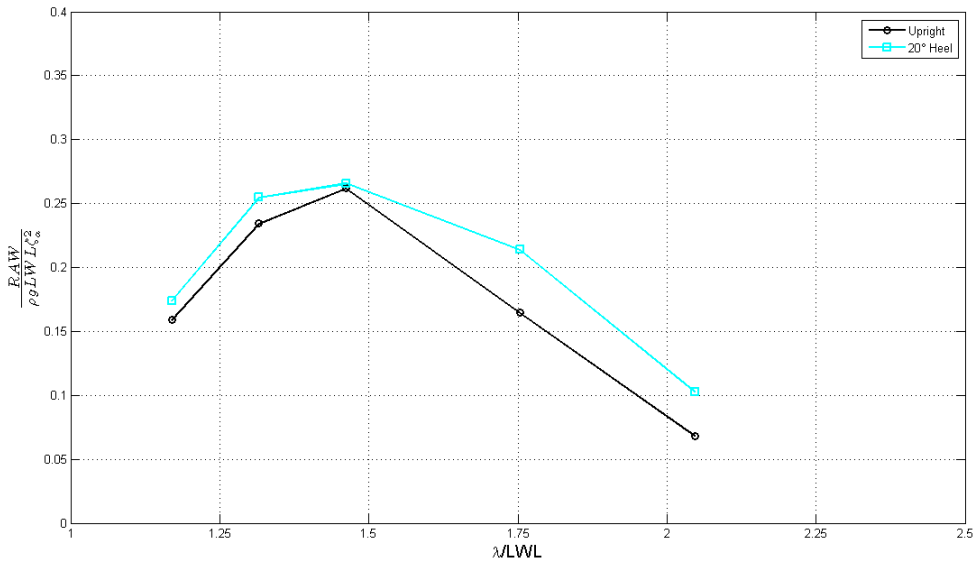

Figure D.39: Model # 45· Upright vs 20° Heel - Added resistance: Fn=0.325, $\zeta_a = 25$ mm

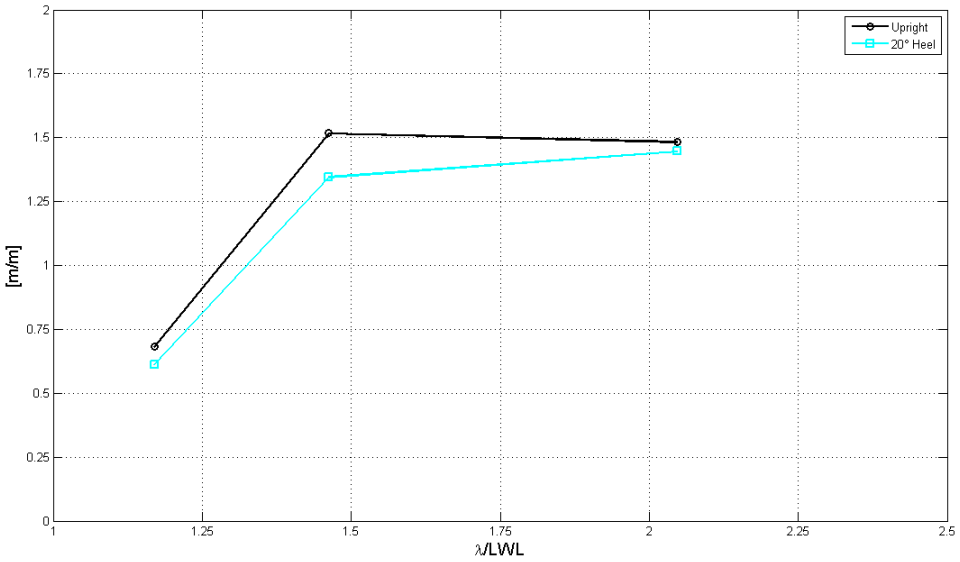

Figure D.40: Model # 45· Upright vs 20° Heel - Heave: Fn=0.325, $\zeta_a = 35$ mm

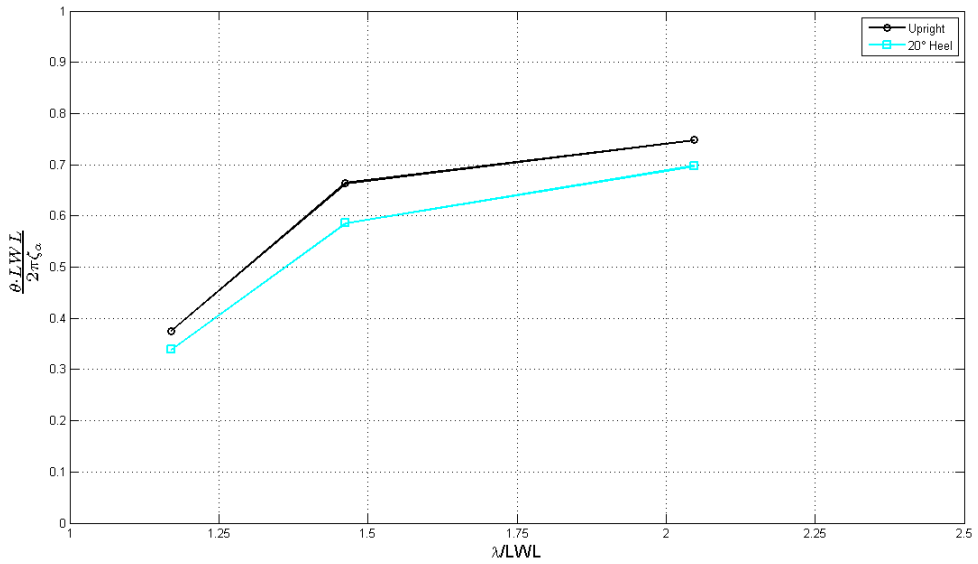

Figure D.41: Model # 45· Upright vs 20° Heel - Pitch: Fn=0.325, $\zeta_a = 35$ mm

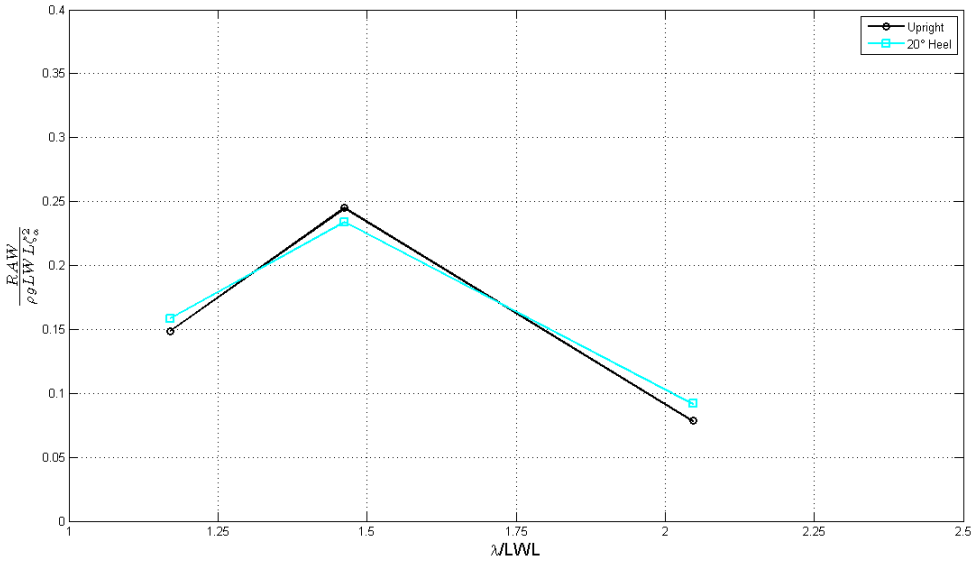

Figure D.42: Model # 45· Upright vs 20° Heel - Added resistance : Fn=0.325, $\zeta_a = 35$ mm

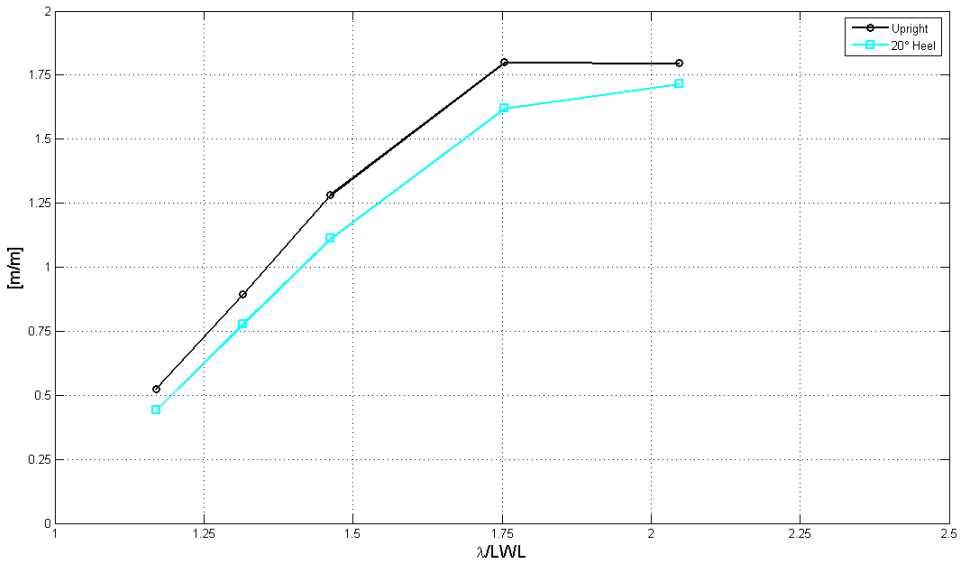

Figure D.43: Model # 45· Upright vs 20° Heel - Heave : Fn=0.4, $\zeta_a = 25$ mm

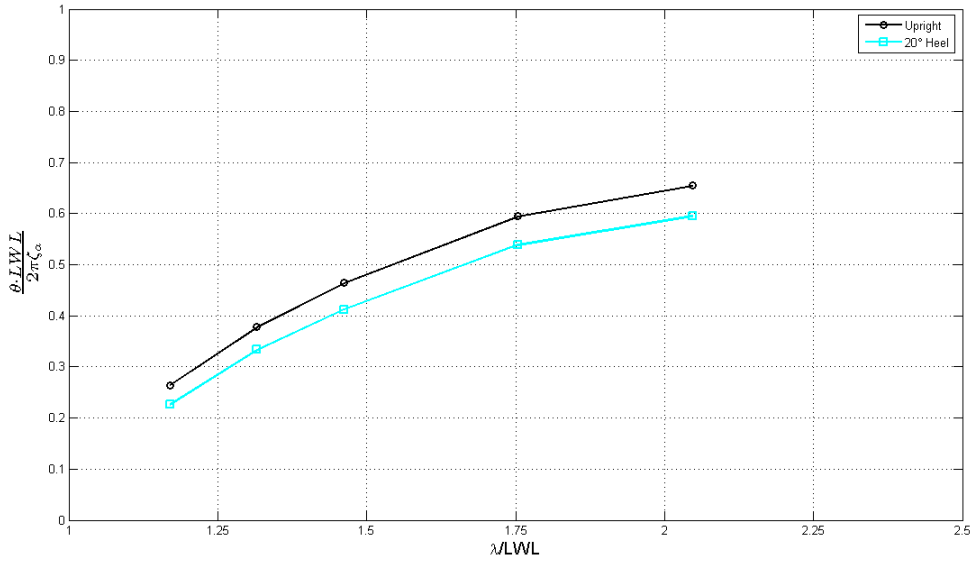

Figure D.44: Model # 45· Upright vs 20° Heel - Pitch : Fn=0.4, $\zeta_a = 25$ mm

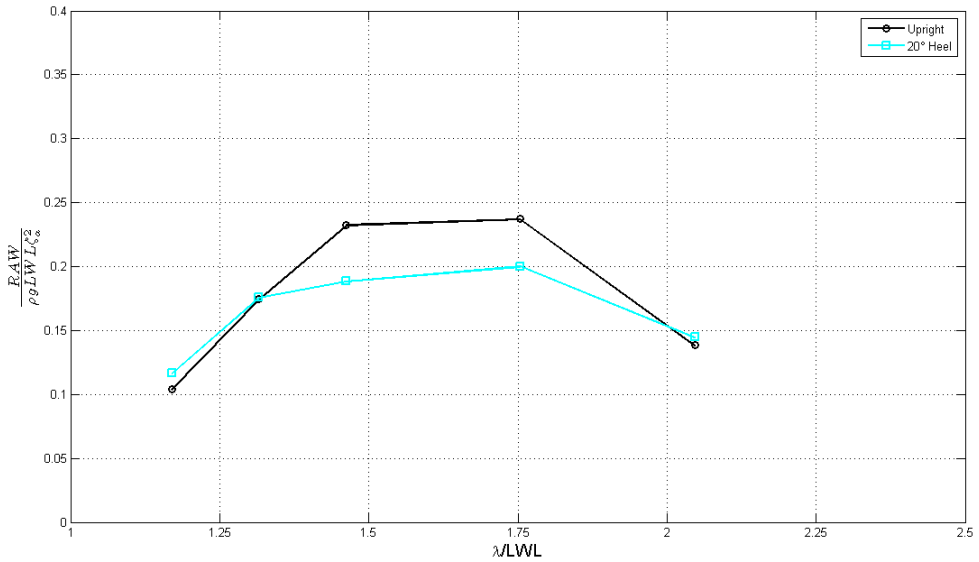

Figure D.45: Model # 45· Upright vs 20° Heel - Added resistance : Fn=0.4, $\zeta_a = 25$ mm

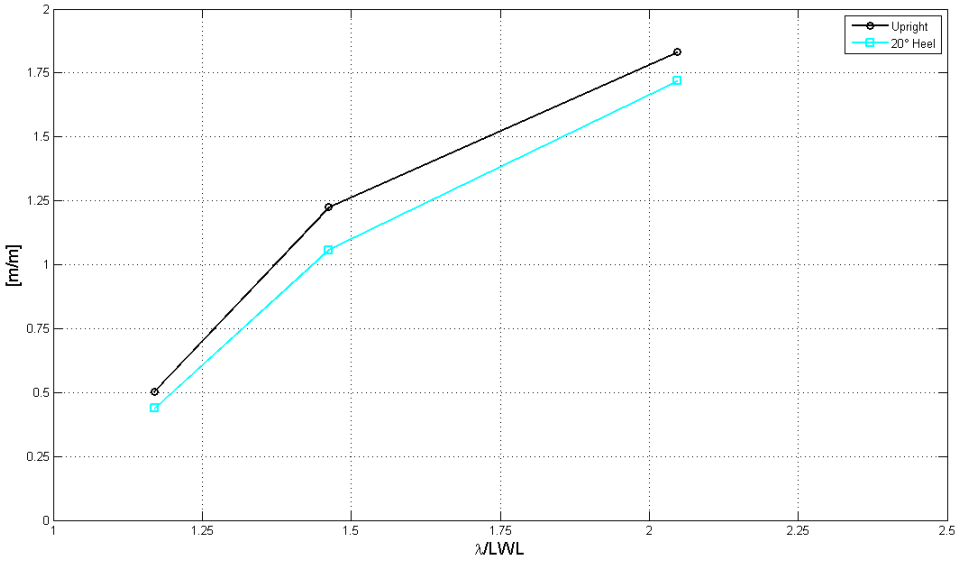

Figure D.46: Model # 45· Upright vs 20° Heel - Heave : Fn=0.4, $\zeta_a = 35$ mm

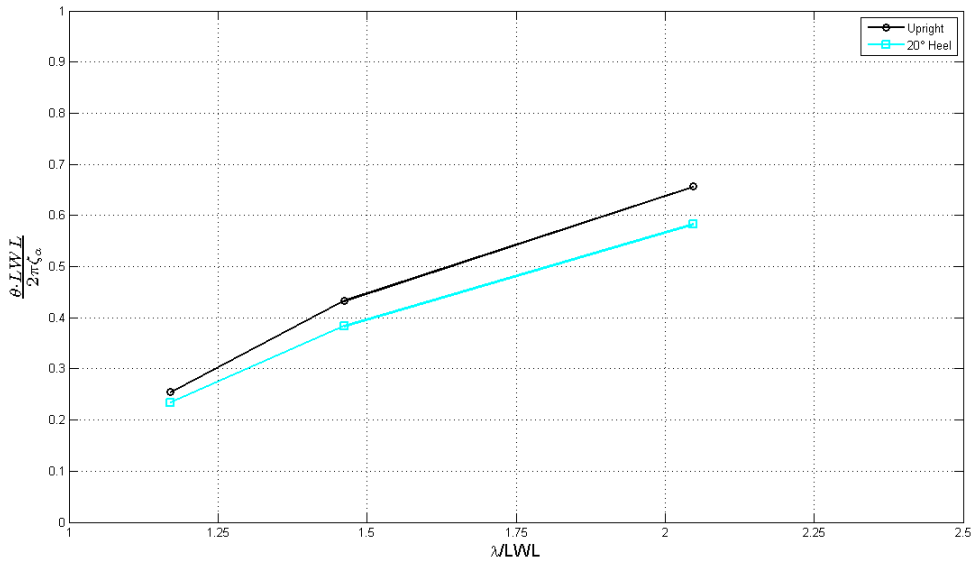

Figure D.47: Model # 45· Upright vs 20° Heel - Pitch : Fn=0.4, $\zeta_a = 35$ mm

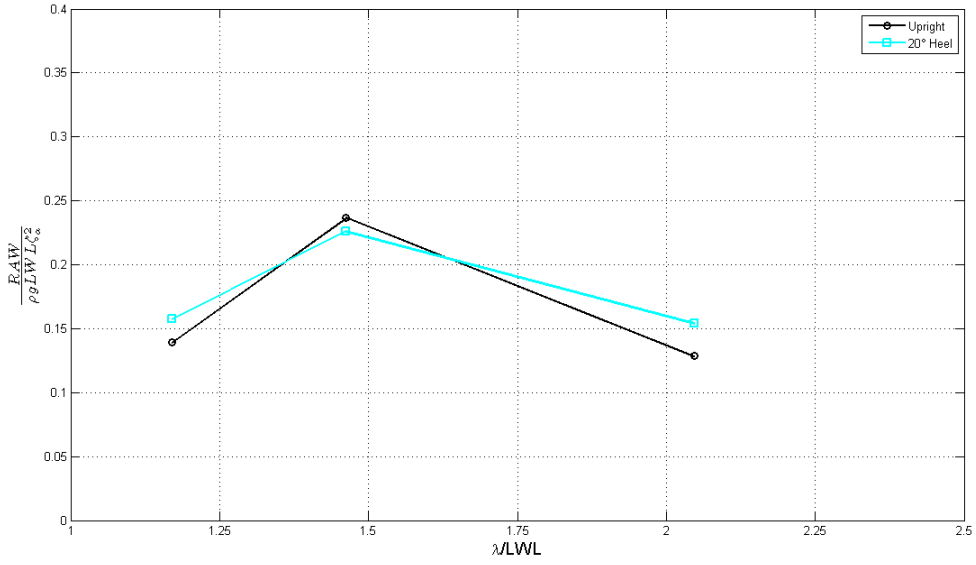

Figure D.48: Model # 45· Upright vs 20° Heel - Added resistance : Fn=0.4, $\zeta_a = 35$ mm

D.3 Study of the surge force

Model # 43

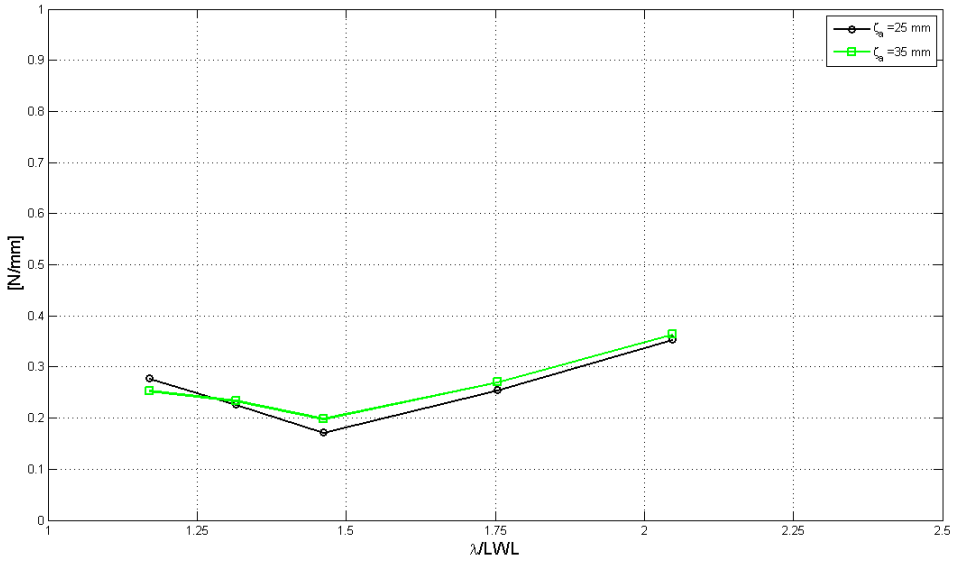

Figure D.49: Model # 43· $\frac{|\text{Surge Force}|}{\zeta_a}$ - Fn=0.325, Upright, No surge

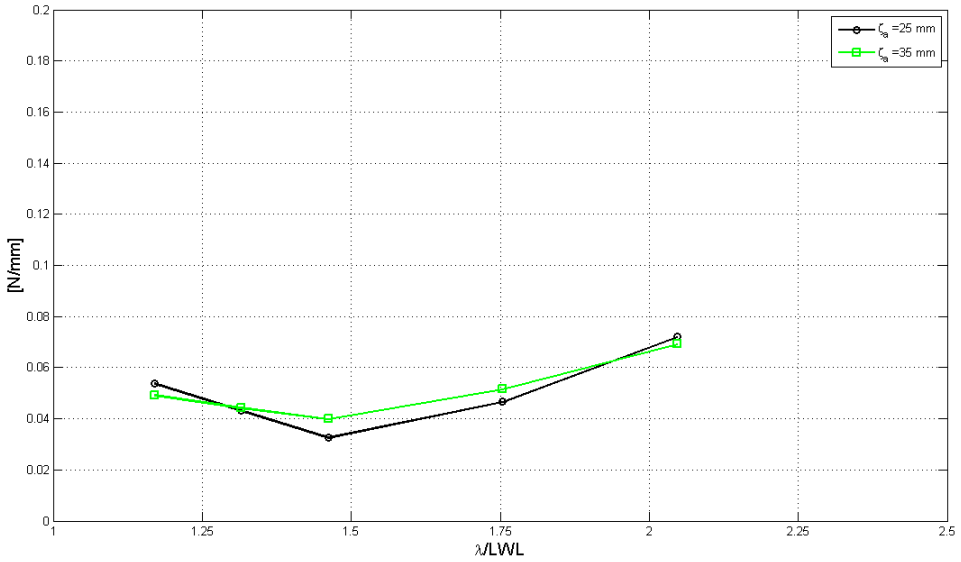

Figure D.50: Model # 43· $\frac{|\text{Surge Force}|}{\zeta_a}$ - Fn=0.325, Upright, Free to surge

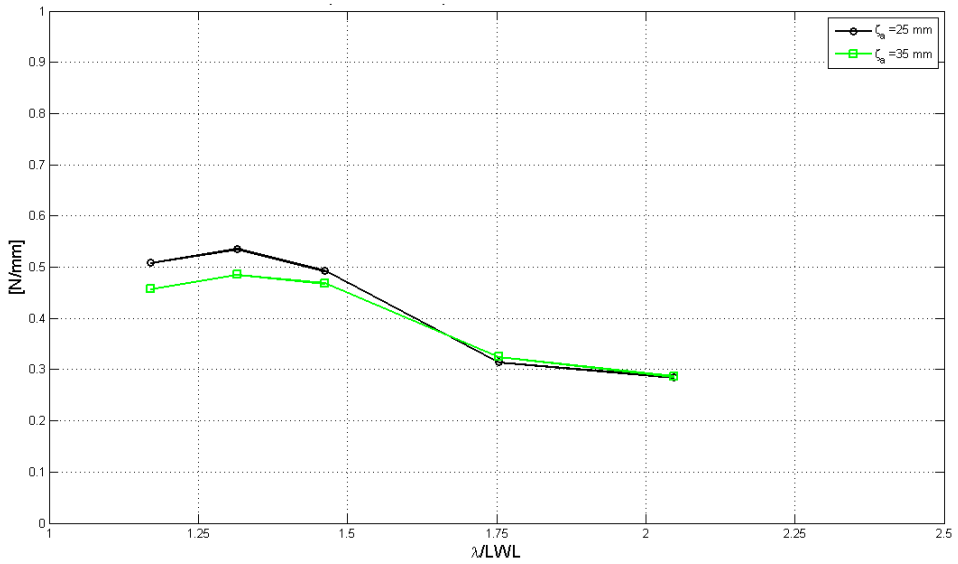

Figure D.51: Model # 43· $\frac{|\text{Surge Force}|}{\zeta_a}$ - Fn=0.4, Upright, No surge

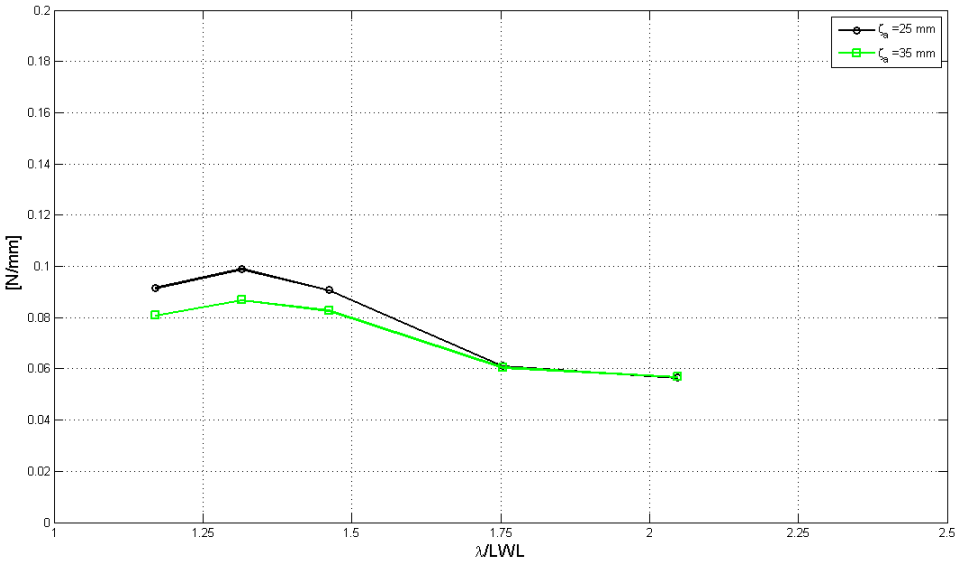

Figure D.52: Model # 43· $\frac{|\text{Surge Force}|}{\zeta_a}$ - Fn=0.4, Upright, Free to surge

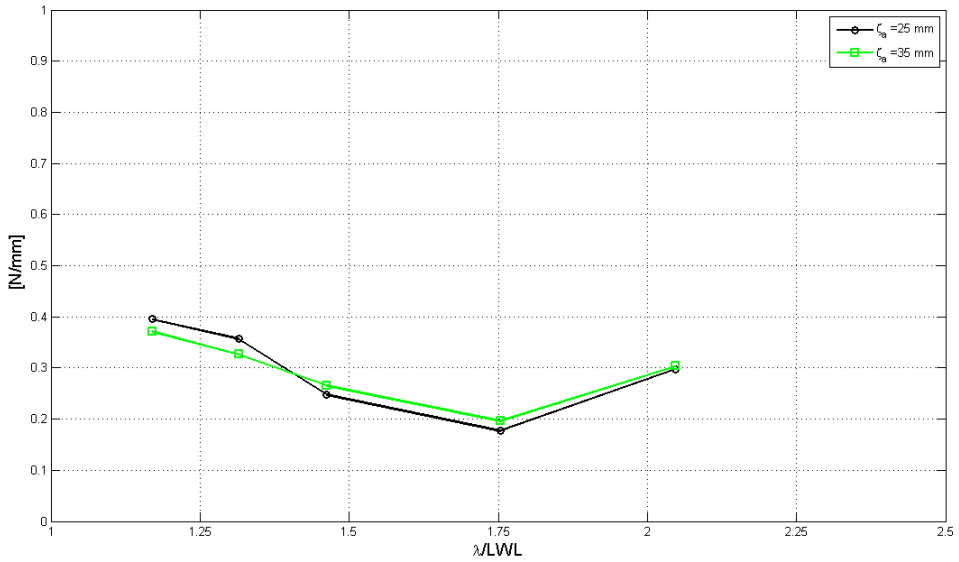

Figure D.53: Model # 43· $\frac{|\text{Surge Force}|}{\zeta_a}$ - Fn=0.325, 20° Heel, No surge

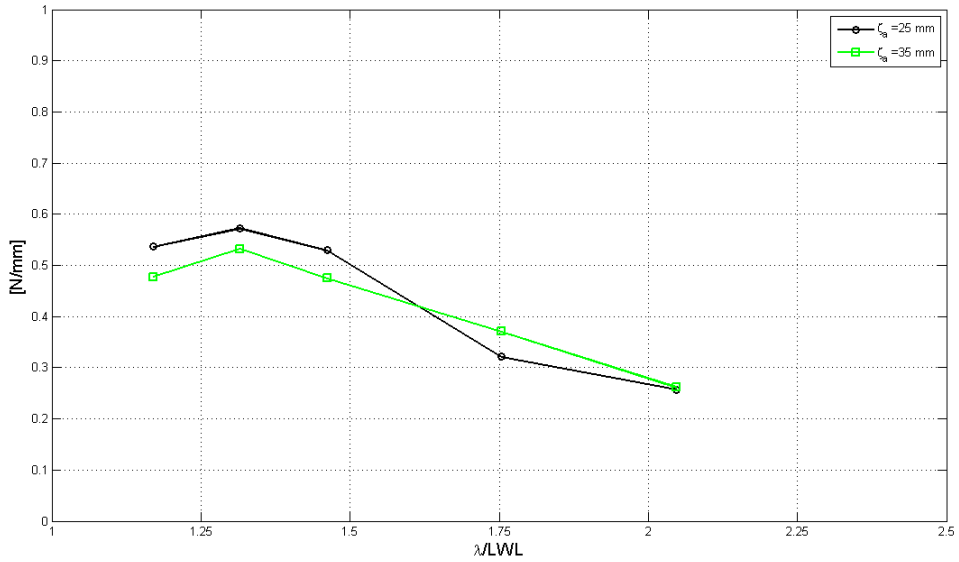

Figure D.54: Model # 43· $\frac{|\text{Surge Force}|}{\zeta_a}$ - Fn=0.4, 20° Heel, No surge

Model # 45

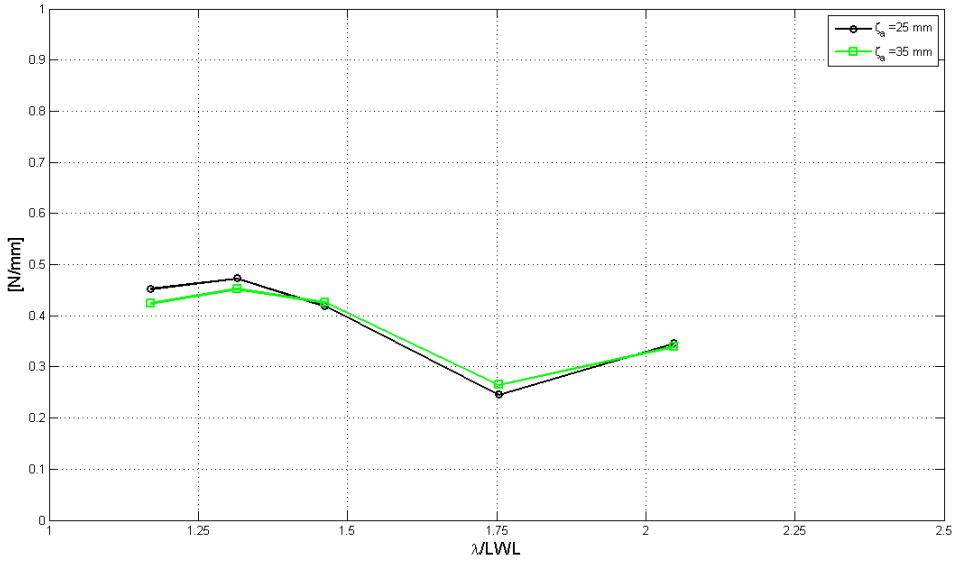

Figure D.55: Model # 45· $\frac{|\text{Surge Force}|}{\zeta_a}$ - Fn=0.325, Upright, No surge

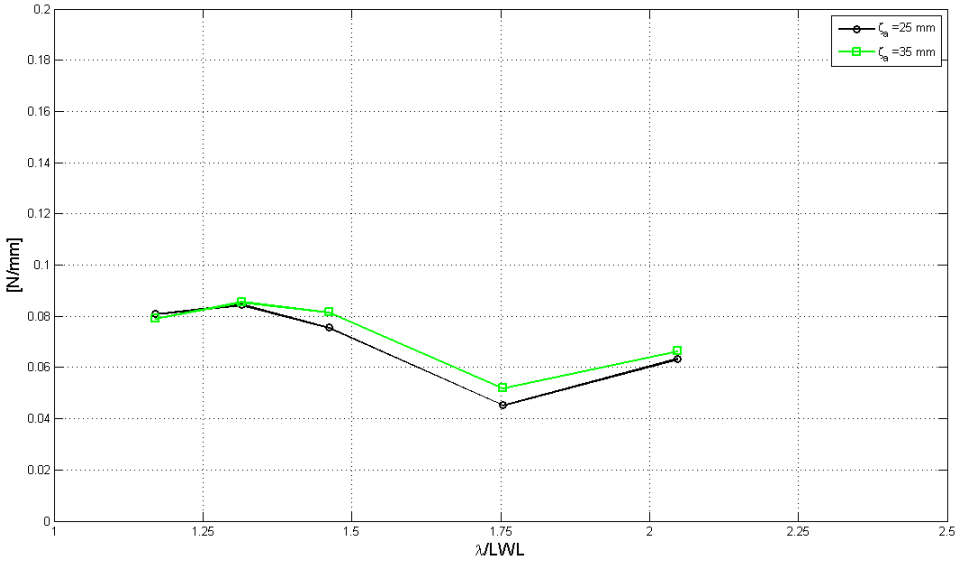

Figure D.56: Model # 45· $\frac{|\text{Surge Force}|}{\zeta_a}$ - Fn=0.325, Upright, Free to surge

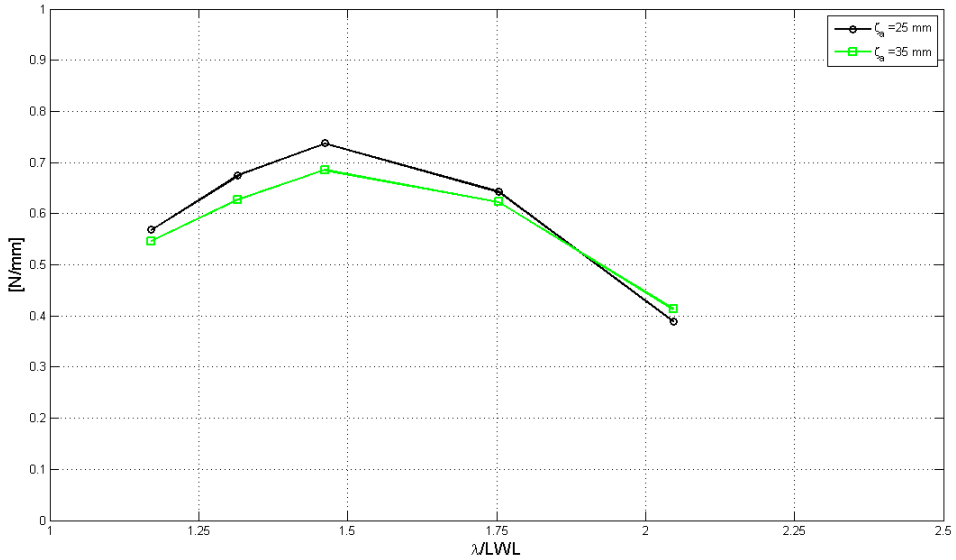

Figure D.57: Model # 45· $\frac{|\text{Surge Force}|}{\zeta_a}$ - Fn=0.4, Upright, No surge

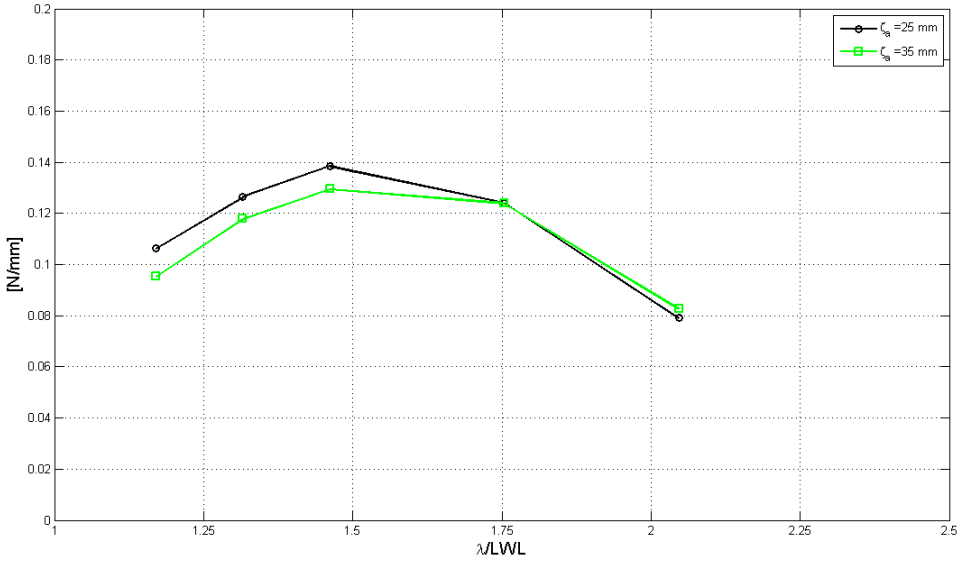

Figure D.58: Model # 45· $\frac{|\text{Surge Force}|}{\zeta_a}$ - Fn=0.4, Upright, Free to surge

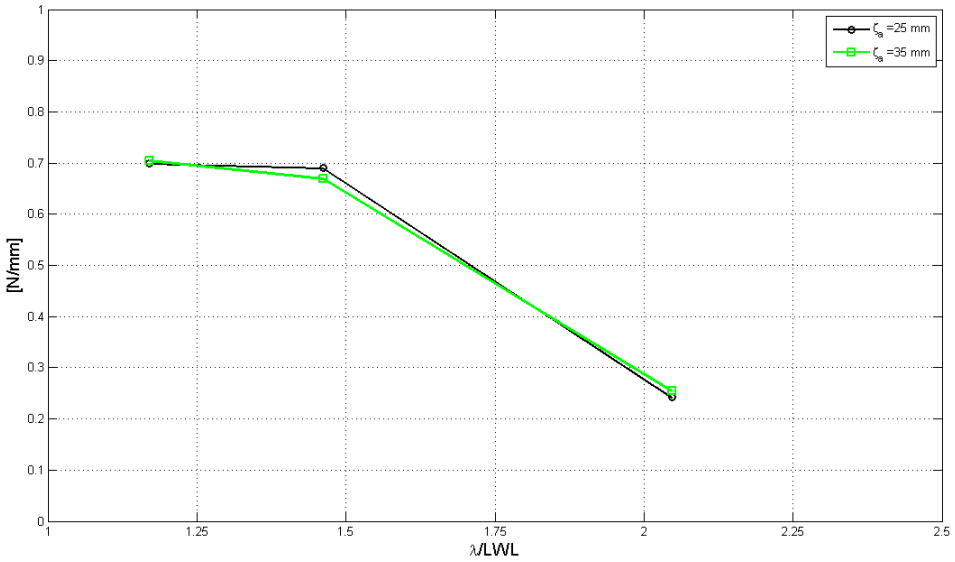

Figure D.59: Model # 45· $\frac{|\text{Surge Force}|}{\zeta_a}$ - Fn=0.325, 20° Heel, No surge

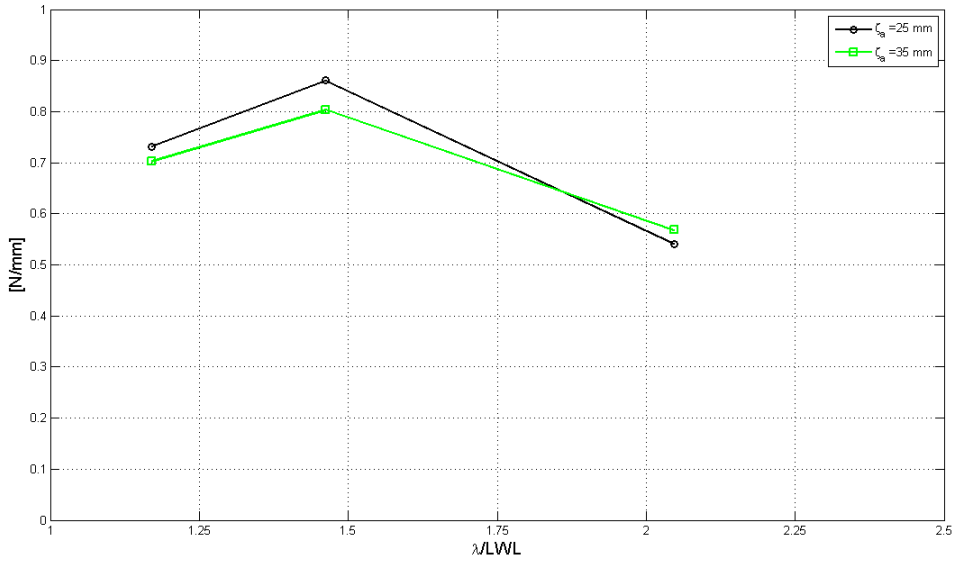

Figure D.60: Model # 45· $\frac{|\text{Surge Force}|}{\zeta_a}$ - Fn=0.4, 20° Heel, No surge

D.4 Comparison with previous experiments: study of the trim angle

Model # 43[2]

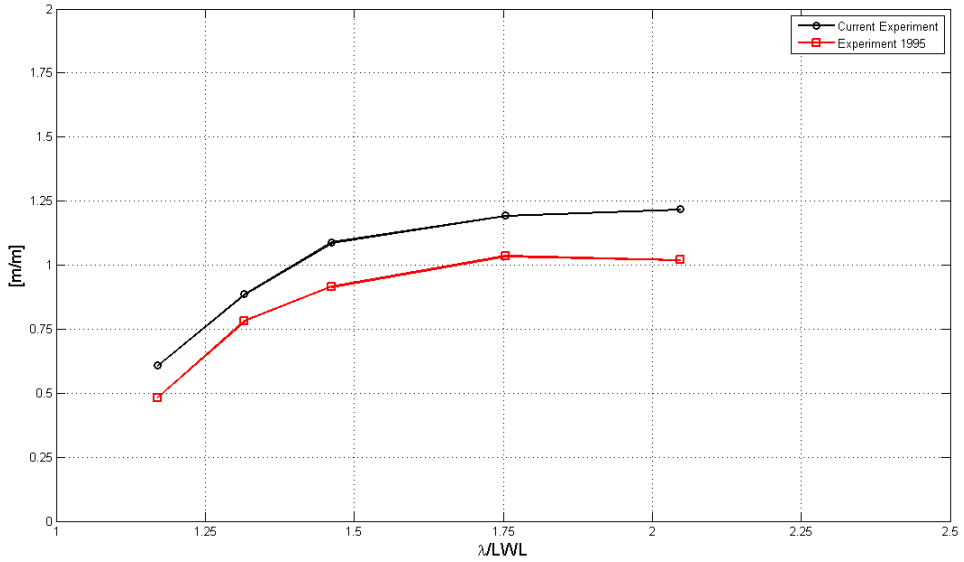

Figure D.61: Model # 43· Comparison with experiments 1995 - Heave: Fn=0.325, Upright

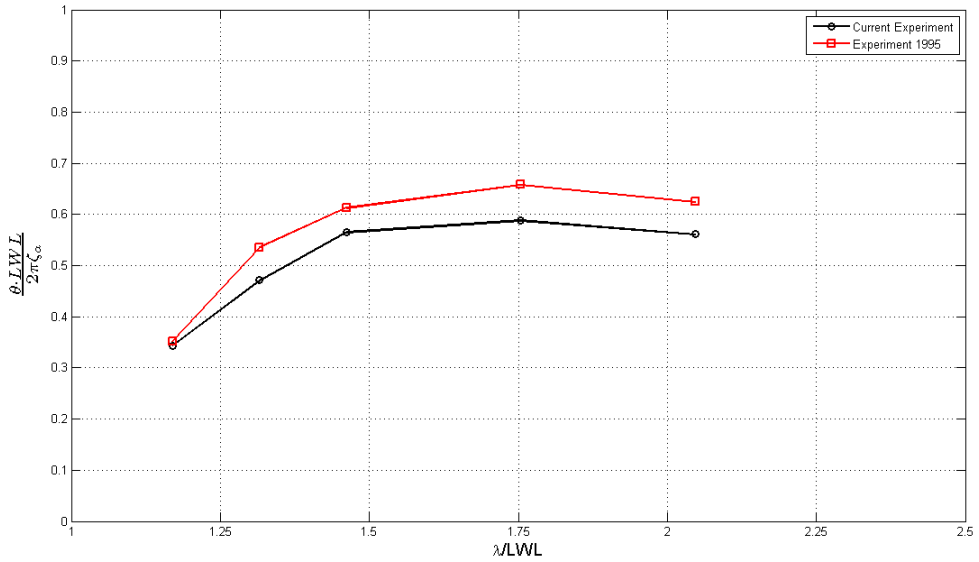

Figure D.62: Model # 43· Comparison with experiments 1995 - Pitch: Fn=0.325, Upright

[2]It should be recalled that, for this model, the radius of gyration k_{yy} used during the current experiments and the experiments performed in 1995 were different ($k_{yy} = 0.28$ and $k_{yy} = 0.25$ respectively).

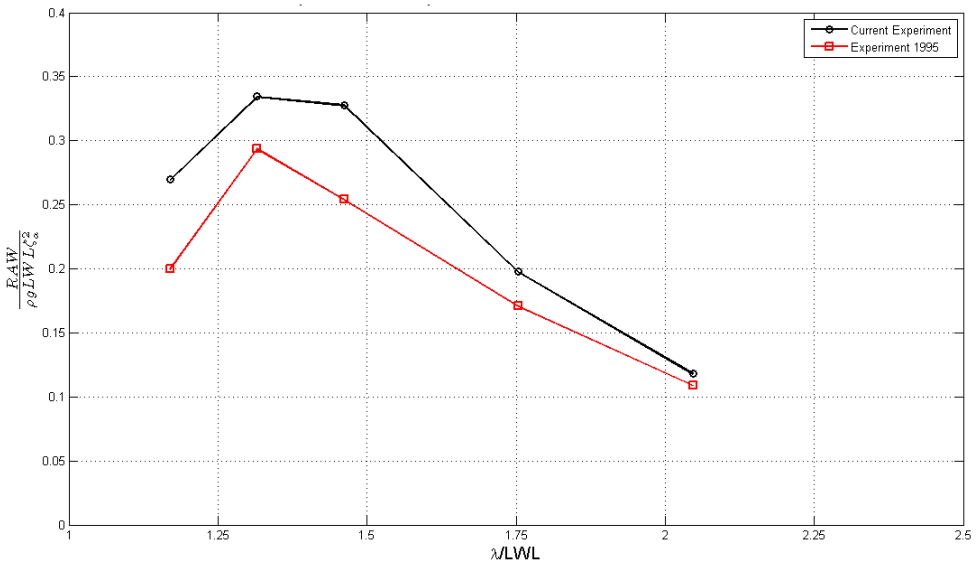

Figure D.63: Model # 43· Comparison with experiments 1995 - RAW: Fn=0.325, Upright

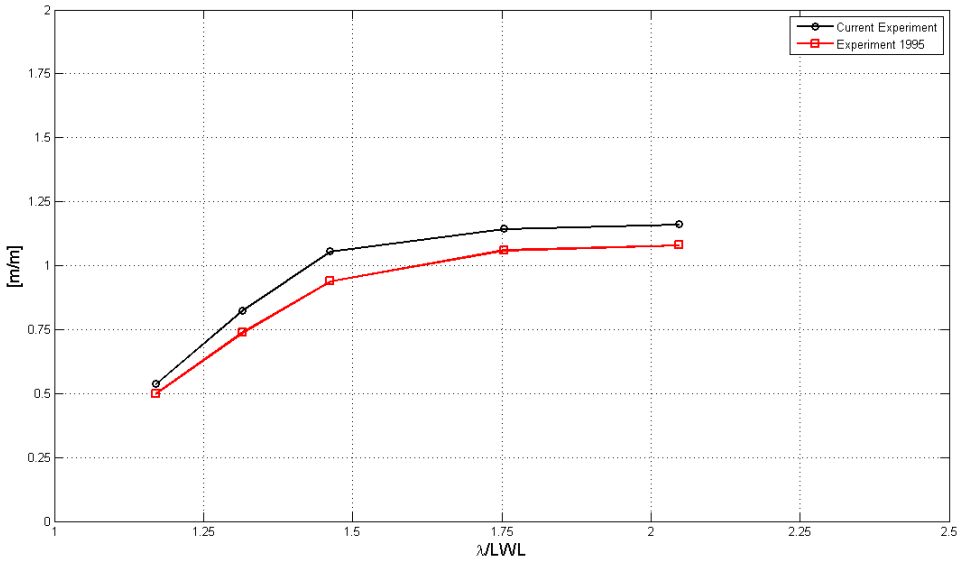

Figure D.64: Model # 43· Comparison with experiments 1995 - Heave: Fn=0.325, 20° Heel

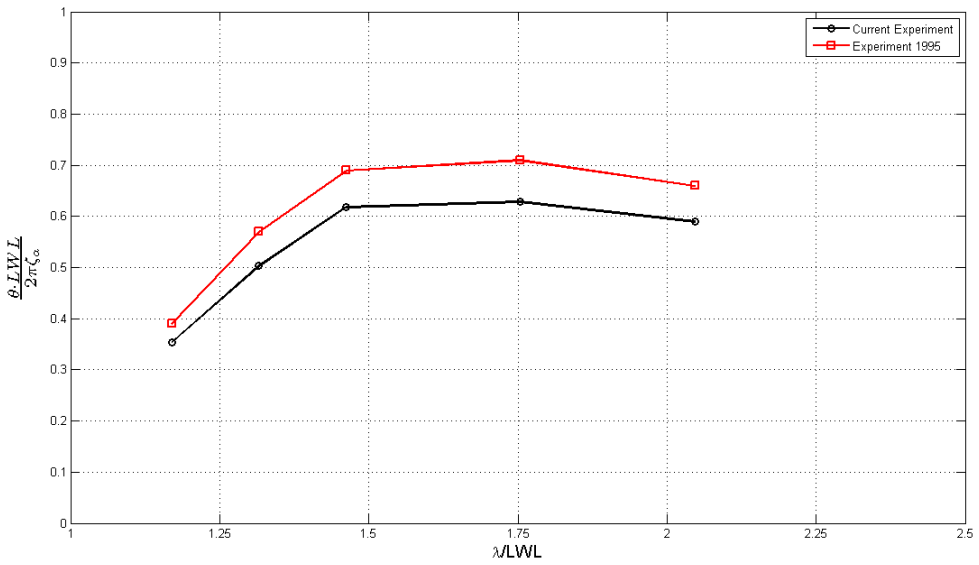

Figure D.65: Model # 43· Comparison with experiments 1995 - Pitch: Fn=0.325, 20° Heel

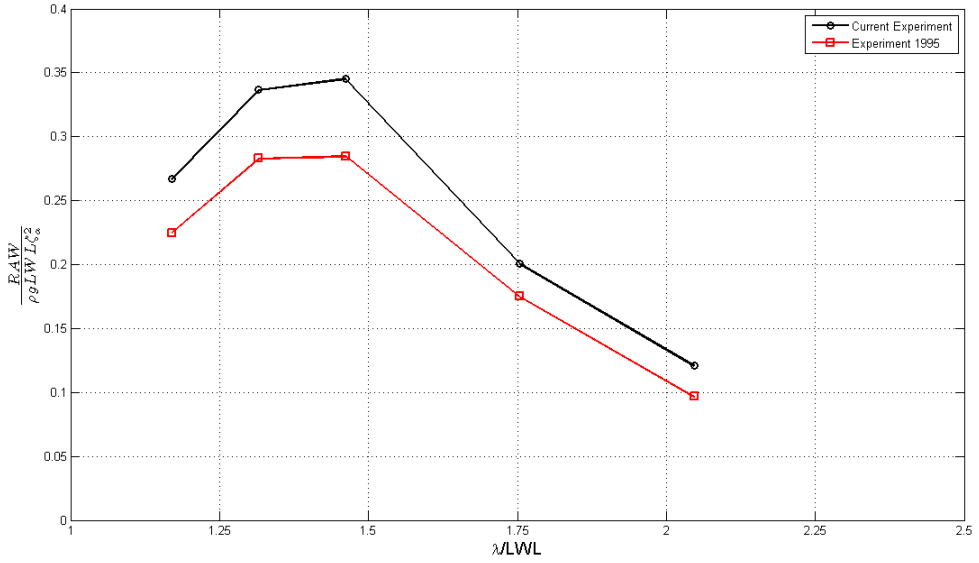

Figure D.66: Model # 43· Comparison with experiments 1995 - RAW: Fn=0.325, 20° Heel

Model # 45

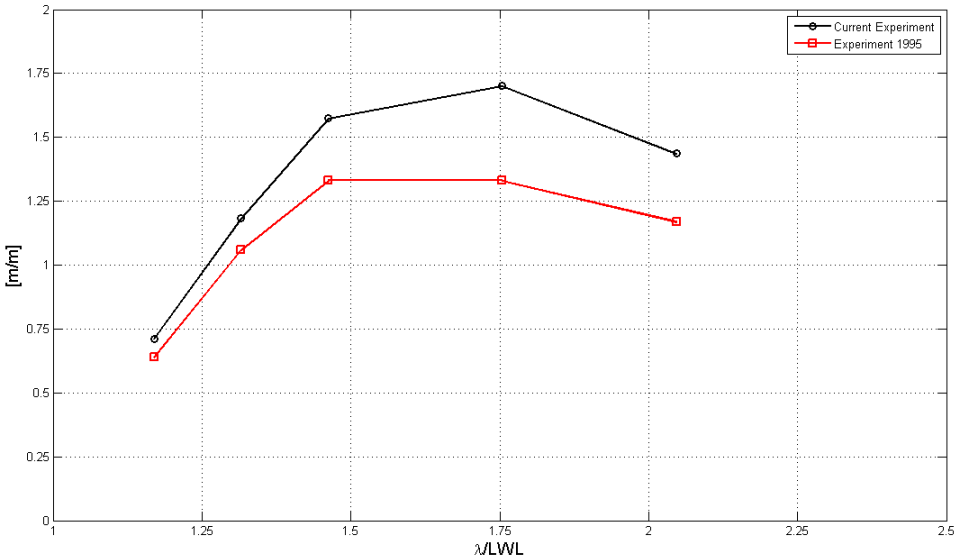

Figure D.67: Model # 45· Comparison with experiments 1995 - Heave: Fn=0.325, Upright

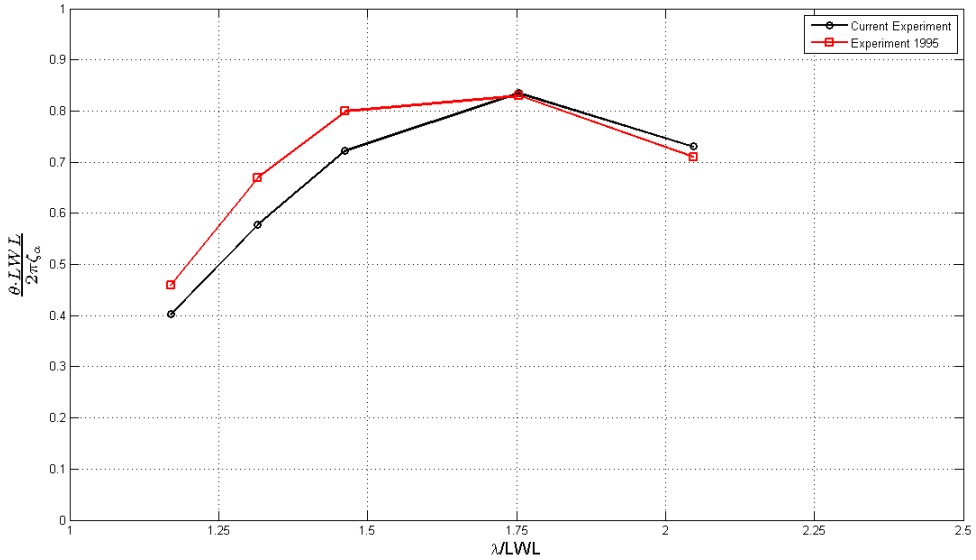

Figure D.68: Model # 45· Comparison with experiments 1995 - Pitch: Fn=0.325, Upright

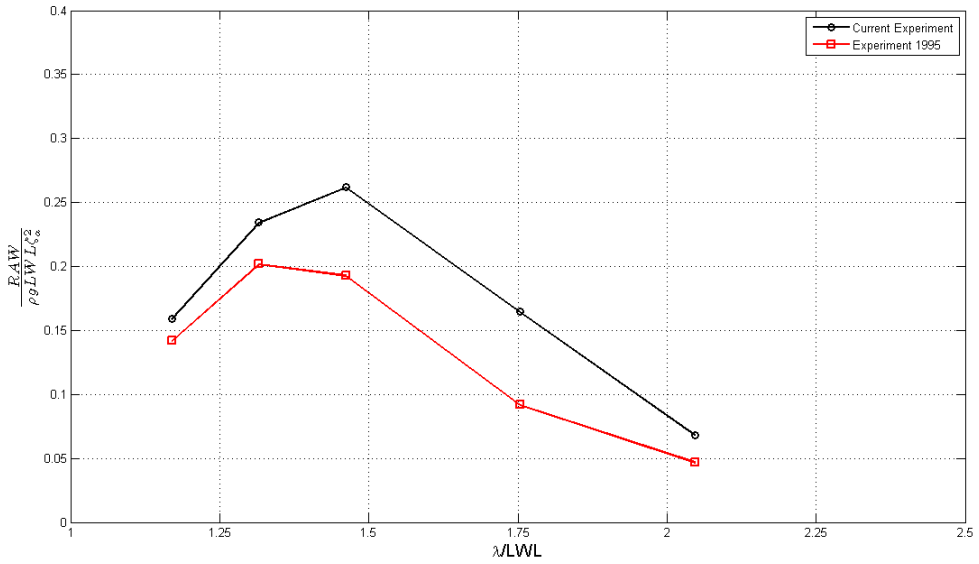

Figure D.69: Model # 45· Comparison with experiments 1995 - RAW: Fn=0.325, Upright

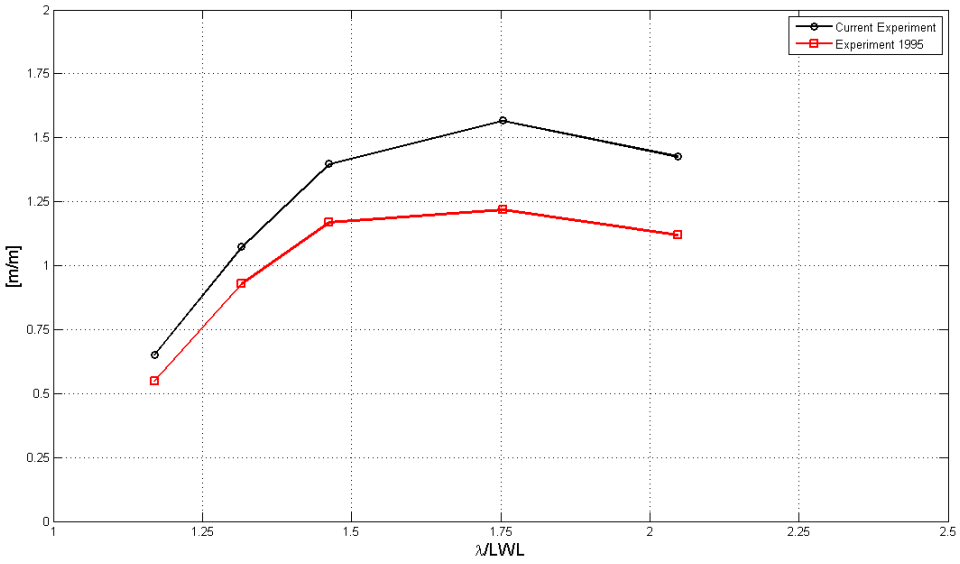

Figure D.70: Model # 45· Comparison with experiments 1995 - Heave: Fn=0.325, 20° Heel

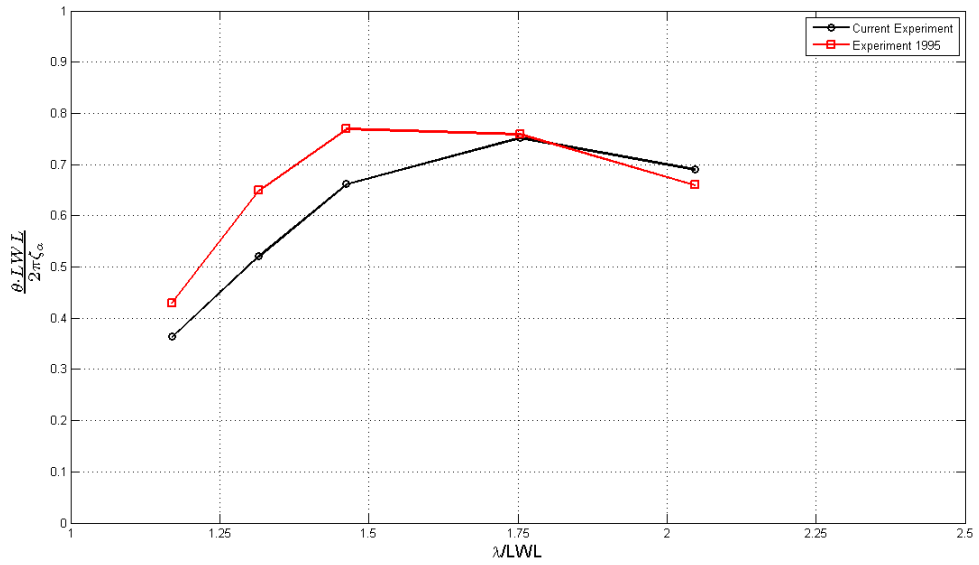

Figure D.71: Model # 45· Comparison with experiments 1995 - Pitch: Fn=0.325, 20° Heel

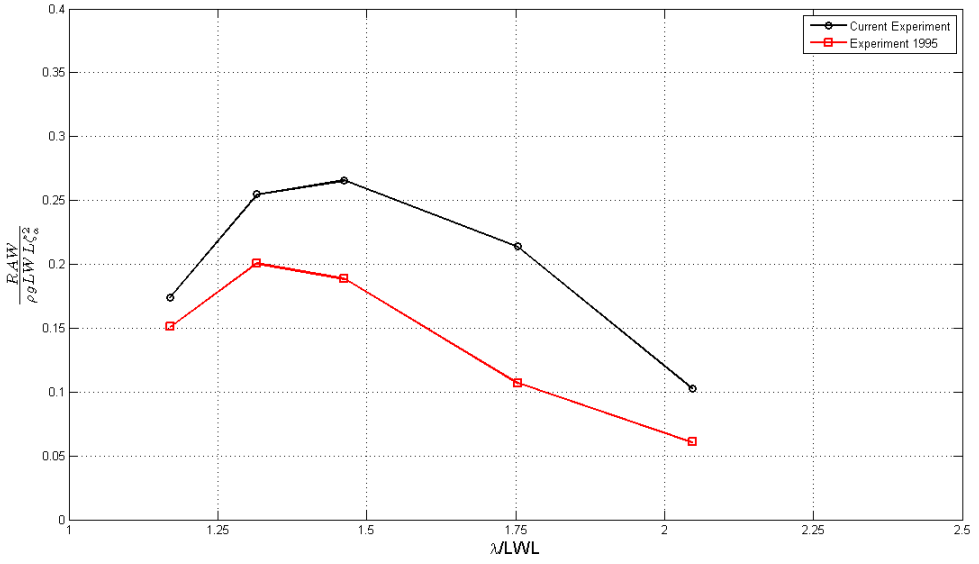

Figure D.72: Model # 45· Comparison with experiments 1995 - RAW: Fn=0.325, 20° Heel

D.5 Study of the effect of the heeling angle with PDSTRIP

Model # 43

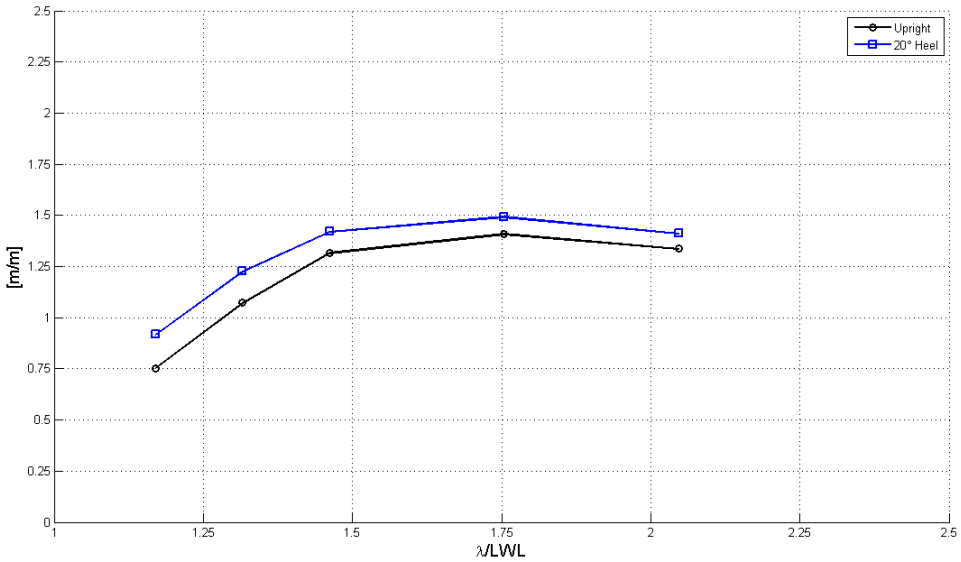

Figure D.73: Model # 43· Upright vs 20° Heel - Heave: Fn=0.325. PDSTRIP

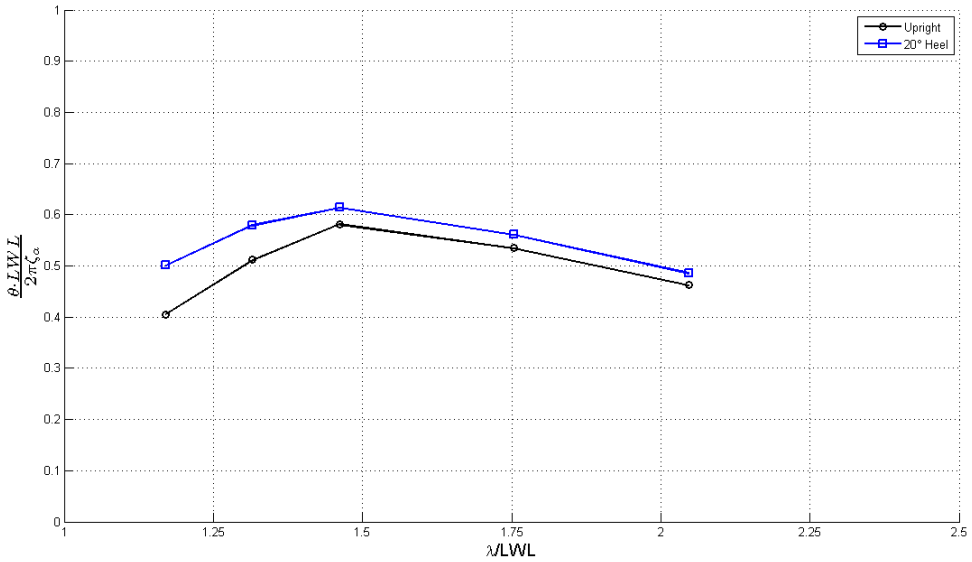

Figure D.74: Model # 43· Upright vs 20° Heel - Pitch: Fn=0.325. PDSTRIP

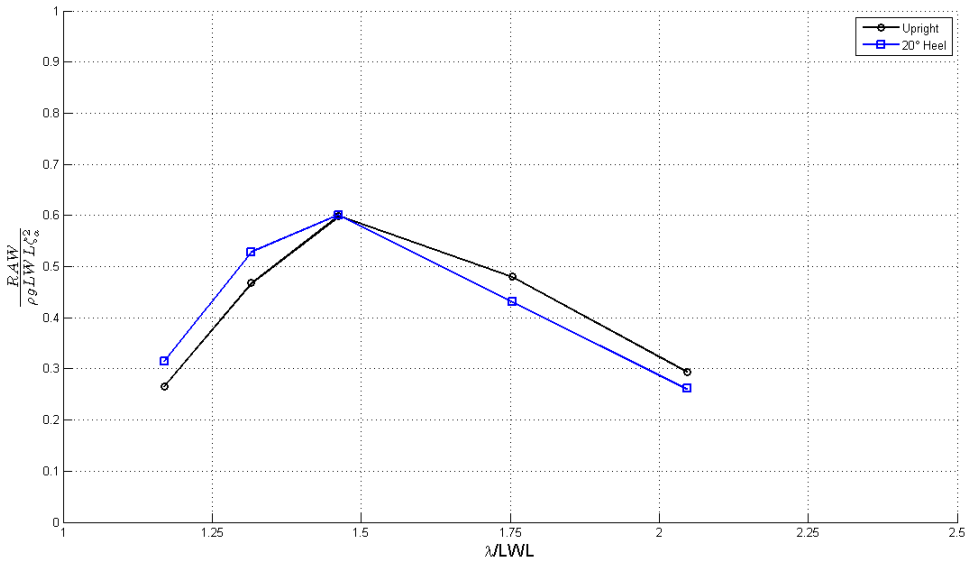

Figure D.75: Model # 43· Upright vs 20° Heel - Added resistance: Fn=0.325. PDSTRIP

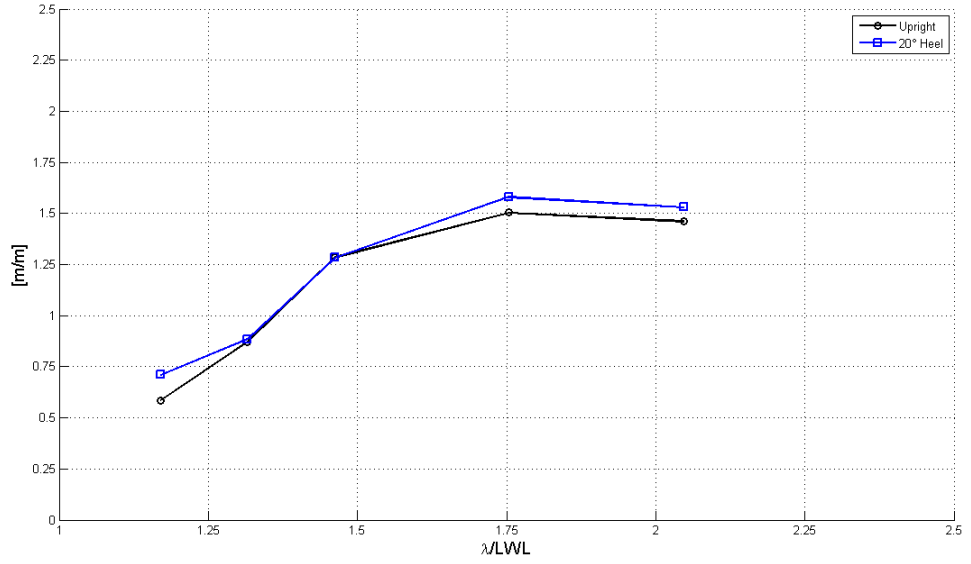

Figure D.76: Model # 43· Upright vs 20° Heel - Heave: Fn=0.4. PDSTRIP

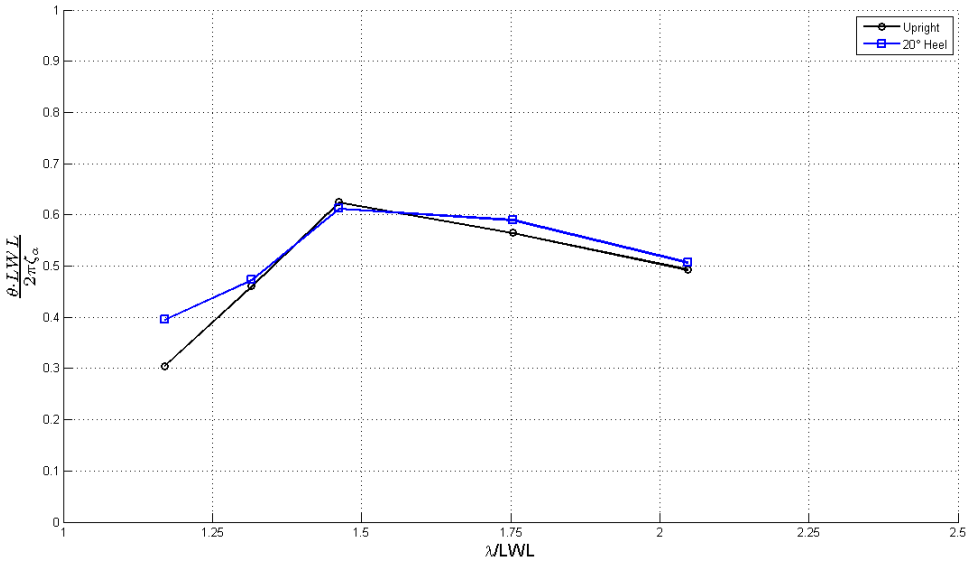

Figure D.77: Model # 43· Upright vs 20° Heel - Pitch: Fn=0.4. PDSTRIP

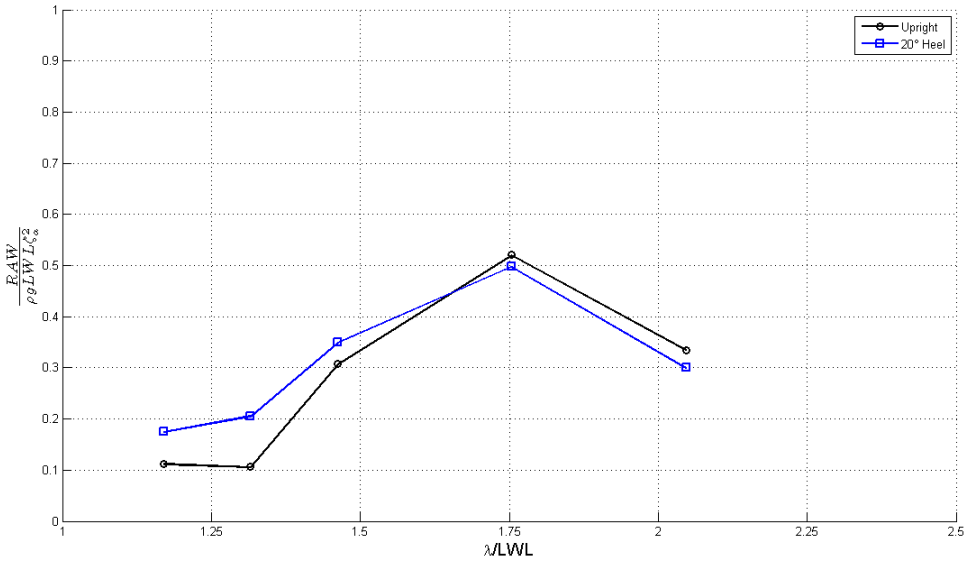

Figure D.78: Model # 43· Upright vs 20° Heel - Added resistance: Fn=0.4. PDSTRIP

Model # 45

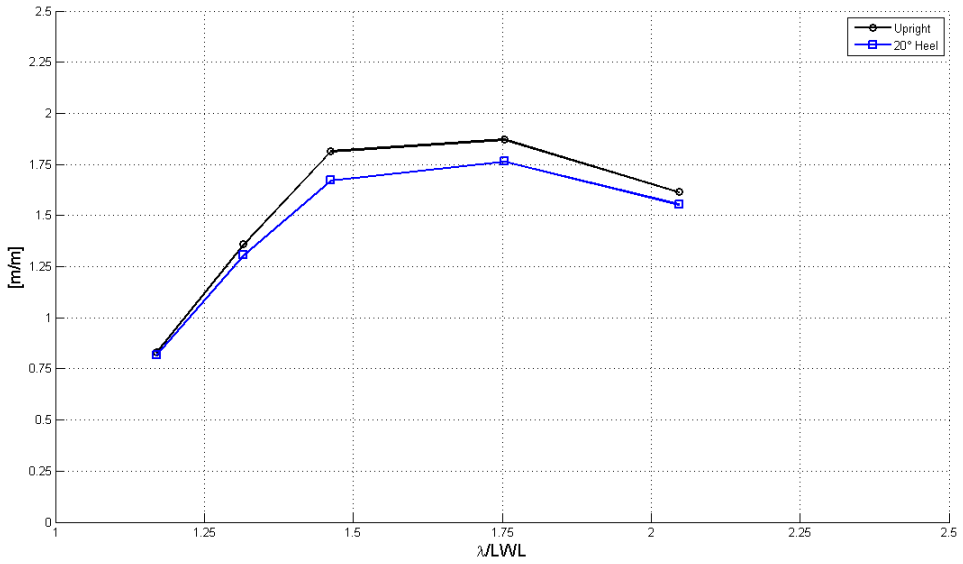

Figure D.79: Model # 45· Upright vs 20° Heel - Heave: Fn=0.325. PDSTRIP

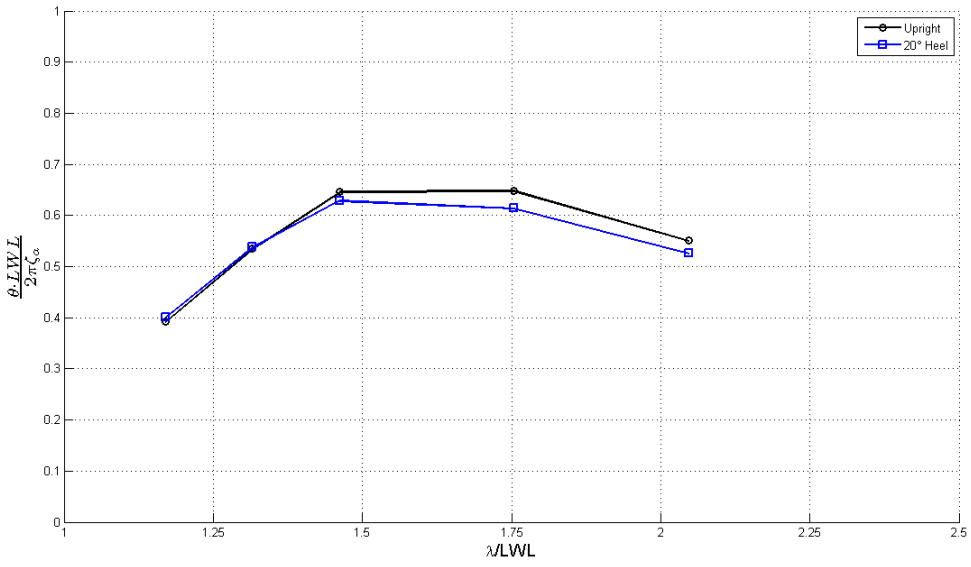

Figure D.80: Model # 45· Upright vs 20° Heel - Pitch: Fn=0.325. PDSTRIP

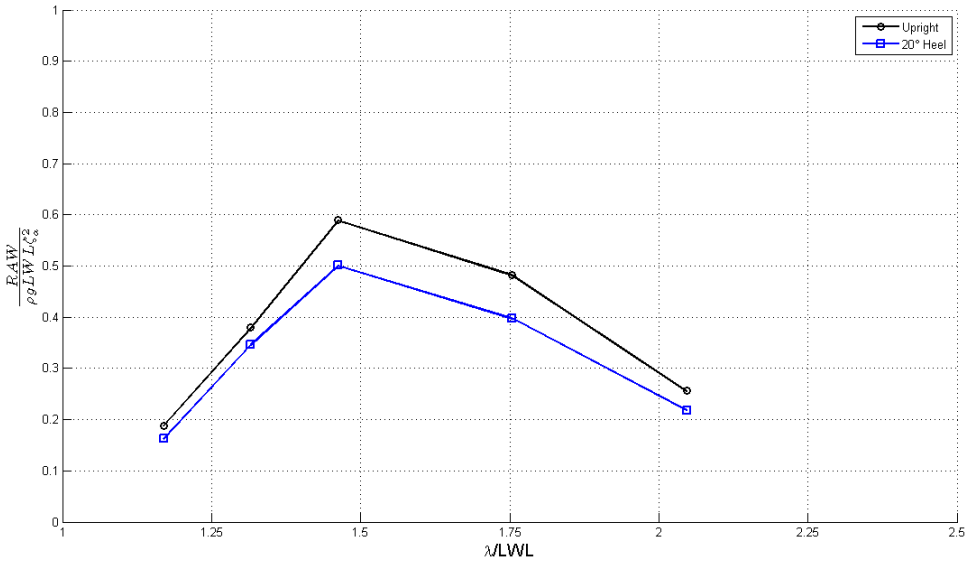

Figure D.81: Model # 45· Upright vs 20° Heel - Added resistance: Fn=0.325. PDSTRIP

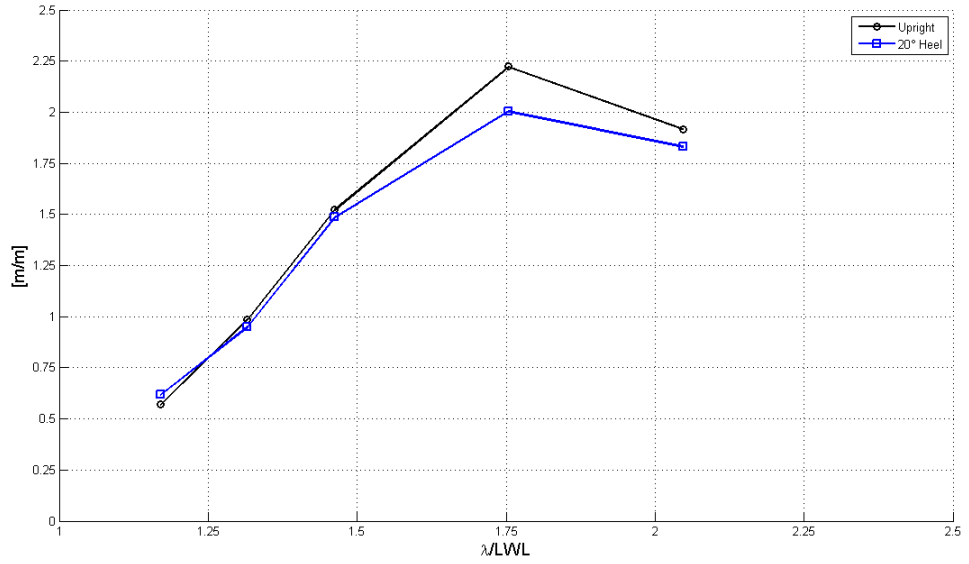

Figure D.82: Model # 45· Upright vs 20° Heel - Heave: Fn=0.4. PDSTRIP

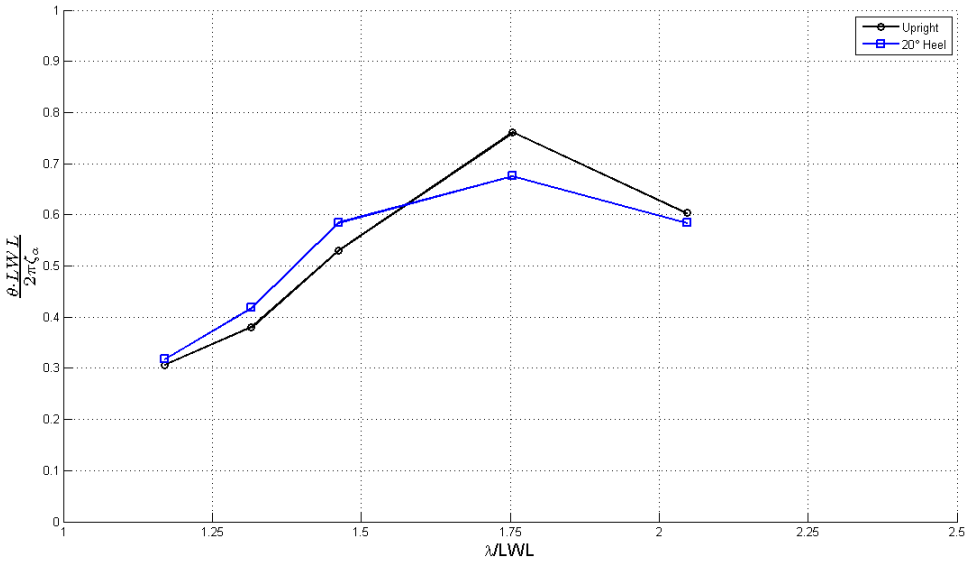

Figure D.83: Model # 45· Upright vs 20° Heel - Pitch: Fn=0.4. PDSTRIP

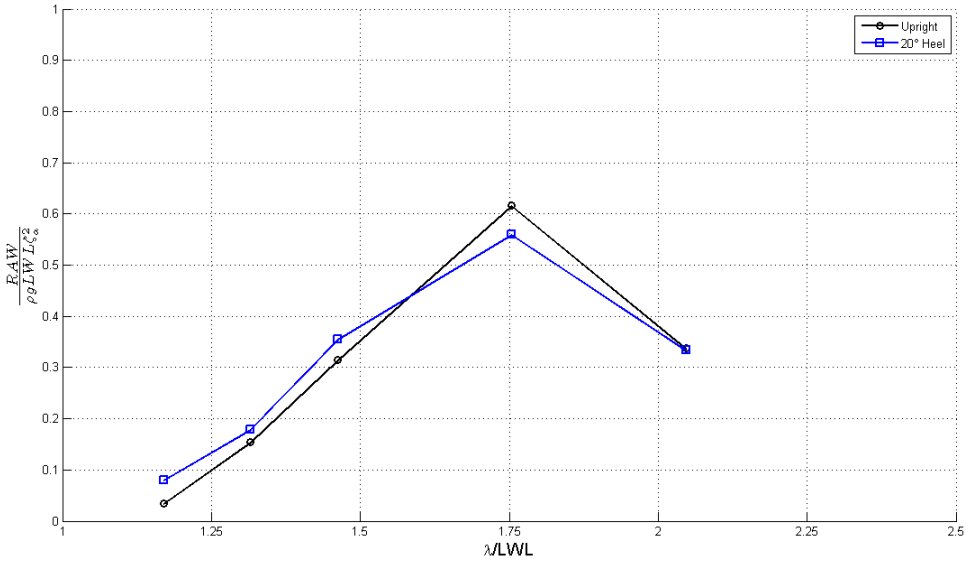

Figure D.84: Model # 45· Upright vs 20° Heel - Added resistance: Fn=0.4. PDSTRIP

D.6 Time-domain simulations

Model # 43

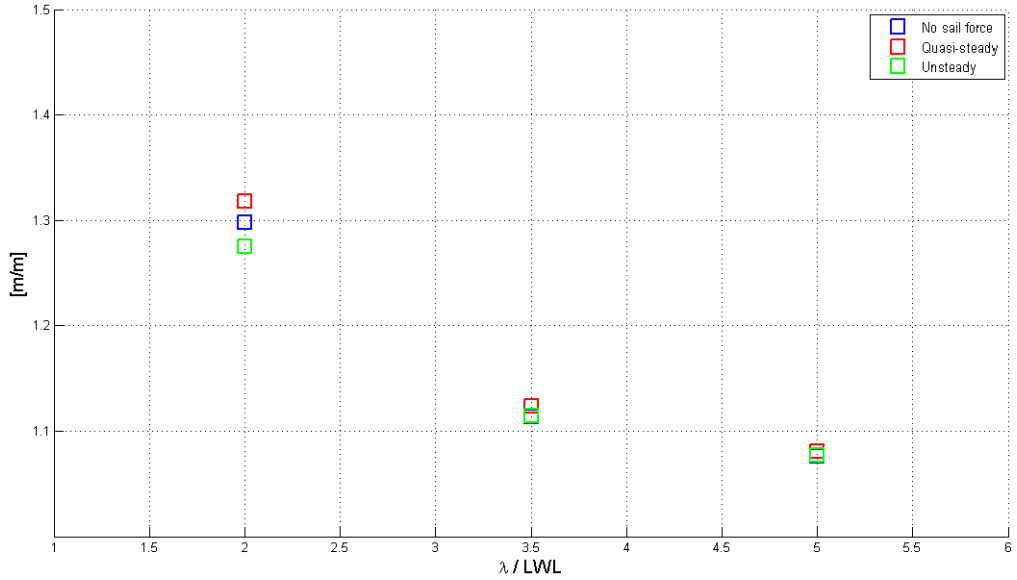

Figure D.85: Model # 43· Heave mean and amplitude: Fn=0.35, $\zeta_a = 0.25$ m, Upright

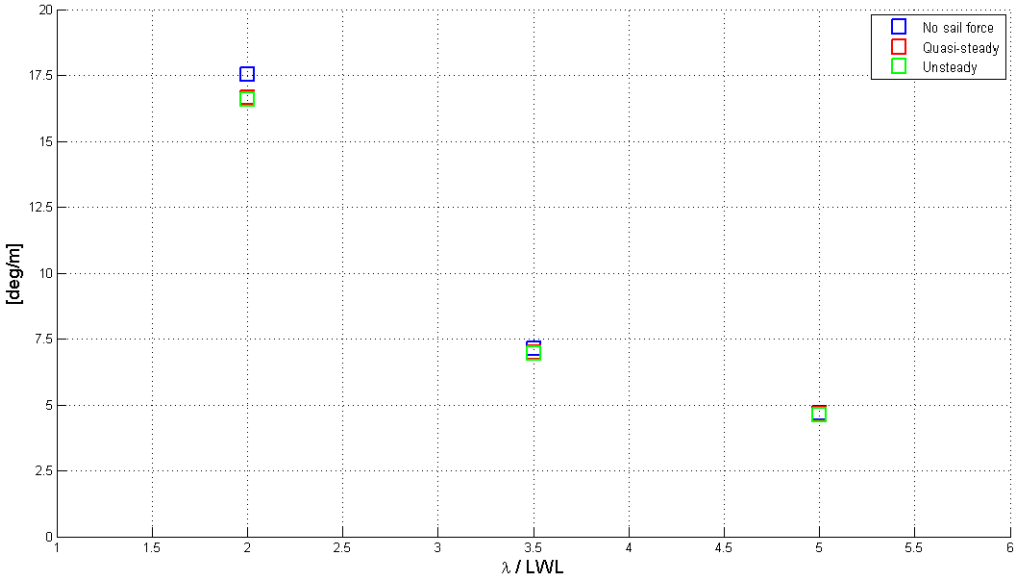

Figure D.86: Model # 43· Pitch mean and amplitude: Fn=0.35, $\zeta_a = 0.25$ m, Upright

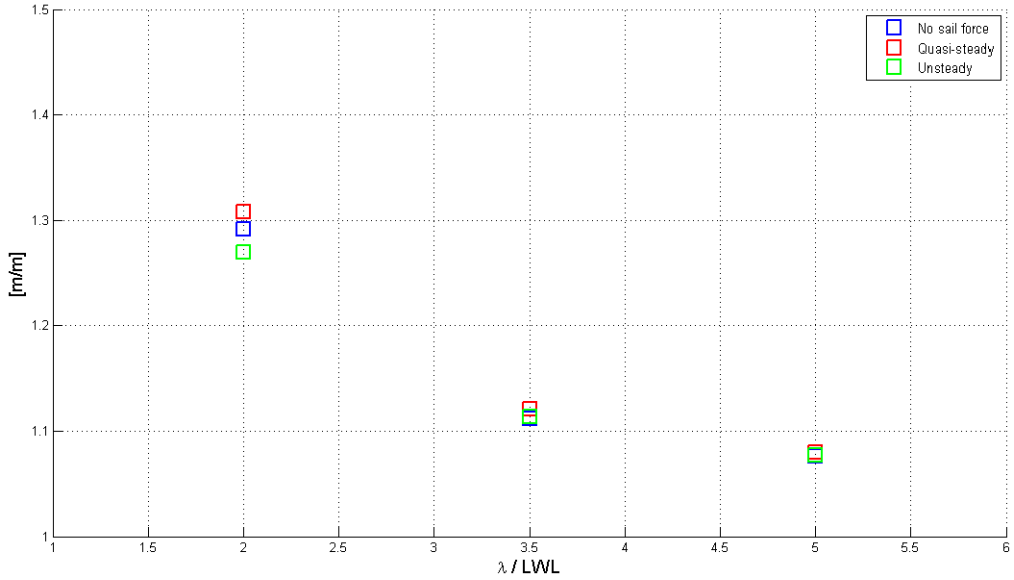

Figure D.87: Model # 43· Heave mean and amplitude: Fn=0.35, $\zeta_a = 0.6$ m, Upright

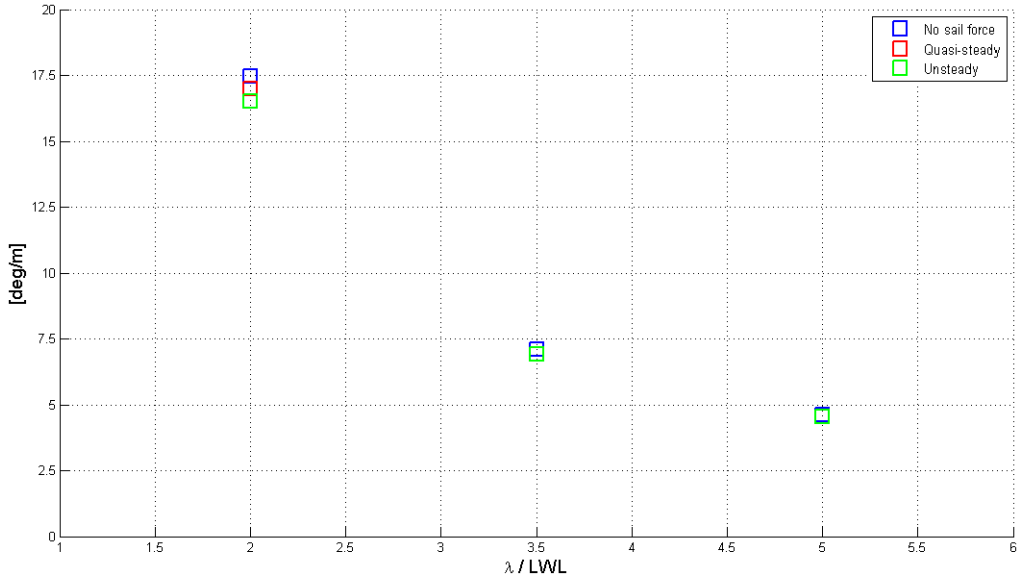

Figure D.88: Model # 43· Pitch mean and amplitude: Fn=0.35, $\zeta_a = 0.6$ m, Upright

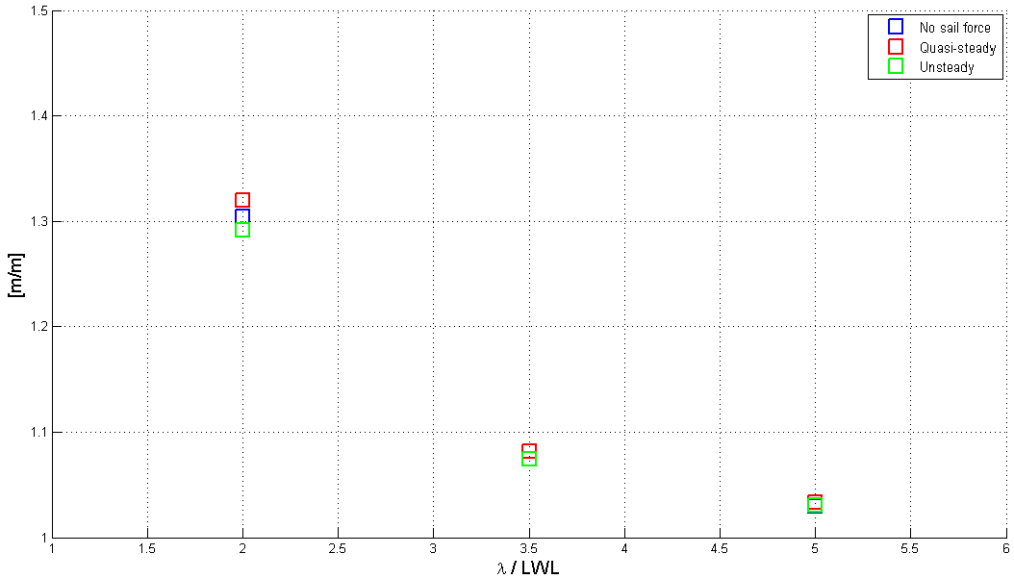

Figure D.89: Model # 43· Heave mean and amplitude: Fn=0.35, $\zeta_a = 0.25$ m, 20° Heel

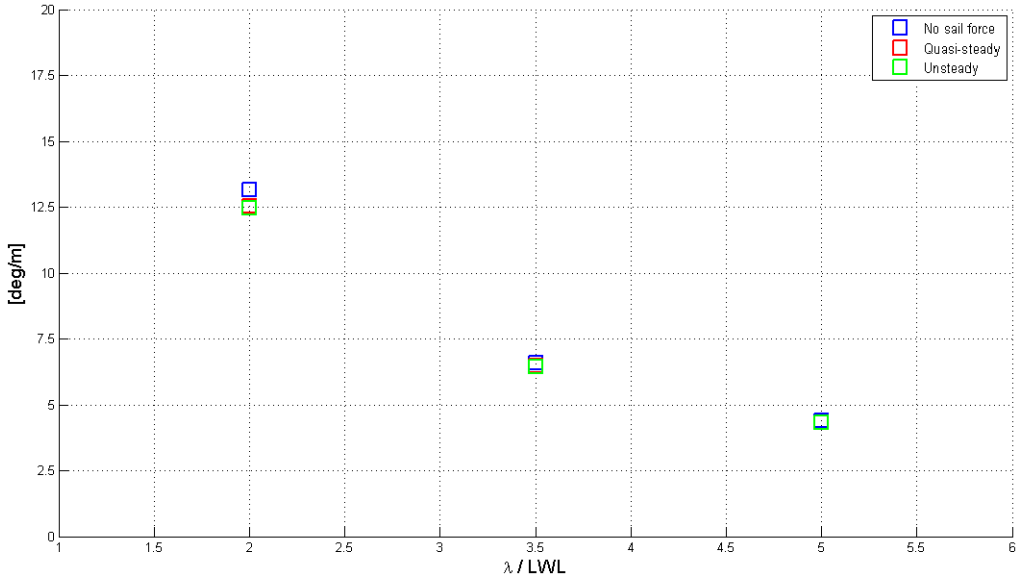

Figure D.90: Model # 43· Pitch mean and amplitude: Fn=0.35, $\zeta_a = 0.25$ m, 20° Heel

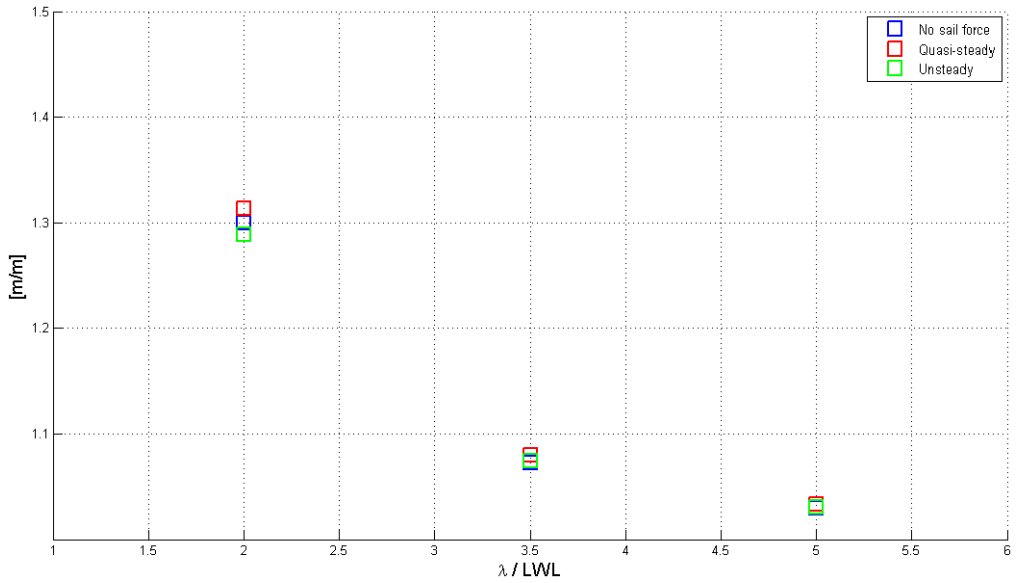

Figure D.91: Model # 43· Heave mean and amplitude: Fn=0.35, $\zeta_a = 0.6$ m, 20° Heel

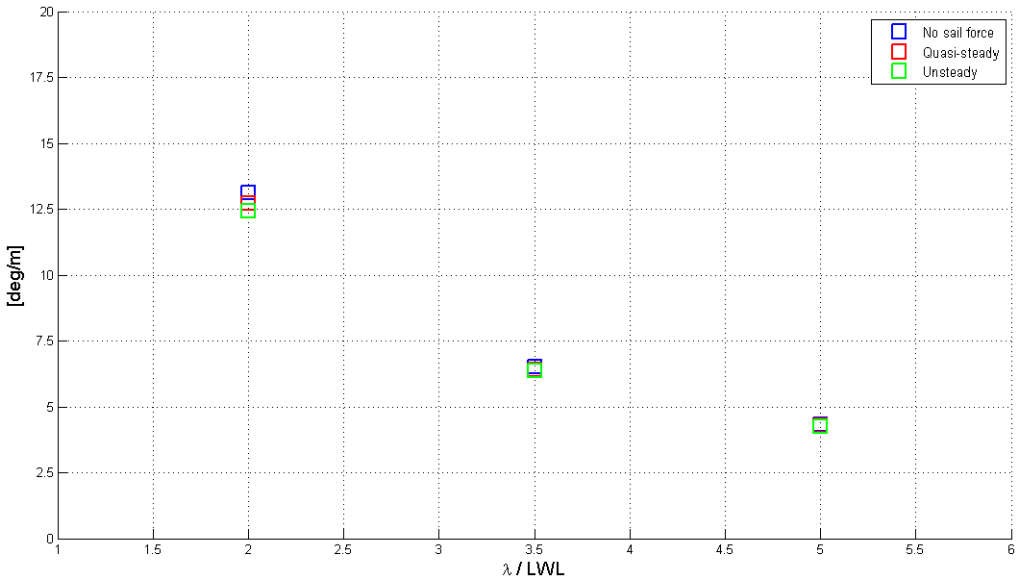

Figure D.92: Model # 43· Pitch mean and amplitude: Fn=0.35, $\zeta_a = 0.6$ m, 20° Heel

Model # 45

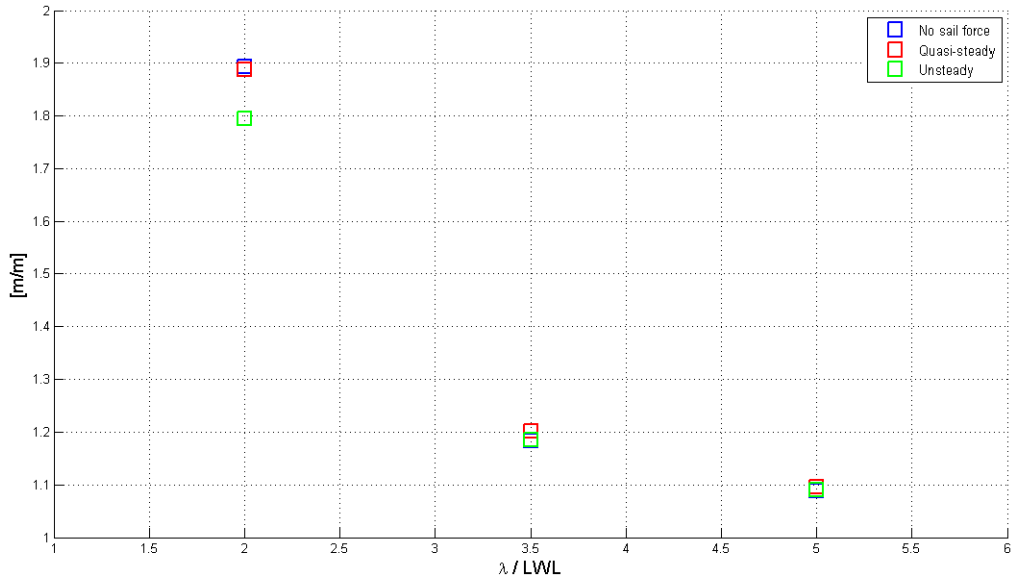

Figure D.93: Model # 45· Heave mean and amplitude: Fn=0.35, $\zeta_a = 0.25$ m, Upright

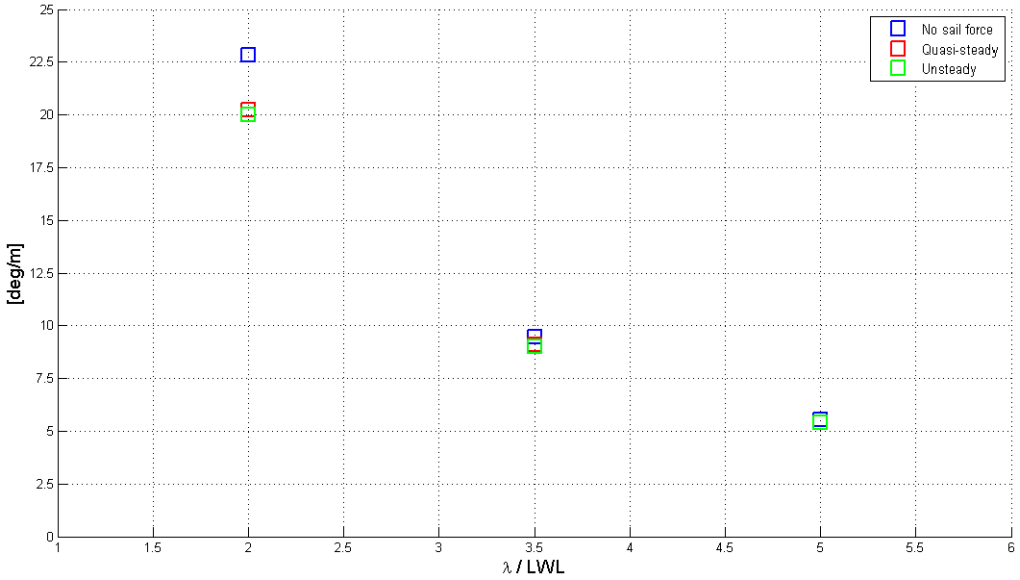

Figure D.94: Model # 45· Pitch mean and amplitude: Fn=0.35, $\zeta_a = 0.25$ m, Upright

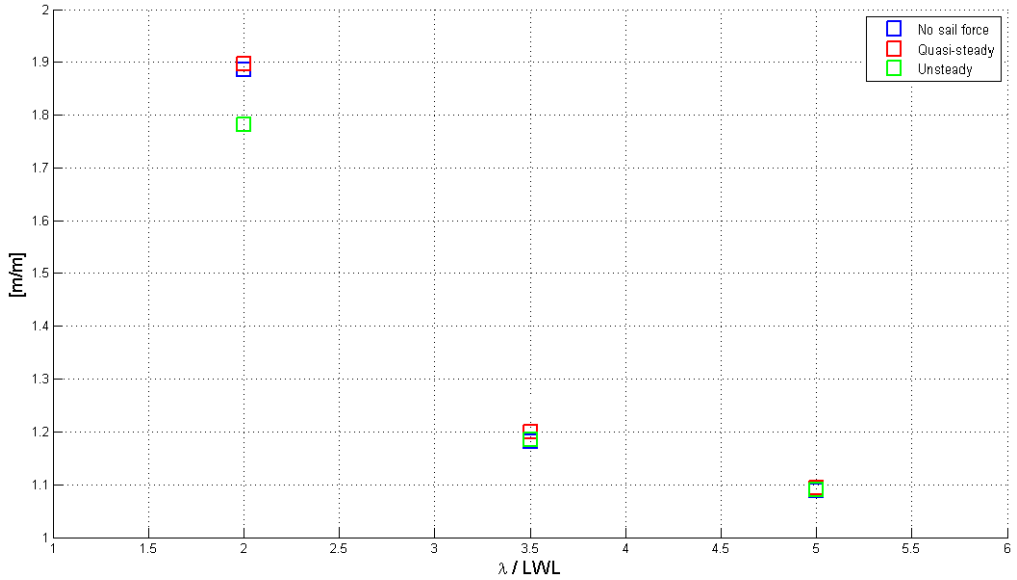

Figure D.95: Model # 45· Heave mean and amplitude: Fn=0.35, $\zeta_a = 0.6$ m, Upright

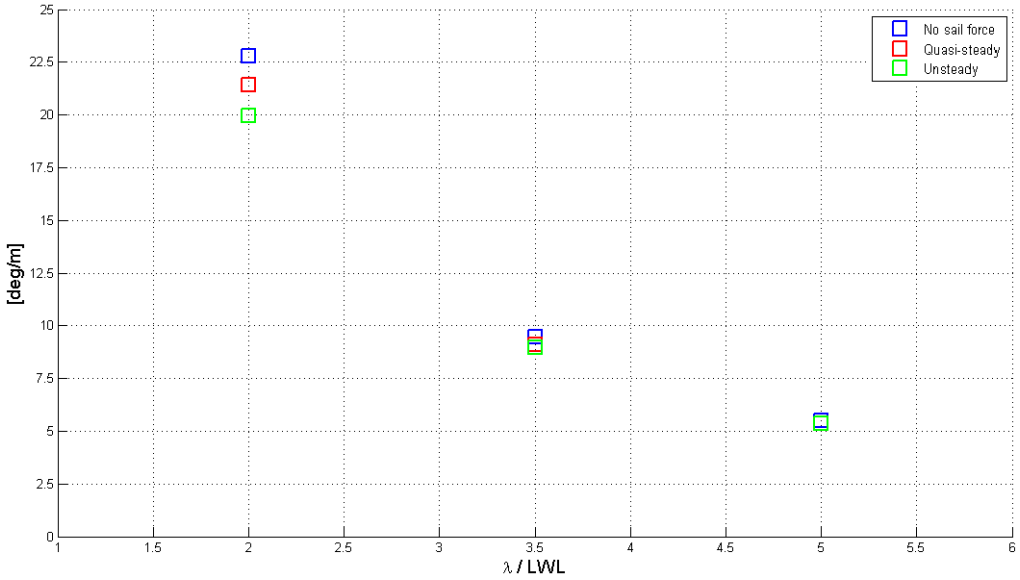

Figure D.96: Model # 45· Pitch mean and amplitude: Fn=0.35, $\zeta_a = 0.6$ m, Upright

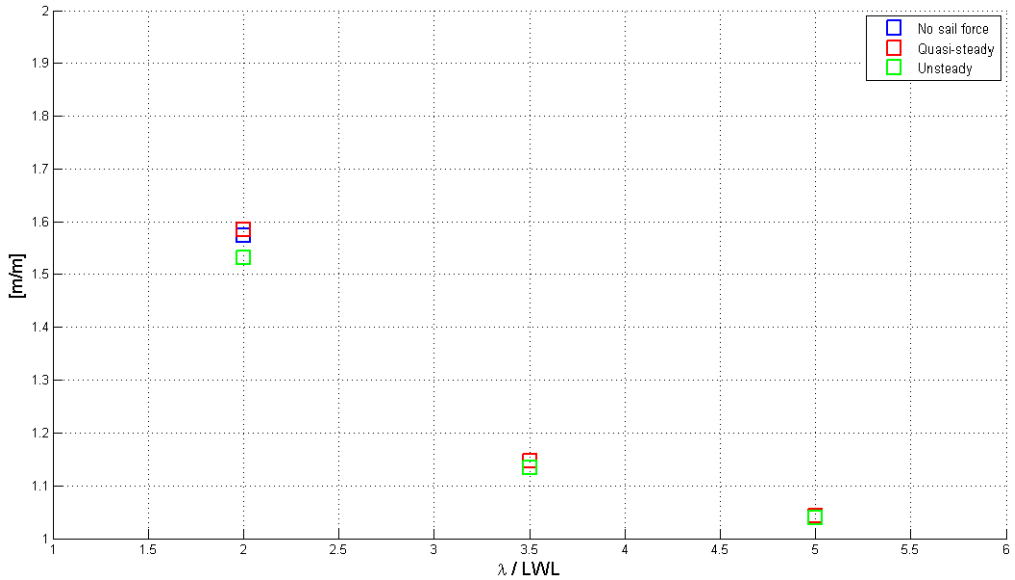

Figure D.97: Model # 45· Heave mean and amplitude: Fn=0.35, $\zeta_a = 0.25$ m, 20° Heel

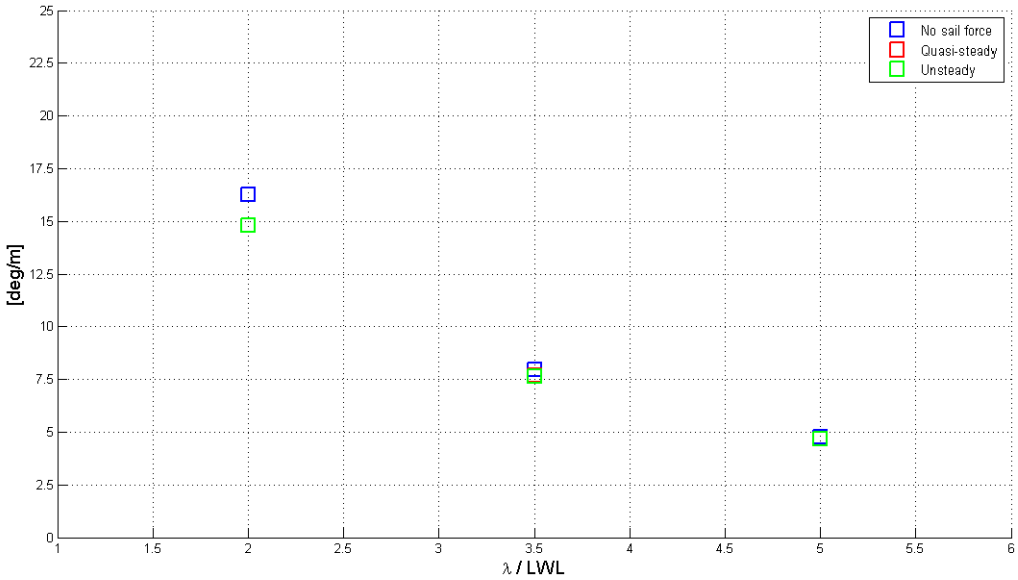

Figure D.98: Model # 45· Pitch mean and amplitude: Fn=0.35, $\zeta_a = 0.25$ m, 20° Heel

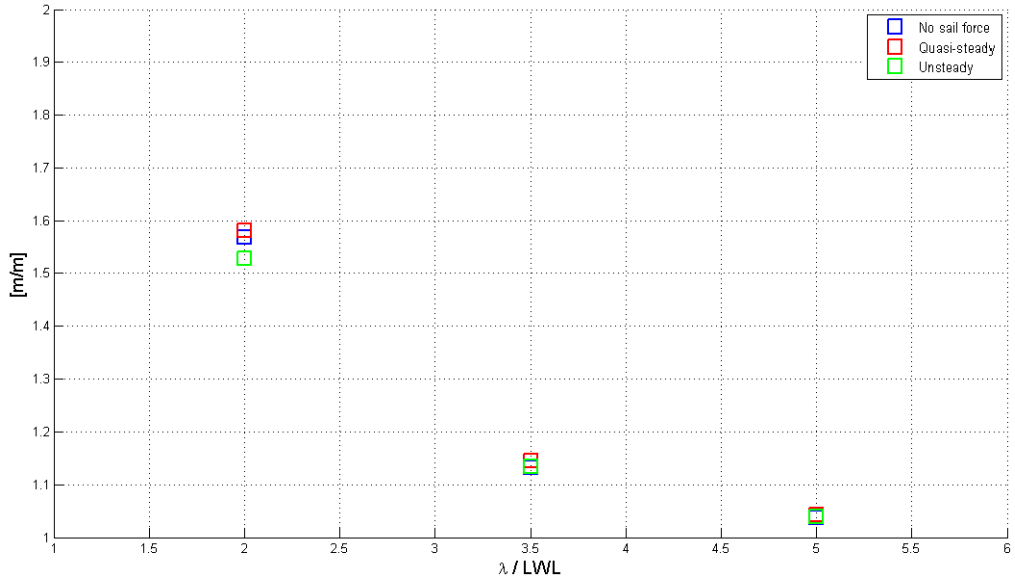

Figure D.99: Model # 45· Heave mean and amplitude: Fn=0.35, $\zeta_a = 0.6$ m, 20° Heel

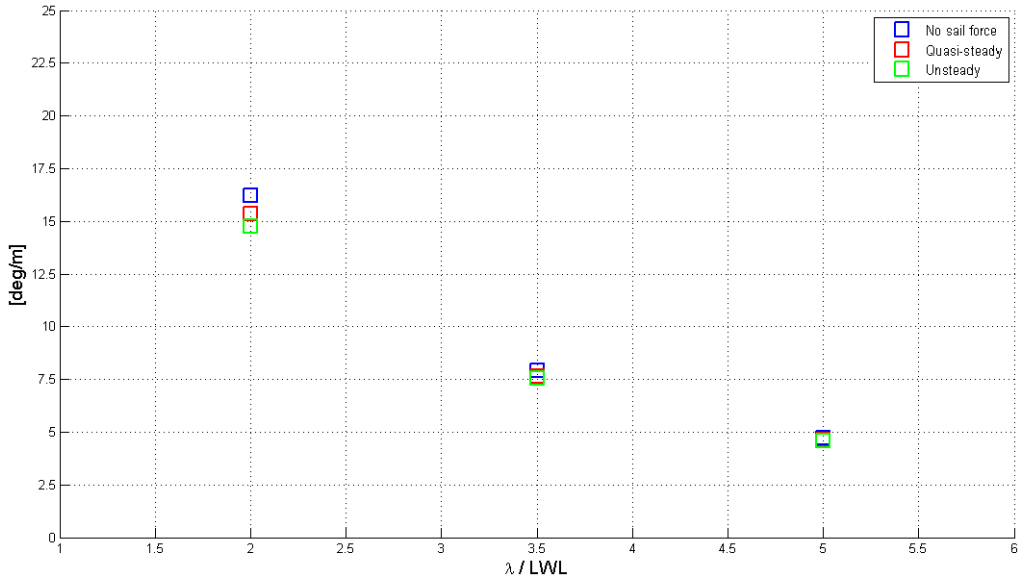

Figure D.100: Model # 45· Pitch mean and amplitude: Fn=0.35, $\zeta_a = 0.6$ m, 20° Heel